COMPREHENSIVE ANALYSIS AND MODELING OF

THREE-PHASE Z-SOURCE CONVERTERS

—————————————————

A Thesis

Presented to

The Faculty of the Graduate School

Tennessee Technological University

By

Gayathri Murthi

—————————————————

In Partial Fulfillment

Of the Requirements of the Degree

MASTER OF SCIENCE

Electrical Engineering

—————————————————

August 2007

CERTIFICATE OF APPROVAL OF THESIS

COMPREHENSIVE ANALYSIS AND MODELING OF

THREE-PHASE Z-SOURCE CONVERTERS

by

Gayathri Murthi

Graduate Advisory Committee:

_____   _____
Joseph O. Ojo, Chairperson   Date

_____   _____
Arun Sekar   Date

_____   _____
Mohamed A. Abdelrahman   Date

Approved for the Faculty:

_____

Francis Otuonye

Associate Vice President of Research and
Graduate Studies

_____

Date

STATEMENT OF PERMISSION TO USE

In presenting this thesis in partial fulfillment of the requirements for a Master of Science degree at Tennessee Technological University, I agree that the University Library shall make it available to borrowers under rules of the Library. Brief quotations from this thesis are allowable without special permission, provided that accurate acknowledgement of the source is made.

Permission for extensive quotation from or reproduction of this thesis may be granted by my major professor when the proposed use of the material is for scholarly purposes. Any copying or use of the material in this thesis for financial gain shall not be allowed without my written permission.

Signature _____

Date _____

DEDICATION

This work is dedicated to my parents.

ACKNOWLEDGEMENTS

TABLE OF CONTENTS

LIST OF FIGURES

Page

LIST OF TABLES

CHAPTER 1

INTRODUCTION

1.1 Introduction

In this new century where people keep pursuing higher quality of life, energy seems to be essential to everyone's life no matter when and where they are. Electric energy is one of the most important forms of energy among the different types available which is required everyday. The power systems existing presently have been structured and operated based on the concept of centralized generation power plants. Based on this concept, there are technical and economical justifications for generation, transmission, distribution, and utilization of energy. In power generation systems, high energy conversion efficiency is desirable in order to reduce the cost the energy. Thus the market is largely driven by the need for uninterrupted, high-quality power, as companies are anxious to avoid both the inconvenience and potential financial losses caused by sudden power failures. Rising awareness about environmental concerns and unpredictability of conventional energy prices prompt the Government to emphasize the need for alternative sources of energy.

Power electronic converters play an increasingly important role in the future energy economy. It is essential that there are efficient methodologies for their control, which will also help to improve their design and achieve the optimal, minimalist structures resulting

in cost reduction, efficient improvement, and reduction of the size. A deep understanding of modulation schemes and mathematical concepts that can be used to determine the desired outcome is required in this study. A study of the control of these converters is essential in order to synthesize the various combinations for switching the power devices in order to obtain the desired reference output.

1.2 Power Electronics

Power electronics is a field which has grown rapidly in recent years. This is due to the advances in power semiconductor devices, advanced control techniques, new power converter circuit topologies, and improvements in packaging and manufacturing. The general trend in power electronics devices has been to switch power semiconductors at increased frequencies in order to minimize harmonics and reduce passive component sizes. The fields where Power electronics are useful are AC machine drives, uninterruptible power supplies (UPS), multi-level converters for utility interface applications, adjustable speed drive applications like hybrid electric vehicle (HEV), and industrial power supplies where the industrial applications flourished. Improvement in product performance, cost, new products and features previously not economically feasible are accomplished in the advances in technology and design techniques.

Energy Conservation Law states that "Energy can neither be created nor destroyed. It can only be transformed from one form to another." A switching power converter is a power electronic system, which converts one level of electrical energy into

2

another level of electrical energy. Electrical energy conversion using power converters are of various types. They can be classified as

- DC to AC converters (Inverters)

- AC to DC converters (Rectifiers)

- DC to DC converters

- AC to AC converters (Cycloconverters/Matrix converters)

There has been on-going research on these power converters and as technology evolves and matures various new trends and performance of the converter can be identified. The dominant topology in the low power and some selected medium power applications has been the pulse width modulated two-level converters. Factors like increasing the power density, improving performance of the converter, reducing the cost of the converter, and also increasing the VA ratings of the converter are among the important issues that play a major role in these new trends. There are several ways in which these factors can be achieved. Reducing the switching losses due to the devices by using appropriate switching techniques, good quality switching devices, and providing efficient thermal protection can increase the power density. Another issue is to increase the performance of the system, which can be achieved by reducing the total harmonic distortions, reducing the EMI problems, and by increasing the dynamics of the system.

Another important factor which has to be considered is the cost of the converters. Tremendous amount of research work is going in an attempt to reduce the cost of the converters by reducing number of devices. Various topologies are being studied to produce the similar result by using lesser number of switching devices. By reducing the

cost of the passive devices, the cost of the converter can be reduced. There has been a continuing increase in power demand and hence the converter power ratings also increase. If the conventional two-level converters are to be used in these high power applications, the rating of the devices has to be increased such as the blocking voltage rating, current rating, thermal management, and so on. Hence in case of increasing the power ratings of the converters by using the low rating devices, Z-source converters are being studied.

The Z-source converters make it possible to deliver high performance, lower cost drives for a wide range of commercial, vehicular, military, utility, and residential applications. This is possible because the Z-source converter consists of lesser number of components than other multiple models used in the industry. It thereby contributes to efficient operation of electric power systems, enhance the efficient use of electricity, and thus contribute to environmental protection and sustainable developments around the world.

1.3 Scope of the Work

This thesis will present in detail the issues in the Z-source converter with special attention on development of new PWM strategies for the Inverter and Rectifier and their advantages with respect to the switching loss and the reduction of harmonic content and ripple in the currents.

- Development of various modulation strategies for the Z-Source Inverter and the Z-Source Rectifier.

- Development of the Generalized Discontinuous Pulse Width Modulation (GDPWM) scheme for the Z-source converter using the space vector approach.

- Development of the system model of the Z-Source Inverter and the Z-Source Rectifier detailed.

- Study of the model and development of the steady state model of the Z-source inverter feeding an RL load as well as an induction machine.

- Modeling and analysis of the Z-Source Rectifier using a resistive load and development of the detailed steady state analysis while unity input power factor is achieved.

- Development of a cascaded control system for the Z-Source Rectifier feeding a resistive load while controlling the output DC voltage and the capacitor voltage.

- Development of a rotor flux vector control scheme of a squirrel cage induction motor by controlling the DC capacitor voltage of the Z-source inverter.

1.4 Organization of Thesis

The organization of this thesis is as follows:

- Chapter 1 presented the introduction to the thesis. It gave an overview of the suggested research work and the scope and limitations of the research.

- Chapter 2 presents the literature survey performed in the scope of realization of this research work. A study of the different converter topologies and the modulation schemes for each topology has been discussed. A comparison of the different topologies discussed has been made. The control schemes and their analysis methods have been reviewed.

- Chapter 3 proposes the conventional converter topologies available and studied so far. It gives a description of the Carrier based Pulse Width Modulation (PWM) and the Space Vector Pulse Width Modulation (SVPWM) schemes which have been used. This chapter gives a basic knowledge of the difference in the classical converters and the Z-source converters.

- Chapter 4 illustrates the various conventional VSI pulse width modulation (PWM) strategies (centered space vector modulation (SVM)) can be modified to switch a Z-source converter either continuously or discontinuously for the realization of the Z-Source Converters. It provides the operating principal of the modulation schemes. The stress is laid on the

Space Vector Pulse Width Modulation (SVPWM) and the generalization of the scheme. The concept of shoot-through duty ratio is brought in, in this chapter. The development and determination of this shoot-though duty has been illustrated. It also provides results to validate the proposed control scheme.

- Chapter 5 illustrates the detailed modeling and study of the Z-Source Inverter. Simulation and steady state results prove the theories stated. In this chapter, the model is studied with an RL (impedance) load. The small signal analysis and the stability analysis shown gives a wider knowledge of the model studied.

- Chapter 6 presents the case of an Induction machine driven by the Z-source inverter. Both the steady state and the dynamic analysis have been performed presenting simulation results.

- Chapter 7 illustrates the detailed modeling and study of the Z-Source Rectifier in all the modes of operation. The input power factor is maintained at unity in this case. The load of the Z-source rectifier is a resistive load.

- Chapter 8 provides the detailed analysis of the Z-source rectifier. The simulation and steady state results prove the theories stated. The small signal analysis as well as the stability analysis shows the different state variables and their eigen values.

- Chapter 9 describes the cascaded control system of the Z-Source Rectifier while controlling the unity input power factor, the capacitor voltage as

well as the output DC voltage. In this case, there are three control variables - M_{qs}, M_{ds}, D_o. Simulation results show the concept of the controller used.

- Chapter 10 proposes an indirect vector control of an induction motor. The procedure is illustrated in detail. In addition to it, the block diagram of the control scheme is presented with the control parameters and the control variables.

- Chapter 11 presents the hardware implementation of the Z-Source Inverter and the Z-Source Rectifier. A detailed procedure of selection of the components and a step-by-step procedure in building the converters and the Z-network are explained. The carrier-based implementation using the TMS320LF2407 DSP is explained in detailed in this chapter.

- Chapter 12 presents the contributions of the work with some conclusions. Also it provides some future extension of the present work.

CHAPTER 2

LITERATURE REVIEW

2.1 Introduction

This chapter presents a review on the various research and works previously done on Z-Source Converters. The review also includes the work done in the area of conventional converters and their control methods.

The initial section gives the details about the vast amount of work done in the field of conventional three-phase voltage source inverters, three-phase boost rectifiers, boost-buck ac-dc converter, buck-boost ac-dc converters, Z-source inverters, and Z-source rectifiers and their modulation schemes. This section also highlights the work done on three-phase boost rectifiers and methods of control applied to different connection topologies of these rectifiers.

The second section deals with the Z-Source Inverters and the Z-Source Rectifiers specifically while their analysis methods and characteristics are discussed along with their topologies. The case where minimum ripple is obtained while maintaining a constant voltage boost is highlighted. The control methodology used in the previous work is presented. In the case of the Z-source Inverter, the control of the DC link voltage is being controlled using suitable PID controllers and this concept has been established in

the earlier work. The vast amount of work done is discussed and the method of study of the process of the control scheme developed in this thesis is put forth in contrast.

2.2 Topologies of Converters

This section deals with the topologies of the conventional converters like the voltage source inverter, boost rectifier, boost-buck ac-dc converter, buck-boost ac-dc converter and the Z-source converters.

2.2.1 Voltage Source Inverter

Voltage Source Inverters (VSI's) are used as a means for DC $\Rightarrow$ AC electric energy conversion in ac motor drive, active filters, unified power flow controllers in power systems, utility interface, and uninterruptible power supplies (UPS) applications. They are also used to generate controllable frequency and AC voltage magnitudes with the help of various Pulse Width Modulation (PWM) techniques [C.1]-[C.3]. However, the classical VSI has a simple structure as shown in Figure 2.1.

From various studies on PWM over the past several decades, the following characteristics could be stated as the most desirable in the PWM scheme :

- Minimum switching loss

- Minimum total harmonic distortion (THD) in the switching function spectrum

- Minimum voltage and current harmonics

- Minimum computation time

- Wide linear modulation range

- Easy implementation [C.4]

Among several modulation schemes, Carrier-based PWM which uses the sinusoidal signal as the modulation signal is the earliest type that employs the "per-carrier-cycle volt-second balance" principle in order to program a desirable inverter output voltage waveform. The intersections obtained by comparing the reference voltage (modulation) waveforms with the triangular carrier wave, in the triangular intersection technique, define the switching instants of the controllable switching devices. Direct digital technique is another common technique where the space-vector concept is utilized to calculate the duty cycle of the inverter switching devices which in turn is utilized to program the switch gate signals [C.3].
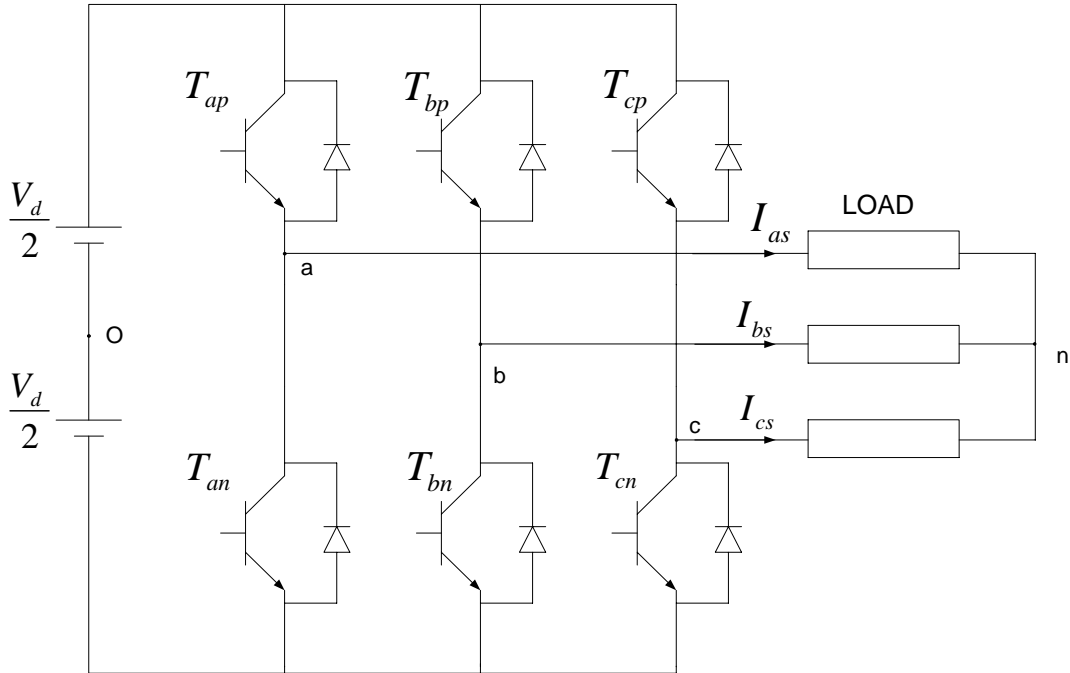
Figure 2.1: Structure of the conventional Voltage Source Inverter

The absence of the neutral current path in three wire loads gives a degree of freedom in determining the duty cycle of the inverter switches. The degree of freedom occasioned by the star-point of the three-phase loads appears as the partitioning of the total time the switching devices in the two zero states are used in the space-vector modulation (SVM) methodology. A degree of freedom appears in choosing the modulation wave, in a triangle intersection implementation, where any zero sequence signal can be injected to the reference modulation waves. However, in direct digital and triangle intersection methods, the voltage linearity, waveform quality (current ripple), and switching losses are all influenced by the choice of the zero-sequence signal (zero-state partitioning) [C.3].

The knowledge of the classical space-vector technique along with the definition of the distribution of the null state times has been helpful for the modulation schemes of inverters in the derivation of generalized equations for the reference voltages and the corresponding methods for their synthesis [C.2]. Discontinuous Pulse Width Modulation (DPWM) methods at the high-modulation range have superior performance while the switching loss and waveform quality comparisons indicate Space Vector Pulse Width Modulation (SVPWM) at low modulation. Magnitude tests and analytical methods were helpful in designing the inverter and determining the performance characteristics as well [C.1].

2.2.2 Boost Rectifier

Now coming to the Boost converters, they are widely used in many industrial applications requiring a high-power dc supply or an intermediate dc link of ac/ac converters and are also used as power-factor corrected pre-regulators [C.6, C.8]. These rectifiers with significant levels of low-frequency harmonics, excessive reactive power, and pulsating input current (EMI interference) may pollute the ac supply. Pulse Width Modulation (PWM) technology can now be used to achieve nearly sinusoidal three-phase input currents with unity power factor, as well as satisfying the harmonic standards due to the rapid improvement in high-speed power semiconductor modular devices [C.8]. The structure of the boost rectifier is as shown in Figure 2.2.

For better performance, the conventional step-up/down ac/dc conversion is usually done by means of two cascaded converters while a single-stage converter is certainly a better choice to achieve better efficiency [C.10]. Potential zero-sequence circulating current is a unique feature in the parallel three-phase converters. Most present technology uses isolation approach, such as transformers or separate power supplies to avoid the circulating current. Some of the approaches followed are given below.

- Isolation: Separate ac or dc power supplies or a transformer isolated ac side is configured for the overall parallel system. This parallel system is bulky and costly because of additional power supplies or the ac line-frequency transformer.

13
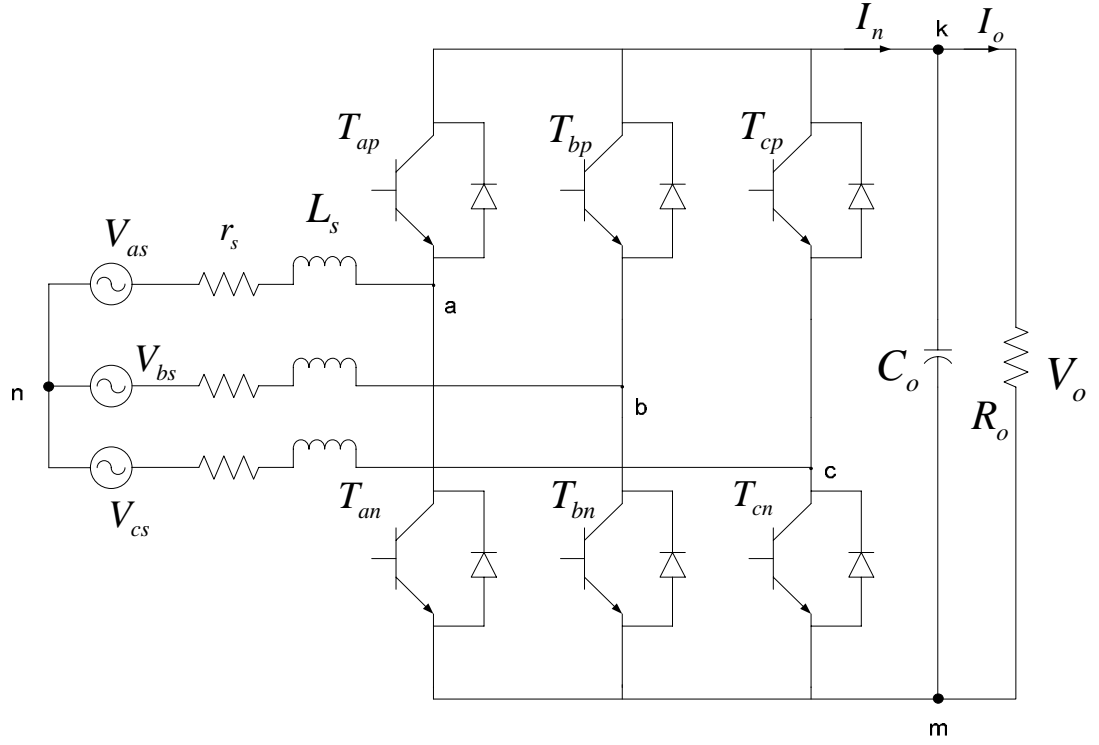
Figure 2.2: Structure of Boost Rectifier

- High impedance: High zero-sequence impedance is provided by the use of Inter-phase reactors, but only at medium and high frequencies as they cannot prevent a low-frequency circulating current.

- Synchronized control: In this approach, parallel converters are treated as one converter. For instance, two parallel three-phase three-leg converters are controlled as a three-phase six-leg converter. This approach is not appropriate for modular converter design. The system becomes very complicated to design and control when more converters are in parallel [C.7].

A new control scheme has been proposed for regulating the instantaneous power for PWM boost type rectifiers under generalized unbalanced operating conditions [C.5].

14

The harmonics in the output DC voltage can be eliminated more effectively under generalized unbalanced operating conditions in the ac input side, by simplifying the oscillating components of instantaneous power at the poles of the converter instead of the front-end through solving a set of nonlinear control equations in real time. The control scheme allows the PWM rectifier to generate a DC output without substantial even-order harmonics as well as to maintain nearly unity power factor under generalized unbalanced operating conditions making it possible to reduce the size of the DC-link capacitor and AC inductors leading to reduced total cost. Feasibility of the new control method is confirmed by the simulation results along with experimental results for the open-loop control using a laboratory prototype converter.

2.2.3 Boost-Buck ac-dc Converters

It is basically a single phase diode rectifier followed by a dc-dc converter power stage. The principal of operation here is a dc-dc converter operating in the current mode control with a rectified input voltage. The illustration of the Boost-Buck ac-dc converter is as shown in Figure 2.3.
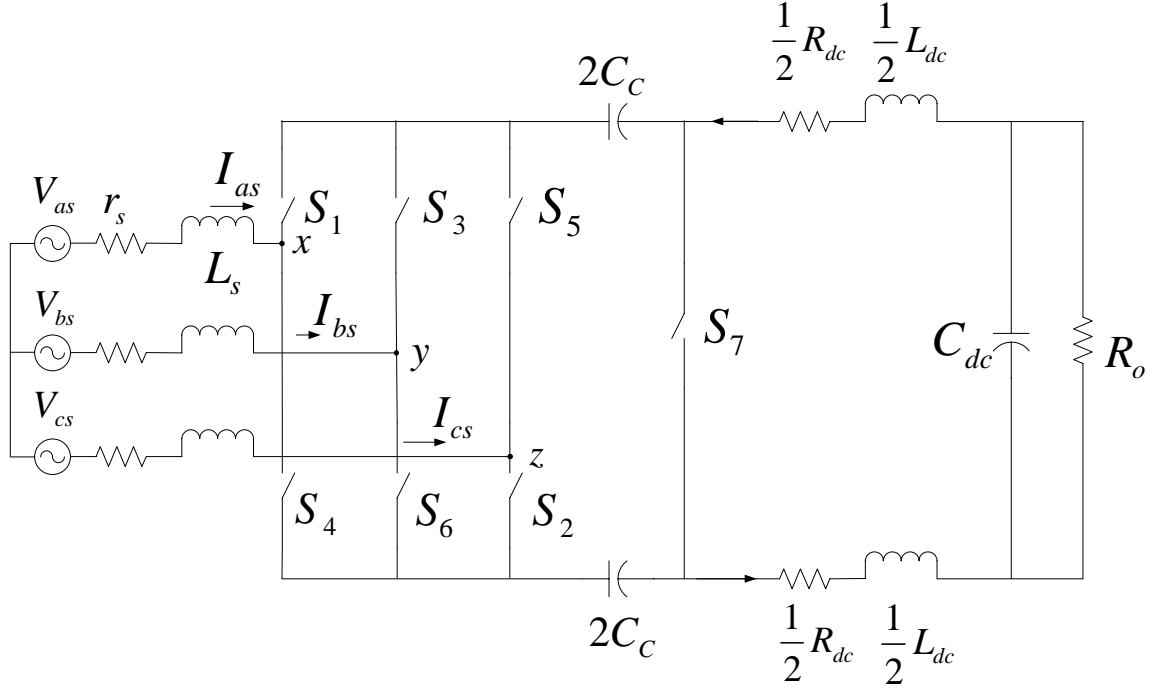
Figure 2.3 Structure of a Boost-Buck ac-dc Converter

The modeling of the boost-buck ac-dc converter is realized using the Ćuk- Ćuk representative [T.4]. They are often called the power factor preregulator since the topology is that of a single phase diode rectifier followed by a dc-dc converter power stage. If the continuous inductor current mode of operation is selected in their current control scheme, they have an inherent input current distortion at the beginning of every half cycle due to lack of a negative ac terminal voltage synthesizing capability [C.13]. In this case they have no power regenerating capability. Generally, single phase applications are low power oriented and quite cost sensitive. The advantage in this case is the low cost realization with this approach.

It has a clear difference in the PWM schemes between the conventional boost rectifier and the boost-buck based rectifier from the viewpoint of power transfer. The boost-buck based rectifiers have an intermediate energy storage stage and the power

transfer from the ac source to the intermediate energy storage stage occurs with an active voltage state vector and that from the intermediate energy storage stage to the dc load occurs with a zero voltage state vector. Experimental demonstration has been performed in [C.14] and [C.15]. In the case mentioned, bidirectional power conversion is not possible in spite of utilizing six active switches with anti-parallel diodes.

Both the upper and lower switches of any leg can be turned ON together in this case. That is the most significant difference between the conventional boost rectifier and the boost-buck rectifier where the zero voltage space vector is applied in the z interval. By turning ON both the upper and the lower switches in a phase leg, a current path for the coupling capacitor discharge is established; thereby power transfer from the coupling capacitor to the dc load is realized. Since the diode D_7 is naturally turned OFF, the shoot-through failure does not occur in the phase leg. One-leg, two-legs or three-legs short mode of operation can be followed. It is seen that the required maximum current carrying capability for the devices in the three-phase bridge is lower because the coupling capacitor discharge current is separated into three-phase legs.

2.2.4 Buck-Boost ac-dc Converters

The simple application of duality to the boost or the boost-buck converter operating principle leads to two current sources connected via a parallel capacitor. In reality, the available ac source is a voltage source. Hence the ac current source must be a series combination of an ac voltage source and an inductor. The LC network between the ac voltage source and the ac current chopping source has a function to filter out the
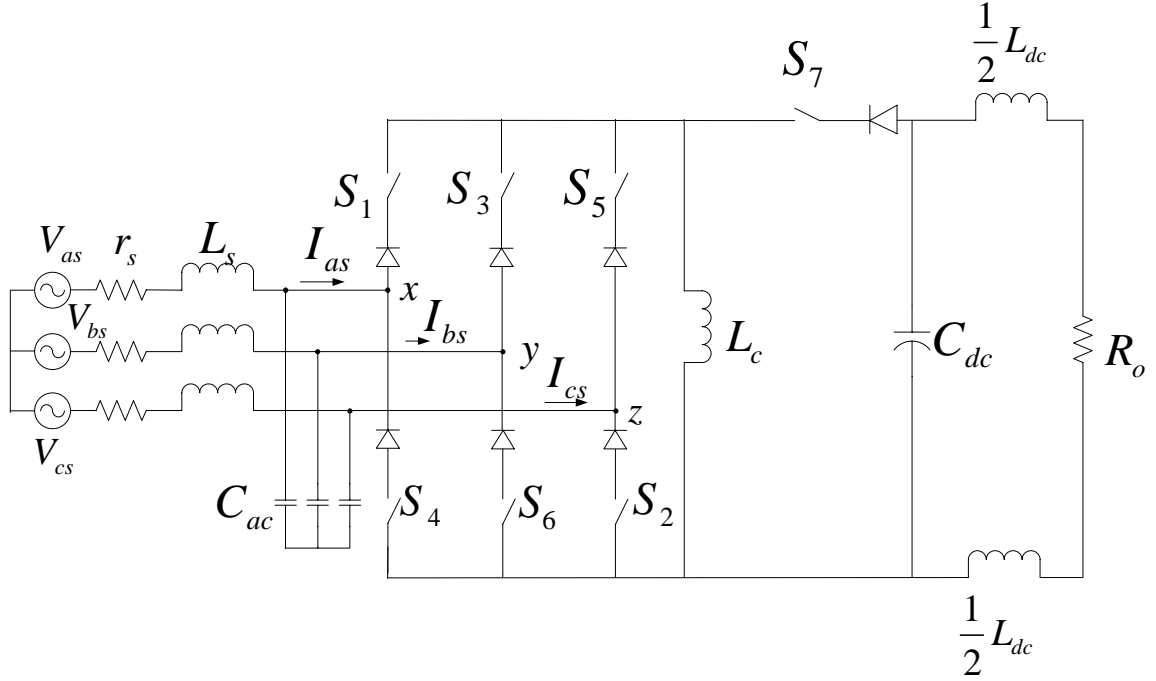
Figure 2.4 Structure of a Buck-Boost ac-dc Converter

switching frequency components due to the current chopping on the rectifier/inverter side. The illustration of a buck-boost ac-dc converter is as shown in Figure 2.4.

It utilizes a simple control scheme with discontinuous inductor current mode of operation and simultaneous switching. Three ac side active switches are turned ON and OFF simultaneously. The active switch on the dc link is necessary to prevent the diode bridge from conducting in its step-down operation. The ac side active switches and the dc side switches operate in complementary fashion which results in a unidirectional power converter [C.16, C.17, C.18].

The topology suggested in [C.18] brings in another reduced switch count version of the buck-boost based converter. It is claimed to have higher efficiency than the six switch realization because only one reverse blocking switch is conducting at any time.

18

The converter reviewed in [T.4] offers bidirectional operation following the schematics of the Ćuk topology in it. The inverter operation with open loop voltage control is studied in [C.19], although the authors mentioned a possibility to operate as a rectifier as well.

The dc-dc converters can be made bidirectional power converters from unidirectional power converters by adding a series diode to the active switch and a series active switch to the freewheeling diode as shown in Figure 2.4. The buck-boost based bidirectional dc-dc converter appears to be a buck-boost converter from both sides. The reversal of polarity in both the input and output voltages is necessary to change the direction of the power flow. The left side source or load is expressed as a parallel combination of a current source and a bipolar capacitor, and the right side source or load is expressed as a series combination of split inductors and a voltage source, where the voltage source polarity must be changed depending on the direction of the power flow [T.4].

In the case of the boost-buck ac-dc converters for power transfer, the necessity of bridge-leg-short is taken into consideration and the application of duality implies the necessity of bridge-leg-open in the buck-boost ac-dc converter operation as unconventional zero current space vector in order to make power transfer possible. Unlike the boost-buck ac-dc converter operation, there is effectively only one zero current space vector to realize the bridge-leg-open because none of the switching devices in the three-phase Current Source Converter (CSC) bridge can carry current during the bridge-leg-open zero current space vector period [T.4].

The most significant difference from the conventional buck rectifier is in the interval z during which a zero current space vector is applied. By opening all three phase

legs, the magnetic energy stored in the inductor L_c is released to dc load side via S_7 and D_7. Whichever the interval is an active current space vector period or a zero current space vector period, S_7 always has a positive gate signal as long as rectification is under operation and D_7 is naturally turned ON or turned OFF depending on the voltage across it. Unlike the buck rectifier, the overlap period conduction period between an outgoing device and an incoming device is not necessary [T.4].

2.2.5 Z-Source Inverter

In the late nineties, Dr. Fang Zheng Peng popularized the concept of the Z-Source Converters, which employ a unique impedance network (or circuit) to couple the converter main circuit to the power source. They provide unique features that cannot be obtained in the traditional voltage-source (or voltage-fed) and current-source (or current-fed) converters which use capacitor and inductor, respectively. The conceptual and theoretical barriers and limitations of the traditional voltage-source converter (abbreviated as V-source converter) and current-source converter (abbreviated as I-source converter) are overcome by the Z-source converter providing a novel power conversion concept that can be applied to all dc-to-ac, ac-to-dc, ac-to-ac, and dc-to-dc power conversion [I.1]. The structure is as shown in Figure 2.5.
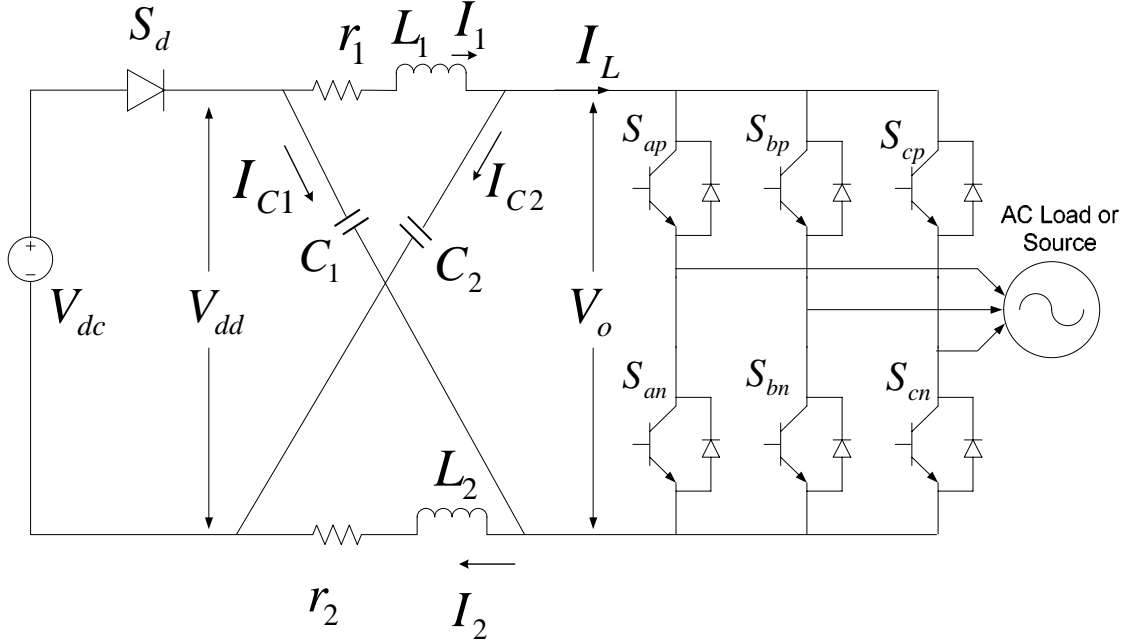
Figure 2.5: Structure of a Z-source inverter

Z-source inverters are single-stage electronic power converters which have both voltage-buck and boost capabilities. The dc-side phenomenon, associated with the Z-source impedance network, is shown through small-signal and signal-flow-graph analyses to be having a right-half-plane zero in its control-to-output transfer function. The ac-side phenomenon is shown through space vector analysis to depend on the time intervals of inverter states used for reconstructing the desired inverter output voltage. A method for improving the inverter transient response is presented on the basis of ac vectorial analysis [I.1, I.2, and I.7]. A Z-source inverter is proposed, which can operate at wide range load (even no-load) with small inductor, eliminating the possibility of the dc-link voltage drops, and simplifying the inductor and controller design [I.5].

The widely used V-source converter has the following conceptual and theoretical barriers and limitations.

- The ac output voltage is limited below and cannot exceed the dc-rail voltage or the dc-rail voltage has to be greater than the ac input voltage. Therefore, the V-source converter is a boost (step-up) rectifier (or boost converter) for ac-to-dc power conversion while the V-source inverter is a buck (step-down) inverter for dc-to-ac power conversion. Some applications where the available dc voltage is limited and over drive is desirable need an additional dc-dc boost converter so as to obtain a needed ac output. The system cost increases and efficiency decreases due to the additional power converter stage.

- If the upper and lower devices of each phase leg are gated on simultaneously either by purpose or by EMI noise, a shoot-through would occur that destroys the devices. This shoot-through problem caused by electromagnetic interference (EMI) noise's mis-gating-on heavily effects the converter's reliability. V-source converter has to provide the dead time to block both upper and lower devices, which causes waveform distortion, etc.

- An output *LC* filter is required to provide a sinusoidal voltage compared with the current-source inverter that causes additional power loss and control complexity [I.1].

The current source converter circuit, a three-phase bridge is fed by a DC current source that can be a relatively large dc inductor which is fed by a voltage source such as a battery, fuel-cell stack, diode rectifier, or thyristor converter.

I-source converter has the following conceptual and theoretical barriers and limitations.

- The ac output voltage has to be greater than the original dc voltage that feeds the dc inductor or the dc voltage produced is always smaller than the ac input voltage. Therefore, the I-source converter is a buck rectifier (or buck converter) for ac-to-dc power conversion while the I-source inverter is a boost inverter for dc-to-ac power conversion. Applications in which a wide voltage range is desirable, need an additional dc–dc buck (or boost) converter. The system cost increases and efficiency decreases due to the additional power converter stage.

- At any given time, at least one of the upper devices and one of the lower devices have to be gated on and maintained. If not, an open circuit of the dc inductor would occur that destroys the devices. This open-circuit problem caused due to EMI noise's mis-gating-off is a major concern of the converter's reliability. I-source converter needs overlap time for safe current commutation, which also causes waveform distortion, etc.

- The main switches of the I-source converter should block reverse voltage which requires a series diode to be used in conjunction with high-speed and high-performance transistors such as insulated gate bipolar transistors (IGBTs). This avoids the direct use of low-cost and high-performance IGBT modules and intelligent power modules (IPMs) [I.1].

Several problems related to high frequency switching are faced with the Traditional 2-level high-frequency pulse width modulation (PWM) inverters for motor drives, which produce common-mode voltages and high voltage change (dV/dt) rates to

23

the motor windings. The concept of utilizing a dc-dc boost converter in series with the inverter was introduced, which uses the Z-network to boost the DC voltage.

In order to minimize the voltage stress for any given voltage gain, the boost factor and the modulation index have to be minimized and maximized, with the restriction of that their product is the desired value. However, to achieve the maximum voltage gain, the boost factor should be maximized for any given modulation index. When the triangular carrier wave is either greater than the maximum curve of the three phase references or smaller than the minimum of the references, the circuit is said to be in shoot through state. The shoot through duty cycle varies each cycle. The average shoot through duty cycle aids to calculate the voltage gain [I.10].

Low-frequency current ripple has to be eliminated by using a constant shoot-through duty ratio so that the volume and cost of the *Z*-source network can be reduced. Simultaneously, to reduce the voltage stress across the switches, a greater voltage boost for any given modulation index is desired. This control method has five modulation curves out of which three are reference signals and two shoot-through envelope signals. The inverter is turned to a shoot-through zero state, when the carrier triangle wave is higher than the upper shoot-through envelope or lower than the bottom shoot-through envelope. Meanwhile, the inverter switches in a similar fashion as in the traditional carrier based PWM control. Maximum voltage gain is achieved and the voltage stress is also minimized, keeping the shoot-through duty ratio a constant [I.11].

2.2.6 Z-Source Rectifier

Although several single-stage single-phase ac/dc converters have been proposed in the existing literature [C.11, C.12, R.4, T.4], not much work is done in the area of three-phase step-up/down converters. Only a few buck–boost-type three-phase ac/dc converters have been proposed. However, the disadvantages of the pulsating input and output currents still exist. An equivalent duty cycle for the zero-voltage space vectors is proposed so that control of the ac and dc parts of the converter circuit can be integrated to achieve the ideal characteristic of a single-stage step-up/down ac/dc converter. The input current can be made clean sinusoidal with unity power factor and the output can be stepped up/down without ripples. Based on how many modes are chosen and which class of generalized zero-voltage space vectors is selected to increase the equivalent dc duty cycle, different control schemes can be derived. In specific, elimination of the dead time circuit also simplifies the drive circuit and adoption of fixed switching frequency renders the design of the filter simple [C.9, C.10].
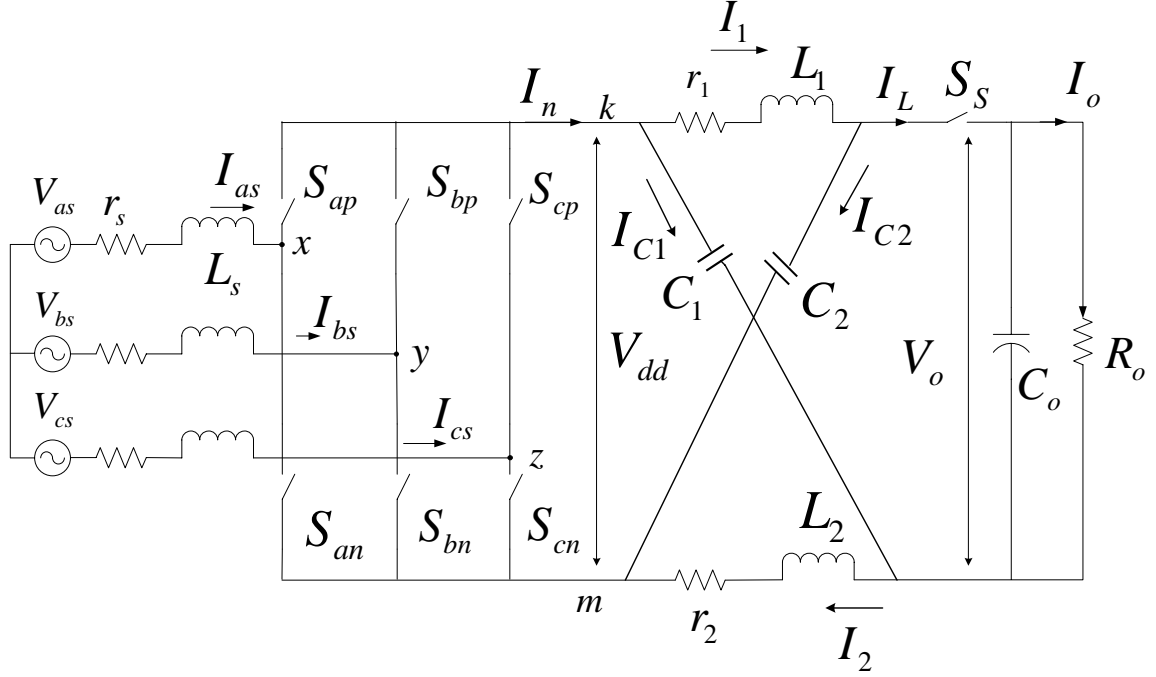
Figure 2.6: Structure of a Z-source rectifier

Z-Source Rectifier concept has been introduced to prevent the problems stated above. The three-phase ZVS Z-Source rectifier implements the zero voltage turn-on (ZVS) for power transistors and zero current turn-off (ZCOFF) for the diodes without any additional circuits [R.1].

The voltage source rectifier (VSR) is widely used in the four-quadrant AC motor driver system in which case, the DC voltage that is greater than AC voltage has to be obtained, that benefits the motor driving performance at the same time being a disadvantage to the motor starting course. Thus, the inverter should be able to take the high DC voltage during starting course, and the modulation index of the inverter has to be set in a low value, reducing the quality of output AC voltage. Additionally, the method of

increasing dead time has been applied to avoid the shoot-through which would result in the distortion of the current waveform.

Employing the Z-Source rectifier's impedance network to couple the rectifier main circuit to the load provides unique features that cannot be obtained in a traditional full-bridge rectifier. The Z-source network is coupled between the bridge and the load, with the unique control strategy, some virtues should be achieved.

- Flexibly adjust the output DC voltage, greater or smaller than the line ac voltage.

- Shoot-through allowed in a bridge leg, which increase the EMI noises resistance.

- The dead time need not be applied, and the clear sinusoidal current wave is obtained.

- The size of both the dc-link inductor and the output capacitor are reduced compared to traditional two-stage buck rectifier.

The unique features of Z-source network make it better to be used in AC-DC converter, and obtain more virtues than traditional cascaded rectifier. As the Z-Source rectifier can access buck or boost function without using two-stage power conversion, it overcomes the drawbacks of the traditional cascaded buck rectifier. A non-shoot-through allowed in a bridge leg, which lead to lower EMI reliability is one of the limitations in traditional two-stage circuit. In addition, the cascaded system may be lower efficiency and more complicated. Basically, the Z-source rectifier utilizes the shoot-through states to achieve buck-boost DC voltage [R.2].

27

The capacitors are charged during the extra zero voltage state (Shoot-through state), and during the active state, the charged capacitor voltage is supplied to the load along with the voltage output of the boost rectifier. The shoot-through interval (inserted during the traditional zero vector) can achieve buck-boost output voltage while not leading to circuit disorder. The average voltage of the inductors over one switching period can be zero in steady state by charging Z-source inductors [R.2].

The configuration provides favorable characteristics that exceed the traditional voltage source rectifier. It can buck and boost the input voltage and increase the reliability of the system to a great extent. Thus the Z-Source Rectifier provides a low-cost, reliable and highly efficient single-stage structure for the buck and boost power conversion [R.1].

2.3 Modulation Scheme

The modulation scheme is the most important in terms of realizing the Z-source converter. The modulation scheme is the one which makes the model different from the conventional converter and the required output is obtained. The modulation scheme used in the previous work is as shown below.

The shoot-through duty ratio which determines the buck factor has to be kept constant. It is proposed in [I.1], a simple boost method and a similar method is given in [R.1] where the triangle signal shifts to the right where the shoot-through signal is produced. The six active states are maintained unchanged in this method just like it is in the traditional PWM control. The switches which are in the ON state during the free-

wheel states are turned ON just during the shoot-through state. The extra zero state is injected on the forepart of these free-wheel time zones along with the diode-clamp characteristic. The switches operate in the ZVS condition and the diodes operate in the ZCOFF condition. Except for the shoot-through states, the operating principle is similar to that of the traditional PWM control method [R.1].

2.4 Analysis Methods

The analysis methods followed in most of the previous work is as mentioned below. Jinbo Liu in [T.2] has utilized the AC small signal models of the Z-source converters operating in the Continuous Conduction Mode (CCM). It is assumed that

- Z source converter is operating in continuous conduction mode
- The passive components used in the Z-source network are ideal and lossless
- The input voltage is an independent voltage source. The forward voltage drop of the switch is modeled by a fixed voltage drop
- Because the on-resistance of the switch is much smaller than the load impedance, it is neglected in the modeling and analysis

The model is analyzed using a resistive load, and inductive load [T.4].

In the case of P. C. Loh et al in [I.7, I.8, I.13, I.15, I.19], three methods of analysis were performed while taking into consideration the dc side transient analysis of the Z-source impedance network. Namely

- Small-Signal Mathematical Analysis

29

- Signal-Flow Graphical Analysis

- Root Locus Analysis of RHP Zero

For ac side transient analysis of the Z-source inverter, two analysis methods are performed. Namely

- Significance of Inverter Null Switching Vectors

- Gradual Tuning of Active State Interval with Improved Transient Performance

In the case of the dc analysis, both small-signal and signal-flow graph methods are used with an intention of developing a comprehensive guide on the Z-source network modeling. A feature revealed by both modeling methods is that the Z-source network has a RHP zero in its control-to-output transfer function, resulting in the dc-link voltages having a non-minimum-phase response. Non-minimum-phase response is also proved to be in existence through vectorial analysis on the inverter ac-side when PWM state sequence with constant (or zero) null interval is used. This ac response with an initial dip and slower rise time can be improved by using PWM sequence with a variable cushioning null interval and gradual tuning of active interval [I.7].

2.5 Control Scheme

Fang Z. Peng et al in [I.3] introduces a PID controller for dc-link boost voltage in Z-source inverter which utilizes the shoot-through zero states to boost dc voltage and produces an output voltage greater than the original dc voltage. A constant capacitor

voltage can be achieved with this technique along with an excellent transient performance that enhances the rejection of disturbance, including the input voltage ripple and load current variation with good ride-through for voltage-sags. A detail description of the shoot-through duty cycle modulation strategy for controlling the dc-link boost voltage is given to simplify the controller design and improve the transient response [I.3, I.4]. Fang Z. Peng et al in [I.4] introduces a PID controller for direct peak dc-link boost voltage in Z-source inverter and describes the peak dc-link voltage direct sensing and scaling method, and modified modulation strategy, which simplify the controller design, improve the transient response, and decrease the voltage stress across the switches.

The ZSI makes use of the shoot-through state to rise the dc link voltage by conducting both upper and lower switches of any phase legs. Therefore, the ZSI can boost voltage to desired ac output voltage that is greater than the available dc link voltage. The capacitor voltage is equivalent to the dc link voltage of inverter which can be increased by controlling the shoot-through time duty ratio. The shoot-through time cannot linearly control the capacitor voltage as the relationship between the ratio of the capacitor voltage to the dc link voltage and the shoot-through time duty ratio has nonlinear characteristics. This nonlinearity may deteriorate the transient response of capacitor voltage [I.6].

Miaosen Shen et al in [I.29] describes and presents the controller for the Z-source inverter feeding an inductive load. It aims at controlling the output voltage as well as the Z-network capacitor with two control parameters – modulation index as well as the shoot-through duty ratio. A gain scheduling controller has been designed using Taylor series for all possible equilibrium points.

Fang Z. Peng et al in [R.3] presents the analysis of dynamic response of the ZVS Z-source rectifier and design of the closed-loop controllers for both the Z-source rectifier and the Z-network circuit. The transient response is found to be challenging in controlling the ZVS Z-source rectifier due to the unique Z-network. The ZVS Z-Source rectifier model is proposed by combining the traditional PWM rectifier model and equivalent model of the Z-network. The controllers are designed through detailed analysis in order to obtain the steady DC-link voltage and a sinusoidal AC voltage under linear loads. The recently presented Z-source rectifier can provide good input power factor, low line current distortion, regeneration and also a wide range of output dc bus voltage due to using the impedance network (Z-network) [R.1]. Hence, the z-source rectifier can both buck and boost voltage to a desired output voltage, greater or smaller than the input ac voltage, that can be used in the ASD system to make the PWM inverter operating with the high modulation index while in the low voltage condition, M=1. Shoot-through can no longer destroy the circuit, thus improving the reliability of the rectifier. The small-signal model of the Z-network circuit is given based on which the PD controller is designed providing better transient response and steady dc-link output voltage. The ZVS Z-source rectifier in conjunction with the PD compensator has better dynamic response, smaller voltage ripple, a single-stage power conversion topology, high reliability, good dynamic response, and high efficiency.

2.6 Conclusion

This chapter dealt with the previous work performed in this field of study. A detailed analysis of the conventional converters such as voltage source inverters, boost rectifiers, boost-buck ac-dc converters, and buck-boost ac-dc converters has been performed. A deep review of the Z-source inverters and Z-source rectifiers has been done and it can be concluded that in all the work performed so far, a detailed step by step analysis of all the modes of operation has not been performed. At the same time, the resistances in the Z-network have always been neglected. A comprehensive analysis of the system has not been performed in the work done so far. Also, in all the work studied so far, the control parameters are limited to two which leads to controlling only two variables. In this thesis, a comprehensive analysis of the system as well as the designing a controller with three control variables has been considered.

CHAPTER 3

CONVERTER TOPOLOGIES – THREE-PHASE VOLTAGE SOURCE INVERTER AND BOOST RECTIFIER

3.1 Voltage Source Inverter

A conventional three-phase Voltage Source Inverter (VSI) feeding a three-phase load is as shown in Figure 3.1. The main purpose of this topology is to generate a three-phase voltage source with controllable amplitude, phase angle, and frequency. Three-phase DC/AC voltage source inverters are extensively used in motor drives, active filters, and power flow controllers and uninterrupted power supplies (UPS) using various pulse width modulation (PWM) strategies. There are totally six power semiconductor devices with anti-parallel diodes, which can be transistors, MOSFETs, IGBTs, or any other components that can operate as switches and transfer power. The input DC source is usually obtained from a single-phase or three-phase diode-bridge rectifier with a filter or a battery. Voltages can be generated from the voltage source converter by turning on and off the switches under certain combinations.

The carrier-based PWM scheme and the Space vector PWM scheme are discussed in the following section. The voltage vectors are used to synthesize the desired voltage.
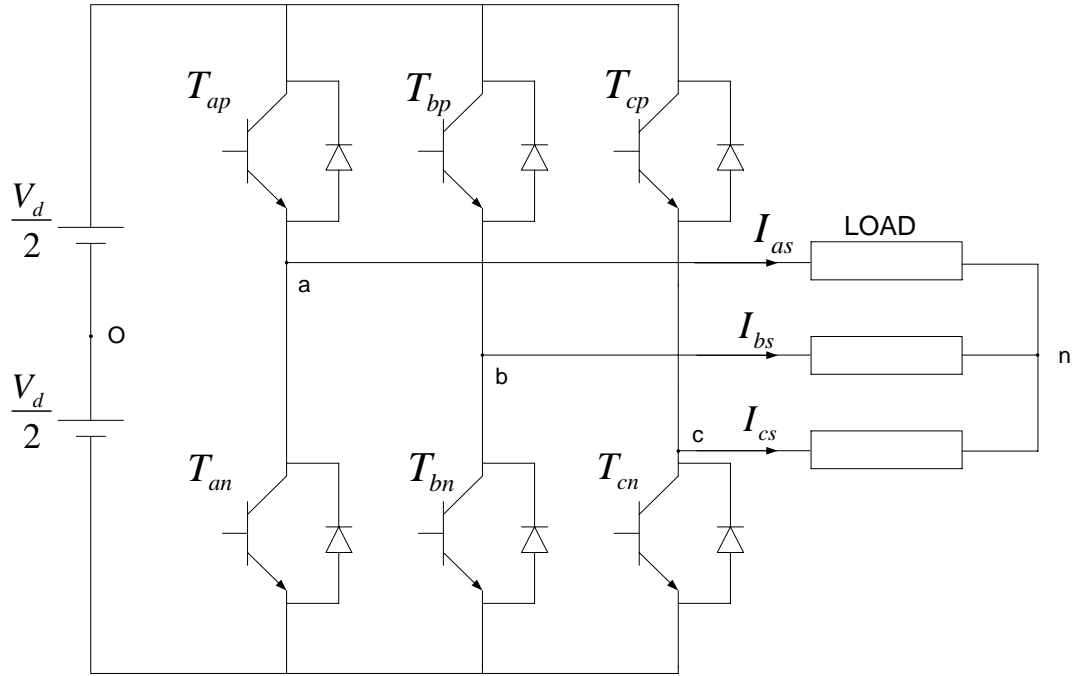
Figure 3.1: Conventional Voltage Source Inverter feeding three-phase load.

Table 3.1: Variables used for the Three-phase Boost Rectifier

V_d	INPUT DC VOLTAGE
V_{as} V_{bs} V_{cs}	THREE-PHASE OUTPUT VOLTAGES
I_{as} I_{bs} I_{cs}	THREE-PHASE OUTPUT CURRENTS
V_{no}	NEUTRAL VOLTAGE
T_{ap} T_{bp} T_{cp}	TOP DEVICES
T_{an} T_{bn} T_{cn}	BOTTOM DEVICES

3.1.1 Carrier-Based PWM

The turn-on and turn-off action of the switch produces a rectangular waveform known as the switching pulse. It is obtained by comparing a sinusoidal signal with a high frequency triangle signal. This principle is known as Sinusoidal Pulse Width Modulation (SPWM) where a sine weighted modulating signal is obtained [B.2]. This is shown in Figure 3.2.

The three phase shifted reference signals are compared with the carrier signal in the three-phase VSI, which eventually define the switching instants for the power devices. The harmonics generated in this scheme are around the carrier frequency and its multiples. The output voltage is equal to the input voltage, $\frac{V_d}{2}$ when the switch is turned ON and it is equal to zero when the switch is turned off. Thus, the continuous turning ON and turning OFF produces a train of pulses.

Due to the Kirchoff's Voltage law, the two switching devices on the same leg cannot be turned ON simultaneously as the DC source will be shorted. At the same time, they cannot be turned OFF simultaneously as it will result in an uncertain voltage to the phase it is connected to. This implies that either one of the switches in each leg of the inverter have to be turned ON at every instant. That is, the nature of the switches on each leg is complementary.

The turn-on and turn off sequences of a switching device are represented by the existence function. Generally, an existence function of a two-level converter with switching devices, T_{ij} is given as S_{ij}

where

$i = $ a, b, c.

i represents the phase on the load side to which the device is connected.

$j = $ p, n.

j represents the top (p) or the bottom (n) device of a leg.

Here, the existence functions of the phase 'a' top device, T_{ap} is S_{ap} and that of the

bottom device, T_{an} is S_{an} and so on and so forth. The following expressions are obtained

to ensure that the devices in one leg are not turned ON together.

$$S_{ap} + S_{an} = 1$$

$$S_{bp} + S_{bn} = 1 \tag{3.1}$$
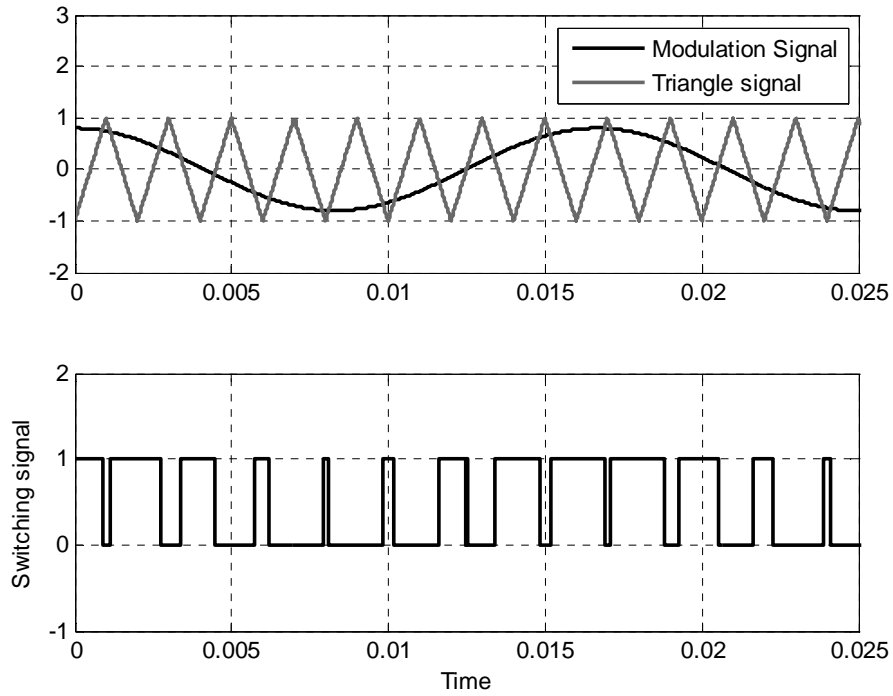
$$S_{cp} + S_{cn} = 1$$

Figure 3.2: Illustration of Sinusoidal Pulse Width Modulation

The output phase voltages of the VSI from Figure 3.1 can be expressed as

$$\frac{V_d}{2}\left(S_{ap} - S_{an}\right) = V_{an} + V_{no}$$

$$\frac{V_d}{2}\left(S_{bp} - S_{bn}\right) = V_{bn} + V_{no} \qquad (3.2)$$

$$\frac{V_d}{2}\left(S_{cp} - S_{cn}\right) = V_{cn} + V_{no}$$

The switching functions for the two switching devices on a leg are dependent. Hence only one switching function can be used to represent the switching status of each leg, which is usually chosen as the switching function of upper device. So the turn-on and turn-off actions of the switches produce series of rectangular waveform and the ratio between the on-duration and a full period is defined as duty cycle, which is varying between 0 and 1. Thus (3.2) can be written as

$$\frac{V_d}{2}\left(2S_{ap} - 1\right) = V_{an} + V_{no}$$

$$\frac{V_d}{2}\left(2S_{bp} - 1\right) = V_{bn} + V_{no} \qquad (3.3)$$

$$\frac{V_d}{2}\left(2S_{cp} - 1\right) = V_{cn} + V_{no}$$

The switching function can be written in terms of the fourier series of the modulation signal. The switching function comprises of a fundamental frequency component and an average component.

$$S_{ap} = \frac{1}{2}\left(1 + M_{ap}\right)$$

$$S_{bp} = \frac{1}{2}\left(1 + M_{bp}\right) \qquad (3.4)$$

$$S_{cp} = \frac{1}{2}\left(1 + M_{cp}\right)$$

where

M_{ip} = three-phase carrier-based modulation signal

To obtain the modulation signal, (3.4) is substituted into (3.3) to get

$$M_{ip} = \frac{2\left(V_{in} + V_{no}\right)}{V_d} \qquad (3.5)$$

where

V_{in} = three phase voltages

i = a, b, c

The neutral voltage V_{no} is determined later in (3.6). In the linear modulation range, the three-phase modulation signal varies from -1 to 1. The steps involved in obtaining the output voltage are as follows. The first step is to calculate the modulation signals of the desired frequency. These three-phase modulation signals are compared with the high frequency triangle signal which also varies between -1 to 1. When the modulation signal is greater than the high frequency triangle signal, the corresponding phase upper device turns ON as the output signal is high. When the modulation signal is lesser than the triangle carrier signal, the corresponding lower device of the phase turns ON. When the upper device is turned ON, the positive rail of the DC supply is connected to the phase and while the lower device is turned ON, the negative rail of the DC supply is connected to the phase. Hence the PWM switching pulses are obtained. The triangle signal is of high frequency because the fundamental component of the voltage pulses is equal to the reference signal only at high frequencies.

The modulation index is defined as ratio between the magnitude of the desired output voltage to half the DC supply voltage.

$$M = \frac{V_m^*}{V_d / 2}$$ (3.6)

To calculate the phase voltages, the neutral voltage V_{no} needs to either be eliminated or determined. The neutral voltage V_{no} is obtained from (3.3) as they are summed and the neutral voltage is eliminated from it. Under balanced load conditions, the neutral voltage is obtained as

$$V_{no} = \frac{V_d}{3}\left(S_{ap} + S_{bp} + S_{cp}\right) - \frac{V_d}{2}$$ (3.7)

Hence the phase voltages can be obtained as

$$V_{an} = \frac{V_d}{3}\left(2S_{ap} - S_{bp} - S_{cp}\right)$$

$$V_{bn} = \frac{V_d}{3}\left(-S_{ap} + 2S_{bp} - S_{cp}\right)$$ (3.8)

$$V_{cn} = \frac{V_d}{3}\left(-S_{ap} - S_{bp} + 2S_{cp}\right)$$

The switching pulses are used to drive the switching devices and the phase voltages are applied to the load which results in sinusoidal currents in the case of inductive loads.

The simulation results of the Carrier-based PWM are shown in Figures 3.3, 3.4, 3.5, and 3.6 as the inverter feeds an RL load.
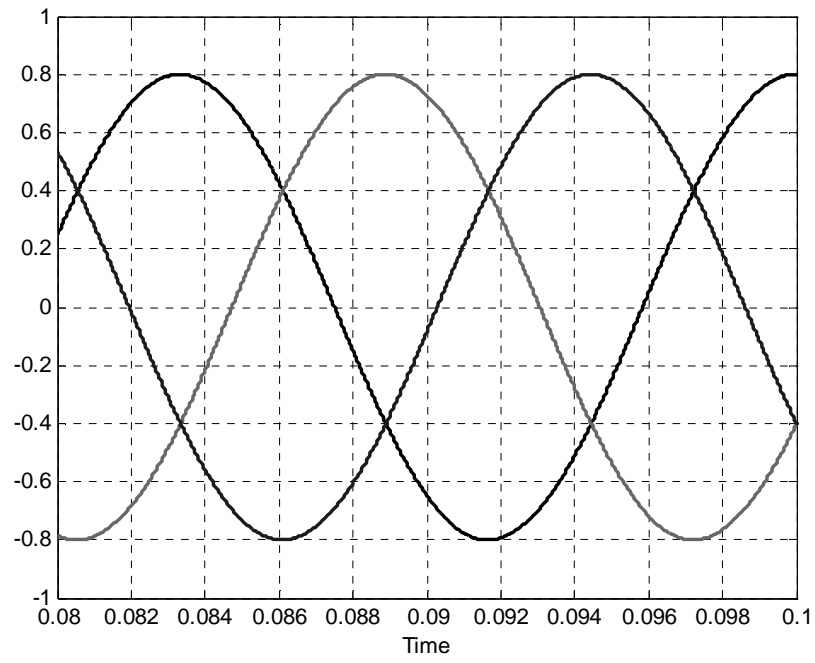
Figure 3.3: Three-Phase modulation signal
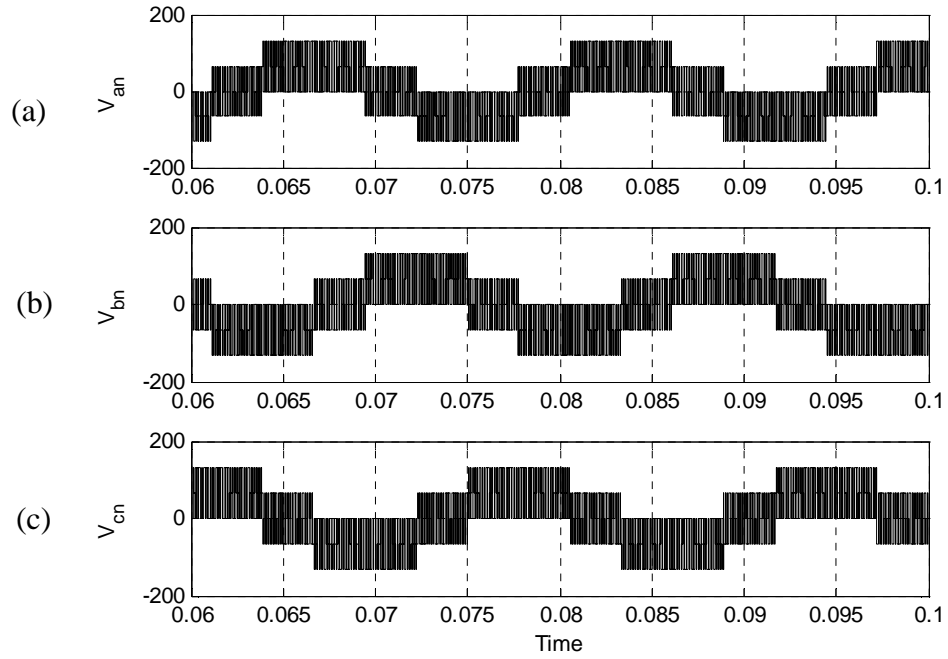
Figure 3.4: Three-phase output voltages (a) phase 'a' voltage, (b) phase 'b' voltage, (c)

phase 'c' voltage

41
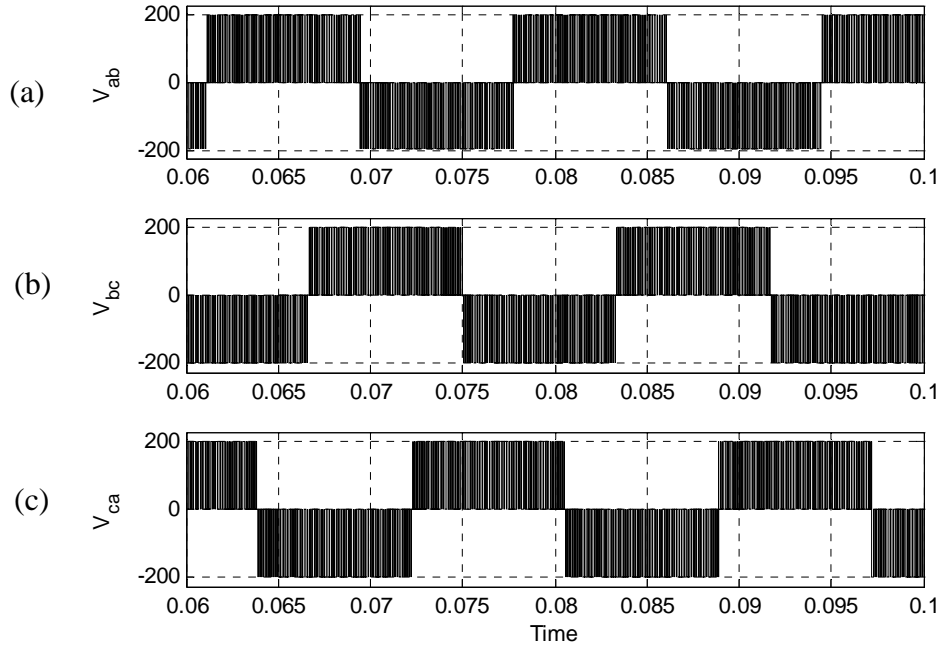
Figure 3.5: Output line voltages (a) Line 'a'-'b', (b) Line 'b'-'c', (c) Line 'c'-'a'
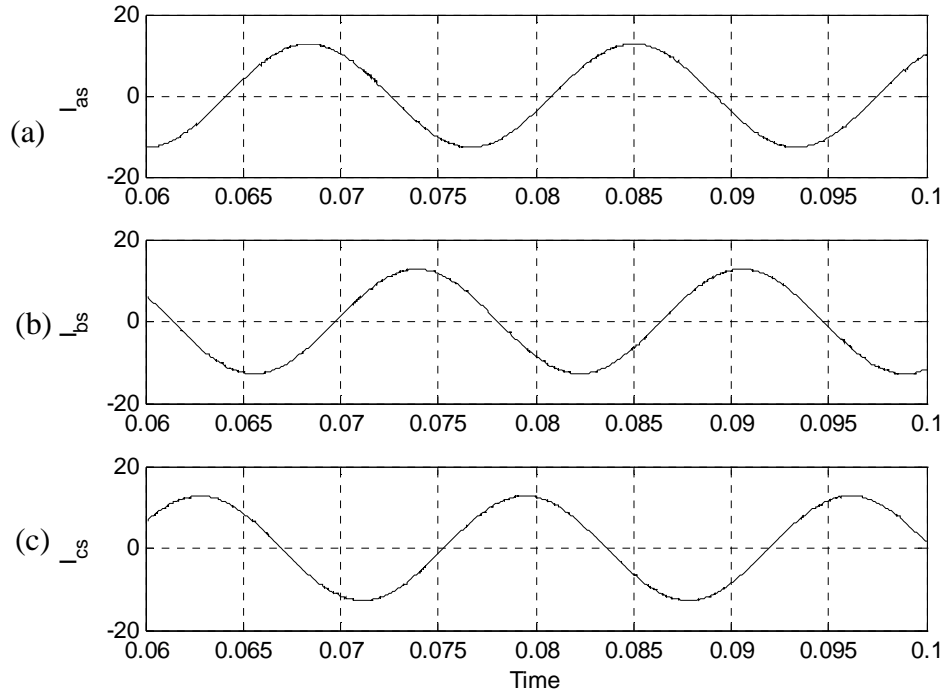
Figure 3.6: Three-phase output currents (a) phase 'a' current, (b) phase 'b' current (c)

phase 'c' current

3.1.2 Space Vector PWM

The maximum fundamental voltage which can be achieved is only 78.5% of $\dfrac{V_d}{2}$ and the output voltage is linear to the reference voltage only until this point. There are six switching devices in the conventional three-phase voltage source inverter. There are eight possible switching combinations. At any instant of time, the inverter would be operating in any one of the eight operating modes. A desired sequence of operating in the eight modes will result in the desired reference voltage as well as minimize the switching loss. Kirchoff's Voltage Law (KVL) and Kirchoff's Current Law (KCL) are kept in mind when the possible eight modes are represented. It is shown in Table 3.2.

Table 3.2: Possible eight switching modes

MODE	S_{ap}	S_{bp}	S_{cp}	S_{an}	S_{bn}	S_{cn}	SWITCHES TURNED ON
NULL, U_0	0	0	0	1	1	1	$S_{an}\, S_{bn}\, S_{cn}$
ACTIVE, U_5	0	0	1	1	1	0	$S_{an}\, S_{bn}\, S_{cp}$
ACTIVE, U_3	0	1	0	1	0	1	$S_{an}\, S_{bp}\, S_{cn}$
ACTIVE, U_4	0	1	1	1	0	0	$S_{an}\, S_{bp}\, S_{cp}$
ACTIVE, U_1	1	0	0	0	1	1	$S_{ap}\, S_{bn}\, S_{cn}$
ACTIVE, U_6	1	0	1	0	1	0	$S_{ap}\, S_{bn}\, S_{cp}$
ACTIVE, U_2	1	1	0	0	0	1	$S_{ap}\, S_{bp}\, S_{cn}$

NULL, U_7	1	1	1	0	0	0	S_{ap} S_{bp} S_{cp}

The neutral voltage V_{no} is obtained from (3.3) as they are summed and the neutral voltage is eliminated from it. Under balanced load conditions, the neutral voltage is obtained as

$$V_{no} = \frac{V_d}{3}\left(S_{ap} + S_{bp} + S_{cp}\right) - \frac{V_d}{2} \qquad (3.9)$$

Hence the phase voltages can be obtained as

$$V_{an} = \frac{V_d}{3}\left(2S_{ap} - S_{bp} - S_{cp}\right)$$

$$V_{bn} = \frac{V_d}{3}\left(-S_{ap} + 2S_{bp} - S_{cp}\right) \qquad (3.10)$$

$$V_{cn} = \frac{V_d}{3}\left(-S_{ap} - S_{bp} + 2S_{cp}\right)$$

These phase voltages can be represented in the q-d reference frame. The transformation between the abc reference frame to the q-d reference frame and the q-d reference frame to the abc stationary reference frame is shown in Figure 3.7. Here 'f' represents the quantity in reference frame which is transformed. It can be current, voltage, flux density and so on. The transformation matrix and the inverse transformation matrix is as shown in (3.11).
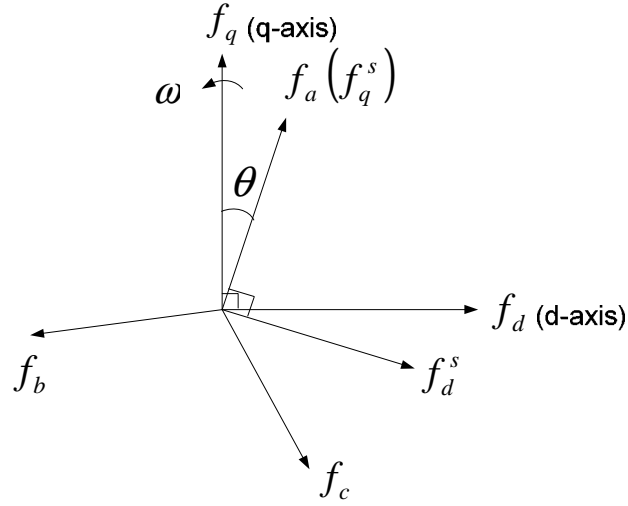
Figure 3.7: Transformation between reference frames

$$
\begin{bmatrix} f_q \\ f_d \\ f_o \end{bmatrix} = T(\theta) \begin{bmatrix} f_a \\ f_b \\ f_c \end{bmatrix}
$$

$$
\begin{bmatrix} f_a \\ f_b \\ f_c \end{bmatrix} = T^{-1}(\theta) \begin{bmatrix} f_q \\ f_d \\ f_o \end{bmatrix}
\tag{3.11}
$$

where $T(\theta) = \dfrac{2}{3} \begin{bmatrix} \cos\theta & \cos\left(\theta - \dfrac{2\pi}{3}\right) & \cos\left(\theta + \dfrac{2\pi}{3}\right) \\ \sin\theta & \sin\left(\theta - \dfrac{2\pi}{3}\right) & \sin\left(\theta + \dfrac{2\pi}{3}\right) \\ \dfrac{1}{2} & \dfrac{1}{2} & \dfrac{1}{2} \end{bmatrix}$

$$
T^{-1}(\theta) = \begin{bmatrix} \cos\theta & \sin\theta & 1 \\ \cos\left(\theta - \dfrac{2\pi}{3}\right) & \sin\left(\theta - \dfrac{2\pi}{3}\right) & 1 \\ \cos\left(\theta + \dfrac{2\pi}{3}\right) & \sin\left(\theta + \dfrac{2\pi}{3}\right) & 1 \end{bmatrix}
$$

θ is the angle between the reference frames

The general transformation for any given three-phase voltage set in the stationary reference frame is given in (3.9).

$$V_{qs}^* = \frac{2}{3}\left(V_{an} - \frac{1}{2}V_{bn} - \frac{1}{2}V_{cn}\right)$$

$$V_{ds}^* = \frac{2}{3}\left(-\frac{\sqrt{3}}{2}V_{bn} - \frac{\sqrt{3}}{2}V_{cn}\right) \tag{3.9}$$

$$V_{os}^* = \frac{2}{3}\left(\frac{1}{2}V_{an} + \frac{1}{2}V_{bn} + \frac{1}{2}V_{cn}\right)$$

The q-d voltages are calculated using (3.8) to get (3.10), (3.11), and (3.12)

$$V_{qp} = V_{an}$$

$$= \frac{V_d}{3}\left(2S_{ap} - S_{bp} - S_{cp}\right) \tag{3.10}$$

$$V_{dp} = \frac{1}{\sqrt{3}}\left(-V_{bn} + V_{cn}\right)$$

$$= \frac{1}{\sqrt{3}}\left(-S_{bp} + S_{cp}\right) \tag{3.11}$$

$$V_{op} = \frac{V_d}{3}\left(S_{ap} + S_{bp} + S_{cp} - \frac{3}{2}\right) \tag{3.12}$$

The q-d voltages can be calculated for the eight operating modes assuming balanced load conditions. Table 3.3 illustrates the switching modes of the conventional VSI and the corresponding stationary reference frame q-d-o voltages.

Table 3.3: Switching modes of the conventional VSI and the corresponding stationary

reference frame q-d-o voltages

MODE	S_{ap}	S_{bp}	S_{cp}	V_{qp}	V_{dp}	V_{op}
NULL, U_0	0	0	0	0	0	$-\dfrac{V_d}{2}$
ACTIVE, U_5	0	0	1	$-\dfrac{V_d}{3}$	$\dfrac{V_d}{\sqrt{3}}$	$-\dfrac{V_d}{6}$
ACTIVE, U_3	0	1	0	$-\dfrac{V_d}{3}$	$-\dfrac{V_d}{\sqrt{3}}$	$-\dfrac{V_d}{6}$
ACTIVE, U_4	0	1	1	$-\dfrac{2V_d}{3}$	0	$\dfrac{V_d}{6}$
ACTIVE, U_1	1	0	0	$\dfrac{2V_d}{3}$	0	$-\dfrac{V_d}{6}$
ACTIVE, U_6	1	0	1	$\dfrac{V_d}{3}$	$\dfrac{V_d}{\sqrt{3}}$	$\dfrac{V_d}{6}$
ACTIVE, U_2	1	1	0	$\dfrac{V_d}{3}$	$-\dfrac{V_d}{\sqrt{3}}$	$\dfrac{V_d}{6}$
NULL, U_7	1	1	1	0	0	$\dfrac{V_d}{2}$

Table 3.3 can be represented in the form of a Space Vector Diagram as shown in
Figure 3.8. A regular hexagon is divided into six equal sectors.
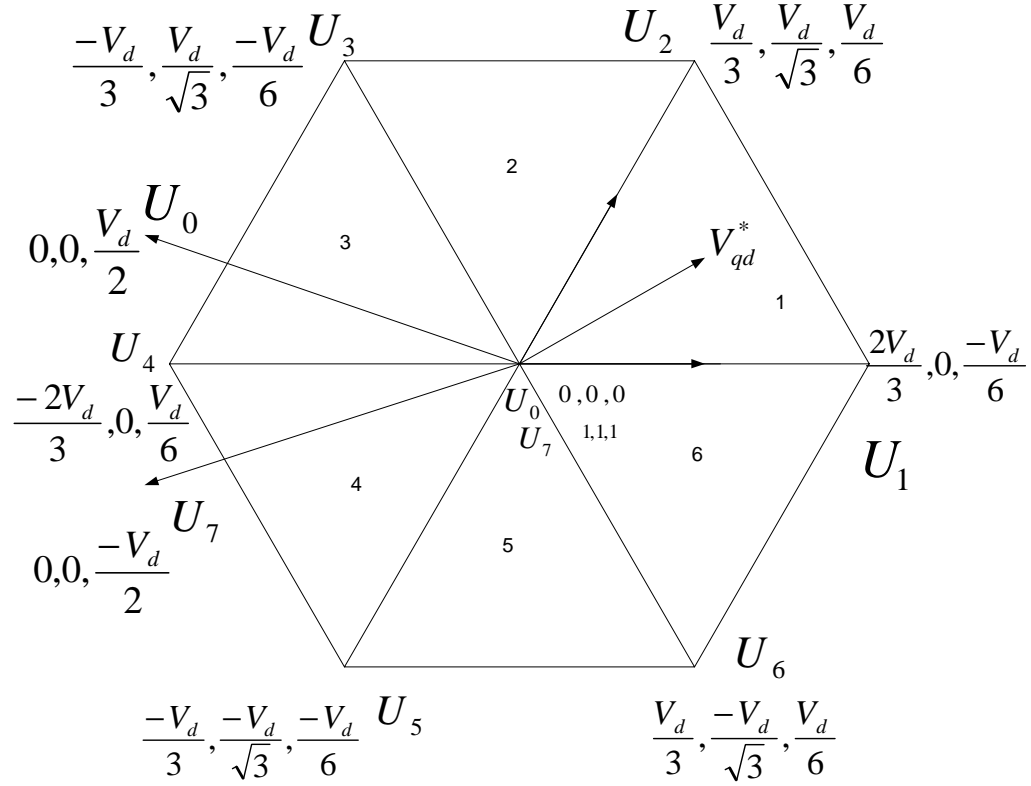
Figure 3.8: Space Vector diagram for the conventional VSI

The q-d reference voltage, V_{qd}^* is calculated in each of the eight sectors to synthesize a reference phase voltage, In general, the three-phase voltages expressed in the stationary reference frame, $V_{qd}^* \Rightarrow V_{qn}^*, V_{dn}^*$, situated in the appropriate sector, are approximated by the time-average over a sampling period (converter switching period T_s) of the two adjacent active voltage inverter vectors and the two zero states U_0 and U_7. The switching turn-on times of the two active and two null states are utilized to determine the duty cycle information to program the active switch gate signals [C.1]. When the inverter is operating in the linear modulation region, the sum of the times the two active switching modes are utilized is less than the switching period, in which case

the remaining time is occupied by using the two null vectors U_0 and U_7. If the four voltage vectors V_{qdpa}, V_{qdpb}, ,V_{qdp0} and V_{qdp7} are called into play for times t_a, t_b, t_0, t_7 (normalized with respect to modulator sampling time or converter switching period T_s), respectively, then the qp and dp components of the reference voltage V_{qd}^* are approximated as

$$V_{qd}^* = V_{qp*} + jV_{dp}^*$$

$$= V_{qdpa}t_a + V_{qdpb}t_b + V_{qdp0}t_0 + V_{qdp7}t_7 \tag{3.12}$$

$$t_c = t_0 + t_7 = 1 - t_a - t_b \tag{3.13}$$

where

$$t_0 = \alpha t_c$$

$$t_7 = (1 - \alpha)t_c$$

t_c is the null state time. t_c constitutes of t_0 and t_7 where they are divided with a ratio of α.

Equation (3.12) is separated into its real and imaginary parts and the zero sequence voltage is approximated as

$$V_{qs}^* = V_{qpa}t_a + V_{qpb}t_b + V_{qp0}t_0 + V_{qp7}t_7 \tag{3.14}$$

$$V_{ds}^* = V_{dpa}t_a + V_{dpb}t_b + V_{dp0}t_0 + V_{dp7}t_7 \tag{3.15}$$

In general the zero sequence voltage,

$$V_{op} = V_{os}^* + V_{no} \tag{3.16}$$

$$\langle V_{os}^* + V_{no} \rangle = V_{opa}t_a + V_{opb}t_b + V_{op0}t_0 + V_{op7}t_7 \tag{3.17}$$

However, it is noticed that V_{qd0} and V_{qd7} do not play a role in obtaining the times, t_a and t_b. Equations (3.14) and (3.15) can be represented in matrix form as

$$\begin{bmatrix} V_{qs}^* \\ V_{ds}^* \end{bmatrix} = \begin{bmatrix} V_{qpa} & V_{qpb} \\ V_{dpa} & V_{dpb} \end{bmatrix} \begin{bmatrix} t_a \\ t_b \end{bmatrix} \tag{3.18}$$

Hence the times, t_a and t_b can be calculated from (3.18) as

$$\begin{bmatrix} t_a \\ t_b \end{bmatrix} = \begin{bmatrix} V_{qpa} & V_{qpb} \\ V_{dpa} & V_{dpb} \end{bmatrix}^{-1} \begin{bmatrix} V_{qs}^* \\ V_{ds}^* \end{bmatrix} \tag{3.19}$$

$$t_a = \frac{V_{dpb}V_{qs}^* - V_{qpb}V_{ds}^*}{V_{qpa}V_{dpb} - V_{qpb}V_{dpa}} \tag{3.20}$$

$$t_b = \frac{-V_{dpa}V_{qs}^* + V_{qpa}V_{ds}^*}{V_{qpa}V_{dpb} - V_{qpb}V_{dpa}} \tag{3.21}$$

The sum of the normalized times t_a, t_b, t_c are equal to 1.

Hence the expression for the normalized time t_c is given in (3.13). In the linear modulation region, the sum of the times, t_a and t_b is less than 1. The remaining time is utilized by the two null states. Here, α which varies between 0 and 1 determines the ratio at which the two null state times are divided. The normalized times are calculated, and the switching pattern in order to have switching loss is brought about. It is noted that a clean voltage synthesis is achieved when the converter is operating in the linear modulation region when $\alpha = 0.5$ [T.7]. The results shown below have been performed for $\alpha = 0.5$. The device switching times in each sector can be represented in terms of the line voltages as shown in Table 3.3.

50

Table 3.4: Switching times of the devices expressed in terms of the reference line

voltages

Sector	t_a	t_b
1	$\dfrac{V_{ab}}{V_d}$	$\dfrac{V_{bc}}{V_d}$
2	$\dfrac{V_{ac}}{V_d}$	$\dfrac{V_{ba}}{V_d}$
3	$\dfrac{V_{bc}}{V_d}$	$\dfrac{V_{ca}}{V_d}$
4	$\dfrac{V_{ba}}{V_d}$	$\dfrac{V_{cb}}{V_d}$
5	$\dfrac{V_{ca}}{V_d}$	$\dfrac{V_{ab}}{V_d}$
6	$\dfrac{V_{cb}}{V_d}$	$\dfrac{V_{ac}}{V_d}$

The sequence used to synthesis the reference voltage vector is by rotating it counter-clockwise for all the six sectors. In each sector, the starting and ending conditions for all upper switching devices are state mode 0 while the state mode 7 happens in the middle of the period. A minimum switching is obtained using this arrangement in order to reduce the switching losses. Figures (3.9), (3.10), (3.11), (3.12), (3.13), and (3.14) show the arrangement of the existence functions of the top devices in each of the sectors respectively.
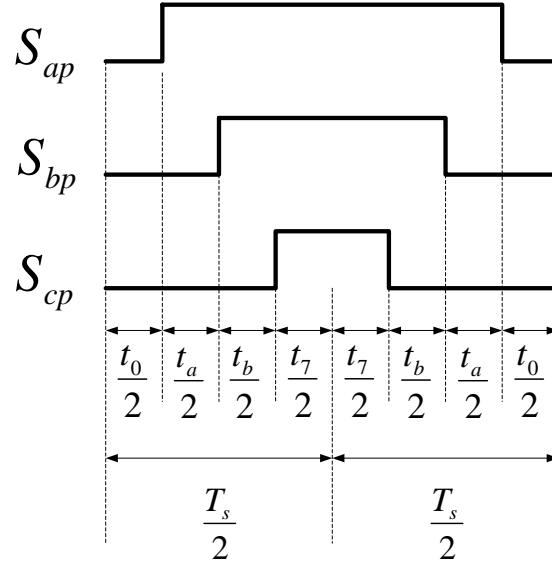
Figure 3.9: Existence function of the top devices in Sector 1
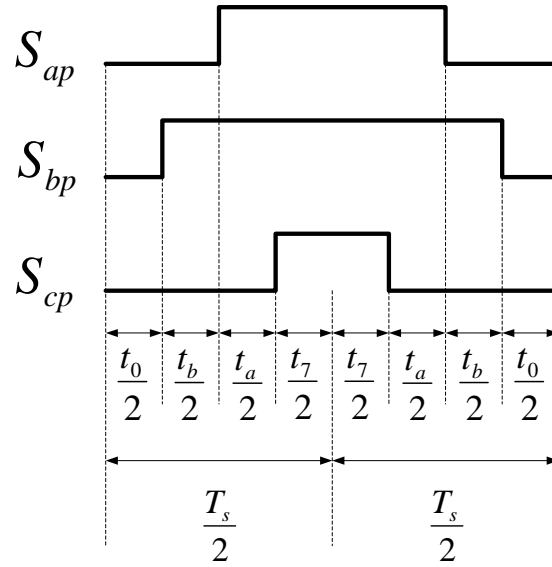
Figure 3.10: Existence function of the top devices in Sector 2
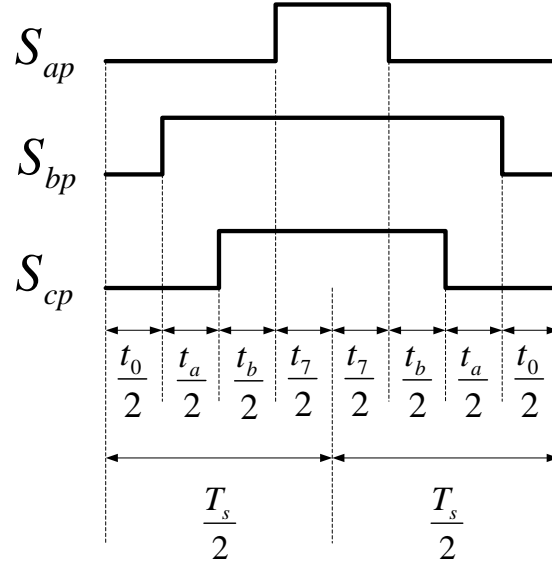
Figure 3.11: Existence function of the top devices in Sector 3
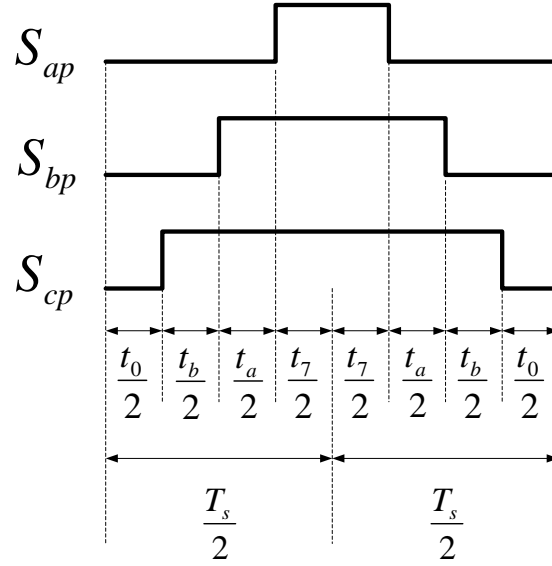
Figure 3.12: Existence function of the top devices in Sector 4
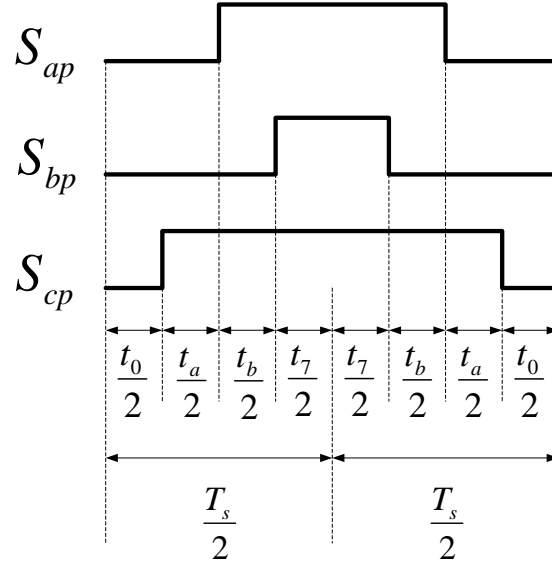
Figure 3.13: Existence function of the top devices in Sector 5
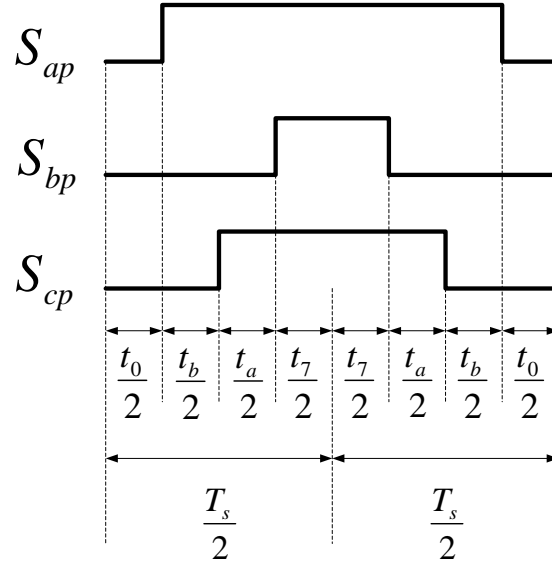
Figure 3.14: Existence function of the top devices in Sector 6

The simulation results of the conventional voltage source inverter are as shown in Figures (3.15), (3.16), (3.17), and (3.18).
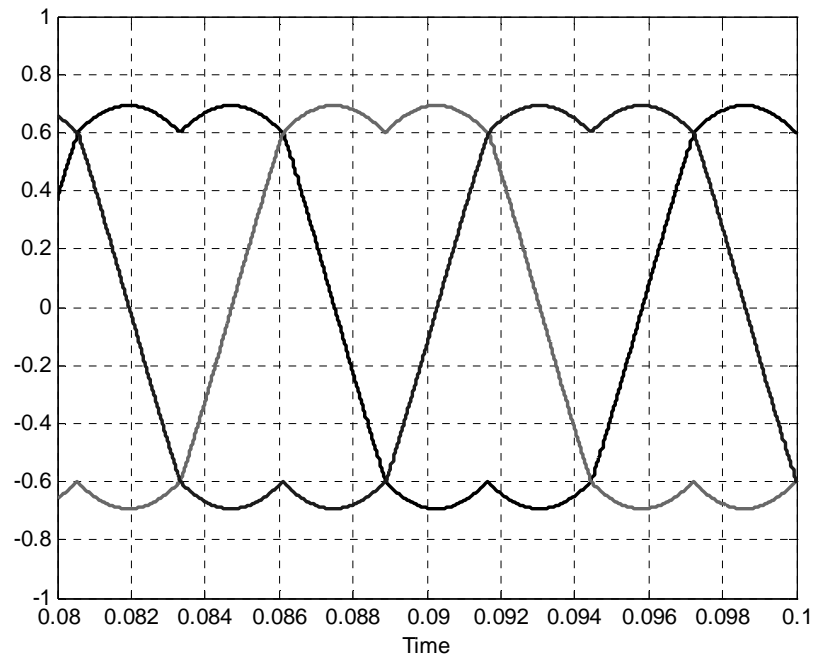
Figure 3.15: Three-Phase modulation signal when $\alpha = 0.5$
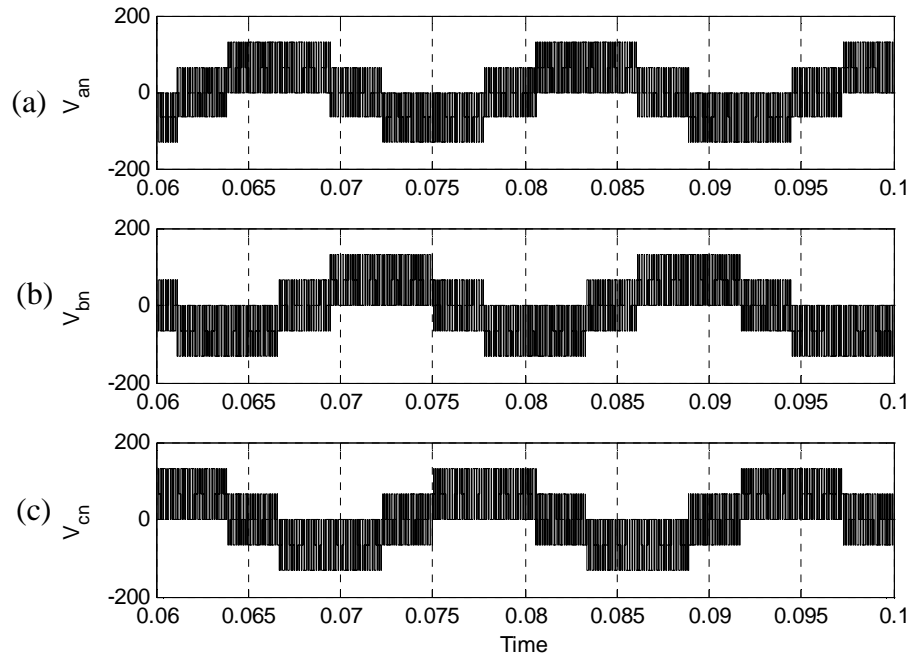
Figure 3.16: Three-phase output voltages when $\alpha = 0.5$ (a) phase 'a' voltage, (b) phase

'b' voltage, (c) phase 'c' voltage

55
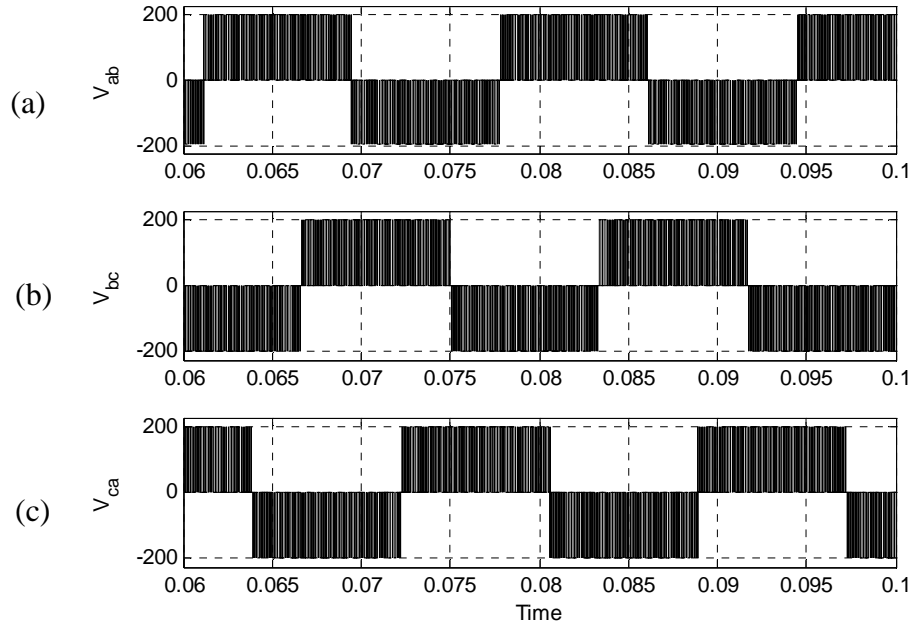
Figure 3.17: Output line voltages when $\alpha = 0.5$ (a) Line 'a'-'b', (b) Line 'b'-'c', (c) Line

'c'-'a'
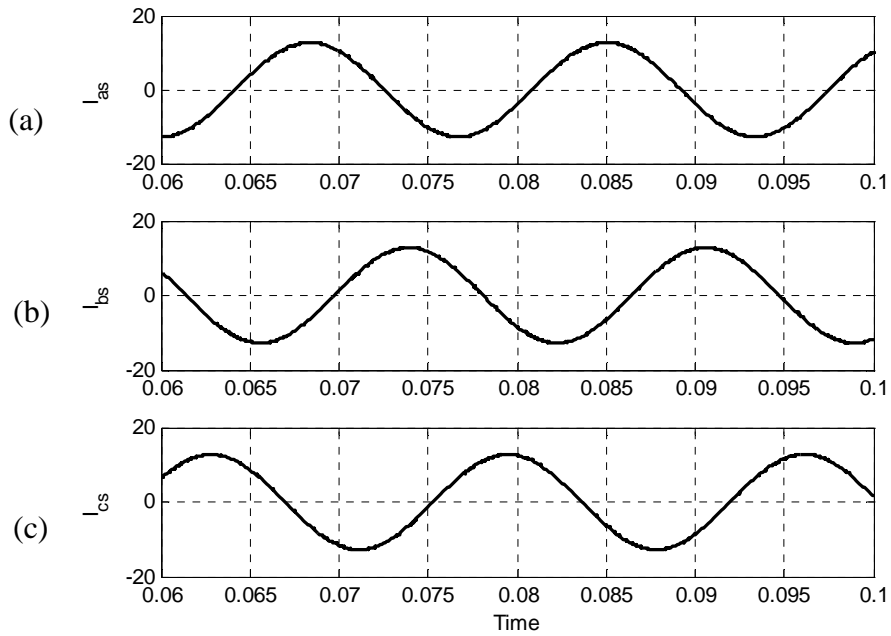
Figure 3.18: Three-phase output currents when $\alpha = 0.5$ (a) phase 'a' current, (b) phase

'b' current (c) phase 'c' current

56

3.2 Boost Rectifier

A conventional boost rectifier feeding a resistive load is as shown in Figure 3.19. It consists of a three-phase voltage supplying to the converter consisting of six switching devices which feeds a resistive load. It differs from the three-phase bridge rectifier by utilizing the switching devices instead of the diodes. A three-phase bridge rectifier has six diodes instead of the switching devices.

The PWM boost rectifier has been increasingly employed in recent years owing to its advanced features including sinusoidal input current at unity power factor and high quality dc output voltage with a filter capacitor of small size [C.2]. The application areas of the boost rectifier are varied and exhaustive because of the boosting of the output voltage as well as the efficient utilization of power in the rectification process.

The three-phase boost rectifier's six switches are switched using the sinusoidal pulse width modulation technique. In general, the operation of a converter can be explained in terms of the input quantities, output quantities and the pattern of the switching used to obtain the reference output. The input ac voltages are defined and the output dc voltage is dependant on the input voltage and the switching pattern of the rectifier. Kirchoff's Voltage Law (KVL) and Kirchoff's Current Law (KCL) is used as the basis of formulating the switching pattern of the switches. The switching pattern for any converter can be expressed as a function, which is a mathematical representation of the switching pattern which is known as the existence function [B.7].
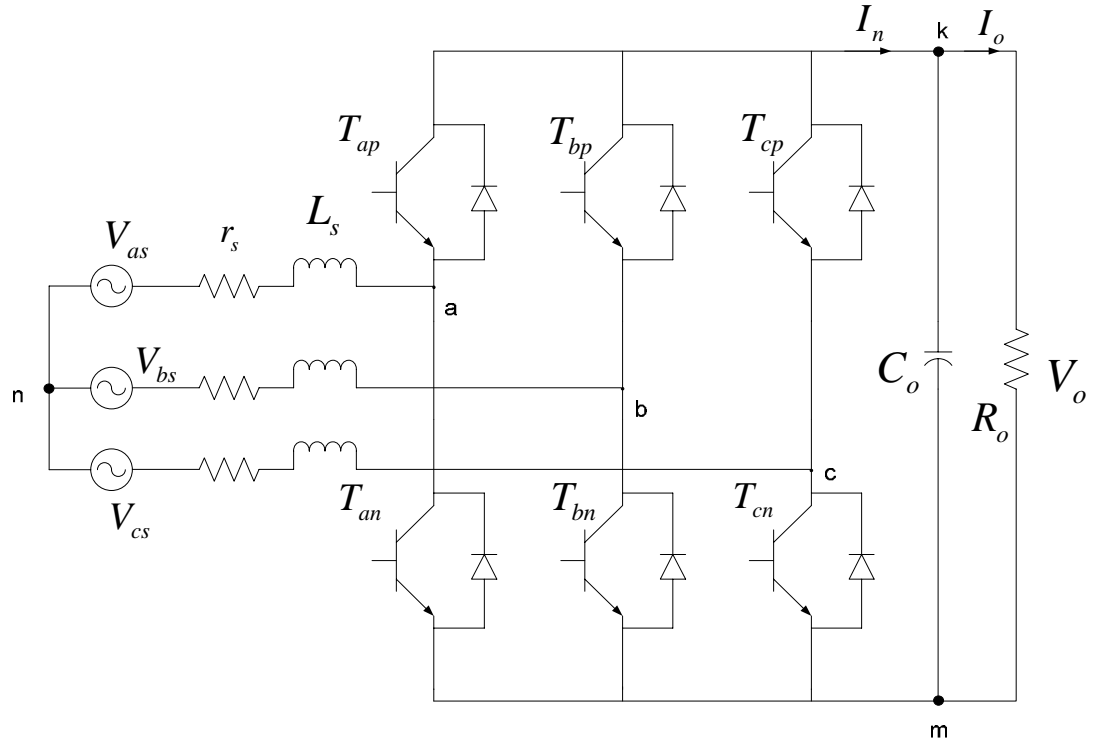
Figure 3.19: Three-phase boost rectifier

Table 3.5: Variables used for the Three-phase Boost Rectifier

V_{as} V_{bs} V_{cs}	THREE-PHASE INPUT VOLTAGES
I_{as} I_{bs} I_{cs}	THREE-PHASE INPUT CURRENTS
r_s	INPUT PER PHASE RESISTANCE
L_s	INPUT PER PHASE INDUCTANCE
C_o	OUTPUT FILTER CAPACITANCE
R_o	LOAD RESISTANCE
V_o	OUTPUT DC VOLTAGE
T_{ap} T_{bp} T_{cp}	TOP DEVICES

T_{an} T_{bn} T_{cn}	BOTTOM DEVICES

The boost rectifier follows the laws same as that of the classical three-phase voltage source inverter. The three-phase voltages supplied to the converter are given as

$$V_a = S_{ap}V_{kn} + S_{an}V_{mn} \tag{3.21}$$

$$V_b = S_{bp}V_{kn} + S_{bn}V_{mn} \tag{3.22}$$

$$V_c = S_{cp}V_{kn} + S_{cn}V_{mn} \tag{3.23}$$

The supply voltages are given as

$$V_{as} = r_s I_{as} + L_s p I_{as} + V_a \tag{3.24}$$

$$V_{bs} = r_s I_{bs} + L_s p I_{bs} + V_b \tag{3.25}$$

$$V_{cs} = r_s I_{cs} + L_s p I_{cs} + V_c \tag{3.26}$$

Now the switching functions of each phase/leg are complementary to each other.

$$\Rightarrow S_{ip} = 1 - S_{in} \tag{3.27}$$

where, $i = a, b, c$

By using (3.27) in (3.21)-(3.23) and substituting the result in (3.24)-(3.26), the following expressions for the voltages are obtained

$$V_{as} = r_s I_{as} + L_s p I_{as} + S_{ap}\left(V_{kn} - V_{mn}\right) + V_{mn} \tag{3.28}$$

$$V_{bs} = r_s I_{bs} + L_s p I_{bs} + S_{bp}\left(V_{kn} - V_{mn}\right) + V_{mn} \tag{3.29}$$

$$V_{cs} = r_s I_{cs} + L_s p I_{cs} + S_{cp}\left(V_{kn} - V_{mn}\right) + V_{mn} \tag{3.30}$$

Here, the voltage difference is given as

$$V_{kn} - V_{mn} = V_o$$

Hence, the voltage equations become

$$V_{as} = r_s I_{as} + L_s p I_{as} + S_{ap} V_o + V_{mn}$$ (3.31)

$$V_{bs} = r_s I_{bs} + L_s p I_{bs} + S_{bp} V_o + V_{mn}$$ (3.32)

$$V_{cs} = r_s I_{cs} + L_s p I_{cs} + S_{cp} V_o + V_{mn}$$ (3.33)

The neutral voltage V_{mn} is eliminated by adding (3.31)-(3.33). In a case where the source is balanced,

$$V_{mn} = -\frac{V_o}{3}\left(S_{ap} + S_{bp} + S_{cp}\right)$$ (3.34)

By substituting (3.34) in (3.31)-(3.33), the voltage equations given in (3.35)-(3.37) are obtained.

$$V_{as} = r_s I_{as} + L_s p I_{as} + \frac{V_o}{3}\left(2S_{ap} - S_{bp} - S_{cp}\right)$$ (3.35)

$$V_{bs} = r_s I_{bs} + L_s p I_{bs} + \frac{V_o}{3}\left(-S_{ap} + 2S_{bp} - S_{cp}\right)$$ (3.36)

$$V_{cs} = r_s I_{cs} + L_s p I_{cs} + \frac{V_o}{3}\left(-S_{ap} - S_{bp} + 2S_{cp}\right)$$ (3.37)

The current exiting the rectifier is given as

$$I_n = S_{ap} I_{as} + S_{bp} I_{bs} + S_{cp} I_{cs}$$

Hence the current through the capacitor is given in (3.38) when the load is a resistive load.

$$C_o p V_o = \left(S_{ap} I_{as} + S_{bp} I_{bs} + S_{cp} I_{cs}\right) - \frac{V_o}{R_o}$$ (3.38)

The simulation results shown in Figures 3.20, 3.21, 3.22, and 3.23 have been performed using Sinusoidal Pulse Width Modulation using a resistive load of 50 Ω and an input ac voltage of 220 V while the modulation index used is m = 0.8.
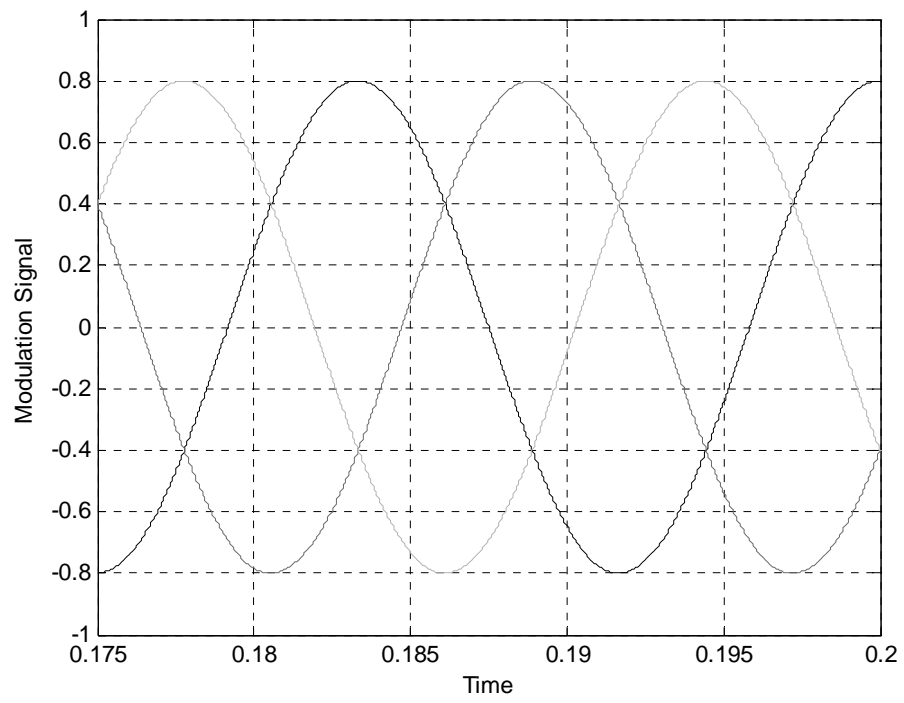
Figure 3.20: Three-phase modulation signal
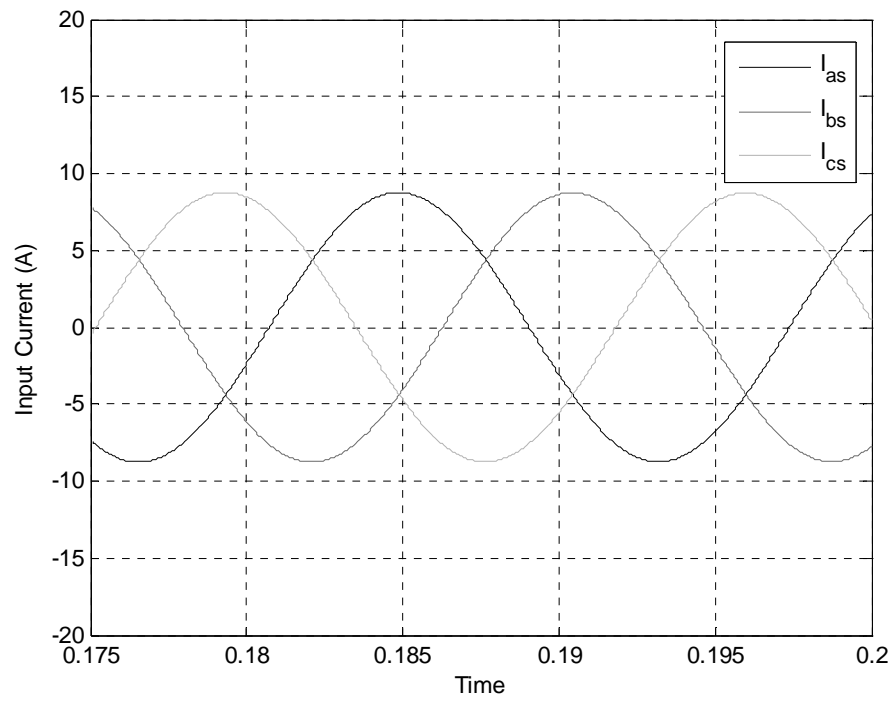
Figure 3.21: Three-phase input current

62
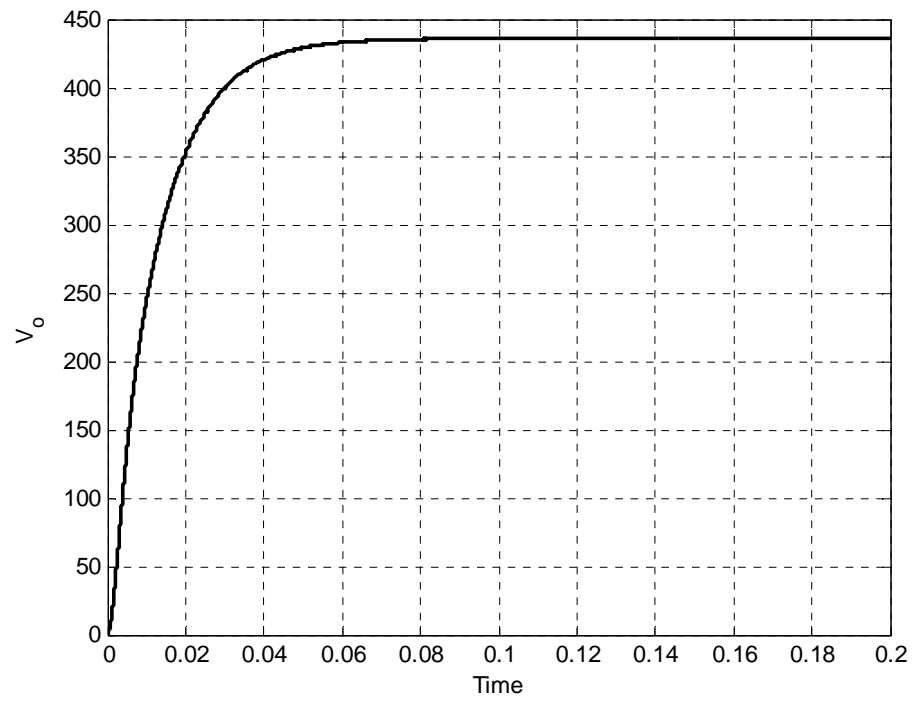
Figure 3.22: Output Load Voltage
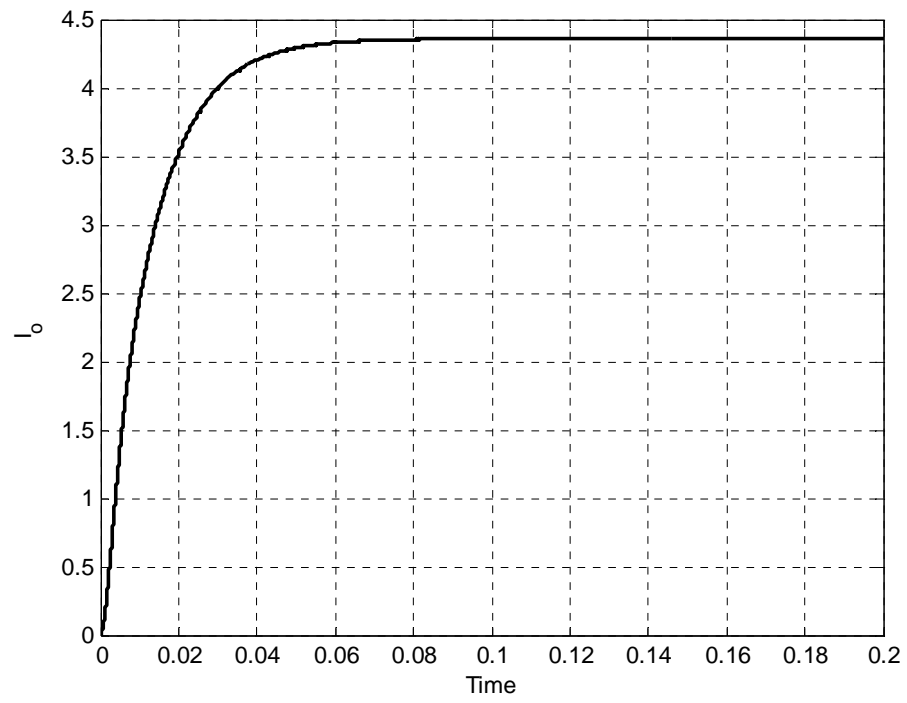
Figure 3.23: DC Load current

63

3.3 Conclusion

In conclusion, this chapter verified the topologies of the conventional voltage source inverter as well as the conventional boost AC-DC rectifier. It can be seen from the simulation results performed in MATLAB/SIMULINK that in the conventional voltage source inverter, the output voltage is always bucked in all operating conditions. As the name suggests, the boost rectifier always boosts the output voltage. In order to achieve the complementary results using the same converter, an additional AC-AC converter or a DC-DC converter is required, respectively. This may increase the component count and make it bulk and expensive. In order to avoid this disadvantage, the study of the Z-source converter is performed in this thesis.

CHAPTER 4

PULSE WIDTH MODULATION (PWM) SCHEME FOR

THE Z-SOURCE CONVERTER

4.1 Introduction

Large inverters operating at ten to hundreds of megawatts in the medium voltage range (2-13 kV) have traditionally been the domains of gate turn off (GTO) thyristors. Semiconductor switch ratings have limited the application of power converters rated in the tens to hundreds of megawatts. However, their switching speed is severely limited compared to the IGBT's so that the carrier frequency of a GTO inverter is generally only a few hundred hertz. High switching frequencies can be achieved by replacing each of the slower switches so that each individual IGBT shares the dc link voltage with others in the string during its off state. The devices are operated in saturation region of operation. This is because there exists higher losses in active region operation of these devices.

In the traditional converter, the two switches of the same phase leg cannot be turned ON at the same time because doing so would create a short circuit and damage the converter. The Z-source converter overcomes this problem by introducing an impedance circuit. In an inverter, the Z-source circuit connects the source and the converter circuit while in a rectifier, the Z-source connects the converter and the load. For applications

requiring both buck and boost power conversions, Z-source inverters have recently been proposed as a possible solution with many performance benefits [I.1]. The Z-source circuit uses split inductors, L_1 and L_2, and capacitors C_1 and C_2 connected in an X-shape. The inductors may also be coupled. This unique impedance network allows the Z-source converter to buck or boost its output voltage. In addition, the reliability of the inverter is greatly improved because the shoot through caused by electromagnetic interference (EMI) noise can no longer destroy the circuit [I.10]. An additional converter is not necessary to boost the output voltage. In turn, the impedance network elements (inductors and capacitors) are all that are utilized. Hence the switching components reduce tremendously which in turn reduces the switching losses as well as the volume of the entire system. Thus it provides a low-cost, reliable, and highly efficient single-stage structure for buck and boost power conversion.

4.2 Modulation Scheme

Pulse-width modulation (PWM) control for the Z-source inverter has to be modified to utilize the shoot-through states for the voltage boost. Figure 4.1 shows the conventional carrier-based PWM scheme of the VSI. There are eight possible states – six active states and 2 null states as explained earlier in Chapter 3. During the null state, either all the top devices are gated together or all the bottom devices are gated together. During the active state, a total of three switches are gated at the same time, that is, one device on each leg/phase is turned ON – either two top devices and one bottom device or

66
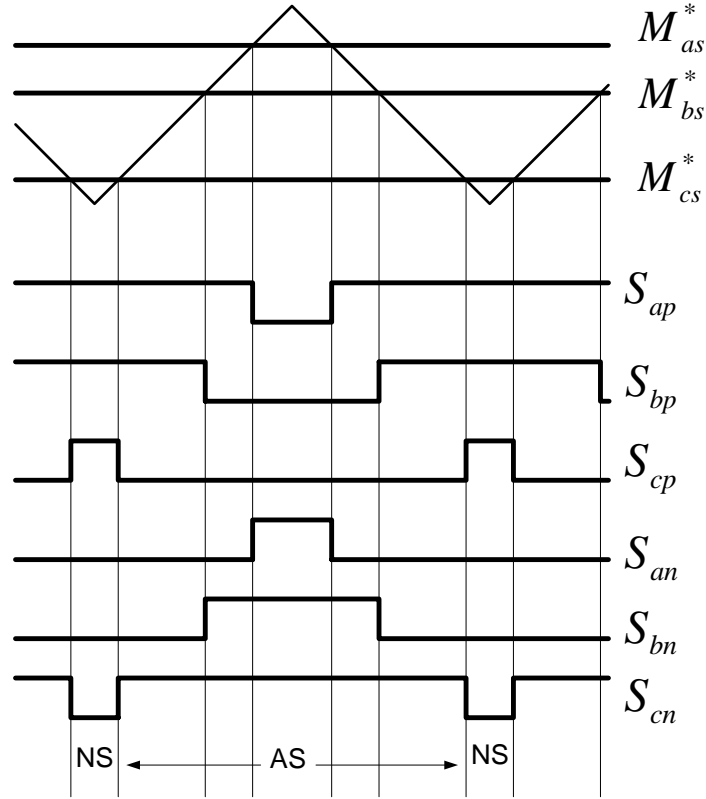
Figure 4.1: Carrier-based PWM for the conventional converter where NS – Null state and

AS – Active state.

one top device and two bottom devices. During the active state, the dc voltage is impressed across the load, positively or negatively [I.10].

In the Z-source converter, it has several shoot-through states, during which both the switches on one leg/phase can be gated together. Multiple legs' switches can also be turned ON together such that either the switches in two legs/phases are turned ON at once or even all the three legs' switches are turned ON together. In the case of realization of this thesis, shorting all the three legs/phases at once is utilized. This implies that all the six switches are gated together in order to realize the shoot-through state. The simulated results of shorting one leg and three legs showed similar results. While implementing the

three legs-short model, lesser components were required. Moreover, the required maximum current carrying capability for the devices in the three phase bridge is lower because the capacitor discharge current is distributed into the three phase legs.

As the name suggests, during the shoot-through state, the output terminals of the inverter are shorted and it does not contribute to the output voltage. They have the same effect of that of the null state of the traditional converter. The difference in this case is that the dc voltage is boosted considerably. The active states are unaltered to maintain the output voltage value. Essentially, a part of the null state or the entire null state is used for shoot-through depending on the desired output voltage. The Z-Source Inverter's schematics feeding an RL load are as shown in Figure 4.2.
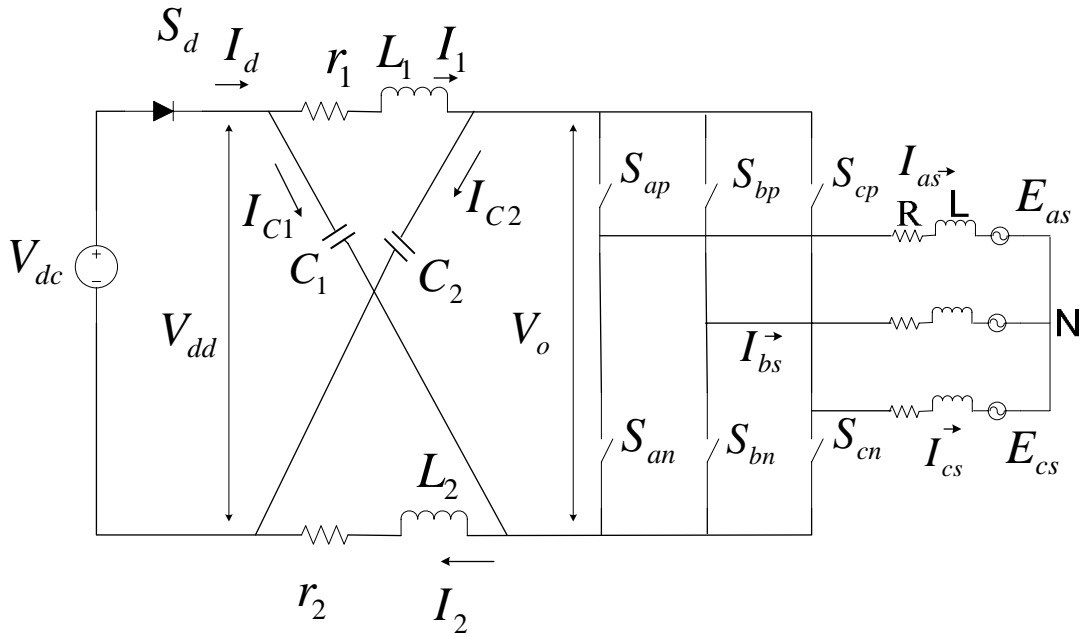
Figure 4.2: Model of a Z-Source Inverter

The possible switching modes for the Z-source converter are shown in Table 4.1. It is obvious from the table that either one leg/phase can be shorted or two legs can be turned ON together or even all the six devices can be turned ON together. There are some advantages and disadvantages of the shoot-through state. The main advantage in this case is that it boosts the dc voltage to a considerable extend. The introduction of the shoot-through state brings about more switching losses. The conventional null state is shared between the Z-source null state and the shoot-through state. In this case, two other reference waveforms, M_{TP} and M_{TN} are introduced to determine the shoot-through duty ratio.

Table 4.1: Possible switching modes of the Z-source converter

	STATE	S_{ap}	S_{bp}	S_{cp}	S_{an}	S_{bn}	S_{cn}
1	ST	0	0	1	0	0	1
2	ST	0	1	0	0	1	0
3	ST	1	0	0	1	0	0
4	ST	0	1	1	0	1	1
5	ST	1	0	1	1	0	1
6	ST	1	1	0	1	1	0
7	ST	1	1	1	1	1	1
U_0	Null	1	1	1	0	0	0
U_7	Null	0	0	0	1	1	1
U_1	Active	1	0	0	0	1	1
U_2	Active	1	0	1	0	1	0
U_3	Active	0	0	1	1	1	0
U_4	Active	0	1	1	1	0	0
U_5	Active	0	1	0	1	0	1
U_6	Active	1	1	0	0	0	1

4.3 Determination of Shoot-through Reference Waveforms

In the Z-Source converter, the shoot-through state is the one which makes it different from the conventional converter. The modulation scheme for the Z-source converter is shown in Figure 4.3.
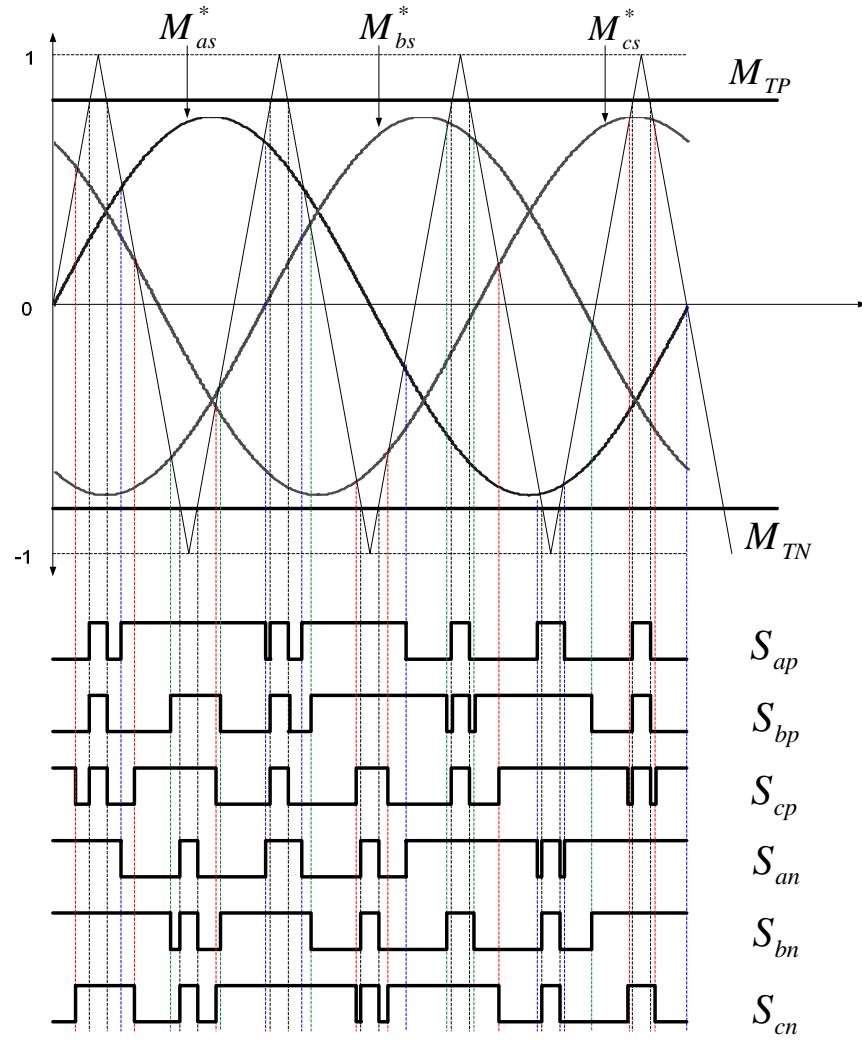
Figure 4.3: Modulation scheme of Z-converters and the switching functions of the individual devices

The volume and cost of the Z-source network has to be reduced. This can be achieved when the low frequency ripple is eliminated. Using a constant shoot through duty ratio simplifies the system as well as eliminates the low frequency current ripple That is, the modulation method reduces the ripple in the current.

In Figure 4.3, there are five modulation curves – three reference signals, M_{as}^*, M_{bs}^*, M_{cs}^* and two shoot-through envelope signals, M_{TP}, M_{TN}. The two shoot-through envelopes are considered as straight lines since a constant shoot-through duty ratio is required. The modulation scheme considered for the three phase reference signals is the conventional modulation scheme where the top device is gated when the reference signal is greater than the high frequency triangular wave and the corresponding bottom device is gated when the same signal is lesser than the high frequency triangular wave. When the carrier triangle wave is higher than the upper shoot-through envelope, M_{TP} and when the carrier triangle wave is lower than the lower shoot-through envelope, M_{TN}, a shoot-through signal is given to the system. That is, all the devices are turned ON to turn the converter to the shoot-through state.

The signals, M_{TP}, M_{TN} are determined as functions of the three-phase modulation reference signals. The shoot-through envelope M_{TP} is always greater than the maximum of the reference signals and the shoot-through envelope M_{TN} is always lesser than the minimum of the reference signals. The expressions can be expressed as

$$M_{TP} = M_{max} + (1 - M_{max})\sigma \tag{4.1}$$

$$M_{TN} = M_{min} + (-1 - M_{min})\sigma \tag{4.2}$$

σ is a ratio between 0 and 1. This determines the value of the shoot-through duty ratio used in the modulation scheme.

M_{max} and M_{min} can either be the instantaneous maximum and minimum of the modulation signals or they can be the absolute maximum and minimum of the modulation signals.

Figure 4.4 shows the waveforms of the ratio of the shoot-through envelope σ and the shoot-through envelopes when absolute maximum and minimum values are used. Figure 4.5 shows the waveforms of the ratio of the shoot-through envelope σ and the shoot-through envelopes when instantaneous maximum and minimum values are used. It can be seen that the ratio of the shoot-through envelope in this case varies with time. This is the only difference between using the absolute maximum and minimum and instantaneous maximum and minimum. The shoot-through envelope remains the same in both the cases. The envelope determines the shoot-through duty ratio. Hence either one of the two methods can be used to determine the shoot-through envelope. By using the absolute maximum and minimum, the realization of the model turns out to be easier than the other, hence the same is used in this case.
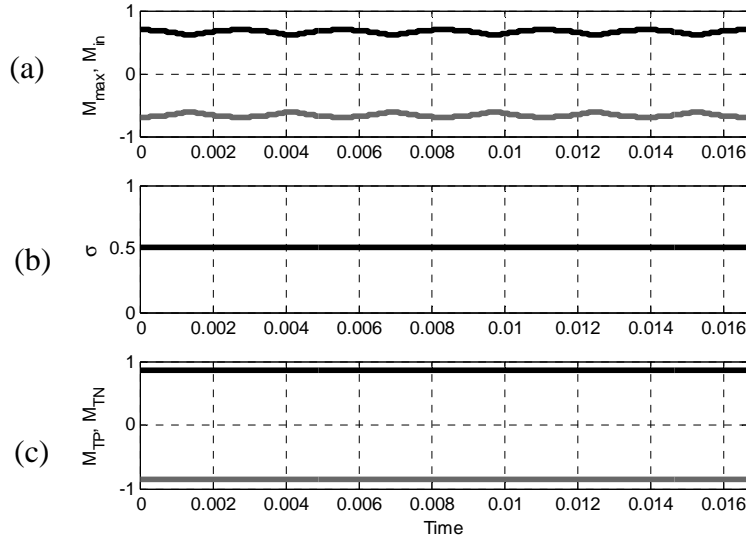
Figure 4.4: Shoot-through envelopes with absolute maximum and minimum of

modulation signals (a) M_{max} and M_{min} (b) Ratio of the shoot-through envelope σ (c)
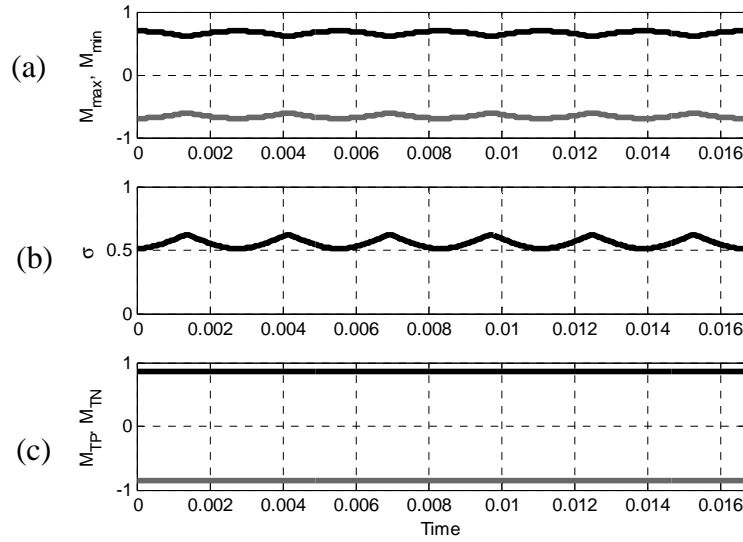
M_{TP} and M_{TN}

Figure 4.5: Shoot-through envelopes with instantaneous maximum and minimum value

of modulation signals (a) M_{max} and M_{min} (b) Ratio of the shoot-through envelope σ (c)

M_{TP} and M_{TN}

4.4 Determination of Shoot-Through Duty Ratio

The shoot-through duty ratio is determined using a simplified analysis. In a switching cycle T, T_o is the shoot-through time, T_1 is the active state time while T_2 is the null state time.

Hence the time period, $T = T_1 + T_2 + T_o$ (4.3)

In the case of Z-source converter analysis, the inductors and capacitors used in the Z-circuit are assumed to be balanced. That is, the two inductors are of same value L and the capacitors are of the same value, C. The Z-source network becomes symmetrical and hence it can be seen that

$$V_{c1} = V_{c2} = V_c \tag{4.4}$$

$$V_{L1} = V_{L2} = V_L \tag{4.5}$$

During the shoot-through state, in a switching cycle,

$$V_L = V_c \tag{4.6}$$

$$V_{dd} = 2V_c \tag{4.7}$$

$$V_o = 0 \tag{4.8}$$

During the non-shoot-through state, in a switching cycle,

$$V_L = V_{dc} - V_c \tag{4.9}$$

$$V_{dd} = V_o \tag{4.10}$$

$$V_o = V_c - V_L$$

$$= 2V_c - V_{dc} \tag{4.11}$$

In one switching cycle, the average voltage of each inductor should be zero. The dc link voltage across the inverter input terminals can hence be represented as

$$V_o = \frac{T_o 0 + (T_1 + T_2)(2V_c - V_{dc})}{T}$$

$$= \frac{(T_1 + T_2)(2V_c - V_{dc})}{T} \tag{4.12}$$

$$V_L = \frac{T_o V_c + (T_1 + T_2)(V_{dc} - V_c)}{T} = 0 \tag{4.13}$$

$$\frac{V_c}{V_{dc}} = \frac{T_1 + T_2}{T_1 + T_2 - T_o} \tag{4.14}$$

The active state is when there is a transfer of power from the source to the load. Hence the peak of the dc link voltage across the inverter bridge is given as

$$\hat{V}_o = 2V_c - V_{dc}$$

$$= \frac{T}{T_1 + T_2 - T_o} V_{dc}$$

$$= BV_{dc} \tag{4.15}$$

where

B is the Boost factor

$$B = \frac{T}{T_1 + T_2 - T_o}$$

$$= \frac{T}{T - 2T_o}$$

$$= \frac{1}{1 - 2\frac{T_o}{T}}$$

$$= \frac{1}{1 - 2D_o} \tag{4.16}$$

$$D_o = \frac{T_o}{T} \tag{4.17}$$

4.4.1 Graphical Illustration of Shoot-Through Duty Ratio

The representation of shoot-through envelopes and one period of the high frequency triangular signal is as shown in Figure 4.6. The individual shoot-through duty ratios for the top triangle peak and the bottom triangle peak are obtained using trigonometric identities. The top triangle peak is represented in Figure 4.7.
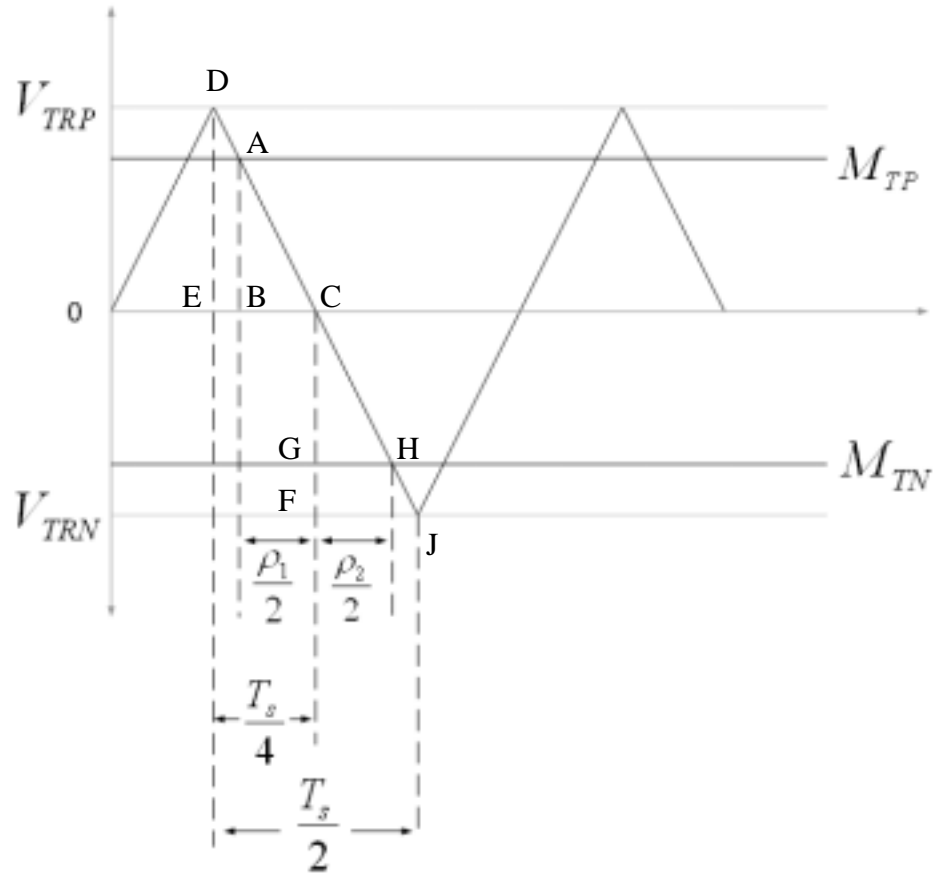
Figure 4.6: Unsymmetrical shoot-through envelopes

Figure 4.7: Method to determine the top shoot-through duty ratio with unsymmetrical

envelopes

From triangle ABC, $\tan \theta = \dfrac{M_{TP}}{\dfrac{\rho_1}{2}}$

$$\Rightarrow \rho_1 = \frac{2M_{TP}}{\tan \theta} \qquad (4.18)$$
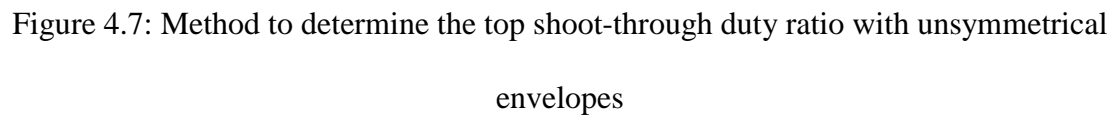
From triangle DEC, $\tan \theta = \dfrac{V_{TRP}}{\dfrac{T_s}{4}}$

$$\Rightarrow T_s = \frac{4V_{TRP}}{\tan \theta} \qquad (4.19)$$

When considering M_{TP} and using (4.18) (4.19), $D_{o1} = \dfrac{1}{2} - \dfrac{\rho_1}{T_s}$ $\qquad (4.20)$

$$= \frac{1}{2} - \frac{M_{TP}}{2V_{TRP}} \qquad (4.21)$$
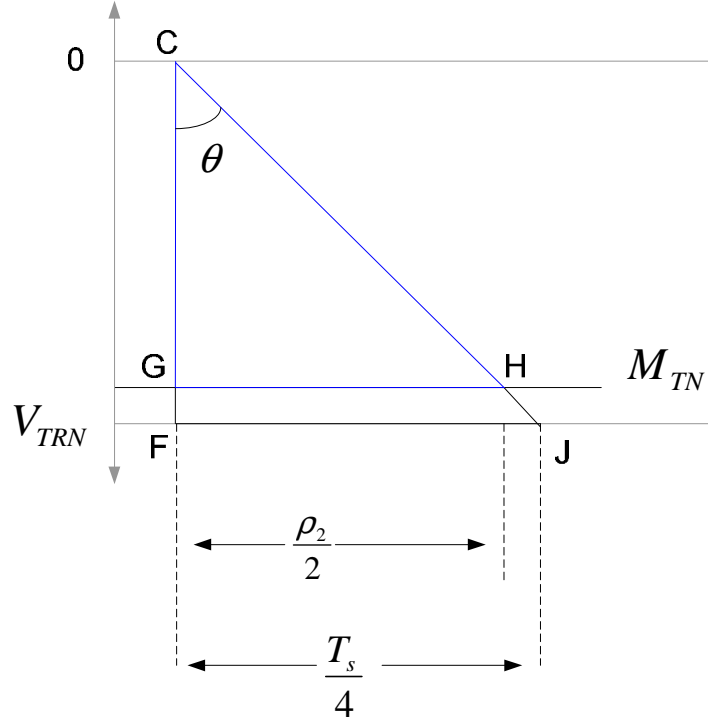
Figure 4.8: Method to determine the bottom shoot-through duty ratio with unsymmetrical

envelopes

$$\text{From triangle CGH, } \tan \theta = \frac{\dfrac{\rho_2}{2}}{M_{TN}}$$

$$\Rightarrow \rho_2 = 2M_{TP} \tan \theta \tag{4.22}$$

$$\text{From triangle CFJ, } \tan \theta = \frac{\dfrac{T_s}{4}}{V_{TRN}}$$

$$\Rightarrow T_s = 4V_{TRP} \tan \theta \tag{4.23}$$

When considering M_{TN} and using (4.22) and (4.23), $D_{o2} = \dfrac{1}{2} - \dfrac{\rho_2}{T_s}$ (4.24)

$$= \frac{1}{2} - \frac{M_{TN}}{2V_{TRN}} \tag{4.25}$$

Hence the shoot-through duty ratio is given as

$$D_o = D_{o1} + D_{o2}$$

$$= 1 - \frac{M_{TP}}{2V_{TRP}} - \frac{M_{TN}}{2V_{TRN}}$$

When the shoot-through envelopes are symmetrical about the x-axis, then Figure 4.9 illustrates the control method. Simple right angle triangles are formed from the structure and the duty ratio is easily determined from the simple control method shown in Figure 4.10.
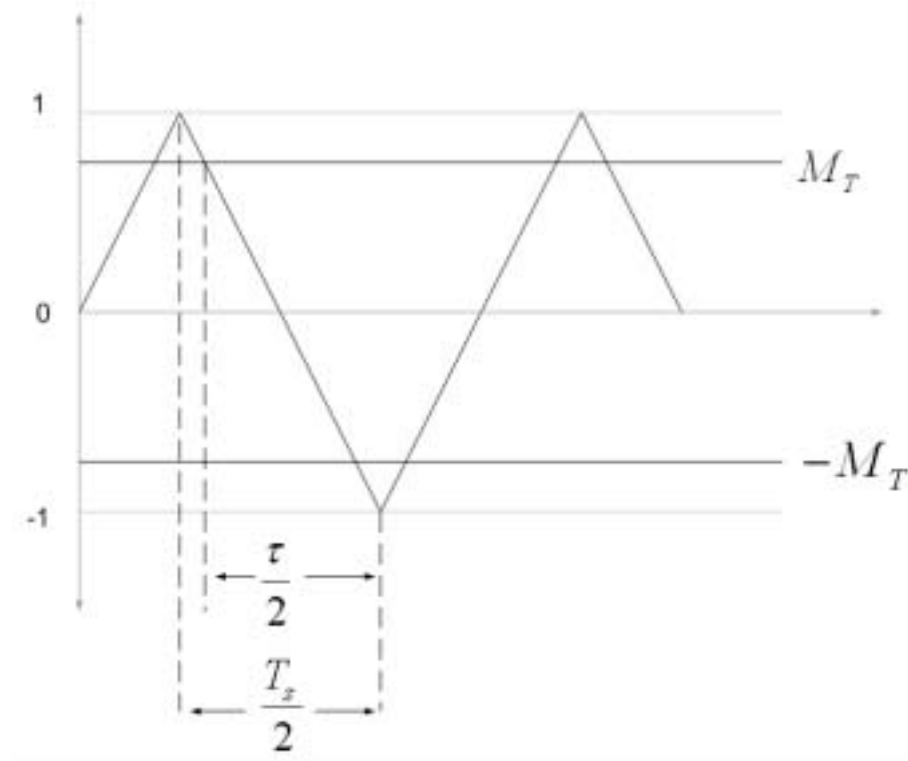
Figure 4.9: Symmetrical shoot-through envelopes
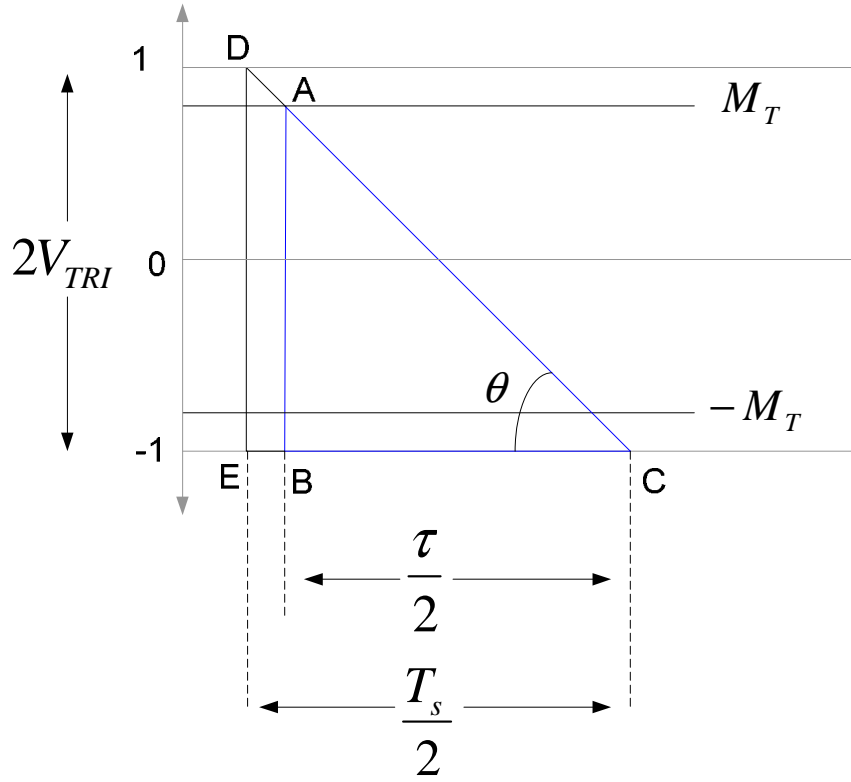
Figure 4.10: Method to determine the shoot-through duty ratio with symmetrical

envelopes

From triangle ABC, $\tan \theta = \dfrac{V_{TRI} + M_T}{\dfrac{\tau}{2}}$

$$\Rightarrow \tau = \frac{2(V_{TRI} + M_T)}{\tan \theta} \qquad (4.26)$$

From triangle DEC, $\tan \theta = \dfrac{2V_{TRI}}{\dfrac{T_s}{2}}$

$$\Rightarrow T_s = \frac{4V_{TRI}}{\tan \theta} \qquad (4.27)$$

The shoot through duty ratio is given as $D_o = 2\left(1 - \dfrac{\tau}{T_s}\right) \qquad (4.28)$

From (4.26) and (4.27) $\dfrac{\tau}{T_s} = \dfrac{V_{TRI} + M_T}{2V_{TRI}}$ (4.29)

$$\Rightarrow D_o = 2\left(1 - \dfrac{1}{2} - \dfrac{M_T}{2V_{TRI}}\right)$$

$$= 1 - \dfrac{M_T}{V_{TRI}}$$ (4.30)

In the earlier case, the shoot-through envelope being used was unsymmetrical about the X-axis. Now to prove the above concept of symmetry, M_{TP} and M_{TN} are considered of equal magnitude but of opposite signs in order to be symmetric.

Now if $M_{TP} = -M_{TN}$

$$V_{TRP} = -V_{TRN}$$

$$D_o = D_{o1} + D_{o2}$$

$$= 1 - \dfrac{M_{TP}}{V_{TRI}}$$ (4.31)

In this case, the reference signal is symmetric

$$M_{TP} = -M_{TN}$$

The reference signal, M_{TP} can be defined in terms of the instantaneous maximum or the absolute maximum of the three-phase modulation signal and a ratio, σ. The expression is as expressed in (4.32). The peak of the triangle is the absolute value of 1.

$$M_{TP} = M_{max} + (1 - M_{max})\sigma$$ (4.32)

$$V_{TRI} = 1$$ (4.33)

The above equations can be used to determine the shoot-through duty ratio, D_o which is used in the simulation.

$$D_o = 1 - M_{max} - (1 - M_{max})\sigma$$

$$= (1 - \sigma)(1 - M_{max}) \tag{4.44}$$

The Shoot-through duty ratio hence has a limit on its value for every modulation index. While using the space vector modulation, the peak of the modulation signal is determined to be $\frac{\sqrt{3}}{2}m$ while m being the modulation index. Hence the maximum limit of the shoot-through duty ratio can be determined by (4.45) and it is observed that it is a linear curve from Figure 4.11 As the modulation index increases, $D_{o\,max}$ decreases linearly.

$$0 \leq D_{o\,max} \leq 1 - \frac{\sqrt{3}}{2}m \tag{4.45}$$
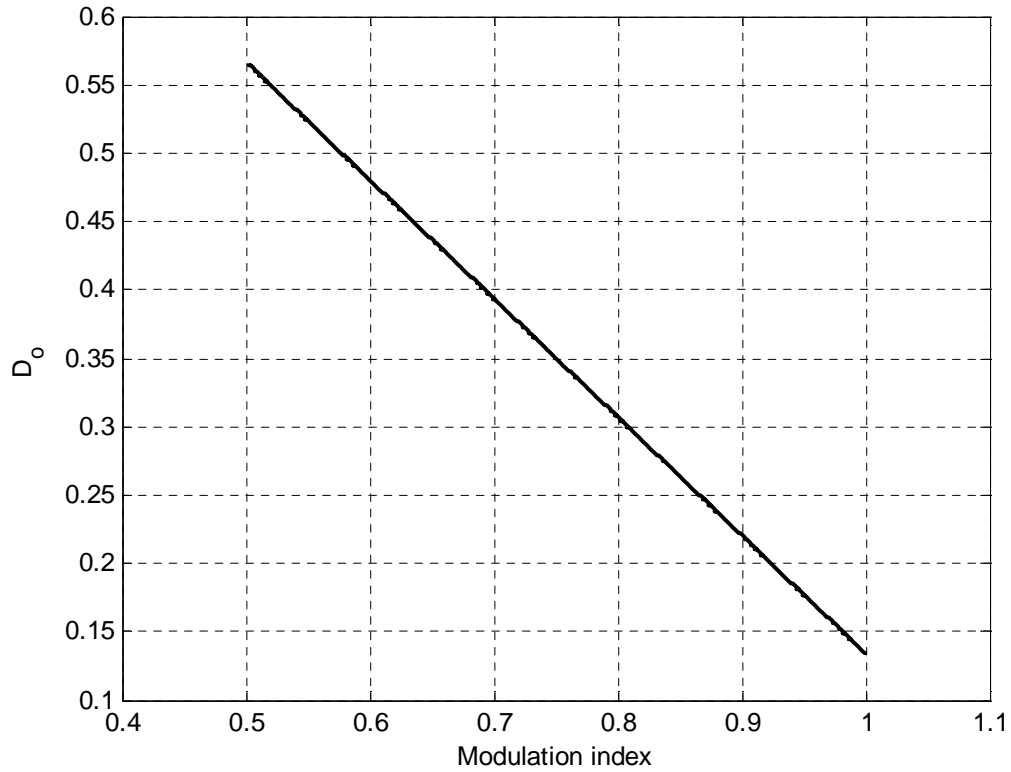
Figure 4.11: Relation between the modulation index and the duty ratio

4.5 Harmonic Analysis of the Shoot-through Duty Ratio

By injecting the third harmonic functions, it is seen that the results are identical to that of the ones without the injection of third harmonics. The third harmonic injection modulation scheme is shown in Figure 4.12. Since the results are the same, the waveforms with the third harmonic injection are used to find the maximum and the minimum of the shoot-through duty ratio curve. When the sequence is formed, it is used to find the Fourier series of the same.

$$M_{as} = m\cos\theta_e - \frac{m}{6}\cos 3\theta_e \tag{4.46}$$

$$M_{bs} = m\cos(\theta_e - \beta) - \frac{m}{6}\cos 3\theta_e \tag{4.47}$$

$$M_{cs} = m\cos(\theta_e + \beta) - \frac{m}{6}\cos 3\theta_e \tag{4.48}$$

$$\frac{dM_{as}}{d\theta_e} = -m\sin\theta_e + \frac{m}{2}\sin 3\theta_e \tag{4.49}$$

To find maximum or minimum: $\dfrac{dM_{as}}{d\theta_e} = 0$

$$\sin\theta_e - \frac{1}{2}(\sin(2\theta_e + \theta_e)) = 0 \tag{4.50}$$

$$\cos\theta_e = \pm\frac{\sqrt{3}}{2}; \quad \theta_e = 30°,150° \tag{4.51}$$

$$\theta_e = 30° = \frac{m\sqrt{3}}{2} - \frac{m}{6} \tag{4.52}$$

$$M_{as} = \frac{m\sqrt{3}}{2} \qquad M_{max} \tag{4.53}$$

$$\theta_e = 150° = \frac{-\sqrt{3}m}{2} - \frac{m}{6} \qquad (4.54)$$

$$M_{as} = -\frac{m\sqrt{3}}{2} \qquad M_{\min} \qquad (4.55)$$

$$\sigma = 0: \quad d = 1 - \frac{\sqrt{3}m}{2} \quad \text{at point } M_2$$

To find the point of intersection,

$$M_{as} = m\cos\theta_e - \frac{m}{6}\cos 3\theta_e \qquad (4.56)$$

$$M_{bs} = m\cos(\theta_e - \beta) - \frac{m}{6}\cos 3\theta_e \qquad (4.57)$$

$$M_{as} = M_{bs} \qquad (4.58)$$

$$\cos\theta_e = \frac{-\cos\theta_e}{2} + \frac{\sqrt{3}\sin\theta_e}{2} \qquad (4.59)$$

$$\tan\theta_e = \sqrt{3} = 60°$$

$$M_{as} = \frac{m}{2} + \frac{m}{3} = \frac{2m}{3} \qquad (4.60)$$

M_{cs} at $\theta_e = 60°$

Minimum:

$$M_{cs} = m\cos(\theta_e + \frac{2\pi}{3}) - \frac{m}{6}\cos 3\theta_e \qquad (4.61)$$

$$M_{cs} = -m + \frac{m}{6} = -\frac{5m}{6} \qquad (4.62)$$

$$d = 1 - \frac{3m}{4} \text{ At point } M_1 \qquad (4.63)$$
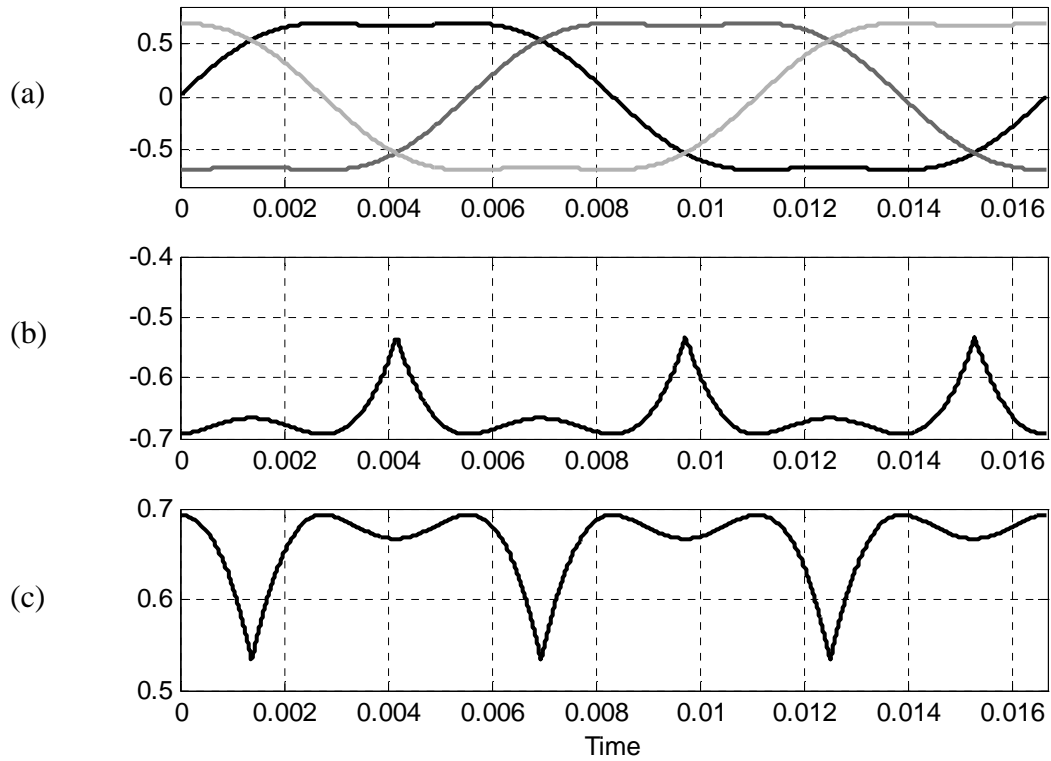
Figure 4.12: Third harmonic injection modulation scheme for 1 cycle operation (a)Three phase Modulation Signal, (b)Maximum of three-phase modulation signal, (c)Minimum of three-phase modulation signal

The shoot-through duty ratio for one cycle of the system by injecting the third harmonics is shown in Figure 4.13. This figure illustrates the maximum point, M_1 and minimum point, M_2.
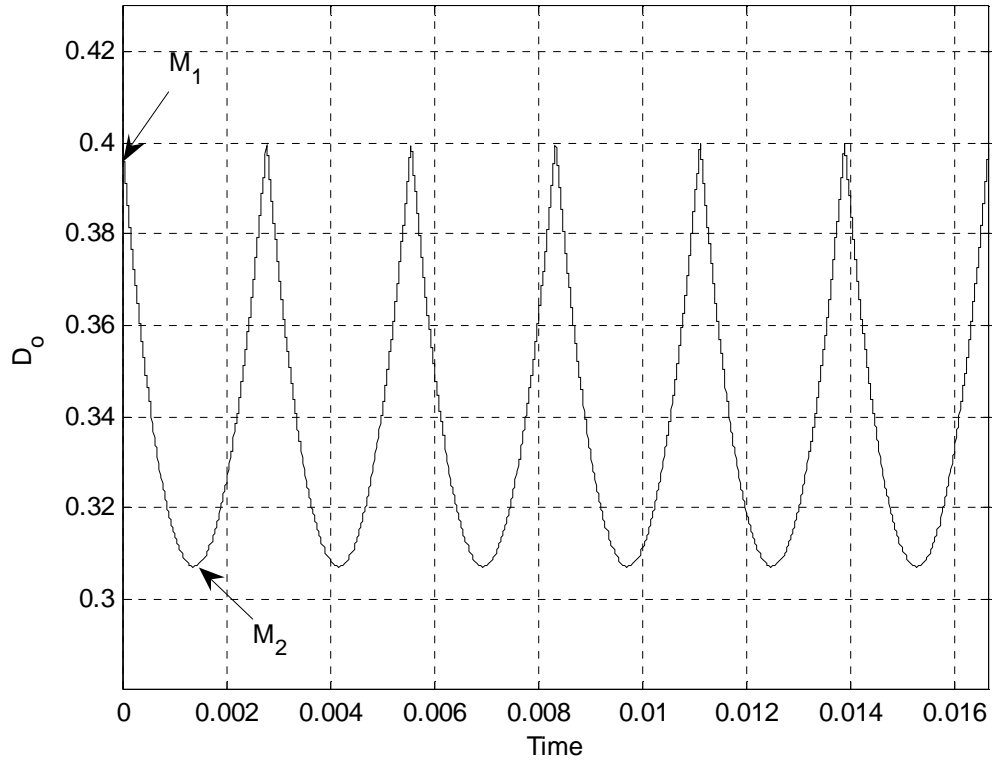
Figure 4.13: Shoot-through duty Ratio using third harmonic injection modulation scheme

for 1 cycle operation

Now the generalized equation for the shoot-through duty ratio is given as

$$d = 1 - \frac{\sqrt{3}m}{2}\cos\left(\theta - \frac{\pi}{6}\right) \qquad (4.64)$$

where $0 \leq \theta \leq \frac{\pi}{3}$

Now assuming $f(\theta) = \frac{\sqrt{3}m}{2}\cos\left(\theta - \frac{\pi}{6}\right)$ $\qquad (4.65)$

The Fourier theorem states that a periodic function $f(\theta)$ can be described by a constant term plus and infinite series of sine and cosine terms of frequency $n\omega$, where n is an integer [B.5]. Therefore, $f(\theta)$ can be expressed as

$$f(\theta) = \frac{a_o}{2} + \sum_{n=1}^{\infty} a_n \cos n\theta + \sum_{n=1}^{\infty} b_n \sin n\theta \tag{4.66}$$

where

$\frac{a_o}{2}$ is the average value of the output. The constants, $\frac{a_o}{2}$, a_n and b_n can be determined from the following expressions

$$\frac{a_o}{2} = \frac{1}{T} \int_{-\frac{T}{2}}^{\frac{T}{2}} f(\theta) d\theta \tag{4.67}$$

$$a_n = \frac{2}{T} \int_{-\frac{T}{2}}^{\frac{T}{2}} f(\theta) \cos(n\theta) d\theta \qquad 1 \le n \le \infty \tag{4.68}$$

$$b_n = \frac{2}{T} \int_{-\frac{T}{2}}^{\frac{T}{2}} f(\theta) \sin(n\theta) d\theta \qquad 1 \le n \le \infty \tag{4.69}$$

Hence the fourier series of $f(\theta)$ is obtained by using the above equations

$$\frac{a_o}{2} = \frac{1}{\pi} \int_{-\frac{\pi}{3} - \frac{\pi}{6}}^{\frac{\pi}{6}} \frac{\sqrt{3}m}{2} \cos\left(\theta - \frac{\pi}{6}\right) d\theta$$

$$= \frac{3\sqrt{3}m}{2\pi} \tag{4.70}$$

$$a_n = \frac{2}{\pi} \int_{-\frac{\pi}{3}}^{\frac{\pi}{6}} \frac{\sqrt{3}m}{2} \cos\left(\theta - \frac{\pi}{6}\right) \cos(n\theta) d\theta$$

$$= \frac{3\sqrt{3}m}{2\pi} \left(\frac{\sin\left((1-2n)\frac{\pi}{6}\right)}{1-n} + \frac{\sin\left((1+2n)\frac{\pi}{6}\right)}{1+n} + \frac{1}{(1-n)(1+n)} \right) \qquad (4.71)$$

$$b_n = \frac{2}{\pi} \int_{-\frac{\pi}{3}}^{\frac{\pi}{6}} \frac{\sqrt{3}m}{2} \cos\left(\theta - \frac{\pi}{6}\right) \sin(n\theta) d\theta$$

$$= \frac{3\sqrt{3}m}{2\pi} \left(\frac{\cos\left((1-2n)\frac{\pi}{6}\right)}{1-n} + \frac{\cos\left((1+2n)\frac{\pi}{6}\right)}{1+n} - \frac{\sqrt{3}n}{(1-n)(1+n)} \right) \qquad (4.72)$$

Substituting the constants, $\frac{a_o}{2}$, a_n, and b_n from (4.70), (4.71), and (4.72) in the fourier

series which is represented in (4.66).

$$f(\theta) = \frac{3\sqrt{3}m}{2\pi} + \sum_{n=1}^{\infty} \frac{3\sqrt{3}m}{2\pi} \left(\frac{\sin\left((1-2n)\frac{\pi}{6}\right)}{1-n} + \frac{\sin\left((1+2n)\frac{\pi}{6}\right)}{1+n} + \frac{1}{(1-n)(1+n)} \right) \cos n\theta$$

$$+ \sum_{n=1}^{\infty} \frac{3\sqrt{3}m}{2\pi} \left(\frac{\cos\left((1-2n)\frac{\pi}{6}\right)}{1-n} + \frac{\cos\left((1+2n)\frac{\pi}{6}\right)}{1+n} - \frac{\sqrt{3}n}{(1-n)(1+n)} \right) \sin n\theta$$

$$(4.73)$$

$$f(\theta) = \frac{3\sqrt{3}m}{2\pi} + \frac{3\sqrt{3}m}{2\pi} \sum_{n=1}^{\infty} \left| \begin{array}{l} \dfrac{\sin\left((1-2n)\dfrac{\pi}{6} - n\theta\right)}{2(1-n)} + \dfrac{\sin\left((1-2n)\dfrac{\pi}{6} + n\theta\right)}{2(1-n)} \\[3mm] + \dfrac{\sin\left((1+2n)\dfrac{\pi}{6} - n\theta\right)}{2(1+n)} + \dfrac{\sin\left((1+2n)\dfrac{\pi}{6} + n\theta\right)}{2(1+n)} \\[3mm] + \dfrac{\cos n\theta}{(1-n)(1+n)} + \dfrac{\sin\left((1-2n)\dfrac{\pi}{6} + n\theta\right)}{2(1-n)} - \dfrac{\sin\left((1-2n)\dfrac{\pi}{6} - n\theta\right)}{2(1-n)} \\[3mm] - \dfrac{\sin\left((1+2n)\dfrac{\pi}{6} + n\theta\right)}{2(1+n)} + \dfrac{\sin\left((1+2n)\dfrac{\pi}{6} - n\theta\right)}{2(1+n)} - \dfrac{\sqrt{3}n\sin n\theta}{(1-n)(1+n)} \end{array} \right|$$

The above equations solves to become (4.74)

$$f(\theta) = \frac{3\sqrt{3}m}{2\pi} - \frac{3\sqrt{3}m}{2\pi} \sum_{n=1}^{\infty} \left(\frac{1}{6n-1} - \frac{1}{6n+1} \right) \cos 6n\theta \qquad (4.74)$$

Now from (4.64), the fourier series of the shoot-through duty ratio is given as

$$d = 1 - \frac{3\sqrt{3}m}{2\pi} + \frac{3\sqrt{3}m}{2\pi} \sum_{n=1}^{\infty} \left(\frac{1}{6n-1} - \frac{1}{6n+1} \right) \cos 6n\theta \qquad (4.75)$$

4.6 Space Vector Modulation Scheme used in the Z-Source Inverter

The phase voltages of the given system as shown in Figure 3.1 are given as from (3.2)

$$V_{an} + V_{no} = \frac{V_{dd}}{2}\left(S_{ap} - S_{an}\right) \qquad (4.76)$$

$$V_{bn} + V_{no} = \frac{V_{dd}}{2}\left(S_{bp} - S_{bn}\right) \qquad (4.77)$$

$$V_{cn} + V_{no} = \frac{V_{dd}}{2}\left(S_{cp} - S_{cn}\right) \qquad (4.78)$$

Adding (4.76), (4.77), and (4.78) gives the neutral voltage

$$V_{no} = \frac{1}{3}\left(\frac{V_{dd}}{2}\left(S_{ap} + S_{bp} + S_{cp} - S_{an} - S_{bn} - S_{cn}\right) - \left(V_{an} + V_{bn} + V_{cn}\right)\right) \qquad (4.79)$$

In a case where the load is balanced; $V_{an} + V_{bn} + V_{cn} = 0$

Therefore,

$$V_{no} = \frac{V_{dd}}{6}\left(S_{ap} + S_{bp} + S_{cp} - S_{an} - S_{bn} - S_{cn}\right) \qquad (4.80)$$

Hence the phase voltages of the system are given below after substituting the neutral voltage (4.76), (4.77) and (4.78).

$$V_{an} = \frac{V_{dd}}{6}\left(2S_{ap} - S_{bp} - S_{cp} - 2S_{an} + S_{bn} + S_{cn}\right) \qquad (4.81)$$

$$V_{bn} = \frac{V_{dd}}{6}\left(-S_{ap} + 2S_{bp} - S_{cp} + S_{an} - 2S_{bn} + S_{cn}\right) \qquad (4.82)$$

$$V_{cn} = \frac{V_{dd}}{6}\left(-S_{ap} - S_{bp} + 2S_{cp} + S_{an} + S_{bn} - 2S_{cn}\right) \qquad (4.83)$$

The qdo equations in the stationary reference frame are given as

$$V_q = \frac{1}{3}\left(V_{an} - V_{bn} - V_{cn}\right)$$

$$V_q = \frac{V_{dd}}{6}\left(2S_{ap} - S_{bp} - S_{cp} - 2S_{an} + S_{bn} + S_{cn}\right) \qquad (4.84)$$

$$V_d = \frac{1}{\sqrt{3}}\left(-V_{bn} + V_{cn}\right)$$

$$V_d = \frac{V_{dd}}{2\sqrt{3}}\left(-S_{bp} + S_{bn} + S_{cp} - S_{cn}\right) \qquad (4.85)$$

90

$$V_o = \frac{V_{dd}}{6}\left(S_{ap} + S_{bp} + S_{cp} - S_{an} - S_{bn} - S_{cn}\right) \qquad (4.86)$$

Table 4.2 illustrates the phase voltages in both the abc reference frame as well as the qdo reference frame in all the switching states. Figure 4.14 shows the space vector diagram of the Z-Source Inverter taking into consideration the qdo equations at each state of operation.

Table 4.2: Phase voltages in the abc and q-d reference frame given the

possible switching states

	STATE	V_{AN}	V_{BN}	V_{CN}	V_q	V_d	V_o
1	ST	0	0	0	0	0	0
2	ST	0	0	0	0	0	0
3	ST	0	0	0	0	0	0
4	ST	0	0	0	0	0	0
5	ST	0	0	0	0	0	0
6	ST	0	0	0	0	0	0
7	ST	0	0	0	0	0	0
U_0	NULL	0	0	0	0	0	$\dfrac{V_{dd}}{2}$
U_7	NULL	0	0	0	0	0	$-\dfrac{V_{dd}}{2}$
U_1	ACTIVE	$\dfrac{2V_{dd}}{3}$	$-\dfrac{V_{dd}}{3}$	$-\dfrac{V_{dd}}{3}$	$\dfrac{2V_{dd}}{3}$	0	$-\dfrac{V_{dd}}{6}$
U_2	ACTIVE	$\dfrac{V_{dd}}{3}$	$-\dfrac{2V_{dd}}{3}$	$\dfrac{V_{dd}}{3}$	$\dfrac{V_{dd}}{3}$	$\dfrac{V_{dd}}{\sqrt{3}}$	$\dfrac{V_{dd}}{6}$
U_3	ACTIVE	$-\dfrac{V_{dd}}{3}$	$-\dfrac{V_{dd}}{3}$	$\dfrac{2V_{dd}}{3}$	$-\dfrac{V_{dd}}{3}$	$\dfrac{V_{dd}}{\sqrt{3}}$	$-\dfrac{V_{dd}}{6}$
U_4	ACTIVE	$-\dfrac{2V_{dd}}{3}$	$\dfrac{V_{dd}}{3}$	$\dfrac{V_{dd}}{3}$	$-\dfrac{2V_{dd}}{3}$	0	$\dfrac{V_{dd}}{6}$
U_5	ACTIVE	$-\dfrac{V_{dd}}{3}$	$\dfrac{2V_{dd}}{3}$	$-\dfrac{V_{dd}}{3}$	$-\dfrac{V_{dd}}{3}$	$-\dfrac{V_{dd}}{\sqrt{3}}$	$-\dfrac{V_{dd}}{6}$

U_6	ACTIVE	$\dfrac{V_{dd}}{3}$	$\dfrac{V_{dd}}{3}$	$-\dfrac{2V_{dd}}{3}$	$\dfrac{V_{dd}}{3}$	$-\dfrac{V_{dd}}{\sqrt{3}}$	$\dfrac{V_{dd}}{6}$

The figure shows a space vector diagram (hexagon) with labeled vectors. The labels around the diagram:

U_3 : $\dfrac{-V_o}{3}, \dfrac{V_o}{\sqrt{3}}, \dfrac{-V_o}{6}$

U_2 : $\dfrac{V_o}{3}, \dfrac{V_o}{\sqrt{3}}, \dfrac{V_o}{6}$

U_0 : $0,0,\dfrac{V_o}{2}$

V_{qd}^*

U_4 : $\dfrac{-2V_o}{3},0,\dfrac{V_o}{6}$

$\dfrac{2V_o}{3},0,\dfrac{-V_o}{6}$

U_0 $0,0,0$

U_7 $1,1,1$

U_1

$0,0,\dfrac{-V_o}{2}$ U_7

U_6

U_5 : $\dfrac{-V_o}{3}, \dfrac{-V_o}{\sqrt{3}}, \dfrac{-V_o}{6}$

$\dfrac{V_o}{3}, \dfrac{-V_o}{\sqrt{3}}, \dfrac{V_o}{6}$

Sectors numbered 1, 2, 3, 4, 5, 6.
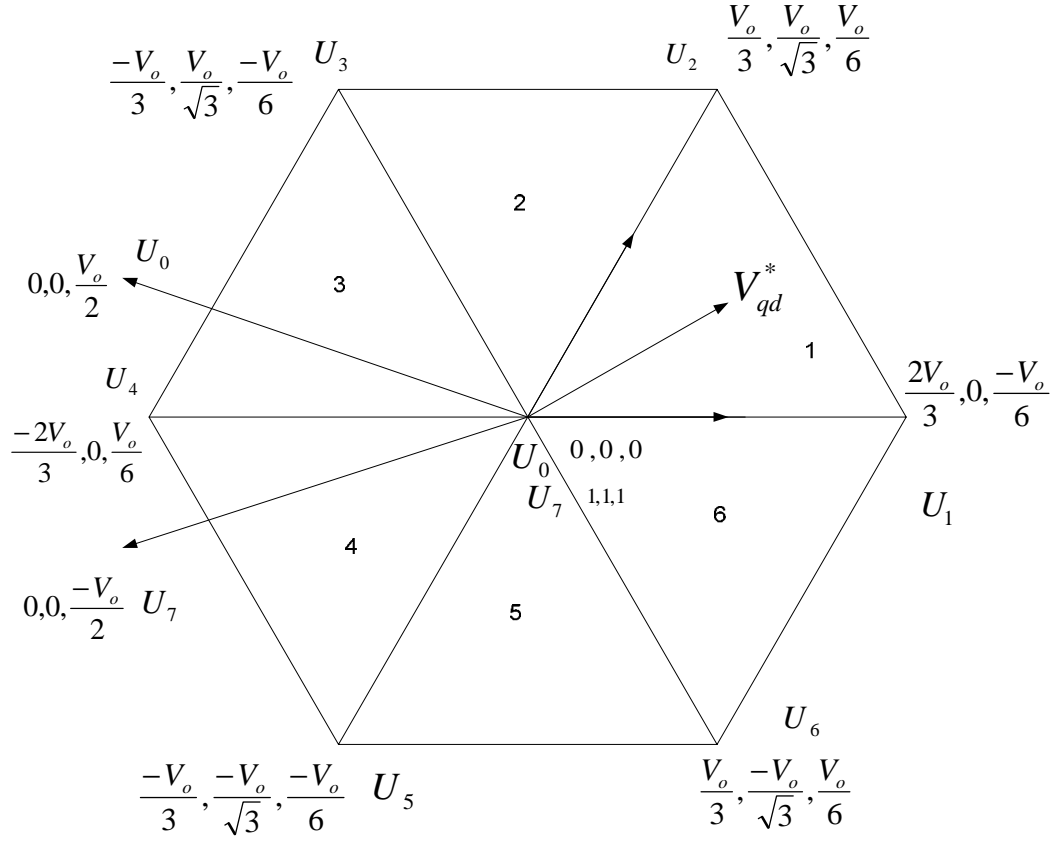
Figure 4.14: Space Vector Diagram of the Z-Source Inverter

Here,

$$\text{Null state } U_o\left(0,0,\frac{V_{dd}}{2}\right) = \alpha_1 t_c \qquad (4.87)$$

$$\text{Null State } U_7\left(0,0,-\frac{V_{dd}}{2}\right) = \alpha_2 t_c \qquad (4.88)$$

$$\text{Shoot-through state} = \gamma t_c \qquad (4.89)$$

where

t_a and t_b are the normalized active state times, t_c is the normalized non-active state time

$$t_c = 1 - t_a - t_b \qquad (4.90)$$

$$\alpha_1 + \alpha_2 + \gamma = 1 \tag{4.91}$$

The stationary reference frame qdo voltage is expressed as

$$V_{qd}^* = V_q^* + jV_d^* = V_{qda}t_a + V_{qdb}t_b + V_{qd0}t_0 + V_{qd7}t_7 \tag{4.92}$$

The device switching times and the individual maximum and minimum voltages when the reference voltages are in the six sectors are given in Table 4.3.

Table 4.3 Device switching times in each sector

SECTOR	t_a	t_b	MAXIMUM VOLTAGE	MINIMUM VOLTAGE
I	$\dfrac{V_{ab}}{V_{dd}}$	$\dfrac{V_{bc}}{V_{dd}}$	V_{an}	V_{cn}
II	$\dfrac{V_{ac}}{V_{dd}}$	$\dfrac{V_{ba}}{V_{dd}}$	V_{bn}	V_{cn}
III	$\dfrac{V_{bc}}{V_{dd}}$	$\dfrac{V_{ca}}{V_{dd}}$	V_{bn}	V_{an}
IV	$\dfrac{V_{ba}}{V_{dd}}$	$\dfrac{V_{cb}}{V_{dd}}$	V_{cn}	V_{an}
V	$\dfrac{V_{ca}}{V_{dd}}$	$\dfrac{V_{ab}}{V_{dd}}$	V_{cn}	V_{bn}

VI	$\dfrac{V_{cb}}{V_{dd}}$	$\dfrac{V_{ac}}{V_{dd}}$	V_{an}	V_{bn}

The average neutral voltage is obtained in each section as follows.

Sector I

$$V_{an} = V_{max}$$

$$V_{cn} = V_{min}$$

$$V_{bn} = -\left(V_{max} + V_{min}\right)$$

$$t_a = \frac{V_{ab}}{V_{dd}} = \frac{V_{max} + V_{max} + V_{min}}{V_{dd}} = \frac{2V_{max} + V_{min}}{V_{dd}}$$

$$t_b = \frac{V_{bc}}{V_{dd}} = \frac{-V_{max} - V_{min} - V_{min}}{V_{dd}} = \frac{-V_{max} - 2V_{min}}{V_{dd}}$$

$$t_c = 1 - t_a - t_b = 1 - \frac{\left(V_{max} - V_{min}\right)}{V_{dd}}$$

$$\left\langle V_{no} \right\rangle = \frac{V_{dd}}{6}\left(-t_a + t_b\right) + \frac{V_{dd}}{2}\alpha_1 t_c - \frac{V_{dd}}{2}\alpha_2 t_c$$

$$\left\langle V_{no} \right\rangle = \frac{V_{dd}}{2}\left(\alpha_1 - \alpha_2\right) + \frac{V_{max}}{2}\left(-1 - \alpha_1 + \alpha_2\right) + \frac{V_{min}}{2}\left(-1 + \alpha_1 - \alpha_2\right)$$

$$\left\langle V_{no} \right\rangle = \frac{V_{dd}}{2}\beta - \frac{V_{max}}{2}\left(1 + \beta\right) - \frac{V_{min}}{2}\left(1 - \beta\right)$$

Sector II

$$V_{bn} = V_{max}$$

$$V_{cn} = V_{min}$$

$$V_{an} = -(V_{max} + V_{min})$$

$$t_a = \frac{V_{ac}}{V_{dd}} = \frac{-V_{max} - V_{min} - V_{min}}{V_{dd}} = \frac{-V_{max} - 2V_{min}}{V_{dd}}$$

$$t_b = \frac{V_{ba}}{V_{dd}} = \frac{V_{max} + V_{max} + V_{min}}{V_{dd}} = \frac{2V_{max} + V_{min}}{V_{dd}}$$

$$t_c = 1 - t_a - t_b = 1 - \frac{(V_{max} - V_{min})}{V_{dd}}$$

$$\langle V_{no} \rangle = \frac{V_{dd}}{6}(t_a - t_b) + \frac{V_{dd}}{2}\alpha_1 t_c - \frac{V_{dd}}{2}\alpha_2 t_c$$

$$\langle V_{no} \rangle = \frac{V_{dd}}{2}(\alpha_1 - \alpha_2) + \frac{V_{max}}{2}(-1 - \alpha_1 + \alpha_2) + \frac{V_{min}}{2}(-1 + \alpha_1 - \alpha_2)$$

$$\langle V_{no} \rangle = \frac{V_{dd}}{2}\beta - \frac{V_{max}}{2}(1 + \beta) - \frac{V_{min}}{2}(1 - \beta)$$

Sector III

$$V_{bn} = V_{max}$$

$$V_{an} = V_{min}$$

$$V_{cn} = -(V_{max} + V_{min})$$

$$t_a = \frac{V_{bc}}{V_{dd}} = \frac{V_{max} + V_{max} + V_{min}}{V_{dd}} = \frac{2V_{max} + V_{min}}{V_{dd}}$$

$$t_b = \frac{V_{ca}}{V_{dd}} = \frac{-V_{max} - V_{min} - V_{min}}{V_{dd}} = \frac{-V_{max} - 2V_{min}}{V_{dd}}$$

$$t_c = 1 - t_a - t_b = 1 - \frac{(V_{max} - V_{min})}{V_{dd}}$$

$$\langle V_{no} \rangle = \frac{V_{dd}}{6}(-t_a - t_b) + \frac{V_{dd}}{2}\alpha_1 t_c - \frac{V_{dd}}{2}\alpha_2 t_c$$

$$\langle V_{no} \rangle = \frac{V_{dd}}{2}(\alpha_1 - \alpha_2) + \frac{V_{max}}{2}(-1 - \alpha_1 + \alpha_2) + \frac{V_{min}}{2}(-1 + \alpha_1 - \alpha_2)$$

$$\langle V_{no} \rangle = \frac{V_{dd}}{2}\beta - \frac{V_{max}}{2}(1 + \beta) - \frac{V_{min}}{2}(1 - \beta)$$

Sector IV

$$V_{cn} = V_{max}$$

$$V_{an} = V_{min}$$

$$V_{bn} = -(V_{max} + V_{min})$$

$$t_a = \frac{V_{ba}}{V_{dd}} = \frac{-V_{max} - V_{min} - V_{min}}{V_{dd}} = \frac{-V_{max} - 2V_{min}}{V_{dd}}$$

$$t_b = \frac{V_{cb}}{V_{dd}} = \frac{V_{max} + V_{max} + V_{min}}{V_{dd}} = \frac{2V_{max} + V_{min}}{V_{dd}}$$

$$t_c = 1 - t_a - t_b = 1 - \frac{(V_{max} - V_{min})}{V_{dd}}$$

$$\langle V_{no} \rangle = \frac{V_{dd}}{6}(t_a - t_b) + \frac{V_{dd}}{2}\alpha_1 t_c - \frac{V_{dd}}{2}\alpha_2 t_c$$

$$\langle V_{no} \rangle = \frac{V_{dd}}{2}(\alpha_1 - \alpha_2) + \frac{V_{max}}{2}(-1 - \alpha_1 + \alpha_2) + \frac{V_{min}}{2}(-1 + \alpha_1 - \alpha_2)$$

$$\langle V_{no} \rangle = \frac{V_{dd}}{2}\beta - \frac{V_{max}}{2}(1 + \beta) - \frac{V_{min}}{2}(1 - \beta)$$

Sector V

$$V_{cn} = V_{max}$$

$$V_{bn} = V_{min}$$

$$V_{an} = -(V_{max} + V_{min})$$

$$t_a = \frac{V_{ca}}{V_{dd}} = \frac{V_{max} + V_{max} + V_{min}}{V_{dd}} = \frac{2V_{max} + V_{min}}{V_{dd}}$$

$$t_b = \frac{V_{ab}}{V_{dd}} = \frac{-V_{max} - V_{min} - V_{min}}{V_{dd}} = \frac{-V_{max} - 2V_{min}}{V_{dd}}$$

$$t_c = 1 - t_a - t_b = 1 - \frac{(V_{max} - V_{min})}{V_{dd}}$$

$$\langle V_{no} \rangle = \frac{V_{dd}}{6}(-t_a - t_b) + \frac{V_{dd}}{2}\alpha_1 t_c - \frac{V_{dd}}{2}\alpha_2 t_c$$

$$\langle V_{no} \rangle = \frac{V_{dd}}{2}(\alpha_1 - \alpha_2) + \frac{V_{max}}{2}(-1 - \alpha_1 + \alpha_2) + \frac{V_{min}}{2}(-1 + \alpha_1 - \alpha_2)$$

$$\langle V_{no} \rangle = \frac{V_{dd}}{2}\beta - \frac{V_{max}}{2}(1 + \beta) - \frac{V_{min}}{2}(1 - \beta)$$

Sector VI

$$V_{an} = V_{max}$$

$$V_{bn} = V_{min}$$

$$V_{cn} = -(V_{max} + V_{min})$$

$$t_a = \frac{V_{cb}}{V_{dd}} = \frac{-V_{max} - V_{min} - V_{min}}{V_{dd}} = \frac{-V_{max} - 2V_{min}}{V_{dd}}$$

$$t_b = \frac{V_{ac}}{V_{dd}} = \frac{V_{max} + V_{max} + V_{min}}{V_{dd}} = \frac{2V_{max} + V_{min}}{V_{dd}}$$

$$t_c = 1 - t_a - t_b = 1 - \frac{(V_{max} - V_{min})}{V_{dd}}$$

$$\langle V_{no} \rangle = \frac{V_{dd}}{6}(t_a - t_b) + \frac{V_{dd}}{2}\alpha_1 t_c - \frac{V_{dd}}{2}\alpha_2 t_c$$

$$\langle V_{no} \rangle = \frac{V_{dd}}{2}(\alpha_1 - \alpha_2) + \frac{V_{max}}{2}(-1 - \alpha_1 + \alpha_2) + \frac{V_{min}}{2}(-1 + \alpha_1 - \alpha_2)$$

$$\langle V_{no} \rangle = \frac{V_{dd}}{2}\beta - \frac{V_{max}}{2}(1 + \beta) - \frac{V_{min}}{2}(1 - \beta)$$

Hence, the generalized equation for the neutral voltage is,

$$\langle V_{no} \rangle = \frac{V_{dd}}{2}\beta - \frac{V_{max}}{2}(1 + \beta) - \frac{V_{min}}{2}(1 - \beta) \tag{4.93}$$

where

$$\beta = \alpha_1 - \alpha_2 \tag{4.94}$$

Also, the generalized equation for the active state duty ratio in terms of the maximum and minimum voltages can be expressed as

$$\frac{t_a + t_b}{T} = \frac{V_{max} - V_{min}}{V_{dd}} \tag{4.95}$$

The switching pattern for the model in order to obtain minimum switching loss for the Z-source converter is as shown in Figures 4.15, 4.16, 4.17, 4.18, 4.19, and 4.20 in each sector of operation respectively.
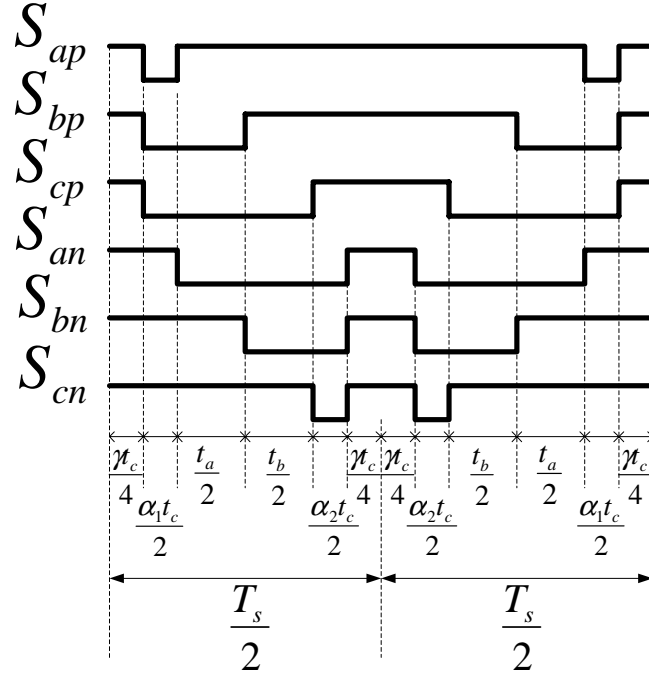
Figure 4.15: Existence function of all the devices in Sector 1 operation
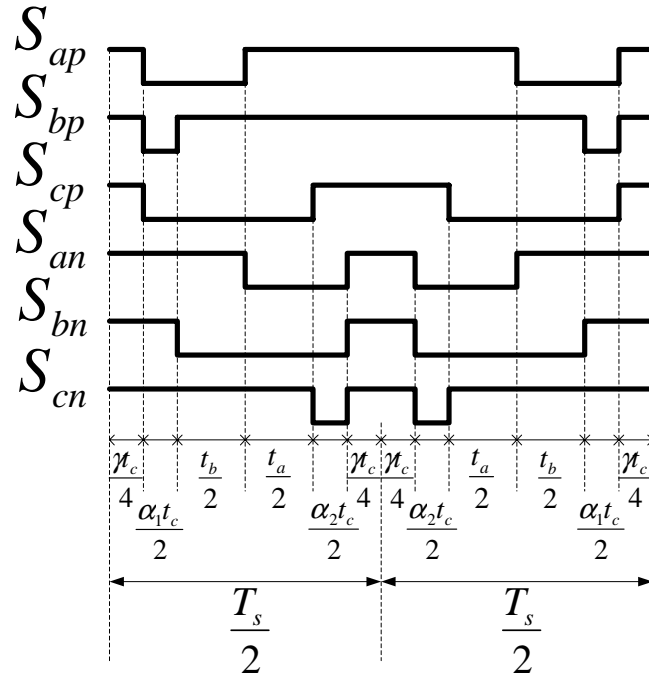
Figure 4.16: Existence function of all the devices in Sector 2 operation

101
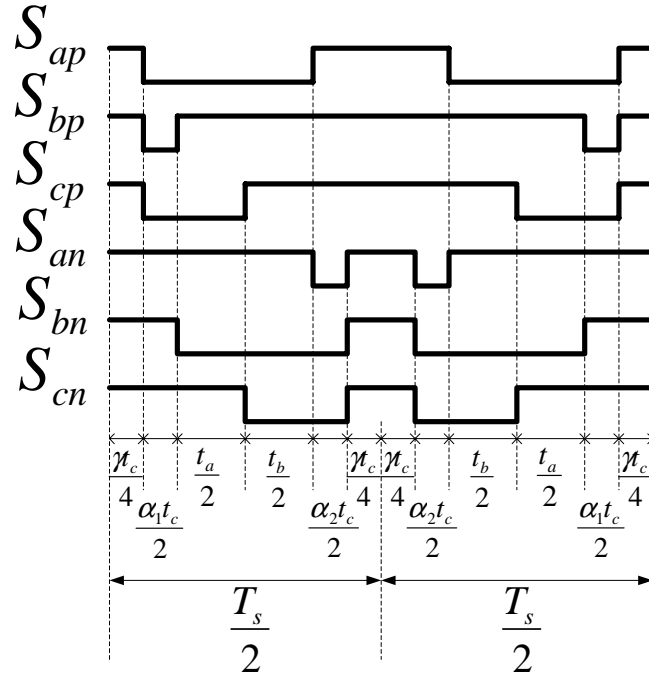
Figure 4.17: Existence function of all the devices in Sector 3 operation
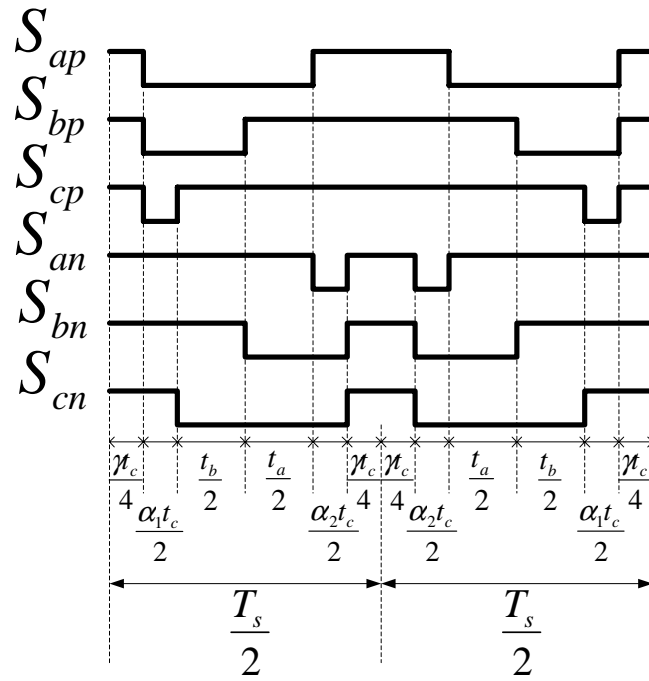
Figure 4.18: Existence function of all the devices in Sector 4 operation

S_{ap}

S_{bp}

S_{cp}

S_{an}

S_{bn}

S_{cn}

$\dfrac{t_c}{4}$ $\dfrac{t_a}{2}$ $\dfrac{t_b}{2}$ $\dfrac{t_c}{4}$ $\dfrac{t_c}{4}$ $\dfrac{t_b}{2}$ $\dfrac{t_a}{2}$ $\dfrac{t_c}{4}$

$\dfrac{\alpha_1 t_c}{2}$ $\dfrac{\alpha_2 t_c}{2}$ $\dfrac{\alpha_2 t_c}{2}$ $\dfrac{\alpha_1 t_c}{2}$

$\dfrac{T_s}{2}$ $\dfrac{T_s}{2}$
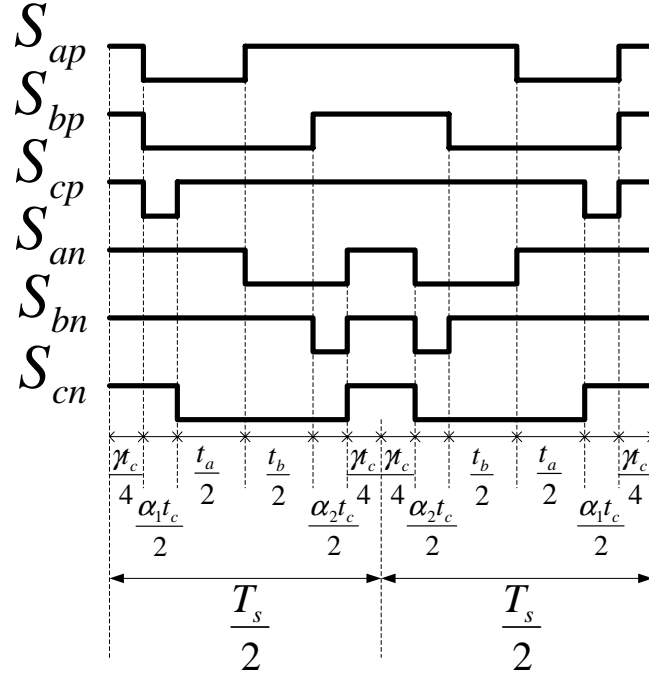
Figure 4.19: Existence function of all the devices in Sector 5 operation

S_{ap}

S_{bp}

S_{cp}

S_{an}

S_{bn}

S_{cn}

$\dfrac{t_c}{4}$ $\dfrac{t_b}{2}$ $\dfrac{t_a}{2}$ $\dfrac{t_c}{4}$ $\dfrac{t_c}{4}$ $\dfrac{t_a}{2}$ $\dfrac{t_b}{2}$ $\dfrac{t_c}{4}$

$\dfrac{\alpha_1 t_c}{2}$ $\dfrac{\alpha_2 t_c}{2}$ $\dfrac{\alpha_2 t_c}{2}$ $\dfrac{\alpha_1 t_c}{2}$

$\dfrac{T_s}{2}$ $\dfrac{T_s}{2}$
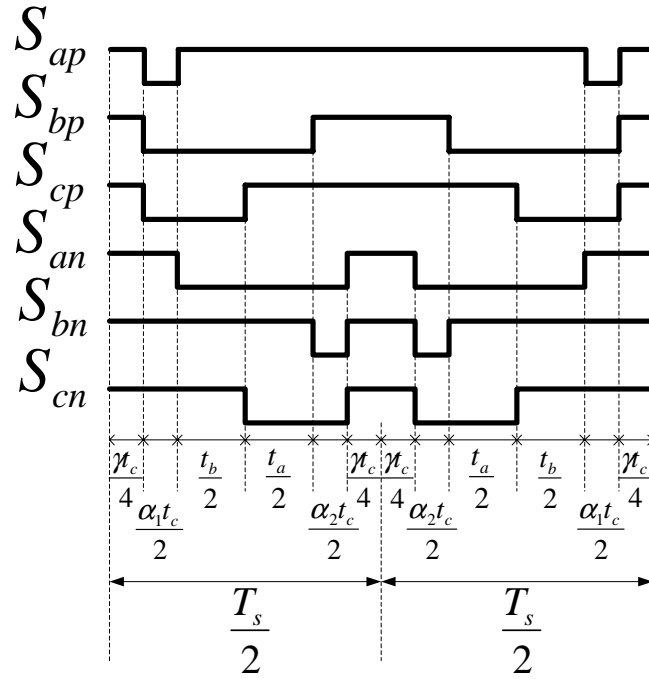
Figure 4.20: Existence function of all the devices in Sector 6 operation

4.7 Conclusion

In this chapter, the modulations scheme used in this thesis has been explained in detail. The shoot-through pulses are injected in the previously total null state region. A constant portion of the null state is used for the shoot-through state. Hence the shoot-through duty ratio is maintained constant. The injection of third harmonics brings out the same shoot-through duty ratio for a particular value of modulation index. Hence the analysis is performed with the injection of third harmonics. The generalized expression for the average neutral voltage of the Z-source Inverter is obtained showing details in the determination of the times. The arrangement of the switching functions in each sector has been illustrated.

CHAPTER 5

MODELING OF Z-SOURCE INVERTER WITH RL LOAD

5.1 Introduction

A new type of converter, Z Source converter (ZSC), was introduced for adjustable speed applications [I.1]. The AC voltage from the Z source inverter can be controlled, theoretically to any value between zero and infinity. For applications such as AC drive systems requiring machine operating over a wide speed range, it is much desirable that the power converter has a buck-boost capability. To differentiate the new DC-AC converter from any conventional VSI and CSI, the author named it Z-source inverter (ZSI). The structure of a VSI based Z-source inverter is shown in Figure 5.1.
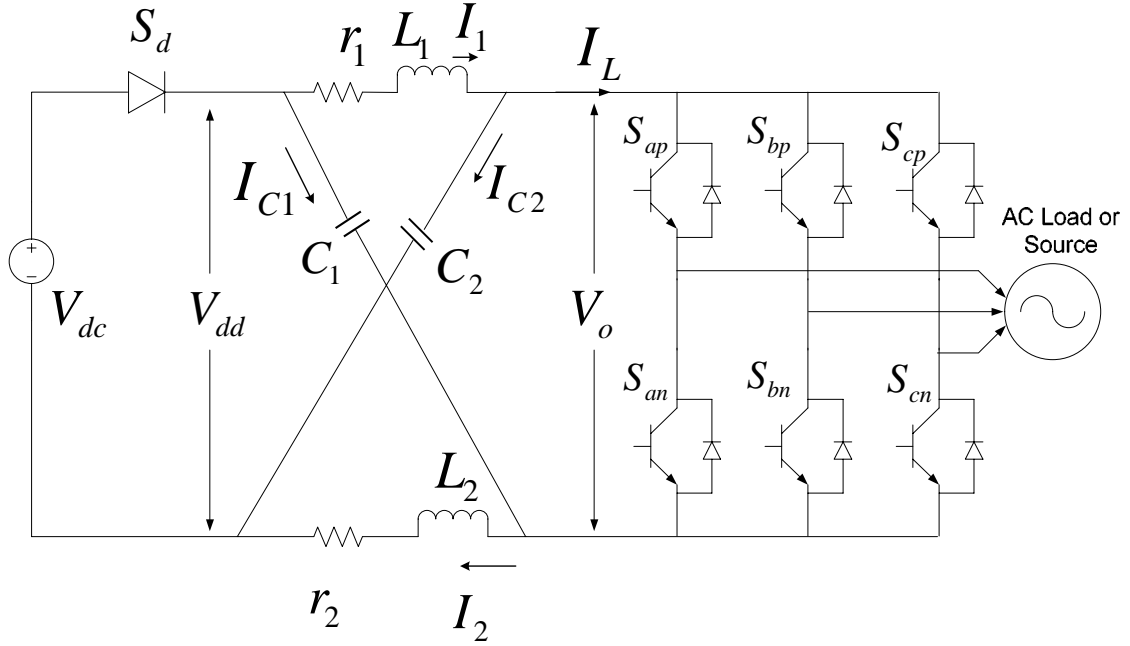
Figure 5.1: Structure of a VSI based Z-Source Inverter

The structure of the Z-source converter shown in Figure 5.1 can be simplified to an equivalent circuit. In the simplified circuit shown in Figure 5.2, the VSI bridge is viewed as an equivalent current source or drain in parallel with an active switch, S [T.2]. In this case, the shoot-through state does not harm the system. The analysis performed in [I.1] shows how the shoot-through state over the non-shoot-through state controls the buck-boost factor of the system. By controlling the shoot-through duty cycle, ZSI can produce any desired AC output voltage.

The AC voltage from ZSC can be controlled theoretically to any value, either higher or lower than the voltage limit imposed by conventional VSI. It is clear that the ZSC can give a large degree of freedom to AC machine design and control so that the performance and costs of overall system is optimized [I.1, I.2, I.26].
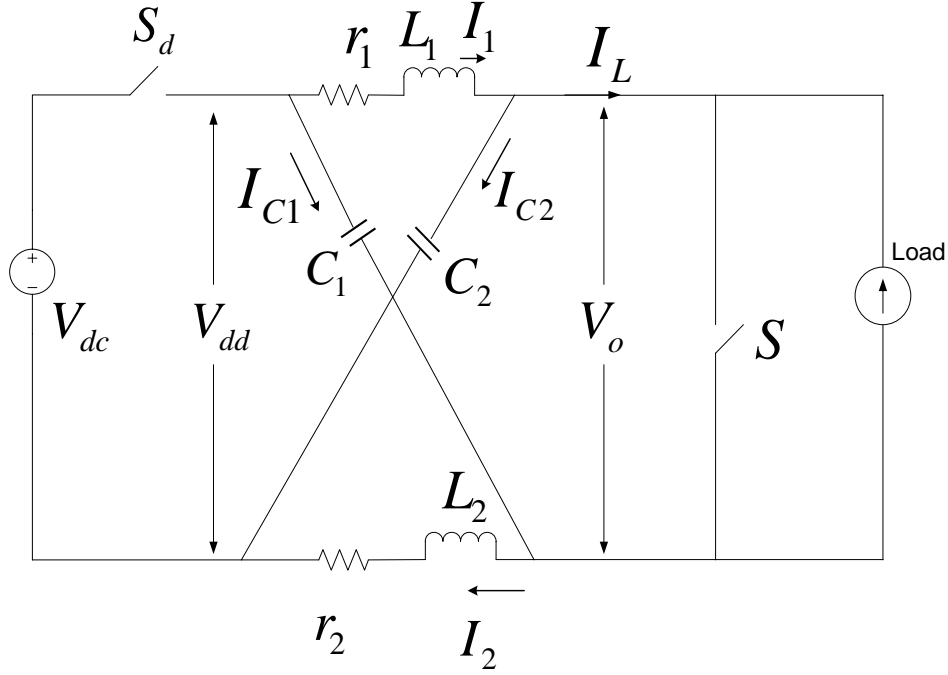
Figure 5.2: Equivalent circuit of voltage source based Z-Source Inverter

Analysis shows that various conventional carrier-based pulse-width modulation strategies could be modified for ZSI [I.13]. Furthermore, two methods were proposed to obtain maximum constant boost control for ZSI, which can achieve maximum voltage gain at any given modulation index without any low-frequency ripple [I.10].

In this chapter, a detailed dynamic analysis of the six modes of operation has been studied. The study has been extended from the previous work by including the dynamics involved when the resistances in the circuits are taken into consideration. Section 5.2 illustrates the details of this analysis. Section 5.3 explains the details regarding the steady state analysis. The entire analysis is performed for two cases of loads

- RL Load

- Induction Motor

Section 5.4 illustrates the accurate small signal model and analysis and also gives a detailed view of the system's stability. The Space vector pulse width modulation (SVPWM) is widely used for variable frequency drive applications because of the various advantages such as the good DC utilization and less harmonics distortion in the output waveforms. In the ZSI, a modified SVPWM is used to inject the shoot-through states into the null states without affecting the active state of operation. This concept is as explained in Chapter 4.

5.2 Dynamic Analysis of ZSI

A detailed analysis of the different modes of operation including the resistances in the circuit is studied and explained. There are basically three modes of operation

- Active State S_A

- Shoot-through State S_B

- Null State S_C

Another detail to be considered is the switch S_d which will be turned ON and OFF in each of the three states. When the switch, S_d is turned ON, it is considered to be high and while it is turned OFF, it is considered to be low.

5.2.1 Active State; S_A

Figure 5.3 represents the active state when $S_d=1$
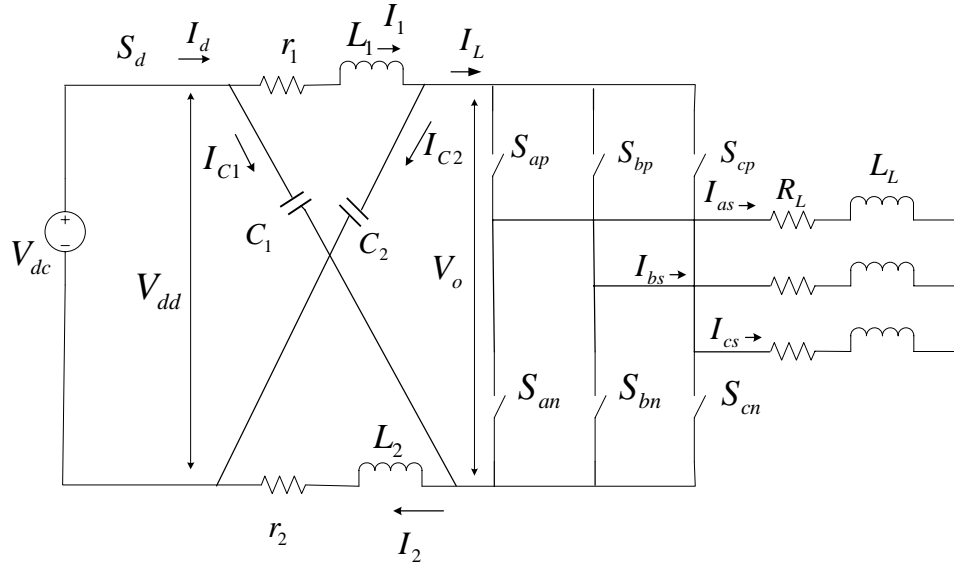
Figure 5.3: Active State of ZSI when $S_d=1$

The model equations for the system during active state of operation is given as the following

$$V_{dd} = r_1 I_1 + L_1 p I_1 + V_{c2} \tag{5.1}$$

$$V_{dd} = r_2 I_2 + L_2 p I_2 + V_{c1} \tag{5.2}$$

$$C_1 p V_{c1} = I_2 - I_L \tag{5.3}$$

$$C_2 p V_{c2} = I_1 - I_L \tag{5.4}$$

$$V_{abcs} = R_L I_{abcs} + L_L p I_{abcs} \tag{5.5}$$

$$V_{dd} = V_{dc} \tag{5.6}$$

$$I_d = I_1 + I_2 - I_L \tag{5.7}$$

$$I_L = S_{ap}I_{as} + S_{bp}I_{bs} + S_{cp}I_{cs} \tag{5.8}$$

$$V_o = V_{c1} + V_{c2} - V_{dd} \tag{5.9}$$

Figure 5.4 represents the active state when $S_d=0$

The model equations for the system while the switch S_d is off is given as the following

$$V_{dd} = r_1 I_1 + L_1 p I_1 + V_{c2} \tag{5.10}$$

$$V_{dd} = r_2 I_2 + L_2 p I_2 + V_{c1} \tag{5.11}$$

$$C_1 p V_{c1} = I_2 - I_L \tag{5.12}$$

$$C_2 p V_{c2} = I_1 - I_L \tag{5.13}$$
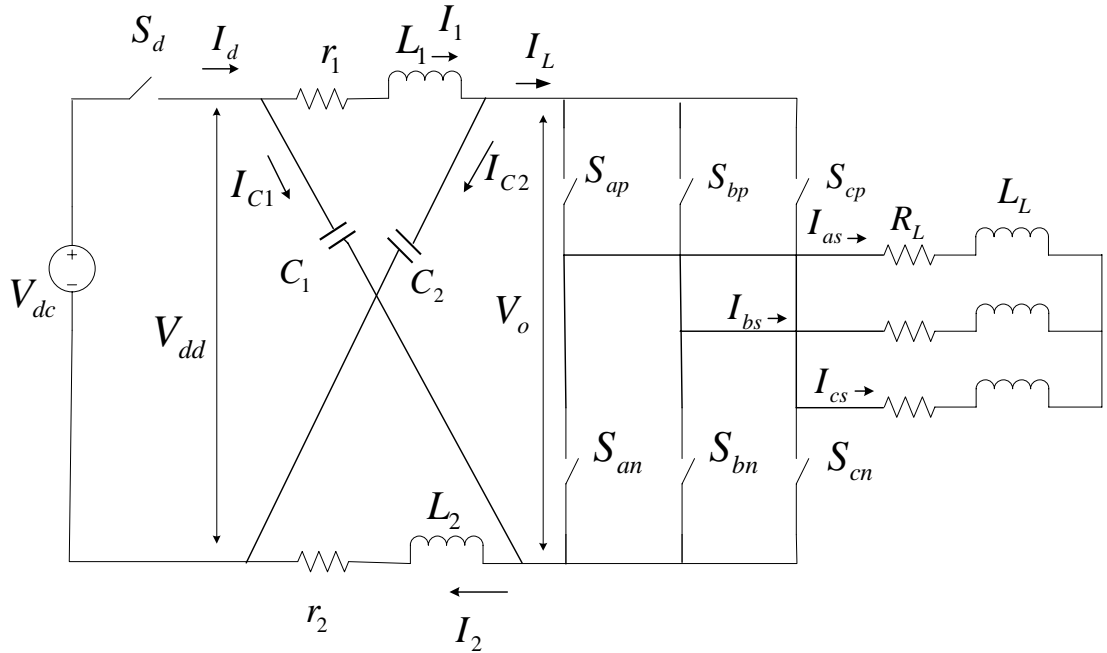
Figure 5.4: Active State of ZSI when $S_d=0$

$$V_{dd} = \frac{L_1}{L_1 + L_2}(r_2 I_2 + V_{c2}) + \frac{L_2}{L_1 + L_2}(r_1 I_1 + V_{c1}) \qquad (5.14)$$

$$I_d = 0 \qquad (5.15)$$

$$I_L = I_1 + I_2 \qquad (5.16)$$

$$V_o = V_{c1} + V_{c2} - V_{dd} \qquad (5.17)$$

5.2.2 Shoot through State; S_B

Figure 5.5 represents the Shoot-through state when either one of the legs or two or all the legs are shorted together when $S_d = 1$.

The model equations for the system during the shoot-through state of operation is given as the following

$$V_{dd} = r_1 I_1 + L_1 p I_1 + V_{c2} \qquad (5.18)$$

$$V_{dd} = r_2 I_2 + L_2 p I_2 + V_{c1} \qquad (5.19)$$

$$C_1 p V_{c1} = I_2 - I_L \qquad (5.20)$$

$$C_2 p V_{c2} = I_1 - I_L \qquad (5.21)$$

$$V_{dd} = V_{dc} \qquad (5.22)$$

$$I_d = I_1 + I_2 - I_L \qquad (5.23)$$
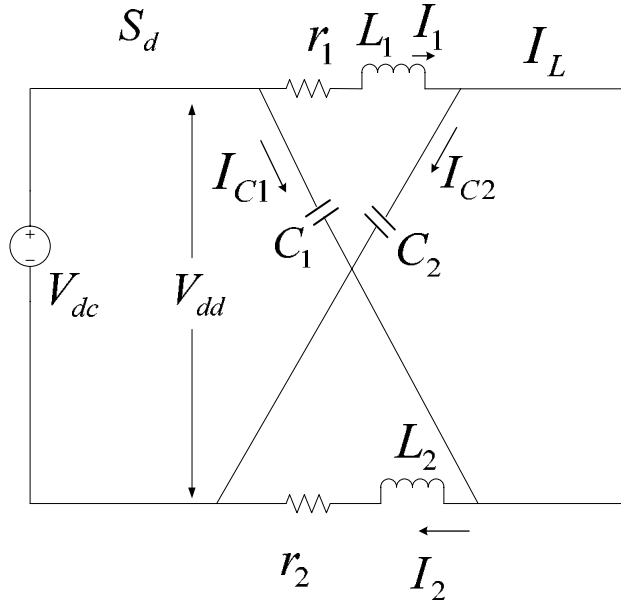
Figure 5.5: Shoot-through State of ZSI when $S_d = 1$

$$I_L = \frac{I_1 C_1 + I_2 C_2}{C_1 + C_2} \tag{5.24}$$

$$V_o = 0 \tag{5.25}$$

Figure 5.6 represents the converter in the shoot-through state when $S_d = 0$.

The model equations for the system while the switch S_d is off is given as the following

$$V_{dd} = r_1 I_1 + L_1 p I_1 + V_{c2} \tag{5.26}$$

$$V_{dd} = r_2 I_2 + L_2 p I_2 + V_{c1} \tag{5.27}$$

$$C_1 p V_{c1} = I_2 - I_L \tag{5.28}$$

$$C_2 p V_{c2} = I_1 - I_L \tag{5.29}$$

$$V_{dd} = V_{c1} + V_{c2} \tag{5.30}$$

$$I_d = 0 \tag{5.31}$$
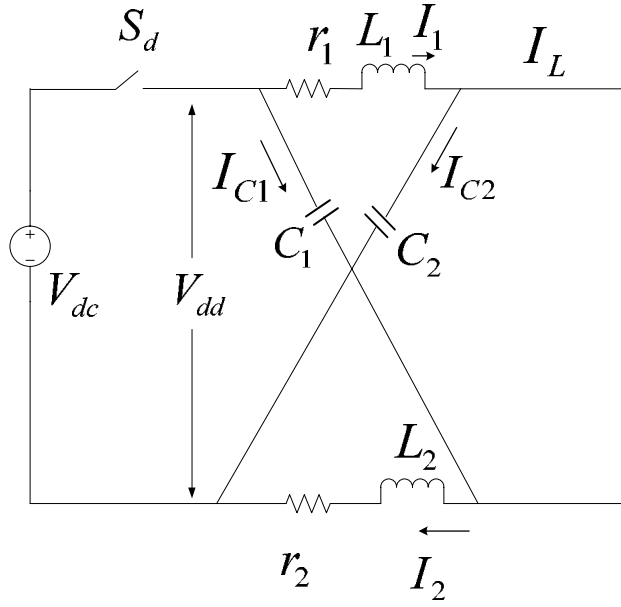
Figure 5.6: Shoot-through State of ZSI when $S_d=0$

$$I_L = I_1 + I_2 \tag{5.32}$$

$$V_o = 0 \tag{5.33}$$

5.2.3 Null State; S_C

Figure 5.7 illustrates the Null state when the switch S_d is turned ON. That is $S_d=1$.

The model equations for the system during the null state of operation is given as the following

$$V_{dd} = r_1 I_1 + L_1 p I_1 + V_{c2} \tag{5.34}$$

$$V_{dd} = r_2 I_2 + L_2 p I_2 + V_{c1} \tag{5.35}$$

$$C_1 p V_{c1} = I_2 - I_L \tag{5.36}$$

113
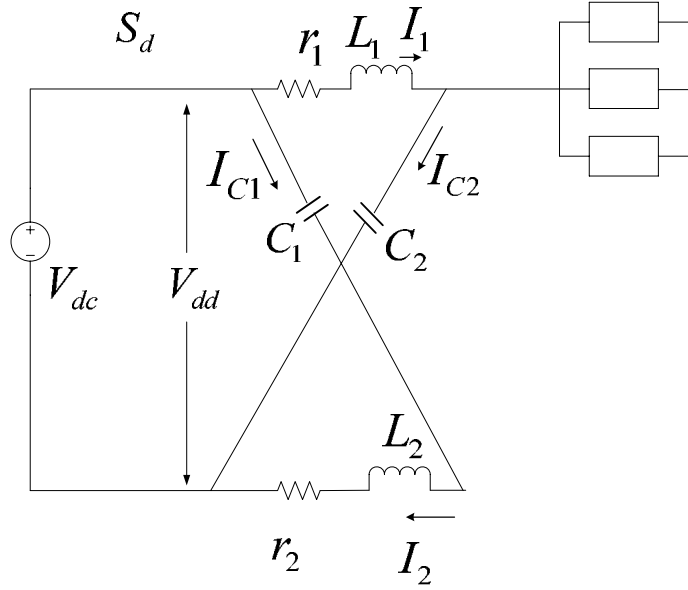
Figure 5.7: Null State of ZSI when $S_d = 1$

$$C_2 p V_{c2} = I_1 - I_L \qquad (5.37)$$

$$V_{dd} = V_{dc} \qquad (5.38)$$

$$I_d = I_1 + I_2 \qquad (5.39)$$

$$I_L = 0 \qquad (5.40)$$

$$V_o = V_{c1} + V_{c2} - V_{dd} \qquad (5.41)$$

Figure 5.8 represents the converter in the null state when $S_d = 0$.

The model equations for the system while the switch S_d is off is given as the following

$$V_{dd} = r_1 I_1 + L_1 p I_1 + V_{c2} \qquad (5.42)$$

$$V_{dd} = r_2 I_2 + L_2 p I_2 + V_{c1} \qquad (5.43)$$

$$C_1 p V_{c1} = I_2 - I_L \qquad (5.44)$$
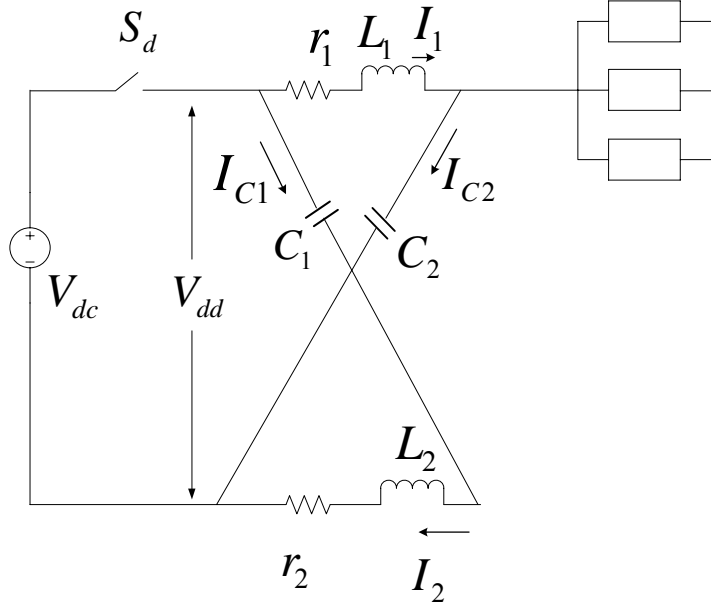
Figure 5.8: Null State of ZSI when $S_d = 0$

$$C_2 p V_{c2} = I_1 - I_L \tag{5.45}$$

$$V_{dd} = \frac{L_1}{L_1 + L_2}\left(r_2 I_2 + V_{c2}\right) + \frac{L_2}{L_1 + L_2}\left(r_1 I_1 + V_{c1}\right) \tag{5.46}$$

$$I_d = 0 \tag{5.47}$$

$$I_L = 0 \tag{5.48}$$

$$V_o = V_{c1} + V_{c2} - V_{dd} \tag{5.49}$$

5.3 Averaging Technique

The averaging technique is performed to generalize the equations in all the modes of operation. Generally, the model is averaged over one period of time. In this case, the averaging is performed for a switching cycle.

5.3.1 Derivation of Generalized Equations

The equations in all the six operating modes can be generalized by utilizing the averaging technique and the equations can be written as the following

$$L_1 pI_1 = S_A\left(S_d\left(V_{dd} - r_1 I_1 - V_{c2}\right) + \left(1 - S_d\right)\left(V_{dd} - r_1 I_1 - V_{c2}\right)\right)$$

$$+ S_B\left(S_d\left(V_{dd} - r_1 I_1 - V_{c2}\right) + \left(1 - S_d\right)\left(V_{dd} - r_1 I_1 - V_{c2}\right)\right)$$

$$+ S_C\left(S_d\left(V_{dd} - r_1 I_1 - V_{c2}\right) + \left(1 - S_d\right)\left(V_{dd} - r_1 I_1 - V_{c2}\right)\right) \quad (5.50)$$

$$L_2 pI_2 = S_A\left(S_d\left(V_{dd} - r_2 I_2 - V_{c1}\right) + \left(1 - S_d\right)\left(V_{dd} - r_2 I_2 - V_{c1}\right)\right)$$

$$+ S_B\left(S_d\left(V_{dd} - r_2 I_2 - V_{c1}\right) + \left(1 - S_d\right)\left(V_{dd} - r_2 I_2 - V_{c1}\right)\right)$$

$$+ S_C\left(S_d\left(V_{dd} - r_2 I_2 - V_{c1}\right) + \left(1 - S_d\right)\left(V_{dd} - r_2 I_2 - V_{c1}\right)\right) \quad (5.51)$$

$$C_1 pV_{c1} = S_A\left(S_d\left(I_2 - I_L\right) + \left(1 - S_d\right)\left(I_2 - I_L\right)\right) + S_B\left(S_d\left(I_2 - I_L\right) + \left(1 - S_d\right)\left(I_2 - I_L\right)\right)$$

$$+ S_C\left(S_d\left(I_2 - I_L\right) + \left(1 - S_d\right)\left(I_2 - I_L\right)\right) \quad (5.52)$$

$$C_2 pV_{c2} = S_A\left(S_d\left(I_1 - I_L\right) + \left(1 - S_d\right)\left(I_1 - I_L\right)\right) + S_B\left(S_d\left(I_1 - I_L\right) + \left(1 - S_d\right)\left(I_1 - I_L\right)\right)$$

$$+ S_C\left(S_d\left(I_1 - I_L\right) + \left(1 - S_d\right)\left(I_1 - I_L\right)\right) \quad (5.53)$$

$$V_{dd} = S_A\left(S_d V_{dc} + \left(1 - S_d\right)\left(\frac{L_1}{L_1 + L_2}\left(\left(r_2 I_2 + V_{c2}\right) + \frac{L_2}{L_1 + L_2}\left(r_1 I_1 + V_{c1}\right)\right)\right)\right)$$

$$+ S_B\left(S_d V_{dc} + \left(1 - S_d\right)\left(V_{c1} + V_{c2}\right)\right)$$

$$+ S_C\left(S_d V_{dc} + \left(1 - S_d\right)\left(\frac{L_1}{L_1 + L_2}\left(\left(r_2 I_2 + V_{c2}\right) + \frac{L_2}{L_1 + L_2}\left(r_1 I_1 + V_{c1}\right)\right)\right)\right) \quad (5.54)$$

$$V_{abcs} = S_A\left(S_d\left(R_L I_{abcs} + L_L pI_{abcs}\right) + \left(1 - S_d\right)\left(R_L I_{abcs} + L_L pI_{abcs}\right)\right) \quad (5.55)$$

$$I_d = S_A S_d\left(I_1 + I_2 - I_L\right) + S_B S_d\left(I_1 + I_2 - I_L\right) + S_C S_d\left(I_1 + I_2\right) \quad (5.56)$$

$$I_L = S_A \left(S_d \left(S_{ap} I_{as} + S_{bp} I_{bs} + S_{cp} I_{cs} \right) + \left(1 - S_d \right) \left(I_1 + I_2 \right) \right)$$

$$+ S_B \left(S_d \left(\frac{I_1 C_1 + I_2 C_2}{C_1 + C_2} \right) + \left(1 - S_d \right) \left(I_1 + I_2 \right) \right) \tag{5.57}$$

$$V_o = S_A \left(S_d \left(V_{c1} + V_{c2} - V_{dd} \right) + \left(1 - S_d \right) \left(V_{c1} + V_{c2} - V_{dd} \right) \right)$$

$$+ S_B \left(S_d \left(V_{c1} + V_{c2} - V_{dd} \right) + \left(1 - S_d \right) \left(V_{c1} + V_{c2} - V_{dd} \right) \right)$$

$$+ S_c \left(S_d \left(V_{c1} + V_{c2} - V_{dd} \right) + \left(1 - S_d \right) \left(V_{c1} + V_{c2} - V_{dd} \right) \right) \tag{5.58}$$

Equations (5.50)-(5.57) are simplified by grouping the common terms and are expressed as shown in (5.59)-(5.67)

$$L_1 p I_1 = \left(S_A + S_B + S_C \right) \left(S_d \left(V_{dd} - r_1 I_1 - V_{c2} \right) \right) + \left(S_A + S_B + S_C \right) \left(\left(1 - S_d \right) \left(V_{dd} - r_1 I_1 - V_{c2} \right) \right)$$
$$\tag{5.59}$$

$$L_2 p I_2 = \left(S_A + S_B + S_C \right) \left(S_d \left(V_{dd} - r_2 I_2 - V_{c1} \right) \right) + \left(S_A + S_B + S_C \right) \left(\left(1 - S_d \right) \left(V_{dd} - r_2 I_2 - V_{c1} \right) \right)$$
$$\tag{5.60}$$

$$C_1 p V_{c1} = \left(S_A + S_B + S_C \right) \left(S_d \left(I_1 - I_L \right) + \left(1 - S_d \right) \left(I_1 - I_L \right) \right) \tag{5.61}$$

$$C_2 p V_{c2} = \left(S_A + S_B + S_C \right) \left(S_d \left(I_2 - I_L \right) + \left(1 - S_d \right) \left(I_2 - I_L \right) \right) \tag{5.62}$$

$$V_{dd} = \left(S_A + S_B + S_C \right) \left(S_d V_{dc} \right)$$

$$+ \left(S_A + S_C \right) \left(\left(1 - S_d \right) \left(\frac{L_1}{L_1 + L_2} \left(\left(r_2 I_2 + V_{c2} \right) + \frac{L_2}{L_1 + L_2} \left(r_1 I_1 + V_{c1} \right) \right) \right) \right) \tag{5.63}$$

$$V_{abcs} = S_A \left(S_d \left(R_L I_{abcs} + L_L p I_{abcs} \right) + \left(1 - S_d \right) \left(R_L I_{abcs} + L_L p I_{abcs} \right) \right) \tag{5.64}$$

$$I_d = \left(S_A + S_B \right) S_d \left(I_1 + I_2 - I_L \right) + S_C S_d \left(I_1 + I_2 \right) \tag{5.65}$$

$$I_L = S_A \left(S_d \left(S_{ap} I_{as} + S_{bp} I_{bs} + S_{cp} I_{cs} \right) \right) + \left(S_A + S_B \right) \left(1 - S_d \right) \left(I_1 + I_2 \right)$$

$$+ S_B \left(S_d \left(\frac{I_1 C_1 + I_2 C_2}{C_1 + C_2} \right) + \left(1 - S_d \right) \left(I_1 + I_2 \right) \right) \tag{5.66}$$

$$V_o = \left(S_A + S_C \right) \left(S_d \left(V_{c1} + V_{c2} - V_{dd} \right) \right) + \left(S_A + S_C \right) \left(\left(1 - S_d \right) \left(V_{c1} + V_{c2} - V_{dd} \right) \right) \tag{5.67}$$

The combined equations (5.59)-(5.67) can be further simplified using the expression (5.68) and the resulting equations are expressed as shown in (5.69)-(5.77)

$$S_A + S_B + S_C = 1 \tag{5.68}$$

$$L_1 pI_1 = V_{dd} - r_1 I_1 - V_{c2} \tag{5.69}$$

$$L_2 pI_2 = V_{dd} - r_2 I_2 - V_{c1} \tag{5.70}$$

$$C_1 pV_{c1} = I_2 - I_L \tag{5.71}$$

$$C_2 pV_{c2} = I_1 - I_L \tag{5.72}$$

$$V_{dd} = S_d V_{dc} + (1 - S_d)(S_A + S_C)\left(\frac{L_1}{L_1 + L_2}(r_2 I_2 + V_{c2}) + \frac{L_2}{L_1 + L_2}(r_1 I_1 + V_{c1})\right) + (1 - S_d)S_B(V_{c1} + V_{c2}) \tag{5.73}$$

$$V_{abcs} = S_A(R_L I_{abcs} + L_L pI_{abcs}) \tag{5.74}$$

$$I_d = S_d(S_A + S_B)(I_1 + I_2 - I_L) + S_d S_C(I_1 + I_2) \tag{5.75}$$

$$I_L = S_d S_A(S_{ap} I_{as} + S_{bp} I_{bs} + S_{cp} I_{cs}) + (1 - S_d)(S_A + S_B)(I_1 + I_2) + S_d S_B\left(\frac{I_1 C_1 + I_2 C_2}{C_1 + C_2}\right) \tag{5.76}$$

$$V_o = (S_A + S_B)(V_{c1} + V_{c2} - V_{dd}) \tag{5.77}$$

For simplifying the simulation, a balanced case as well as the following is assumed.

$$r_1 = r_2 = r$$

$$L_1 = L_2 = L \tag{5.78}$$

$$C_1 = C_2 = C$$

Hence the equations used for the simulation when an RL load is used are given as

$$pI_1 = \frac{1}{L}(V_{dd} - rI_1 - V_{c2}) \tag{5.79}$$

$$pI_2 = \frac{1}{L}\left(V_{dd} - rI_2 - V_{c1}\right) \tag{5.80}$$

$$pV_{c1} = \frac{1}{C}\left(I_2 - I_L\right) \tag{5.81}$$

$$pV_{c2} = \frac{1}{C}\left(I_1 - I_L\right) \tag{5.82}$$

$$V_{dd} = S_d V_{dc} + \left(1 - S_d\right)\left(S_A + S_C\right)\left(\frac{1}{2}\left(rI_2 + V_{c2} + rI_1 + V_{c1}\right)\right) + \left(1 - S_d\right)S_B\left(V_{c1} + V_{c2}\right) \tag{5.83}$$

$$I_d = S_d\left(S_A + S_B\right)\left(I_1 + I_2 - I_L\right) + S_d S_C\left(I_1 + I_2\right) \tag{5.84}$$

$$I_L = S_d S_A\left(S_{ap}I_{as} + S_{bp}I_{bs} + S_{cp}I_{cs}\right) + \left(1 - S_d\right)\left(S_A + S_B\right)\left(I_1 + I_2\right) + S_d S_B\left(\frac{I_1 + I_2}{2}\right) \tag{5.85}$$

$$V_o = \left(S_A + S_B\right)\left(V_{c1} + V_{c2} - V_{dd}\right) \tag{5.86}$$

The load current equations for an RL load are given as

$$pI_{as} = \frac{1}{L_s}\left(\frac{V_o}{3}\left(2S_{ap} - S_{bp} - S_{cp}\right) - r_s I_{as}\right) \tag{5.87}$$

$$pI_{bs} = \frac{1}{L_s}\left(\frac{V_o}{3}\left(-S_{ap} + 2S_{bp} - S_{cp}\right) - r_s I_{bs}\right) \tag{5.88}$$

$$pI_{cs} = \frac{1}{L_s}\left(\frac{V_o}{3}\left(-S_{ap} - S_{bp} + 2S_{cp}\right) - r_s I_{cs}\right) \tag{5.89}$$

5.3.2 Dynamic Analysis Results

The simulation results when an RL Load is used are shown below.

(a)

(b)

(c)
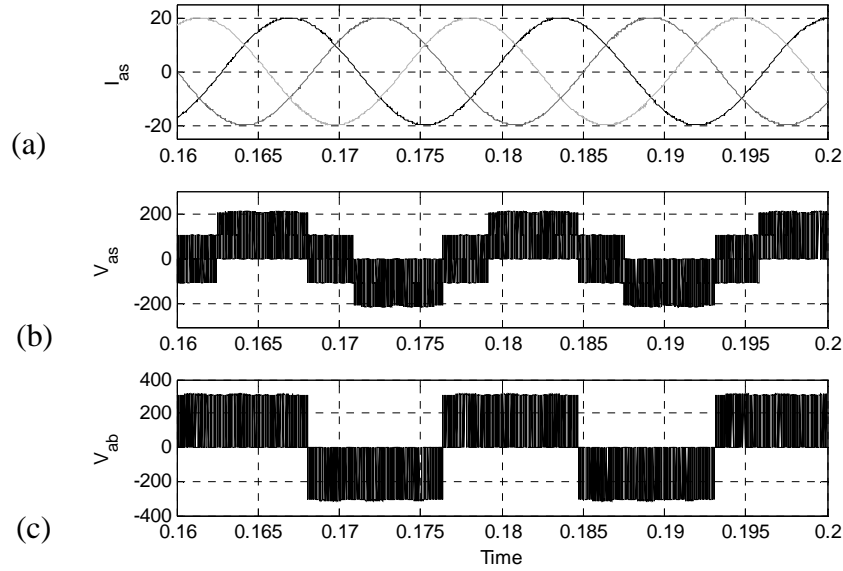
Figure 5.9: (a) Three-phase load currents, (b) Phase 'a' output voltage, (c) Line voltage
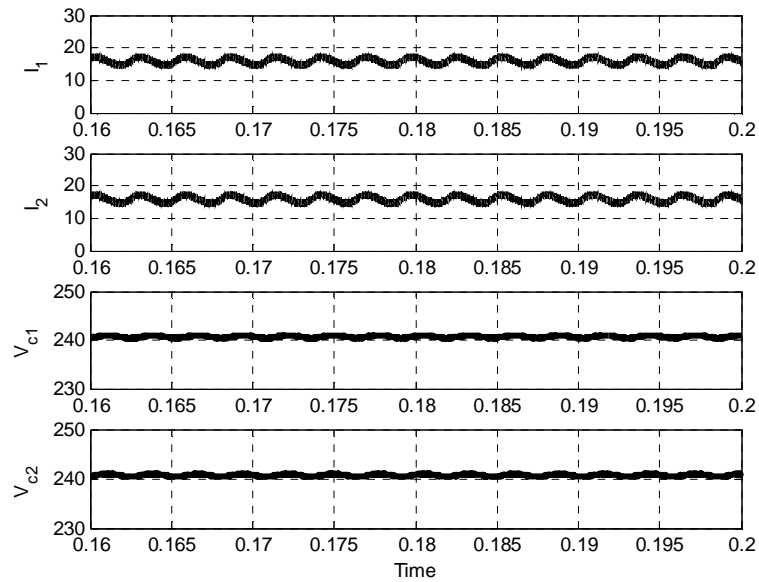
Figure 5.10: (a-b) Inductor currents of the Z-Network, (c-d) Capacitor voltages of the Z-

Network

120
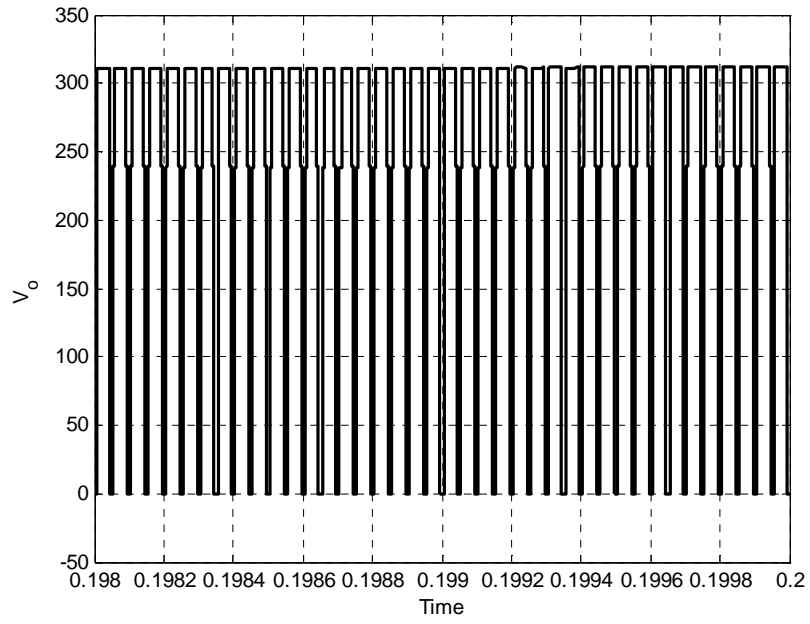
Figure 5.11: Output voltage of the Z-network, V_o
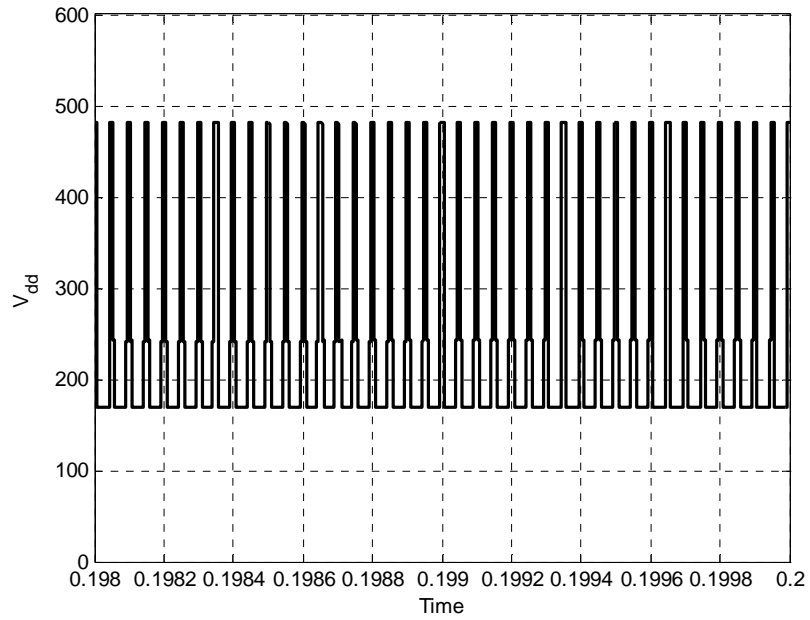
Figure 5.12: Input voltage to the Z-network, V_{dd}
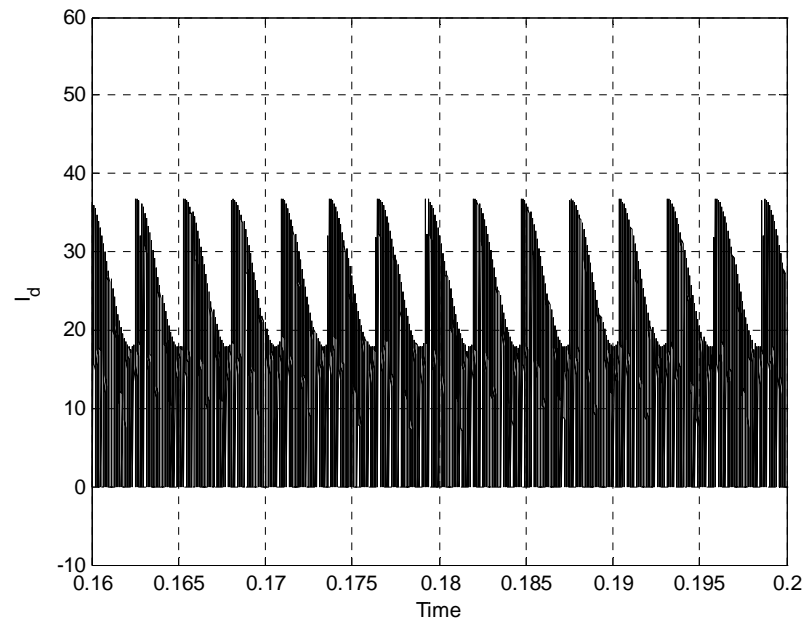
Figure 5.13: Input current to the Z-Network, I_d
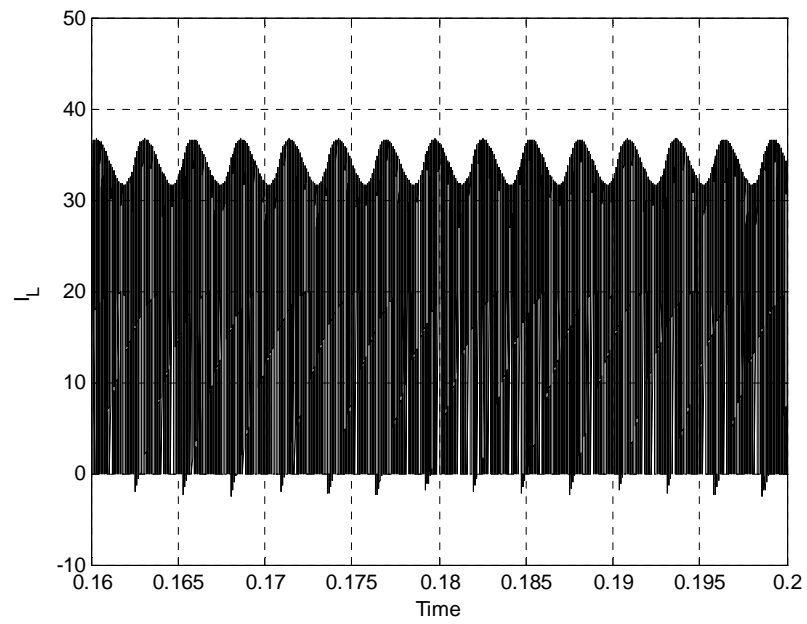
Figure 5.14: Output current of the Z-Network, I_L

122

5.3 Steady State Analysis of Z-Source Inverter

The steady-state analysis of the system is done using the state equations of the system in the synchronous reference frame, as the variables in the equation are time-invariant with respect to the frame of reference. The steady-state analysis of any system is carried out to study the nature of the system at steady state and use the analysis to control the response of the system.

5.3.1 Derivation of the Steady State Analysis

The derivative terms in the above generalized equations are set to zero and the steady state equations of the system after using the averaging technique to eliminate the switching functions are expressed as

$$I_L = \frac{-\dfrac{3R(M_{qs}^2 + M_{ds}^2)(1-D_o)V_{dc}}{2(R^2 + (\omega_e L)^2)(2D_o - 1)}}{1 + \dfrac{3R(M_{qs}^2 + M_{ds}^2)(1-D_o)^2 r}{(R^2 + (\omega_e L)^2)(2D_o - 1)^2}} \tag{5.90}$$

$$I_1 = I_2 = \frac{1-D_o}{2D_o - 1}\left(\frac{-\dfrac{3R(M_{qs}^2 + M_{ds}^2)(1-D_o)V_{dc}}{2(R^2 + (\omega_e L)^2)(2D_o - 1)}}{1 + \dfrac{3R(M_{qs}^2 + M_{ds}^2)(1-D_o)^2 r}{(R^2 + (\omega_e L)^2)(2D_o - 1)^2}}\right) \tag{5.91}$$

$$V_o = \frac{-2(1-D_o)^2 r I_L}{(2D_o - 1)^2} - \frac{(1-D_o)V_{dc}}{(2D_o - 1)} \tag{5.92}$$

$$V_{dd} = \frac{-2D_o(1-D_o)rI_L}{(2D_o-1)^2} - \frac{2(1-D_o)}{(2D_o-1)} \quad (5.93)$$

$$I_d = \frac{I_L(1-D_o)}{(2D_o-1)} \quad (5.94)$$

$$V_{c1} = V_{c2} = \frac{-(1-D_o)rI_L}{(2D_o-1)^2} - \frac{(1-D_o)V_{dc}}{(2D_o-1)} \quad (5.95)$$

5.3.2 Steady State Analysis Results

The steady state results for an RL load. The voltages are normalized with respect to the input DC voltage.
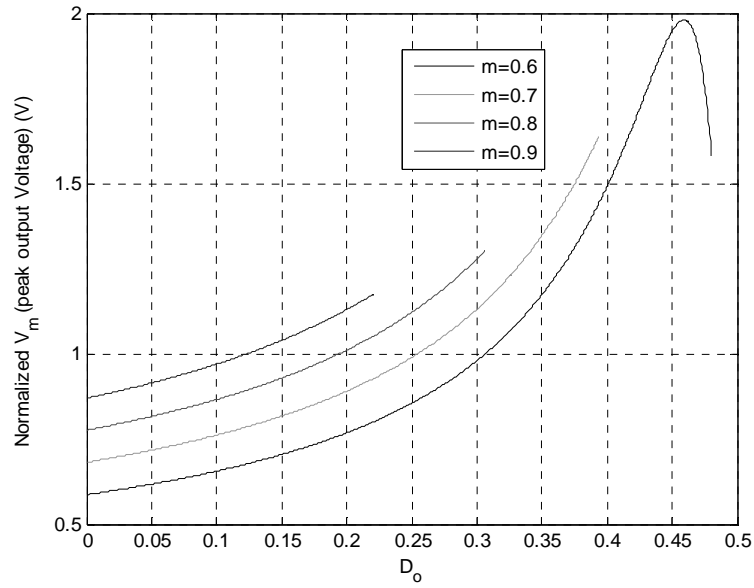
Figure 5.15: Normalized peak output voltage, V_m for varying modulation index
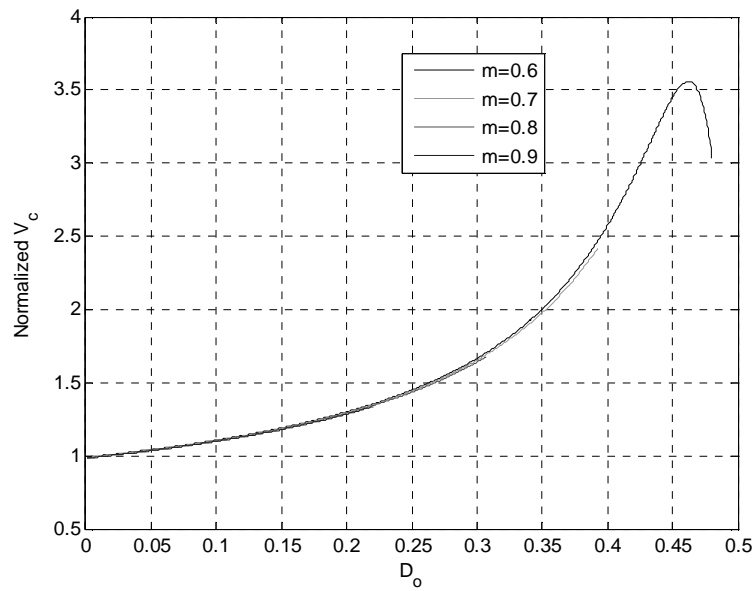
Figure 5.16: Normalized capacitor voltage, V_c of the Z-network, for varying modulation
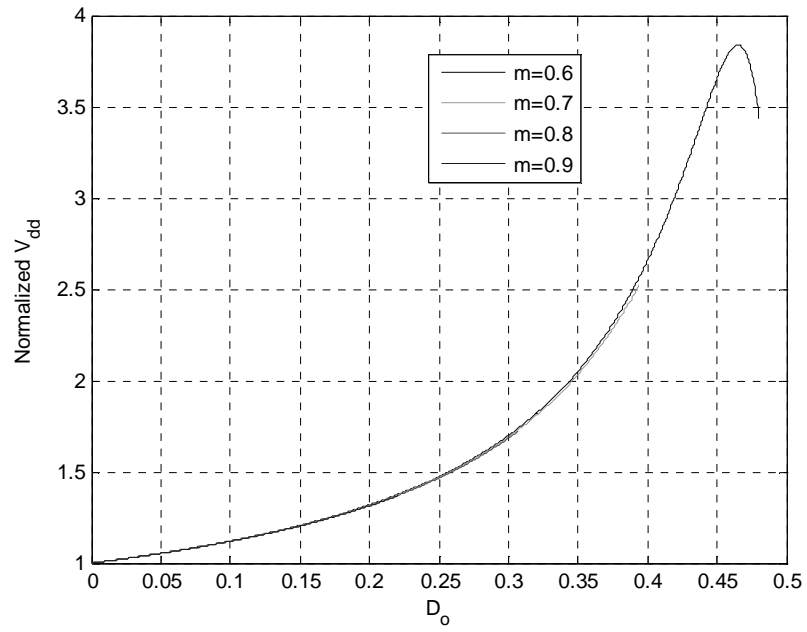
index

Figure 5.17: Normalized input voltage to the Z-network, V_{dd} for varying modulation
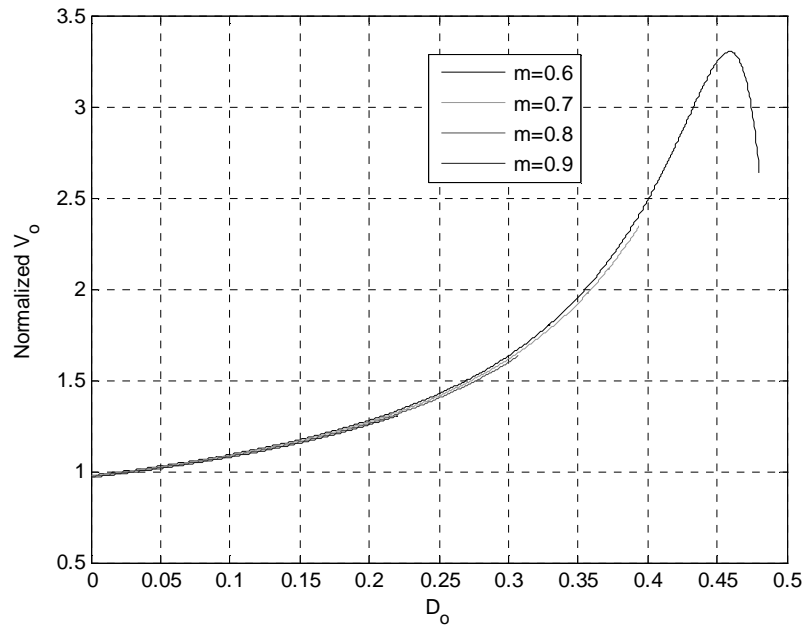
index

Figure 5.18: Normalized DC output voltage of the Z-network, V_o for varying modulation
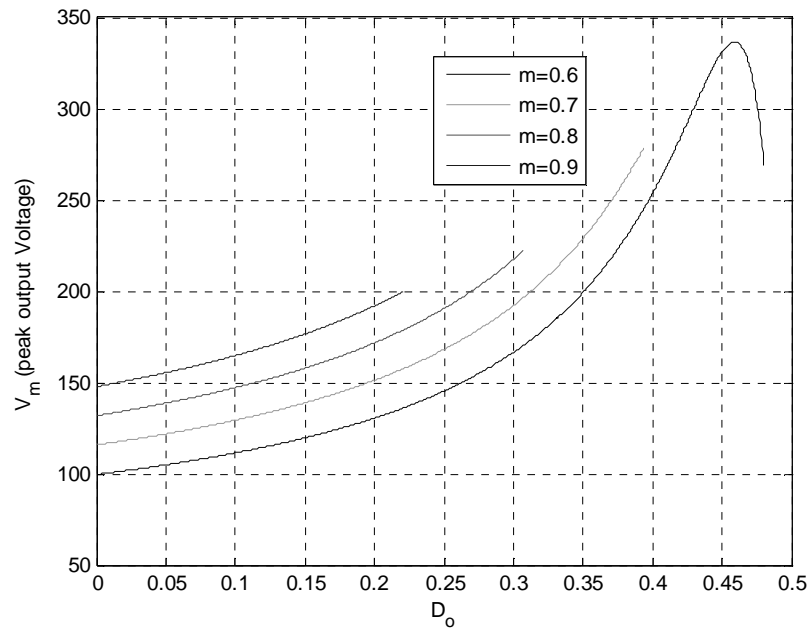
index

Figure 5.19: Output voltage of the inverter, V_m for varying modulation index
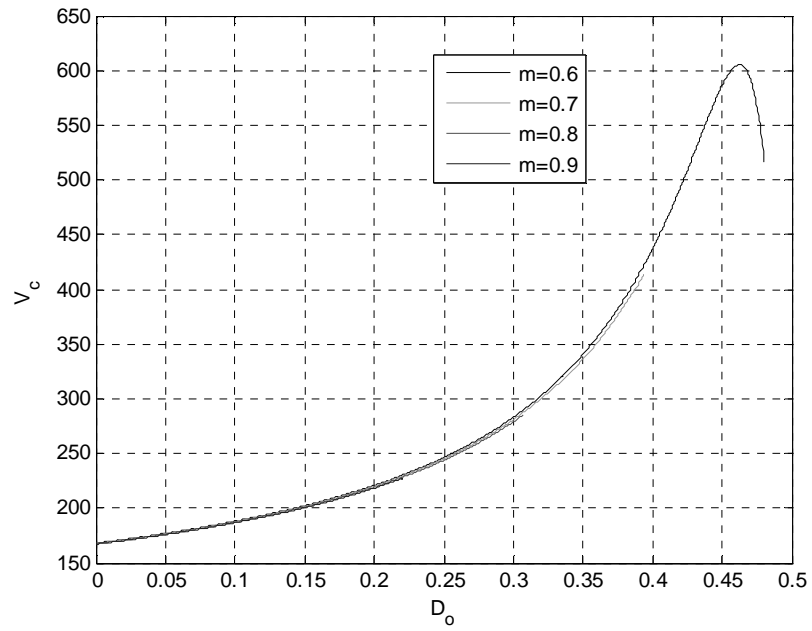
Figure 5.20: Capacitor voltage of the Z-network, V_c for varying modulation index
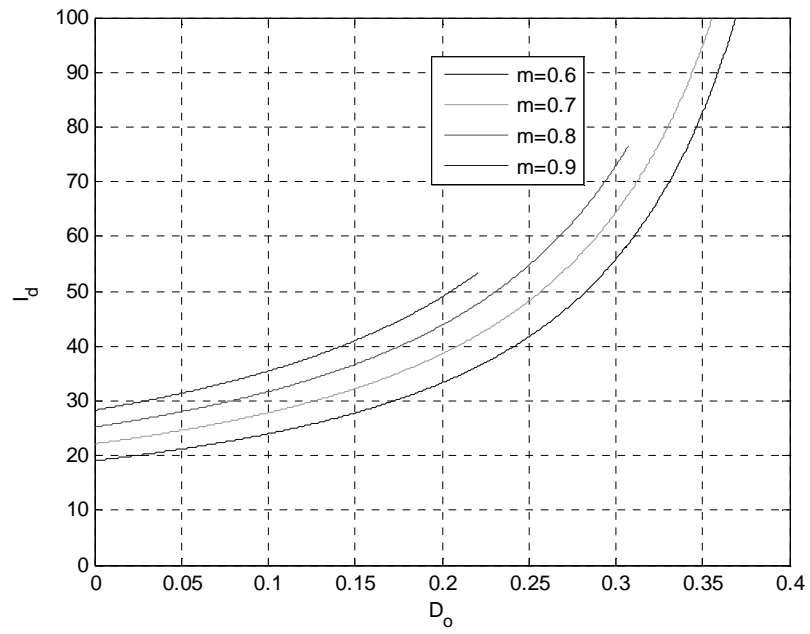
Figure 5.21: Input DC current to the Z-network, I_d for varying modulation index
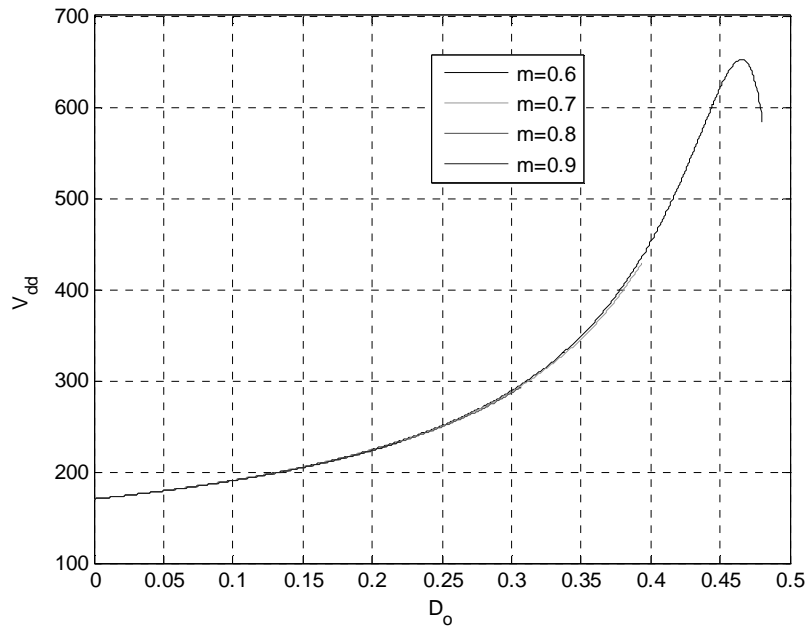
Figure 5.22: Input voltage to the Z-network, V_{dd} for varying modulation index
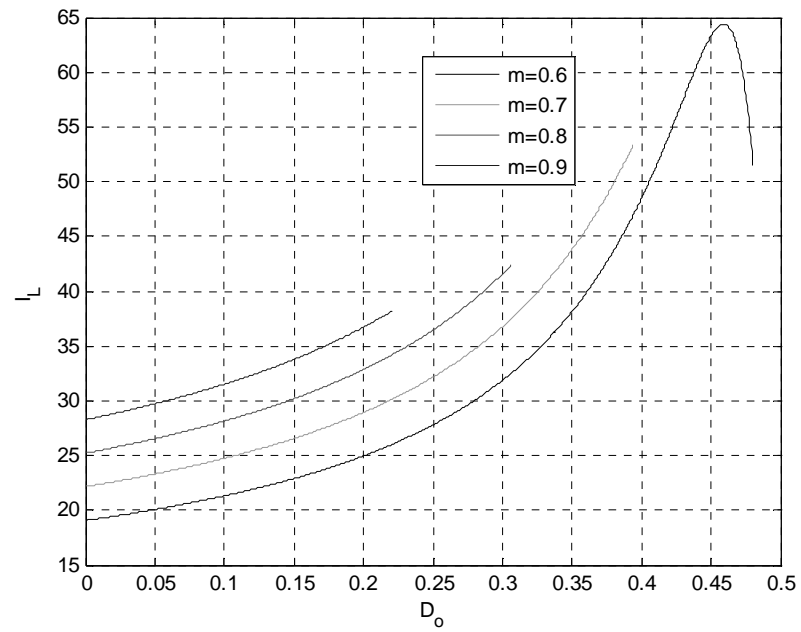
Figure 5.23: Output current of the Z-network, I_L for varying modulation index
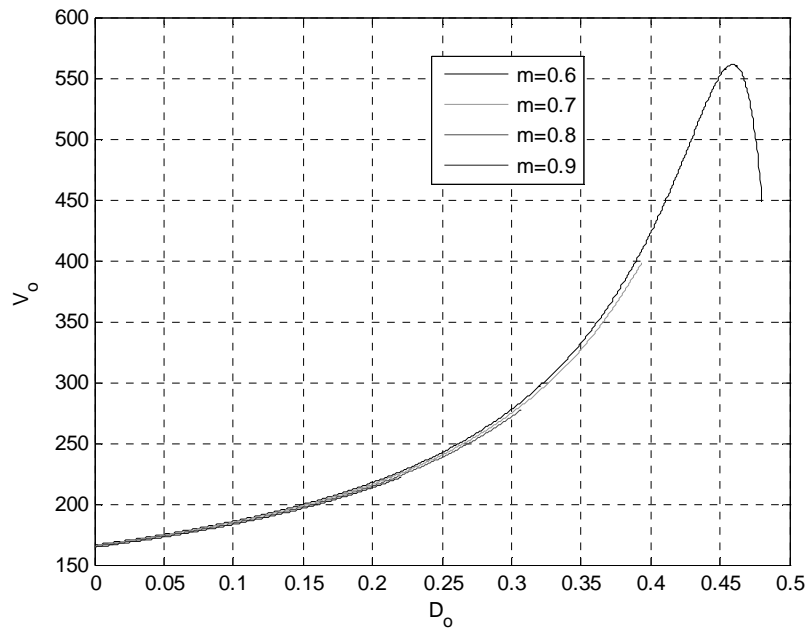
Figure 5.24: Output voltage of the Z-network, V_o for varying modulation index

5.4 Small Signal Analysis

The small signal analysis is performed by state space averaging which is performed as follows.

5.4.1 Derivation of Characteristic Matrix

Let the state equations be of the form

$$\dot{x} = f(x) \tag{5.77}$$

A small change is introduced in all the state variables and they are simplified in order to get the expression as shown below.

$$\Delta\dot{x}(s) = A\Delta x(s) + B\Delta u(s) + D\Delta e(s) \tag{5.78}$$

Where x - equilibrium (dc) state vector

   u - equilibrium (dc) control vector

   e - equilibrium (dc) input vector

   A, B, D - co-efficient matrices

The dynamic equations of the system are used to perform the small signal analysis.

$$pI_1 = \frac{1}{L}\left(\left(S_d V_{dc} + (1-S_d)(S_A + S_C)\left(\frac{1}{2}(rI_2 + V_{c2} + rI_1 + V_{c1})\right) + (1-S_d)S_B(V_{c1} + V_{c2})\right) - rI_1 - V_{c2}\right) \tag{5.96}$$

$$pI_2 = \frac{1}{L}\left(\left(S_d V_{dc} + (1 - S_d)(S_A + S_C)\left(\frac{1}{2}(rI_2 + V_{c2} + rI_1 + V_{c1})\right) + (1 - S_d)S_B(V_{c1} + V_{c2})\right) - rI_2 - V_{c1}\right)$$

(5.97)

$$pV_{c1} = \frac{1}{C}\left(I_2 - S_d S_A(S_{ap} I_{as} + S_{bp} I_{bs} + S_{cp} I_{cs}) + (1 - S_d)(S_A + S_B)(I_1 + I_2) + S_d S_B\left(\frac{I_1 + I_2}{2}\right)\right)$$

(5.98)

$$pV_{c2} = \frac{1}{C}\left(I_1 - S_d S_A(S_{ap} I_{as} + S_{bp} I_{bs} + S_{cp} I_{cs}) + (1 - S_d)(S_A + S_B)(I_1 + I_2) + S_d S_B\left(\frac{I_1 + I_2}{2}\right)\right)$$

(5.99)

$$pI_{as} = \frac{1}{L_s}\left(\frac{V_o}{3}(2S_{ap} - S_{bp} - S_{cp}) - r_s I_{as}\right)$$

(5.100)

$$pI_{bs} = \frac{1}{L_s}\left(\frac{V_o}{3}(-S_{ap} + 2S_{bp} - S_{cp}) - r_s I_{bs}\right)$$

(5.101)

$$pI_{cs} = \frac{1}{L_s}\left(\frac{V_o}{3}(-S_{ap} - S_{bp} + 2S_{cp}) - r_s I_{cs}\right)$$

(5.102)

$$V_o = (S_A + S_B)\left(V_{c1} + V_{c2} - \left(\begin{array}{c} S_d V_{dc} + (1 - S_d)(S_A + S_C)\left(\frac{1}{2}(rI_2 + V_{c2} + rI_1 + V_{c1})\right) \\ + (1 - S_d)S_B(V_{c1} + V_{c2}) \end{array}\right)\right)$$

(5.103)

By perturbing the above equations using the following expressions to bring in a very small change

$$V_{dc} = V_{dco} + \Delta V_{dc}$$

$$I_1 = I_{1o} + \Delta I_{1o}$$

$$I_2 = I_{2o} + \Delta I_{2o}$$

$$V_{c1} = V_{c1o} + \Delta V_{c1}$$

$$V_{c2} = V_{c2o} + \Delta V_{c2}$$

131

$$I_{as} = I_{aso} + \Delta I_{as}$$

$$I_{bs} = I_{bso} + \Delta I_{bs}$$

$$I_{cs} = I_{cso} + \Delta I_{cs}$$

$$S_d = S_{do} + \Delta S_d$$

$$S_A = S_{Ao} + \Delta S_A$$

$$S_B = S_{Bo} + \Delta S_B$$

$$S_C = S_{Co} + \Delta S_C$$

$$S_{ap} = S_{apo} + \Delta S_{ap}$$

$$S_{bp} = S_{bpo} + \Delta S_{bp}$$

$$S_{cp} = S_{cpo} + \Delta S_{cp}$$

$$V_o = \left(S_{Ao} + \Delta S_A + S_{Bo} + \Delta S_B \right) \left(\begin{array}{l} V_{c1o} + \Delta V_{c1} + V_{c2o} + \Delta V_{c2} - \\ \left(\begin{array}{l} \left(S_{do} + \Delta S_d \right)\left(V_{dco} + \Delta V_{dc} \right) \\ + \left(1 - S_{do} - \Delta S_d \right)\left(S_{Ao} + \Delta S_A + S_{Co} + \Delta S_C \right) \end{array} \right) \\ \left(\frac{1}{2}\left(rI_{2o} + r\Delta I_2 + V_{c2o} + \Delta V_{c2} + rI_{1o} + r\Delta I_1 + V_{c1o} + \Delta V_{c1} \right) \right) \\ + \left(1 - S_{do} - \Delta S_d \right)\left(S_{Bo} + \Delta S_B \right)\left(V_{c1o} + \Delta V_{c1} + V_{c2o} + \Delta V_{c2} \right) \end{array} \right)$$

(5.104)

$$p\left(\Delta I_{1o} \right) = \frac{1}{L} \left(\begin{array}{l} \left(V_{dco} - S_{Ao} - S_{Co} - S_{Bo}V_{c1o} - S_{Bo}V_{c2o} \right)\Delta S_d + S_{do}\Delta V_{dc} + \left(1 + S_{do} \right)\Delta S_A \\ + \left(1 - S_{do} \right)\Delta S_C + \left(-\frac{r}{2} \right)\Delta I_{1o} + \left(\frac{r}{2} \right)\Delta I_{2o} + \left(\frac{1}{2} + S_{Bo} - S_{do}S_{Bo} \right)\Delta V_{c1} \\ + \left(-\frac{1}{2} + S_{Bo} - S_{do}S_{Bo} \right)\Delta V_{c2} + \left(V_{c1o} + V_{c2o} - S_{do}V_{c1o} - S_{do}V_{c2o} \right)\Delta S_B \end{array} \right)$$

(5.105)

$$p(\Delta I_{2o}) = \frac{1}{L} \left(\begin{array}{l} (V_{dco} - S_{Ao} - S_{Co} - S_{Bo}V_{c1o} - S_{Bo}V_{c2o})\Delta S_d + S_{do}\Delta V_{dc} + (1 + S_{do})\Delta S_A \\ + (1 - S_{do})\Delta S_C + \left(-\frac{r}{2}\right)\Delta I_{1o} + \left(\frac{r}{2}\right)\Delta I_{2o} + \left(-\frac{1}{2} + S_{Bo} - S_{do}S_{Bo}\right)\Delta V_{c1} \\ + \left(\frac{1}{2} + S_{Bo} - S_{do}S_{Bo}\right)\Delta V_{c2} + (V_{c1o} + V_{c2o} - S_{do}V_{c1o} - S_{do}V_{c2o})\Delta S_B \end{array} \right) \quad (5.106)$$

$$p(\Delta V_{c1}) = \frac{1}{C} \left(\begin{array}{l} \left(1 + S_{Ao} + S_{Bo} - S_{do}S_{Ao} - \frac{1}{2}S_{do}S_{Bo}\right)\Delta I_{2o} + \left(S_{Ao} + S_{Bo} - S_{do}S_{Ao} - \frac{1}{2}S_{do}S_{Bo}\right)\Delta I_{1o} \\ + (-S_{do} + I_{1o} + I_{2o} - S_{do}I_{1o} - S_{do}I_{2o})\Delta S_A + \left(I_{1o} + I_{2o} - \frac{1}{2}S_{do}I_{1o} - \frac{1}{2}S_{do}I_{2o}\right)\Delta S_B \\ + \left(-S_{Ao} - S_{Ao}I_{1o} - S_{Ao}I_{2o} - \frac{1}{2}S_{Bo}I_{1o} - \frac{1}{2}S_{Bo}I_{2o}\right)\Delta S_d + S_{apo}\Delta I_{as} + I_{aso}\Delta S_{ap} \\ + S_{bpo}\Delta I_{bs} + I_{bso}\Delta S_{bp} + S_{cpo}\Delta I_{cs} + I_{cso}\Delta S_{cp} \end{array} \right)$$

$$(5.107)$$

$$p(\Delta V_{c2}) = \frac{1}{C} \left(\begin{array}{l} \left(1 + S_{Ao} + S_{Bo} - S_{do}S_{Ao} - \frac{1}{2}S_{do}S_{Bo}\right)\Delta I_{1o} + \left(S_{Ao} + S_{Bo} - S_{do}S_{Ao} - \frac{1}{2}S_{do}S_{Bo}\right)\Delta I_{2o} \\ + (-S_{do} + I_{1o} + I_{2o} - S_{do}I_{1o} - S_{do}I_{2o})\Delta S_A + \left(I_{1o} + I_{2o} - \frac{1}{2}S_{do}I_{1o} - \frac{1}{2}S_{do}I_{2o}\right)\Delta S_B \\ + \left(-S_{Ao} - S_{Ao}I_{1o} - S_{Ao}I_{2o} - \frac{1}{2}S_{Bo}I_{1o} - \frac{1}{2}S_{Bo}I_{2o}\right)\Delta S_d + S_{apo}\Delta I_{as} + I_{aso}\Delta S_{ap} \\ + S_{bpo}\Delta I_{bs} + I_{bso}\Delta S_{bp} + S_{cpo}\Delta I_{cs} + I_{cso}\Delta S_{cp} \end{array} \right)$$

$$(5.108)$$

$$p(\Delta I_{as}) = \frac{1}{L_s} \left(\frac{(2S_{apo} - S_{bpo} - S_{cpo})\Delta V_o + 2V_o\Delta S_{ap} - V_o\Delta S_{bp} - V_o\Delta S_{cp}}{3} - r_s\Delta I_{as} \right) \quad (5.109)$$

$$p(\Delta I_{bs}) = \frac{1}{L_s} \left(\frac{(-S_{apo} + 2S_{bpo} - S_{cpo})\Delta V_o - V_o\Delta S_{ap} + 2V_o\Delta S_{bp} + V_o\Delta S_{cp}}{3} - r_s\Delta I_{bs} \right) \quad (5.110)$$

$$p(\Delta I_{cs}) = \frac{1}{L_s} \left(\frac{(-S_{apo} - S_{bpo} + 2S_{cpo})\Delta V_o - V_o\Delta S_{ap} - V_o\Delta S_{bp} + 2V_o\Delta S_{cp}}{3} - r_s\Delta I_{cs} \right) \quad (5.111)$$

$$
\begin{bmatrix} p\Delta I_{1o} \\ p\Delta I_{2o} \\ p\Delta V_{c1} \\ p\Delta V_{c2} \\ p\Delta I_{as} \\ p\Delta I_{bs} \\ p\Delta I_{cs} \end{bmatrix} =
\begin{bmatrix}
-\dfrac{r}{2L} & \dfrac{r}{2L} & \dfrac{1}{L}\left(\dfrac{1}{2}+S_{Bo}-S_{do}S_{Bo}\right) & \dfrac{1}{L}\left(-\dfrac{1}{2}+S_{Bo}-S_{do}S_{Bo}\right) & 0 & 0 & 0 \\[2mm]
-\dfrac{r}{2L} & \dfrac{r}{2L} & \dfrac{1}{L}\left(-\dfrac{1}{2}+S_{Bo}-S_{do}S_{Bo}\right) & \dfrac{1}{L}\left(\dfrac{1}{2}+S_{Bo}-S_{do}S_{Bo}\right) & 0 & 0 & 0 \\[2mm]
\dfrac{1}{C}\left(S_{Ao}+S_{Bo}-S_{do}S_{Ao}-\dfrac{1}{2}S_{do}S_{Bo}\right) & \dfrac{1}{C}\left(1+S_{Ao}+S_{Bo}-S_{do}S_{Ao}-\dfrac{1}{2}S_{do}S_{Bo}\right) & 0 & 0 & \dfrac{S_{apo}}{C} & \dfrac{S_{bpo}}{C} & \dfrac{S_{cpo}}{C} \\[2mm]
\dfrac{1}{C}\left(1+S_{Ao}+S_{Bo}-S_{do}S_{Ao}-\dfrac{1}{2}S_{do}S_{Bo}\right) & \dfrac{1}{C}\left(S_{Ao}+S_{Bo}-S_{do}S_{Ao}-\dfrac{1}{2}S_{do}S_{Bo}\right) & 0 & 0 & \dfrac{S_{apo}}{C} & \dfrac{S_{bpo}}{C} & \dfrac{S_{cpo}}{C} \\[2mm]
0 & 0 & 0 & 0 & -\dfrac{r_s}{L_s} & 0 & 0 \\[2mm]
0 & 0 & 0 & 0 & 0 & -\dfrac{r_s}{L_s} & 0 \\[2mm]
0 & 0 & 0 & 0 & 0 & 0 & -\dfrac{r_s}{L_s}
\end{bmatrix}
\begin{bmatrix} \Delta I_{1o} \\ \Delta I_{2o} \\ \Delta V_{c1} \\ \Delta V_{c2} \\ \Delta I_{as} \\ \Delta I_{bs} \\ \Delta I_{cs} \end{bmatrix}
$$

$$
+
\begin{bmatrix}
S_{do} & 0 \\
S_{do} & 0 \\
0 & 0 \\
0 & 0 \\
0 & \dfrac{2S_{apo}-S_{bpo}-S_{cpo}}{3L_s} \\[2mm]
0 & \dfrac{-S_{apo}+2S_{bpo}-S_{cpo}}{3L_s} \\[2mm]
0 & \dfrac{-S_{apo}-S_{bpo}+2S_{cpo}}{3L_s}
\end{bmatrix}
\begin{bmatrix} \Delta V_{dc} \\ \Delta V_o \end{bmatrix}
$$

$$
\begin{bmatrix}
\frac{1}{L}(V_{dco} - S_{Ao} - S_{Co} - S_{Bo}V_{c1o} - S_{Bo}V_{c2o}) & \frac{1}{L}(1+S_{do}) & \frac{1}{L}(V_{c1o} + V_{c2o} - S_{do}V_{c1o} - S_{do}V_{c2o}) & \frac{1}{L}(1-S_{do}) & 0 & 0 & 0 \\[2mm]
\frac{1}{L}(V_{dco} - S_{Ao} - S_{Co} - S_{Bo}V_{c1o} - S_{Bo}V_{c2o}) & \frac{1}{L}(1+S_{do}) & \frac{1}{L}(V_{c1o} + V_{c2o} - S_{do}V_{c1o} - S_{do}V_{c2o}) & \frac{1}{L}(1-S_{do}) & 0 & 0 & 0 \\[2mm]
\frac{1}{C}\left(-S_{Ao} - S_{Ao}I_{1o} - S_{Ao}I_{2o} - \frac{1}{2}S_{Bo}I_{1o} - \frac{1}{2}S_{Bo}I_{2o}\right) & \frac{1}{C}\left(-S_{do} + I_{1o} + I_{2o} - S_{do}I_{1o} - S_{do}I_{2o}\right) & \frac{1}{C}\left(I_{1o} + I_{2o} - \frac{1}{2}S_{do}I_{1o} - \frac{1}{2}S_{do}I_{2o}\right) & 0 & \frac{I_{aso}}{C} & \frac{I_{bso}}{C} & \frac{I_{cso}}{C} \\[2mm]
\frac{1}{C}\left(-S_{Ao} - S_{Ao}I_{1o} - S_{Ao}I_{2o} - \frac{1}{2}S_{Bo}I_{1o} - \frac{1}{2}S_{Bo}I_{2o}\right) & \frac{1}{C}\left(-S_{do} + I_{1o} + I_{2o} - S_{do}I_{1o} - S_{do}I_{2o}\right) & \frac{1}{C}\left(I_{1o} + I_{2o} - \frac{1}{2}S_{do}I_{1o} - \frac{1}{2}S_{do}I_{2o}\right) & 0 & \frac{I_{aso}}{C} & \frac{I_{bso}}{C} & \frac{I_{cso}}{C} \\[2mm]
0 & 0 & 0 & 0 & \frac{2V_o}{3L_s} & -\frac{V_o}{3L_s} & -\frac{V_o}{3L_s} \\[2mm]
0 & 0 & 0 & 0 & -\frac{V_o}{3L_s} & \frac{2V_o}{3L_s} & -\frac{V_o}{3L_s} \\[2mm]
0 & 0 & 0 & 0 & -\frac{V_o}{3L_s} & -\frac{V_o}{3L_s} & \frac{2V_o}{3L_s}
\end{bmatrix}
\begin{bmatrix}
\Delta S_d \\
\Delta S_A \\
\Delta S_B \\
\Delta S_C \\
\Delta S_{ap} \\
\Delta S_{bp} \\
\Delta S_{cp}
\end{bmatrix}
$$

Here the characteristic matrix is

$$
A = \begin{bmatrix}
-\dfrac{r}{2L} & \dfrac{r}{2L} & \dfrac{1}{L}\left(\dfrac{1}{2}+S_{Bo}-S_{do}S_{Bo}\right) & \dfrac{1}{L}\left(-\dfrac{1}{2}+S_{Bo}-S_{do}S_{Bo}\right) & 0 & 0 & 0 \\[3mm]
-\dfrac{r}{2L} & \dfrac{r}{2L} & \dfrac{1}{L}\left(-\dfrac{1}{2}+S_{Bo}-S_{do}S_{Bo}\right) & \dfrac{1}{L}\left(\dfrac{1}{2}+S_{Bo}-S_{do}S_{Bo}\right) & 0 & 0 & 0 \\[3mm]
\dfrac{1}{C}\left(S_{Ao}+S_{Bo}-S_{do}S_{Ao}-\dfrac{1}{2}S_{do}S_{Bo}\right) & \dfrac{1}{C}\left(1+S_{Ao}+S_{Bo}-S_{do}S_{Ao}-\dfrac{1}{2}S_{do}S_{Bo}\right) & 0 & 0 & \dfrac{S_{apo}}{C} & \dfrac{S_{bpo}}{C} & \dfrac{S_{cpo}}{C} \\[3mm]
\dfrac{1}{C}\left(1+S_{Ao}+S_{Bo}-S_{do}S_{Ao}-\dfrac{1}{2}S_{do}S_{Bo}\right) & \dfrac{1}{C}\left(S_{Ao}+S_{Bo}-S_{do}S_{Ao}-\dfrac{1}{2}S_{do}S_{Bo}\right) & 0 & 0 & \dfrac{S_{apo}}{C} & \dfrac{S_{bpo}}{C} & \dfrac{S_{cpo}}{C} \\[3mm]
0 & 0 & 0 & 0 & -\dfrac{r_s}{L_s} & 0 & 0 \\[3mm]
0 & 0 & 0 & 0 & 0 & -\dfrac{r_s}{L_s} & 0 \\[3mm]
0 & 0 & 0 & 0 & 0 & 0 & -\dfrac{r_s}{L_s}
\end{bmatrix}
$$

5.4.2 Stability Analysis

The stability of a system is studied by determining the eigen values and checking the real part of all the eigen values. The real part of the eigen values have to be less than zero to ensure that the system is stable. Figure 5.25 shows the plot of the eigen values of the parameters where the real part was plotted against the imaginary part. The real part of the eigen value of all the state variables are negative. Hence for the given conditions, the Z-source inverter is stable.
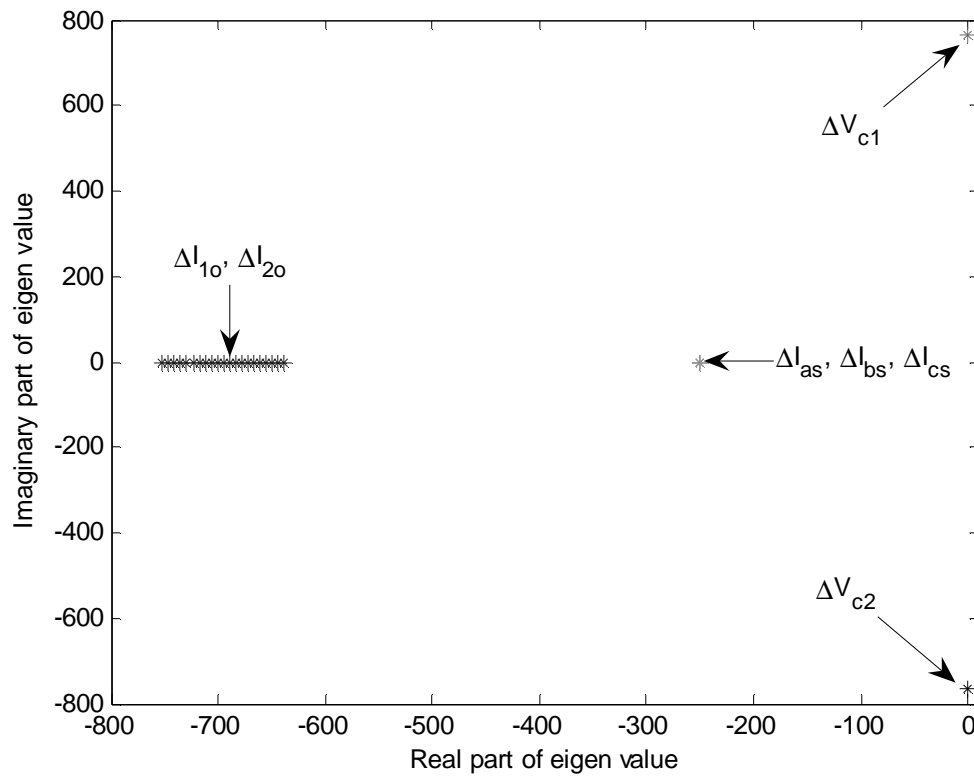
Figure 5.25: Eigen values of the state variables of the Z-source inverter

5.5 Conclusion

In this chapter, the Z-Source Inverter's operating modes were explained in detail. The steady state results were shown for the RL load. The system parameters were plotted for various values of modulation index in the case of RL load and for various reasonable values of shoot-through duty ratio. It was noticed that as the shoot-through duty ratio, D_o increased, the ripple in the circuit increased. The simulation results showed the system's behavior under loaded operating conditions. The small signal analysis was performed and the characteristic matrix was obtained. The eigen values were determined and it was shown that the Z-source inverter was stable for the given operating conditions.

CHAPTER 6

ANALYSIS OF Z-SOURCE INVERTER WITH AN INDUCTION MOTOR LOAD

6.1 Introduction

The Z Source converter (ZSC), is used to control general-purpose motor drives. By controlling the shoot-through duty cycle, the Z-source inverter can produce any desired output ac voltage, even greater than the line voltage. As a result, the new Z-source inverter system provides ride-through capability during voltage sags, reduces line harmonics, improves power factor and reliability, and extends output voltage range [I.26]. The structure of a VSI based Z-source inverter is shown in Figure 6.1.

This chapter deals with the analysis of the Z-source inverter when the load is an Induction Motor. The dynamic analysis of the system along with steady state analysis is put forth. The simulation results hence prove the theory stated.
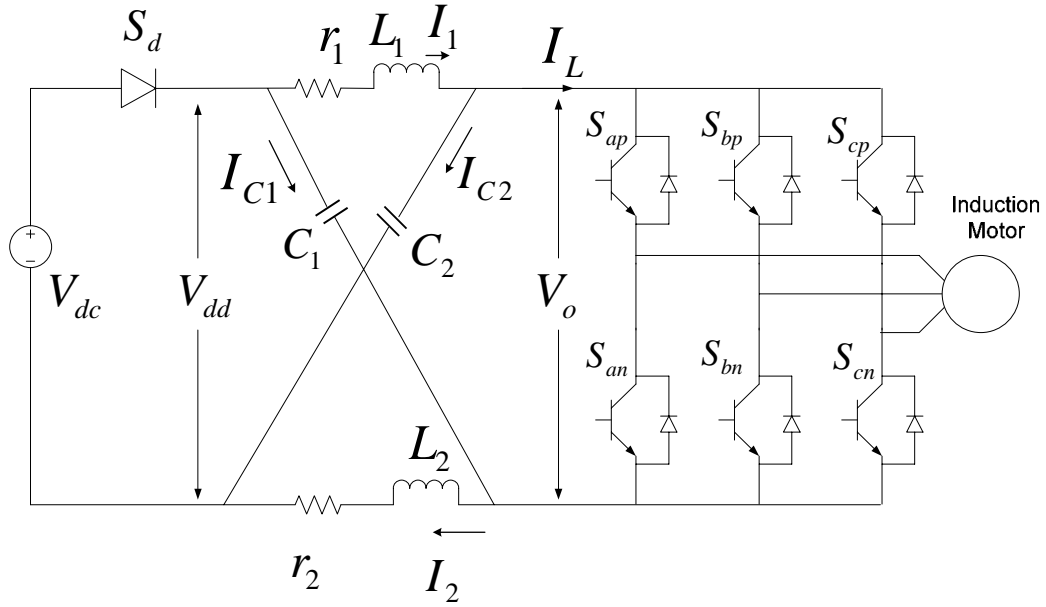
Figure 6.1: Structure of a VSI based Z-Source Inverter

6.2 Dynamic Analysis of the Z-source Inverter Feeding an Induction Motor Load

The dynamic analysis helps in studying the transients of the system. It gives the real time characteristics of the model.

6.2.1 Derivation of Transient Analysis on the Model

The simplified equations in all the six operating modes for a balanced case of operation can be generalized equations and it can be written as the following

140

$$pI_1 = \frac{1}{L}(V_{dd} - rI_1 - V_{c2}) \tag{6.1}$$

$$pI_2 = \frac{1}{L}(V_{dd} - rI_2 - V_{c1}) \tag{6.2}$$

$$pV_{c1} = \frac{1}{C}(I_2 - I_L) \tag{6.3}$$

$$pV_{c2} = \frac{1}{C}(I_1 - I_L) \tag{6.4}$$

$$V_{dd} = S_d V_{dc} + (1 - S_d)(S_A + S_C)\left(\frac{1}{2}(rI_2 + V_{c2} + rI_1 + V_{c1})\right) + (1 - S_d)S_B(V_{c1} + V_{c2}) \tag{6.5}$$

$$I_d = S_d(S_A + S_B)(I_1 + I_2 - I_L) + S_d S_C(I_1 + I_2) \tag{6.6}$$

$$I_L = S_d S_A(S_{ap}I_{as} + S_{bp}I_{bs} + S_{cp}I_{cs}) + (1 - S_d)(S_A + S_B)(I_1 + I_2) + S_d S_B\left(\frac{I_1 + I_2}{2}\right) \tag{6.7}$$

$$V_o = (S_A + S_B)(V_{c1} + V_{c2} - V_{dd}) \tag{6.8}$$

When an induction machine is used as the load, the dynamic equations for the load phase currents change. The Z-network equations remain the same as that of RL load. The qd equations of the squirrel-cage induction machine load in terms of the stator and rotor flux linkages are given as

$$V_{qs} = r_s I_{qs} + p\lambda_{qs} + \omega_e \lambda_{ds} \tag{6.9}$$

$$V_{ds} = r_s I_{ds} + p\lambda_{ds} - \omega_e \lambda_{qs} \tag{6.10}$$

$$V_{qr}' = r_r' I_{qr}' + p\lambda_{qr}' + (\omega_e - \omega_r)\lambda_{dr}' = 0 \tag{6.11}$$

$$V_{dr}' = r_r' I_{dr}' + p\lambda_{dr}' - (\omega_e - \omega_r)\lambda_{qr}' = 0 \tag{6.12}$$

$$p\omega_r = \frac{P}{2J}(T_e - T_L) \tag{6.13}$$

$$T_e = \frac{3P}{4}\left(I_{qs}\lambda_{ds} - I_{ds}\lambda_{qs}\right) \tag{6.14}$$

where the stator and rotor flux linkages are given as

$$\lambda_{qs} = L_s I_{qs} + L_m I_{qr}' \tag{6.15}$$

$$\lambda_{ds} = L_s I_{ds} + L_m I_{dr}' \tag{6.16}$$

$$\lambda_{qr}' = L_r' I_{qr}' + L_m I_{qs} \tag{6.17}$$

$$\lambda_{dr}' = L_r' I_{dr}' + L_m I_{ds} \tag{6.18}$$

This implies that the stator and rotor currents can be obtained from the flux linkage equations where the flux linkages are determined from the stator and rotor dynamic voltage equations as they are expressed in (6.9)-(6.12).

$$p\lambda_{qs} = V_{qs} - r_s I_{qs} - \omega_e \lambda_{ds} \tag{6.19}$$

$$p\lambda_{ds} = V_{ds} - r_s I_{ds} + \omega_e \lambda_{qs} \tag{6.20}$$

$$p\lambda_{qr}' = -r_r' I_{qr}' - (\omega_e - \omega_r)\lambda_{dr}' \tag{6.21}$$

$$p\lambda_{dr}' = -r_r' I_{dr}' + (\omega_e - \omega_r)\lambda_{qr}' \tag{6.22}$$

The currents are obtained from the flux linkages (6.15)-(6.18).

$$I_{qs} = \frac{1}{\Delta}\left(L_r'\lambda_{qs} - L_m\lambda_{qr}'\right) \tag{6.23}$$

$$I_{ds} = \frac{1}{\Delta}\left(L_r'\lambda_{ds} - L_m\lambda_{dr}'\right) \tag{6.24}$$

$$I_{qr}' = \frac{1}{\Delta}\left(L_s\lambda_{qr}' - L_m\lambda_{qs}\right) \tag{6.25}$$

$$I_{dr}^{'} = \frac{1}{\Delta}\left(L_s \lambda_{dr}^{'} - L_m \lambda_{ds}\right)$$
(6.26)

where

$$\Delta = L_s L_r^{'} - L_m^2$$
(6.27)

6.2.2 Results

The simulation results when an induction machine is connected to the output of the inverter are shown below. The initial results show the transient characteristics of the system as shown in Figures 6.2, 6.3, 6.4, 6.5, 6.6, 6.7, and 6.8.

(a)

(b)
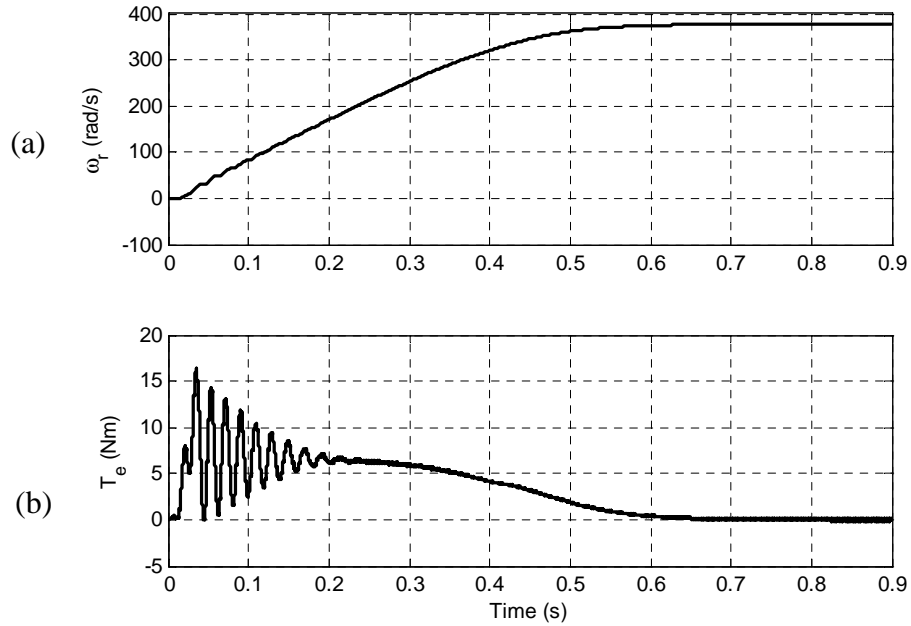
Figure 6.2: Transient characteristics of induction motor (a) rotor speed ω_r (b) torque T_e
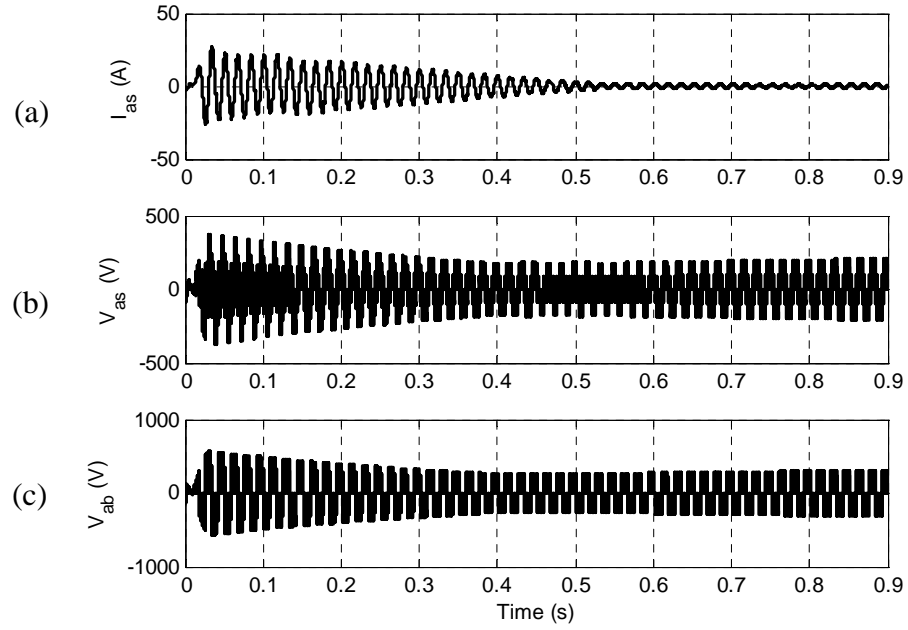
Figure 6.3: Transient characteristics (a) 'a' phase stator current I_{as} (b) Phase 'a' voltage

V_{as} (c) Line voltage V_{ab}
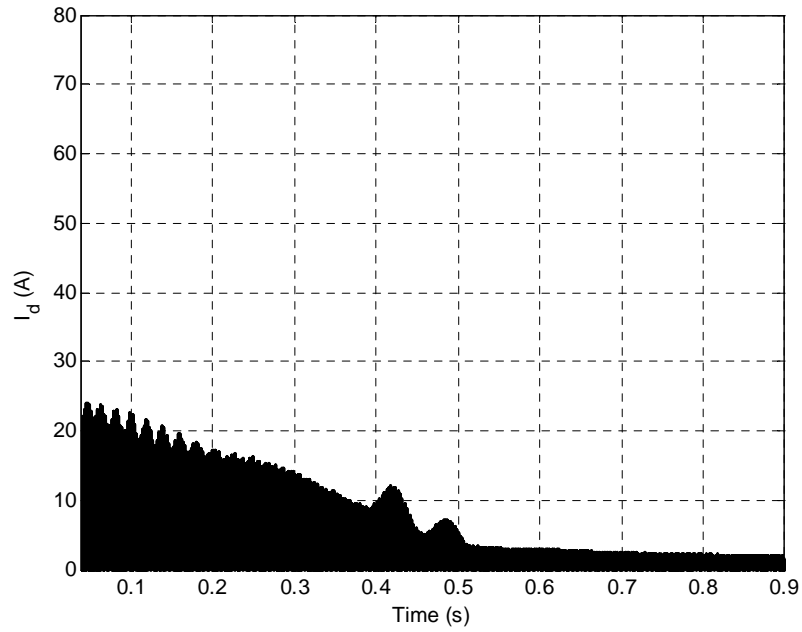
Figure 6.4: Transient characteristics of the Z-source network - DC input current to the Z-

network I_d
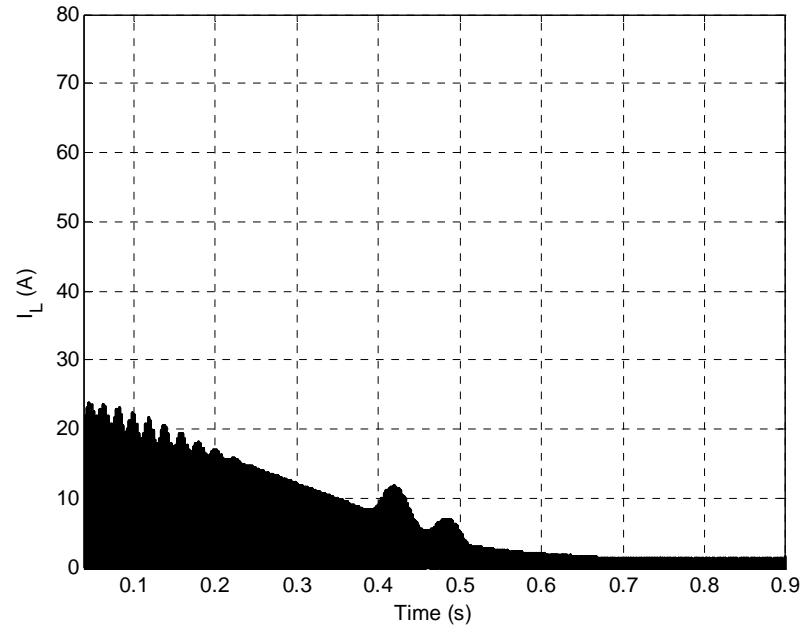
Figure 6.5: Transient characteristics of the Z-source network - DC output current of the
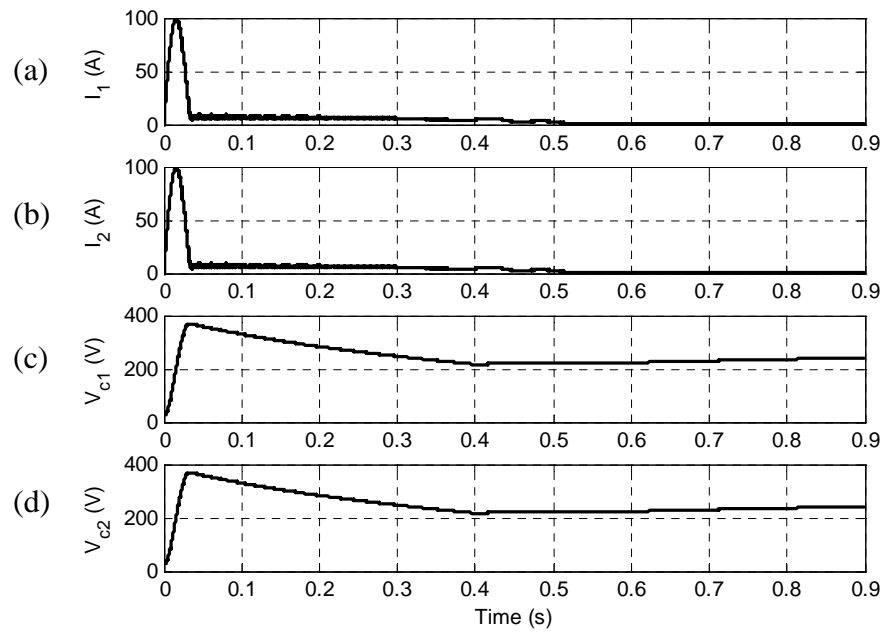
Z-network I_L

Figure 6.6: Transient characteristics of the Z-source network - (a-b) inductor currents,

(c-d) capacitor voltages

145
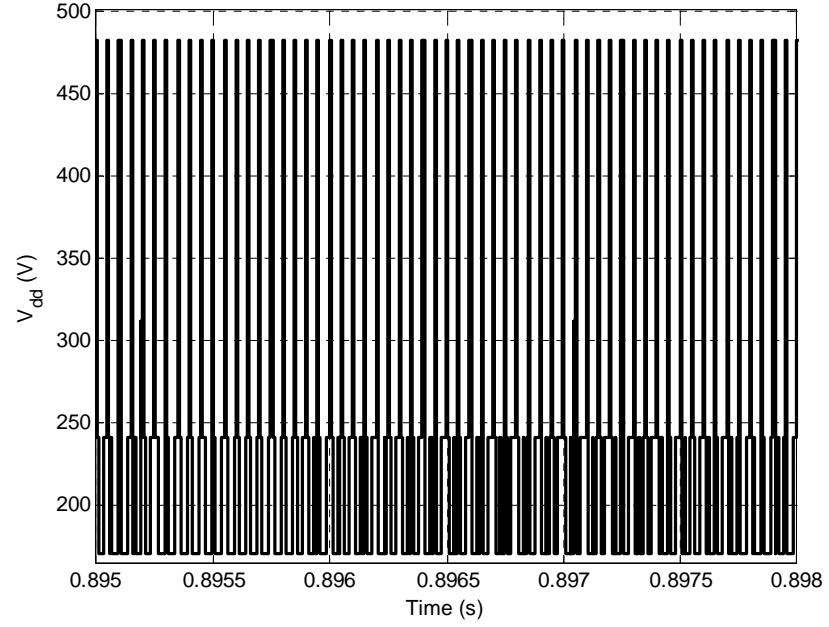
Figure 6.7: Transient characteristics of the Z-source network - DC input voltage to the Z-

network V_{dd}
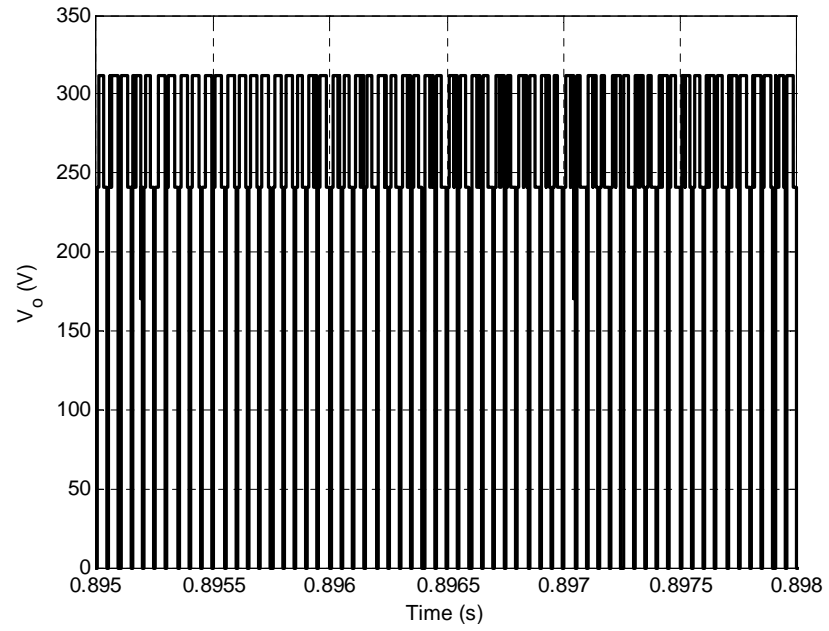
Figure 6.8: Transient characteristics of the Z-source network - DC output voltage of the

Z-network V_o

A load torque of 4 Nm is applied at 0.75 seconds. The behavior of the system is shown below in Figures 6.9, 6.10, 6.11, 6.12, 6.13, 6.14, and 6.15.
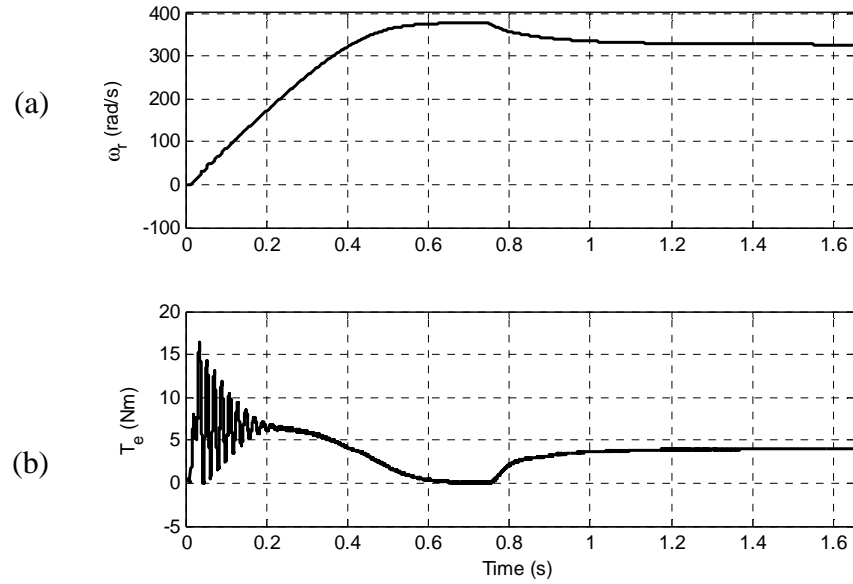
Figure 6.9: Squirrel cage induction motor characteristics (a) Change in rotor speed ω_r (b)

torque at 0.75 seconds
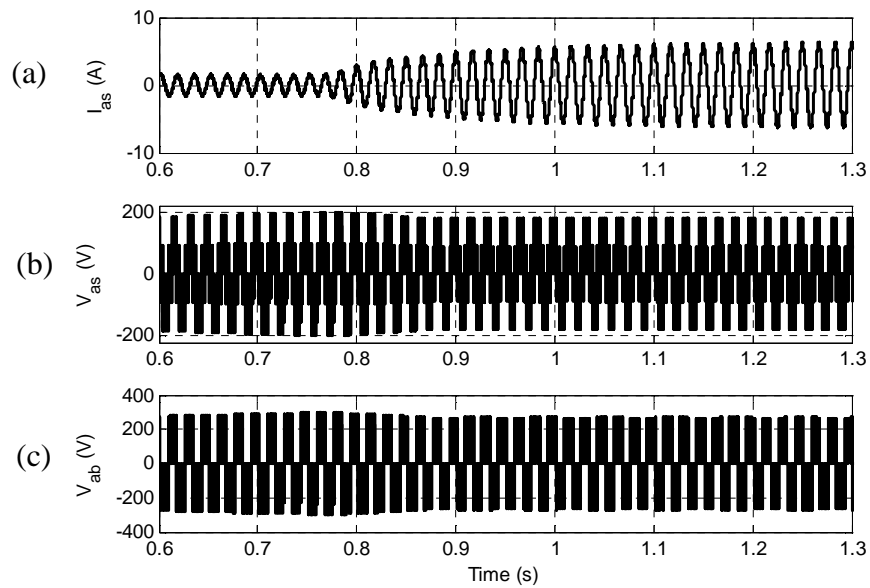
Figure 6.10: Change in (a) 'a' phase stator current (b) Phase 'a' voltage (c) Line voltage

when a load of 4 Nm is applied at 0.75 seconds
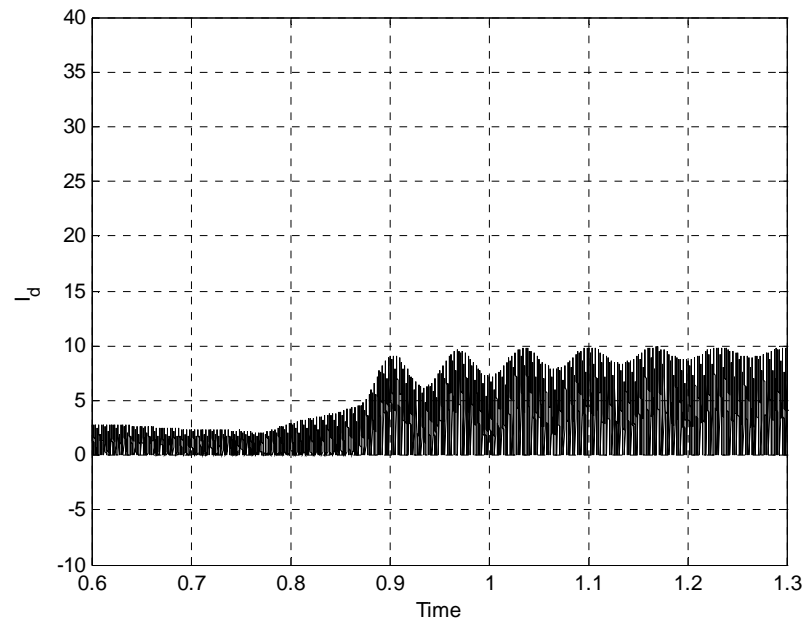
Figure 6.11: Change in the DC input current to the Z-network when a load of 4 Nm is

applied at 0.75 seconds
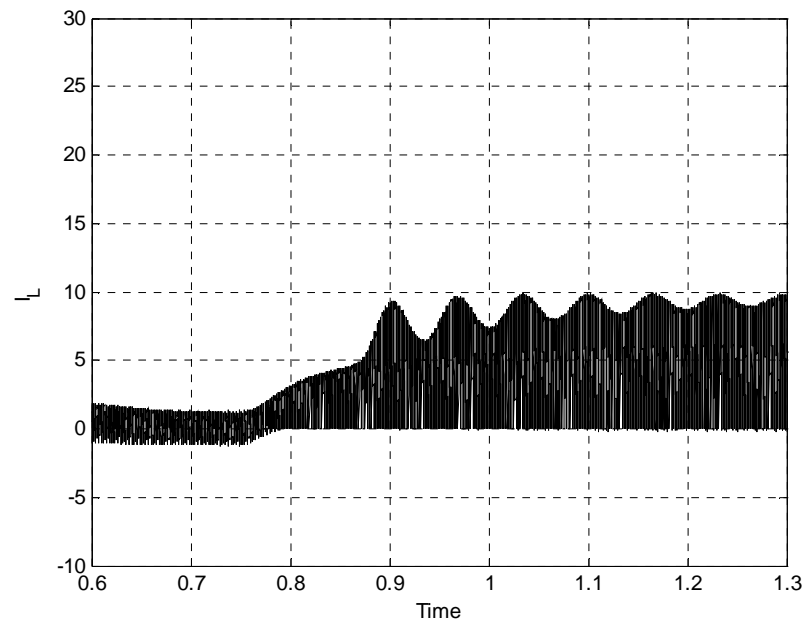
Figure 6.12: Change in the DC output current of the Z-network when a load of 4 Nm is

applied at 0.75 seconds

148
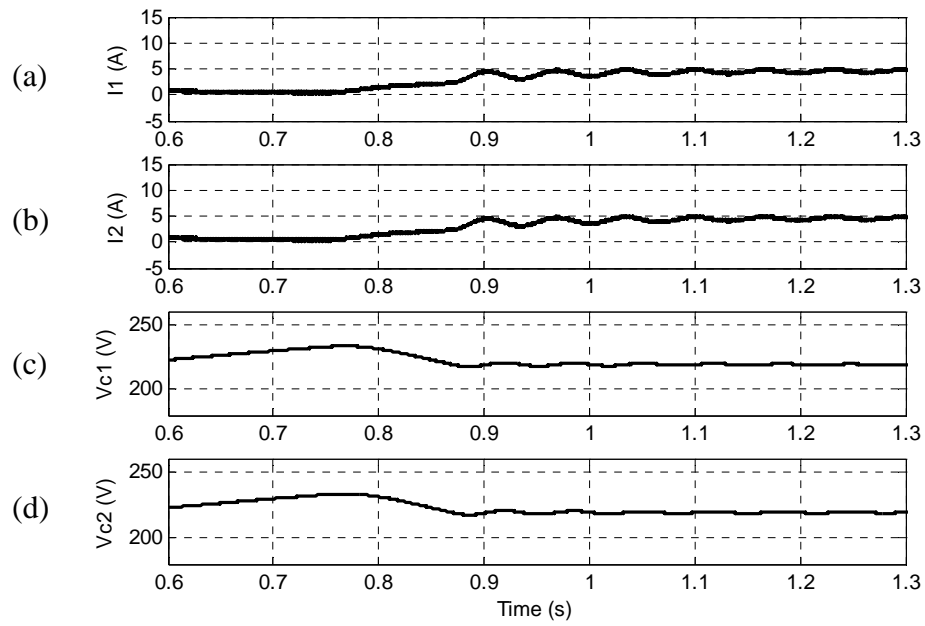
Figure 6.13: Change in the (a-b) Inductor currents, (c-d) Capacitor Voltages of the Z-

network when a load of 4 Nm is applied at 0.75 seconds
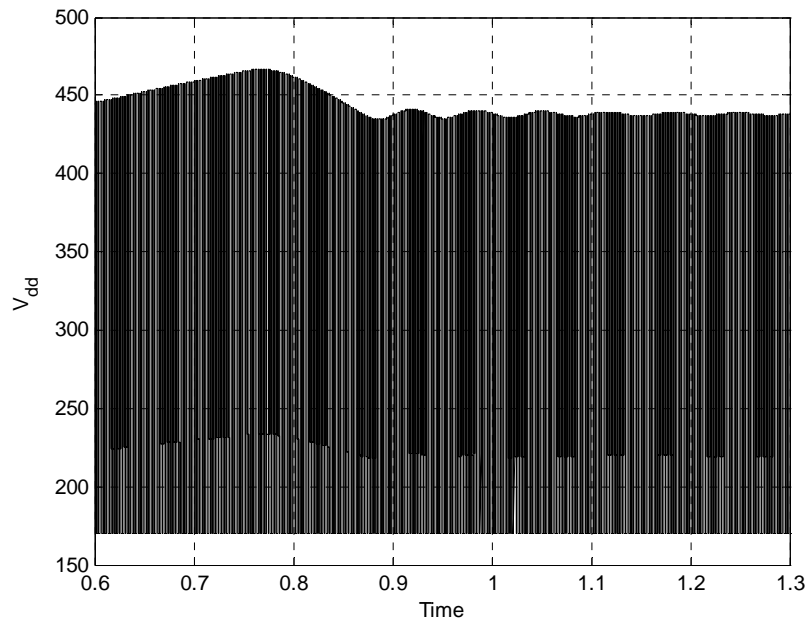
Figure 6.14: Change in the DC input voltage to the Z-network when a load of 4 Nm is

applied at 0.75 seconds
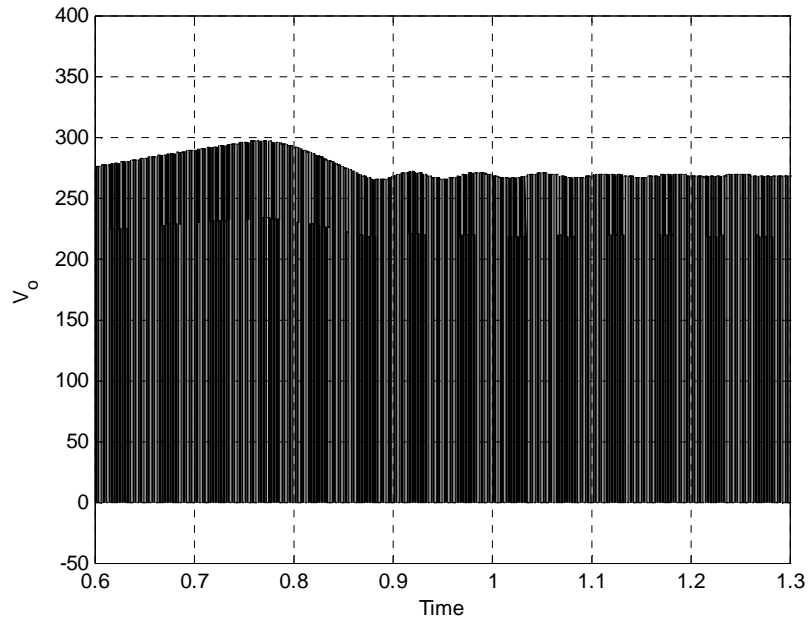
Figure 6.15: Change in the DC output voltage of the Z-network when a load of 4 Nm is

applied at 0.75 seconds

6.3 Steady State Analysis of Z-Source Inverter

The steady-state analysis of any system is carried out to study the nature of the system at steady state and use the analysis to control the response of the system. The steady-state analysis of the system is done using the state equations of the system in the synchronous reference frame, as the variables in the equation are time-invariant with respect to the frame of reference.

6.3.1 Derivation of the Steady State Analysis

The derivative terms in the above generalized equations of the Z-source inverter and the induction machine are set to zero and the steady state equations of the system after using the averaging technique to eliminate the switching functions are expressed as

$$
\begin{bmatrix} I_{qs} \\ I_{ds} \\ I_{qr}' \\ I_{dr}' \end{bmatrix} = \begin{bmatrix} r_s & \omega_e L_s & 0 & \omega_e L_m \\ -\omega_e L_s & r_s & -\omega_e L_m & 0 \\ 0 & (\omega_e - \omega_r)L_m & r_r' & (\omega_e - \omega_r)L_r \\ -(\omega_e - \omega_r)L_m & 0 & -(\omega_e - \omega_r)L_r & r_r^1 \end{bmatrix}^{-1} \begin{bmatrix} V_{qs} \\ V_{ds} \\ 0 \\ 0 \end{bmatrix}
$$

(6.28)

The currents are obtained from (6.28)

Here, I_L is the stator current which is determined from (6.29)

$$
I_L = \sqrt{I_{qs}^2 + I_{ds}^2}
$$

(6.29

$$
V_o = \frac{-2(1 - D_o)^2 r I_L}{(2D_o - 1)^2} - \frac{(1 - D_o)V_{dc}}{(2D_o - 1)}
$$

(6.30)

$$
V_{dd} = \frac{-2D_o(1 - D_o)r I_L}{(2D_o - 1)^2} - \frac{2(1 - D_o)}{(2D_o - 1)}
$$

(6.31)

$$
I_d = \frac{I_L(1 - D_o)}{(2D_o - 1)}
$$

(6.32)

$$
V_{c1} = V_{c2} = \frac{-(1 - D_o)r I_L}{(2D_o - 1)^2} - \frac{(1 - D_o)V_{dc}}{(2D_o - 1)}
$$

(6.33)

6.3.2 Results

For an induction machine load the simulation results are as shown below.
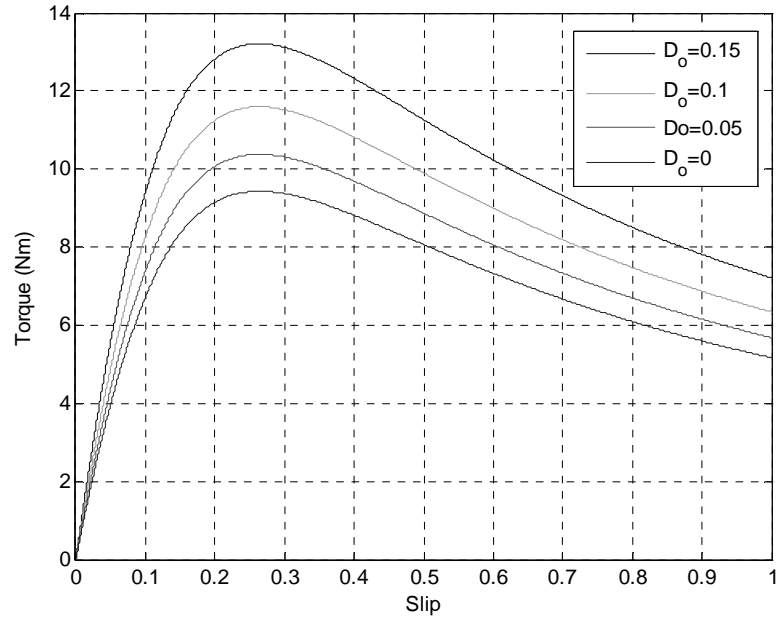
Figure 6.16: Torque of the induction machine for varying shoot-through duty ratio D_o
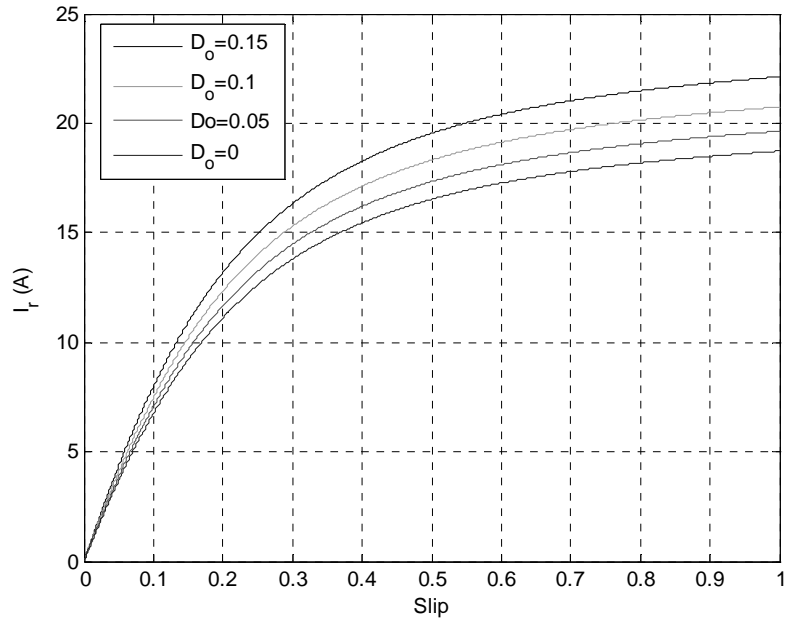
Figure 6.17: Rotor current of the induction machine for varying shoot-through duty ratio

$$D_o$$
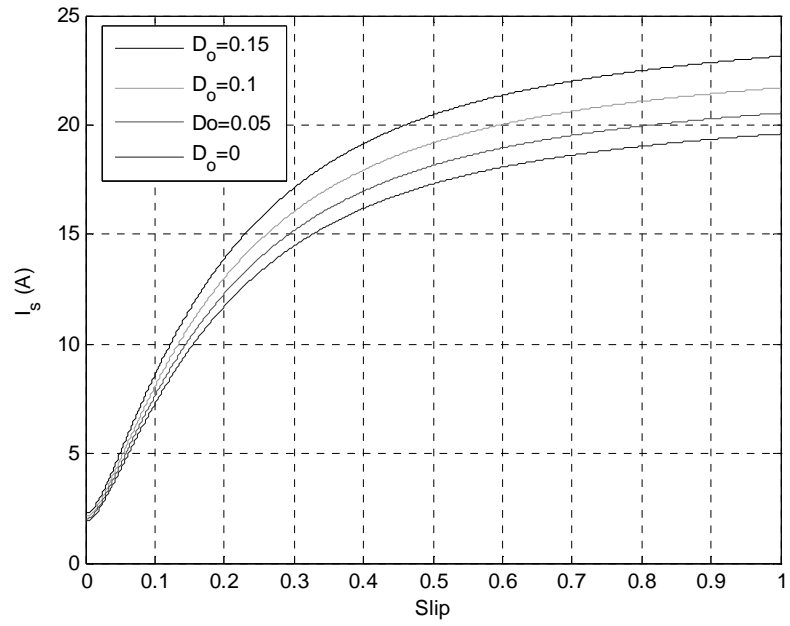
Figure 6.18: Stator current of the induction machine for varying shoot-through duty ratio

D_o
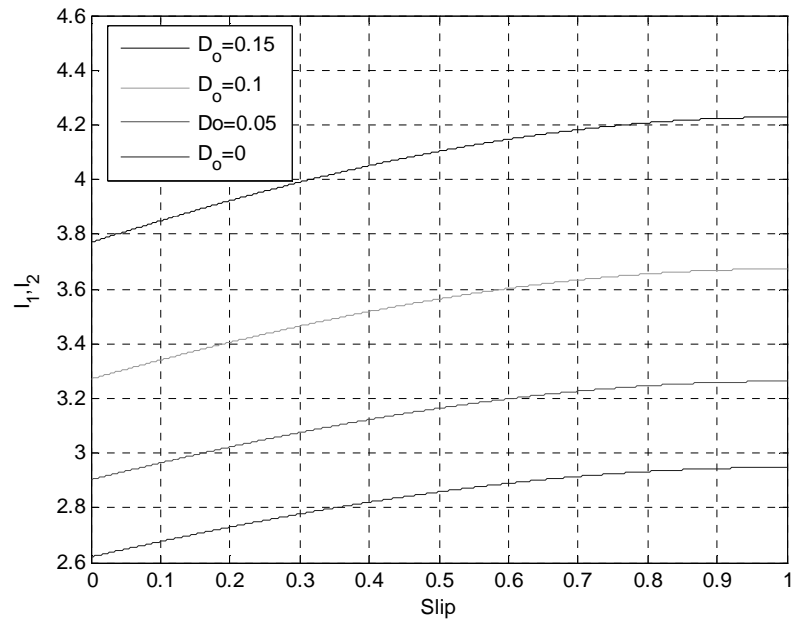
Figure 6.19: Induction currents of the Z-Network for varying shoot-through duty ratio

D_o
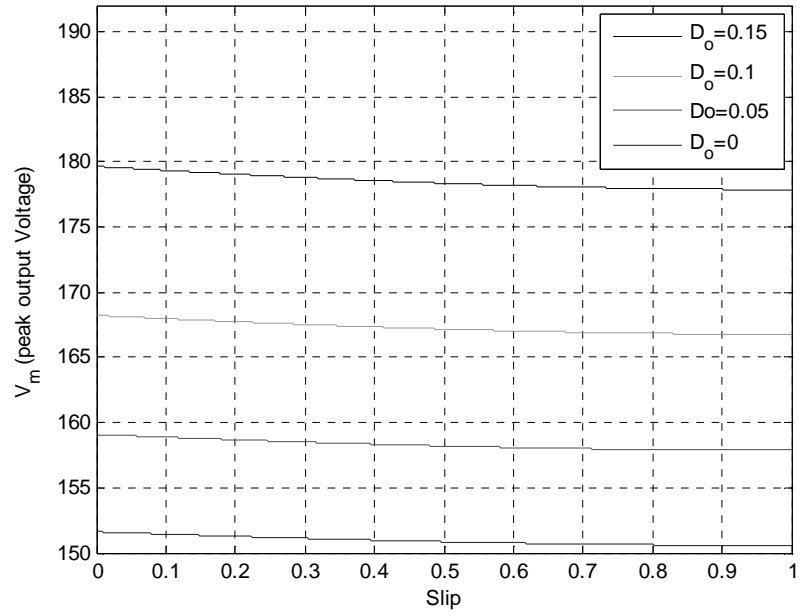
Figure 6.20: Peak output voltage of the inverter for varying shoot-through duty ratio D_o
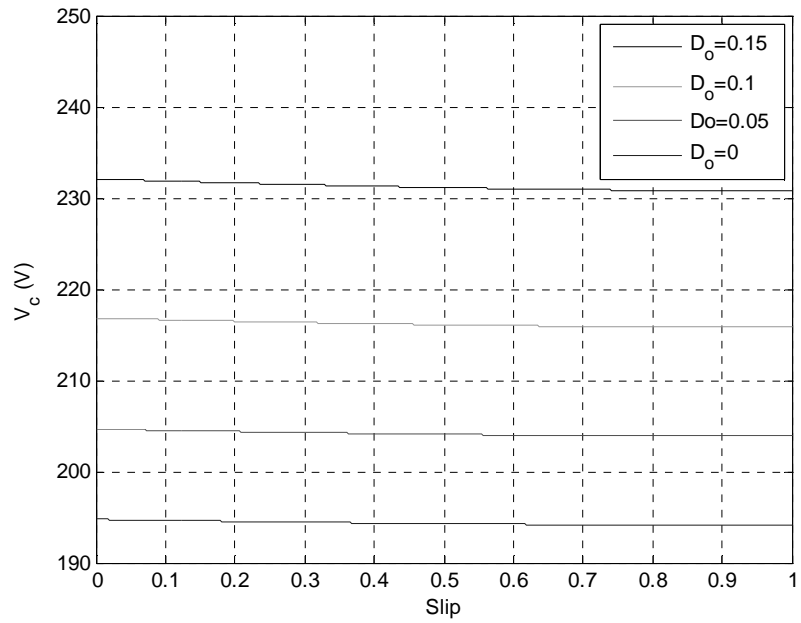
Figure 6.21: Capacitor voltage of the Z-Network for varying shoot-through duty ratio D_o
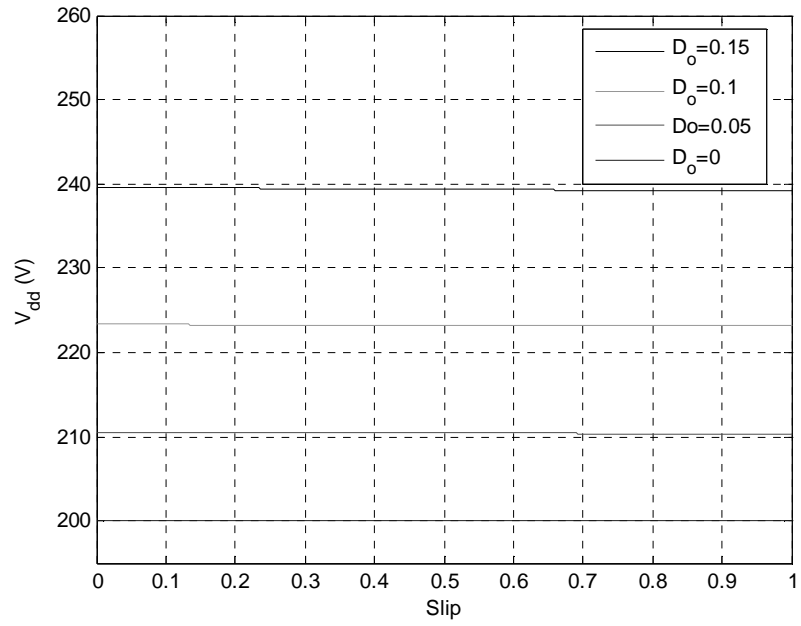
Figure 6.22: Input voltage to the Z-Network for varying shoot-through duty ratio D_o
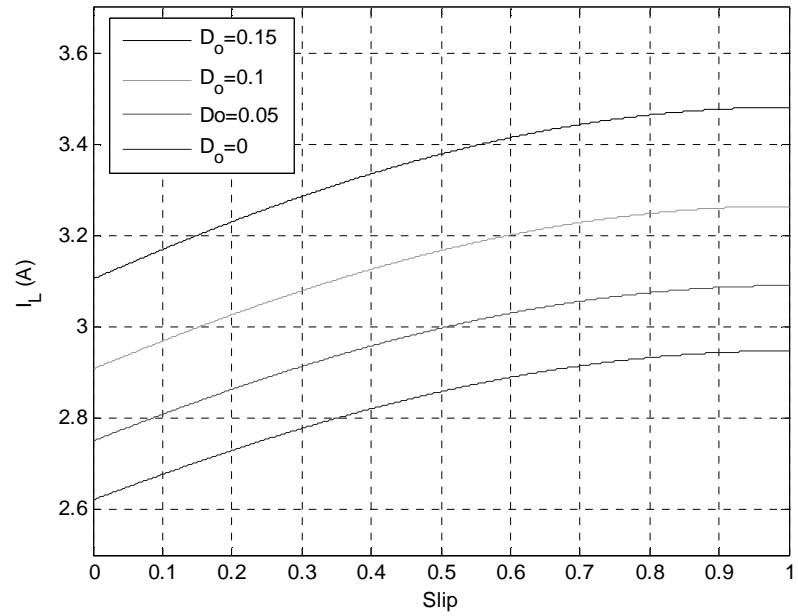
Figure 6.23: Output current of the Z-Network for varying shoot-through duty ratio D_o
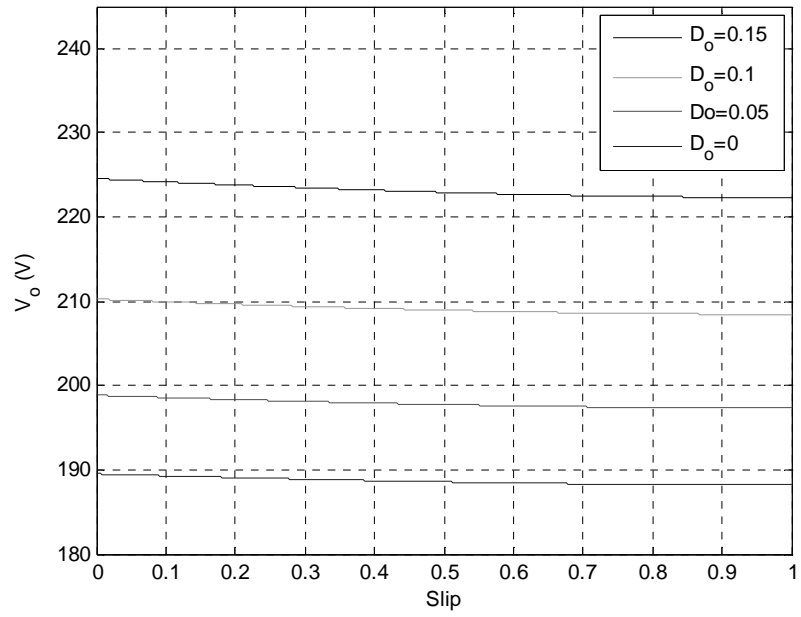
Figure 6.24: Output voltage of the Z-Network for varying shoot-through duty ratio D_o

6.4 Conclusion

In this chapter, the Z-Source Inverter's operation with Induction Machine Load was explained in detail. The system parameters were plotted for various values of modulation index and in addition for various reasonable values of shoot-through duty ratio. The simulation results showed the system's behavior under loaded operating conditions. The Induction motor was loaded up to 4 Nm and the results proved the theories explained earlier.

CHAPTER 7

MODELING OF Z-SOURCE RECTIFIERS

7.1 Introduction

The voltage source rectifier (VSR) is widely used in the four-quadrant AC motor driver system. In this case, the DC voltage that is greater than AC voltage should be obtained, which would benefit the motor driving performance, while it would be disadvantage to the motor starting course. Thus, the inverter must stand the high DC voltage during starting course, and the modulation index of the inverter has to be set in a low value, which reduces the quality of output AC voltage. In addition, to avoid the shoot-through, the method of increase dead time has been applied. This technique would result in the distortion of the current waveform.

The Z-source network is coupled between the bridge and the load, with the unique control strategy, some virtues should be obtained.

- Flexibly adjust the output DC voltage, greater or smaller than the line ac voltage.

- Shoot-through allowed in a bridge leg, which increase the EMI noises resistance.

- The dead time need not be applied, and the sinusoidal current wave is achieved.

- . The size of both the dc-link inductor and the output capacitor are reduced compared to traditional two-stage buck rectifier.

- The switching looses are reduced considerably.

This configuration provides favorable characteristics that exceed the traditional voltage source rectifier [R.2]. This chapter explains the different modes of operation of the Z-Source Rectifier. This configuration is a boost rectifier modified to buck the voltage. This is brought about by the shoot-through state and the modulation index as the voltage is boosted at lower modulation index. It is also capable of unity power factor operation. The structure of the Z-Source Rectifier is shown in Figure 7.1.
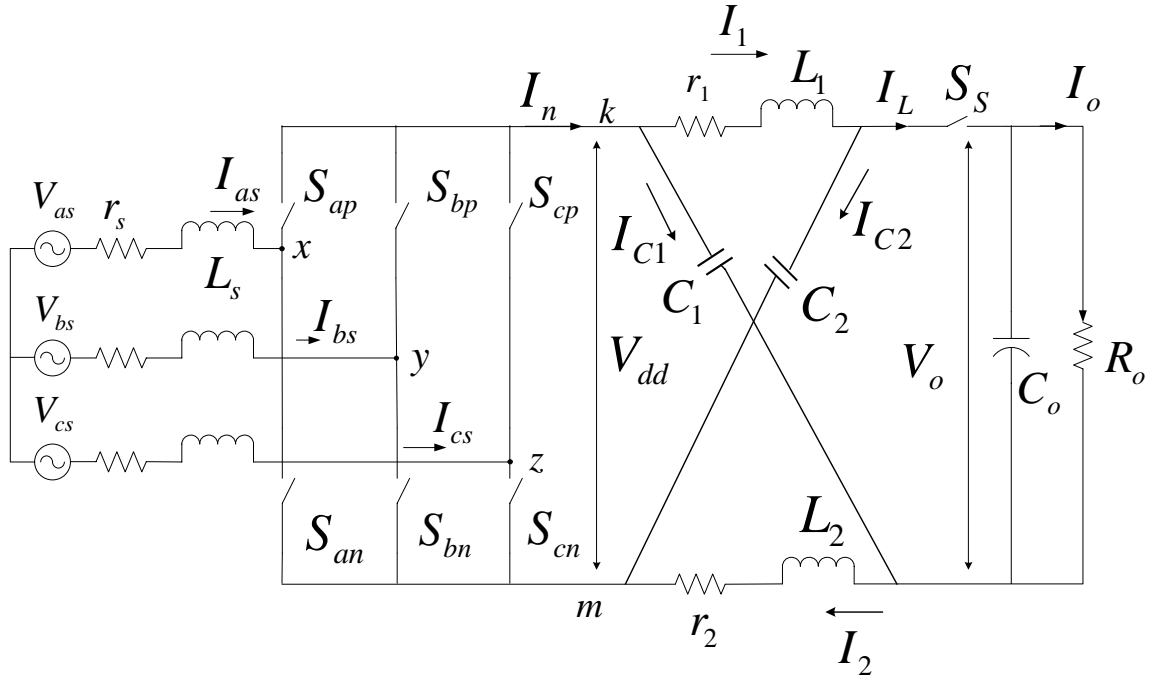
Figure 7.1: Structure of a Z-Source Rectifier

7.2 Dynamic Analysis for ZSR

The Z-Source Rectifier provides unique features that cannot be obtained by the conventional full-bridge rectifier. The three-phase Z-source rectifier is capable of voltage boosting and voltage bucking to the desired output voltage which can be greater than or less than the input voltage. It is also capable of unity power factor operation. The advantage of using the Z-source rectifier is reduced switching losses. The network under consideration can be applied in fuel-cell systems. The shoot-through state leads to the voltage boost and buck requirements. A wide range of output dc bus voltage is obtained due to the introduction of the Z-source network (impedance network). The reliability if the rectifier is increased to a great extent because the shoot-through can no longer destroy the circuit [R.3].

In the case of the Z-source Rectifier, there are three states of operation. Namely

- Active State, S_A

- Shoot-through State, S_B

- Null State, S_C

The switch S_S connects the Z-Source network with the load. This switch is turned ON during the Active state and the Null state. During the shoot-through state, the switch S_S is kept open, that is, turned OFF.

The three states of operation of a Z-source rectifier are illustrated as follows.

7.2.1 Active State ; S_A

The active state of the Z-Source Rectifier is as shown in Figure 7.2. The active state relates to the actual functioning of the model. The three-phase source voltage is supplied to the dc load through the Z-source network. The switch S_S remains closed in this state in order to transfer the three-phase supply, which is converted to dc voltage through the boost rectifier to the dc load which is a dc resistive load in this case. The model equations during this state are given as follows.

The three phase input voltage equations are given as

$$V_{as} = r_s I_{as} + L_s p I_{as} + V_x \tag{7.1}$$

$$V_{bs} = r_s I_{bs} + L_s p I_{bs} + V_y \tag{7.2}$$

$$V_{cs} = r_s I_{cs} + L_s p I_{cs} + V_z \tag{7.3}$$
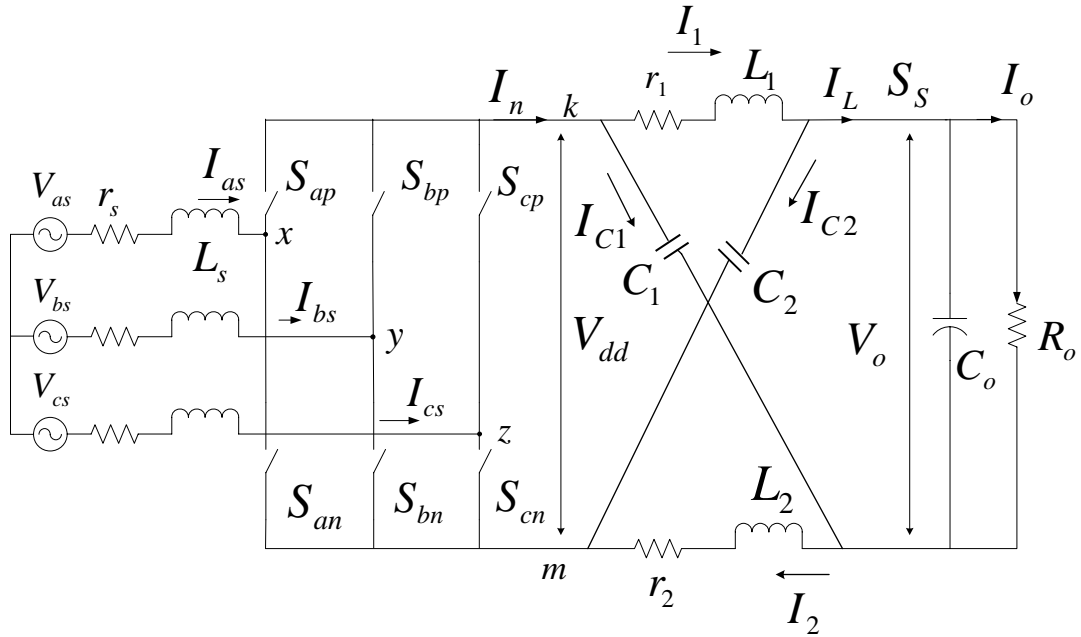
Figure 7.2: Active state of ZSR, S_A

$$\text{where} \quad V_x = S_{ap}V_{kn} + S_{an}V_{mn} \tag{7.4}$$

$$V_y = S_{bp}V_{kn} + S_{bn}V_{mn} \tag{7.5}$$

$$V_z = S_{cp}V_{kn} + S_{cn}V_{mn} \tag{7.6}$$

The output DC voltage of the rectifier is $V_{dd} = V_{km} = V_{kn} - V_{mn}$

$$\Rightarrow \quad V_{kn} = V_{dd} + V_{mn} \tag{7.7}$$

Substituting for V_{kn} in (7.4)-(7.7) and hence substituting for V_x, V_y, and V_z in (7.1)-(7.3) gives

$$V_{as} = r_s I_{as} + L_s p I_{as} + S_{ap}V_{dd} + V_{mn}\left(S_{ap} + S_{an}\right) \tag{7.8}$$

$$V_{bs} = r_s I_{bs} + L_s p I_{bs} + S_{bp}V_{dd} + V_{mn}\left(S_{bp} + S_{bn}\right) \tag{7.9}$$

$$V_{cs} = r_s I_{cs} + L_s p I_{cs} + S_{cp}V_{dd} + V_{mn}\left(S_{cp} + S_{cn}\right) \tag{7.10}$$

By adding the three phase voltage equations (7.8)-(7.10) and eliminating V_{mn} and also using the above equations in a balanced case makes the expressions for the three-phase input voltages as

$$V_{as} = r_s I_{as} + L_s p I_{as} + \frac{V_{dd}}{3}\left(2S_{ap} - S_{bp} - S_{cp}\right) \tag{7.11}$$

$$V_{bs} = r_s I_{bs} + L_s p I_{bs} + \frac{V_{dd}}{3}\left(-S_{ap} + 2S_{bp} - S_{cp}\right) \tag{7.12}$$

$$V_{cs} = r_s I_{cs} + L_s p I_{cs} + \frac{V_{dd}}{3}\left(-S_{ap} - S_{bp} + 2S_{cp}\right) \tag{7.13}$$

$$L_1 p I_1 = V_{dd} - r_1 I_1 - V_{c2} \tag{7.14}$$

$$L_2 p I_2 = V_{dd} - r_2 I_2 - V_{c1} \tag{7.15}$$

$$C_1 p V_{c1} = I_2 - I_L \tag{7.16}$$

$$C_2 p V_{c2} = I_1 - I_L \tag{7.17}$$

$$V_{dd} = V_{c1} + V_{c2} - V_o \tag{7.18}$$

$$I_n = S_{ap} I_{as} + S_{bp} I_{bs} + S_{cp} I_{cs} \tag{7.19}$$

$$I_L = I_1 + I_2 - I_n \tag{7.20}$$

$$C_o p V_o = I_L - I_o = I_L - \frac{V_o}{R_o} \tag{7.21}$$

$$I_o = \frac{V_o}{R_o} \tag{7.22}$$

7.2.2 Shoot-through State; S_B

The shoot-through state of the Z-Source Rectifier is as shown in Figure 7.3. Both the devices on one or all the legs are turned ON together. Here the switch S_S is kept open. In this state, the capacitors are charged. A portion of the conventional null state period is used up for the shoot-though state. The switching functions of the active state, shoot-through state and the null state are shown in Figure 7.5. The individual switching functions of each device including the shoot-through is as shown in Figure 7.6.
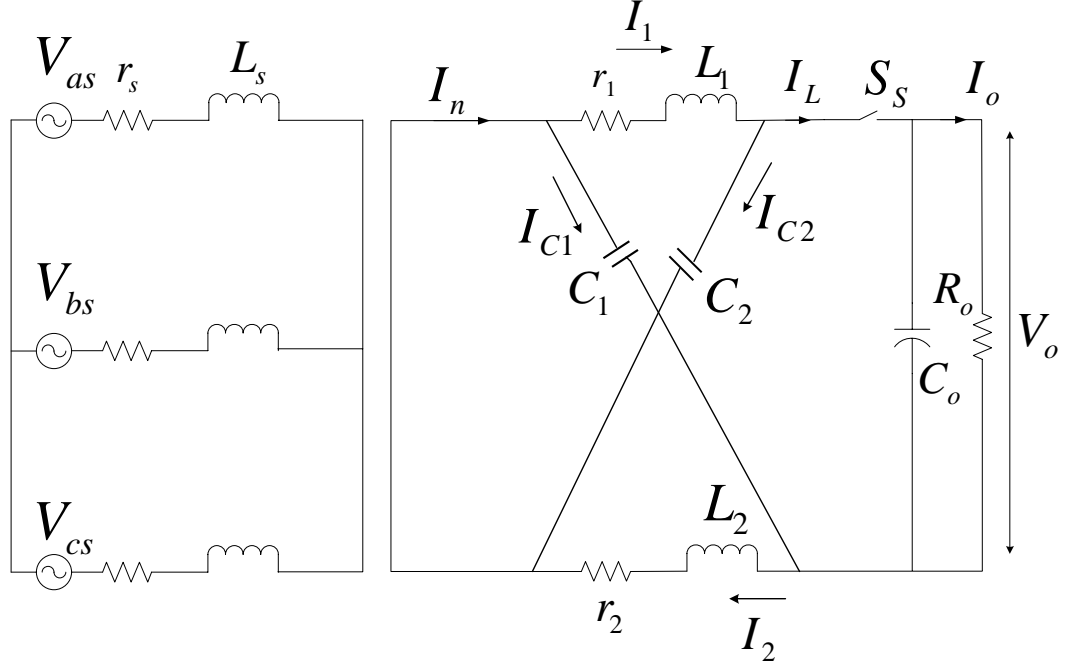
Figure 7.3: Shoot-through State of ZSR, S_B

The model equations during this state of operation are given as follows

$$V_{as} = r_s I_{as} + L_s p I_{as} + \frac{V_{dd}}{3}\left(2S_{ap} - S_{bp} - S_{cp}\right) \tag{7.23}$$

$$V_{bs} = r_s I_{bs} + L_s p I_{bs} + \frac{V_{dd}}{3}\left(-S_{ap} + 2S_{bp} - S_{cp}\right) \tag{7.24}$$

$$V_{cs} = r_s I_{cs} + L_s p I_{cs} + \frac{V_{dd}}{3}\left(-S_{ap} - S_{bp} + 2S_{cp}\right) \tag{7.25}$$

$$L_1 p I_1 = -r_1 I_1 - V_{c2} \tag{7.26}$$

$$L_2 p I_2 = -r_2 I_2 - V_{c1} \tag{7.27}$$

$$C_1 p V_{c1} = I_2 - I_L \tag{7.28}$$

$$C_2 p V_{c2} = I_1 - I_L \tag{7.29}$$

$$V_{dd} = 0 \tag{7.30}$$

$$I_n = I_1 + I_{c1}$$

$$= I_1 + I_2 - I_L$$

$$I_L = 0 \tag{7.31}$$

$$\Rightarrow I_n = I_1 + I_2 \tag{7.32}$$

$$C_o p V_o = -\frac{V_o}{R_o} \tag{7.33}$$

7.2.3 Null State; S_C

The Null state of the Z-Source Rectifier is as shown in Figure 7.4. Here the switch S_s is turned ON.
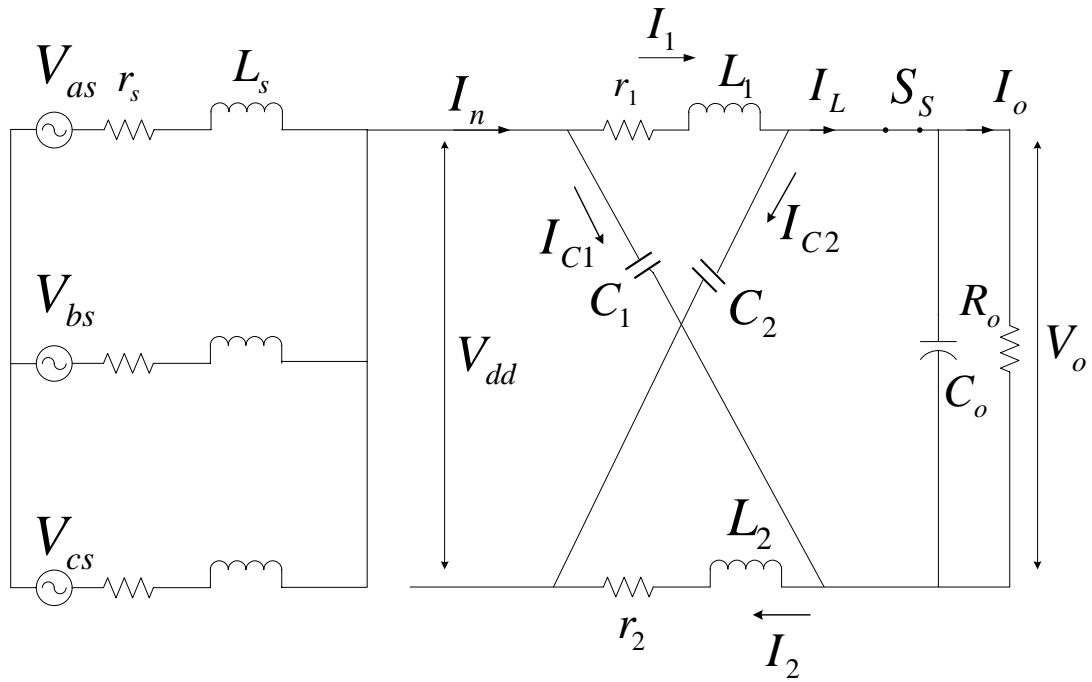
Figure 7.4: Null state of ZSR, S_C

The model equations for this state of operation are given as follows.

$$V_{as} = r_s I_{as} + L_s p I_{as} + \frac{V_{dd}}{3} \left(2S_{ap} - S_{bp} - S_{cp} \right) \tag{7.34}$$

$$V_{bs} = r_s I_{bs} + L_s p I_{bs} + \frac{V_{dd}}{3} \left(-S_{ap} + 2S_{bp} - S_{cp} \right) \tag{7.35}$$

$$V_{cs} = r_s I_{cs} + L_s p I_{cs} + \frac{V_{dd}}{3} \left(-S_{ap} - S_{bp} + 2S_{cp} \right) \tag{7.36}$$

$$L_1 p I_1 = V_{dd} - r_1 I_1 - V_{c2} \tag{7.37}$$

$$L_2 p I_2 = V_{dd} - r_2 I_2 - V_{c1} \tag{7.38}$$

$$V_{dd} = r_1 I_1 + L_1 p I_1 + V_o + r_2 I_2 + L_2 p I_2 \tag{7.39}$$

By substituting (7.37) and (7.38) in (7.39), gives (7.40)

$$V_{dd} = V_{c1} + V_{c2} - V_o \tag{7.40}$$

$$C_1 p V_{c1} = I_2 - I_L \tag{7.41}$$

$$C_2 p V_{c2} = I_1 - I_L \tag{7.42}$$

$$I_n = 0 \tag{7.43}$$

$$C_o p V_o = I_L - \frac{V_o}{R_o} \tag{7.44}$$

$$I_L = I_1 + I_2 \tag{7.45}$$

7.3 Averaging Technique

The equations in all the three operating modes can be generalized by averaging and the equations can be written as the following

$$V_{as} = S_A\left(r_s I_{as} + L_s pI_{as} + \frac{V_{dd}}{3}\left(2S_{ap} - S_{bp} - S_{cp}\right)\right) + S_B\left(r_s I_{as} + L_s pI_{as} + \frac{V_{dd}}{3}\left(2S_{ap} - S_{bp} - S_{cp}\right)\right)$$
$$+ S_C\left(r_s I_{as} + L_s pI_{as} + \frac{V_{dd}}{3}\left(2S_{ap} - S_{bp} - S_{cp}\right)\right) \tag{7.46}$$

$$V_{bs} = S_A\left(r_s I_{bs} + L_s pI_{bs} + \frac{V_{dd}}{3}\left(-S_{ap} + 2S_{bp} - S_{cp}\right)\right) + S_B\left(r_s I_{bs} + L_s pI_{bs} + \frac{V_{dd}}{3}\left(-S_{ap} + 2S_{bp} - S_{cp}\right)\right)$$
$$+ S_C\left(r_s I_{bs} + L_s pI_{bs} + \frac{V_{dd}}{3}\left(-S_{ap} + 2S_{bp} - S_{cp}\right)\right) \tag{7.47}$$

$$V_{cs} = S_A\left(r_s I_{cs} + L_s pI_{cs} + \frac{V_{dd}}{3}\left(-S_{ap} - S_{bp} + 2S_{cp}\right)\right) + S_B\left(r_s I_{cs} + L_s pI_{cs} + \frac{V_{dd}}{3}\left(-S_{ap} - S_{bp} + 2S_{cp}\right)\right)$$
$$+ S_C\left(r_s I_{cs} + L_s pI_{cs} + \frac{V_{dd}}{3}\left(-S_{ap} - S_{bp} + 2S_{cp}\right)\right) \tag{7.48}$$

$$L_1 pI_1 = S_A\left(V_{dd} - r_1 I_1 - V_{c2}\right) + S_B\left(-r_1 I_1 - V_{c2}\right) + S_C\left(V_{dd} - r_1 I_1 - V_{c2}\right) \tag{7.49}$$

$$L_2 pI_2 = S_A\left(V_{dd} - r_2 I_2 - V_{c1}\right) + S_B\left(-r_2 I_2 - V_{c1}\right) S_C\left(V_{dd} - r_2 I_2 - V_{c1}\right) \tag{7.50}$$

$$C_1 pV_{c1} = S_A\left(I_2 - I_L\right) + S_B\left(I_2 - I_L\right) + S_C\left(I_2 - I_L\right) \tag{7.51}$$

$$C_2 pV_{c2} = S_A\left(I_1 - I_L\right) + S_B\left(I_1 - I_L\right) + S_C\left(I_1 - I_L\right) \tag{7.52}$$

$$C_o pV_o = S_A\left(I_L - \frac{V_o}{R_o}\right) + S_B\left(-\frac{V_o}{R_o}\right) + S_C\left(I_L - \frac{V_o}{R_o}\right) \tag{7.53}$$

$$I_L = S_A\left(I_1 + I_2 - \left(S_{ap} I_{as} + S_{bp} I_{bs} + S_{cp} I_{cs}\right)\right) + S_C\left(I_1 + I_2\right) \tag{7.54}$$

$$V_{dd} = S_A\left(V_{c1} + V_{c2} - V_o\right) + S_B\left(V_{c1} + V_{c2} - V_o\right) \tag{7.55}$$

$$I_n = S_A\left(S_{ap} I_{as} + S_{bp} I_{bs} + S_{cp} I_{cs}\right) + S_B\left(I_1 + I_2\right) \tag{7.56}$$

$$I_o = S_A\left(\frac{V_o}{R_o}\right) + S_B\left(\frac{V_o}{R_o}\right) + S_C\left(\frac{V_o}{R_o}\right) \tag{7.57}$$

Equations (7.46)-(7.57) are simplified by grouping the common terms and is expressed as

$$V_{as} = (S_A + S_B + S_C)\left(r_s I_{as} + L_s p I_{as} + \frac{V_{dd}}{3}(2S_{ap} - S_{bp} - S_{cp})\right) \tag{7.58}$$

$$V_{bs} = (S_A + S_B + S_C)\left(r_s I_{bs} + L_s p I_{bs} + \frac{V_{dd}}{3}(-S_{ap} + 2S_{bp} - S_{cp})\right) \tag{7.59}$$

$$V_{cs} = (S_A + S_B + S_C)\left(r_s I_{cs} + L_s p I_{cs} + \frac{V_{dd}}{3}(-S_{ap} - S_{bp} + 2S_{cp})\right) \tag{7.60}$$

$$L_1 p I_1 = (S_A + S_C)V_{dd} + (S_A + S_B + S_C)(-r_1 I_1 - V_{c2}) \tag{7.61}$$

$$L_2 p I_2 = (S_A + S_C)V_{dd} + (S_A + S_B + S_C)(-r_2 I_2 - V_{c1}) \tag{7.62}$$

$$C_1 p V_{c1} = (S_A + S_B + S_C)(I_2 - I_L) \tag{7.63}$$

$$C_2 p V_{c2} = (S_A + S_B + S_C)(I_1 - I_L) \tag{7.64}$$

$$C_o p V_o = (S_A + S_C)I_L + (S_A + S_B + S_C)\left(-\frac{V_o}{R_o}\right) \tag{7.65}$$

The switching functions S_{ap}, S_{bp}, S_{cp} constitute to the active state S_A. That is during the shoot through state and the null state, the three phase currents are zero. Hence the term S_A can be neglected and (7.54) and (7.56) can be re-written as

$$I_L = (S_A + S_C)(I_1 + I_2) - (S_{ap} I_{as} + S_{bp} I_{bs} + S_{cp} I_{cs}) \tag{7.66}$$

$$I_n = (S_{ap} I_{as} + S_{bp} I_{bs} + S_{cp} I_{cs}) + S_B(I_1 + I_2) \tag{7.67}$$

$$V_{dd} = (S_A + S_C)(V_{c1} + V_{c2} - V_o) \tag{7.68}$$

$$I_o = (S_A + S_B + S_C)\left(\frac{V_o}{R_o}\right) \tag{7.69}$$

The combined equations (7.58)–(7.69) can be simplified using the expression (7.70) and the resulting equations are expressed as shown in (7.71)-(7.82)

$$S_A + S_B + S_C = 1 \tag{7.70}$$

$$V_{as} = r_s I_{as} + L_s p I_{as} + \frac{V_{dd}}{3}\left(2S_{ap} - S_{bp} - S_{cp}\right) \tag{7.71}$$

$$V_{bs} = r_s I_{bs} + L_s p I_{bs} + \frac{V_{dd}}{3}\left(-S_{ap} + 2S_{bp} - S_{cp}\right) \tag{7.72}$$

$$V_{cs} = r_s I_{cs} + L_s p I_{cs} + \frac{V_{dd}}{3}\left(-S_{ap} - S_{bp} + 2S_{cp}\right) \tag{7.73}$$

$$L_1 p I_1 = (S_A + S_C)(V_{c1} + V_{c2} - V_o) - r_1 I_1 - V_{c2} \tag{7.74}$$

$$L_2 p I_2 = (S_A + S_C)(V_{c1} + V_{c2} - V_o) - r_2 I_2 - V_{c1} \tag{7.75}$$

$$C_1 p V_{c1} = I_2 - (S_A + S_C)(I_1 + I_2) + \left(S_{ap} I_{as} + S_{bp} I_{bs} + S_{cp} I_{cs}\right) \tag{7.76}$$

$$C_2 p V_{c2} = I_1 - (S_A + S_C)(I_1 + I_2) + \left(S_{ap} I_{as} + S_{bp} I_{bs} + S_{cp} I_{cs}\right) \tag{7.77}$$

$$C_o p V_o = (S_A + S_C)(I_1 + I_2) - \left(S_{ap} I_{as} + S_{bp} I_{bs} + S_{cp} I_{cs}\right) - \frac{V_o}{R_o} \tag{7.78}$$

$$I_L = (S_A + S_C)(I_1 + I_2) - \left(S_{ap} I_{as} + S_{bp} I_{bs} + S_{cp} I_{cs}\right) \tag{7.79}$$

$$V_{dd} = (S_A + S_C)(V_{c1} + V_{c2} - V_o) \tag{7.80}$$

$$I_n = \left(S_{ap} I_{as} + S_{bp} I_{bs} + S_{cp} I_{cs}\right) + S_B(I_1 + I_2) \tag{7.81}$$

$$I_o = \frac{V_o}{R_o} \tag{7.82}$$

7.4 Switching Functions of the ZSR

The switching functions of the individual devices are obtained by combining the switching functions of the conventional boost rectifier and that of the shoot-through state. A portion of the conventional null state is used for injecting the shoot-through pulses. The active state S_A, shoot-through state S_B and the null state S_C are shown in Figure 7.5. When $S_A=1$, it refers to the converter being in active state, otherwise the system is operating in either the null state or the shoot-through state. When $S_B=1$, it refers to the converter operating in shoot-through state and when $S_C=1$, it implies that the system is operating in null state. The individual switching functions for the individual devices are shown in Figure 7.6. These switching functions include the shoot-through pulses.
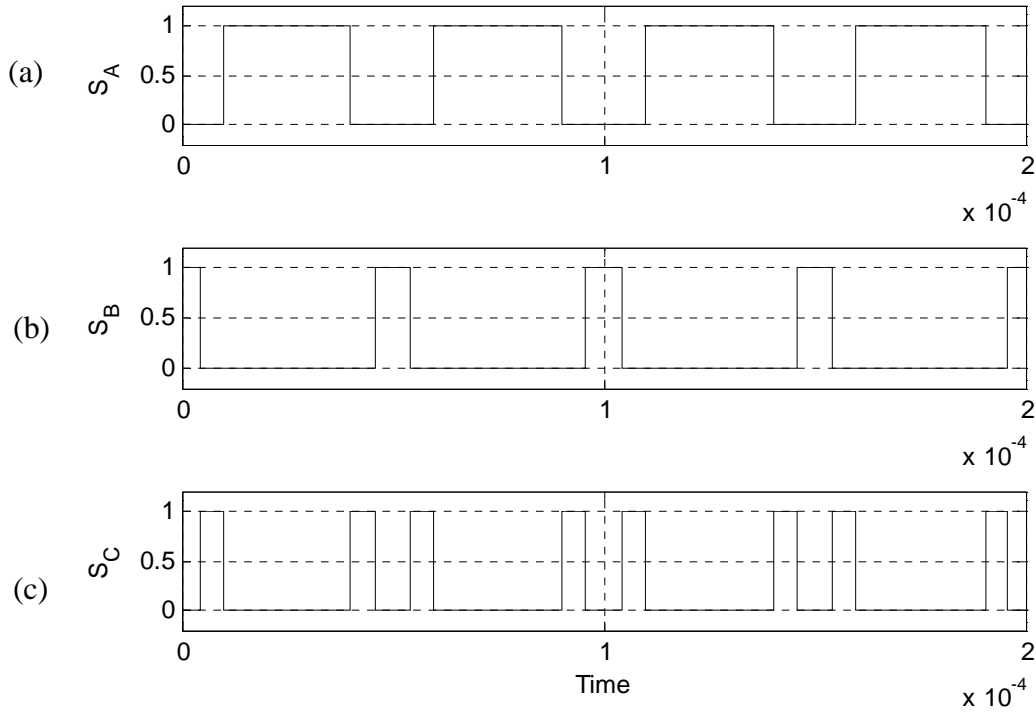
Figure 7.5: Switching function (a) Active State, (b) Shoot-through State, (c) Null state

170
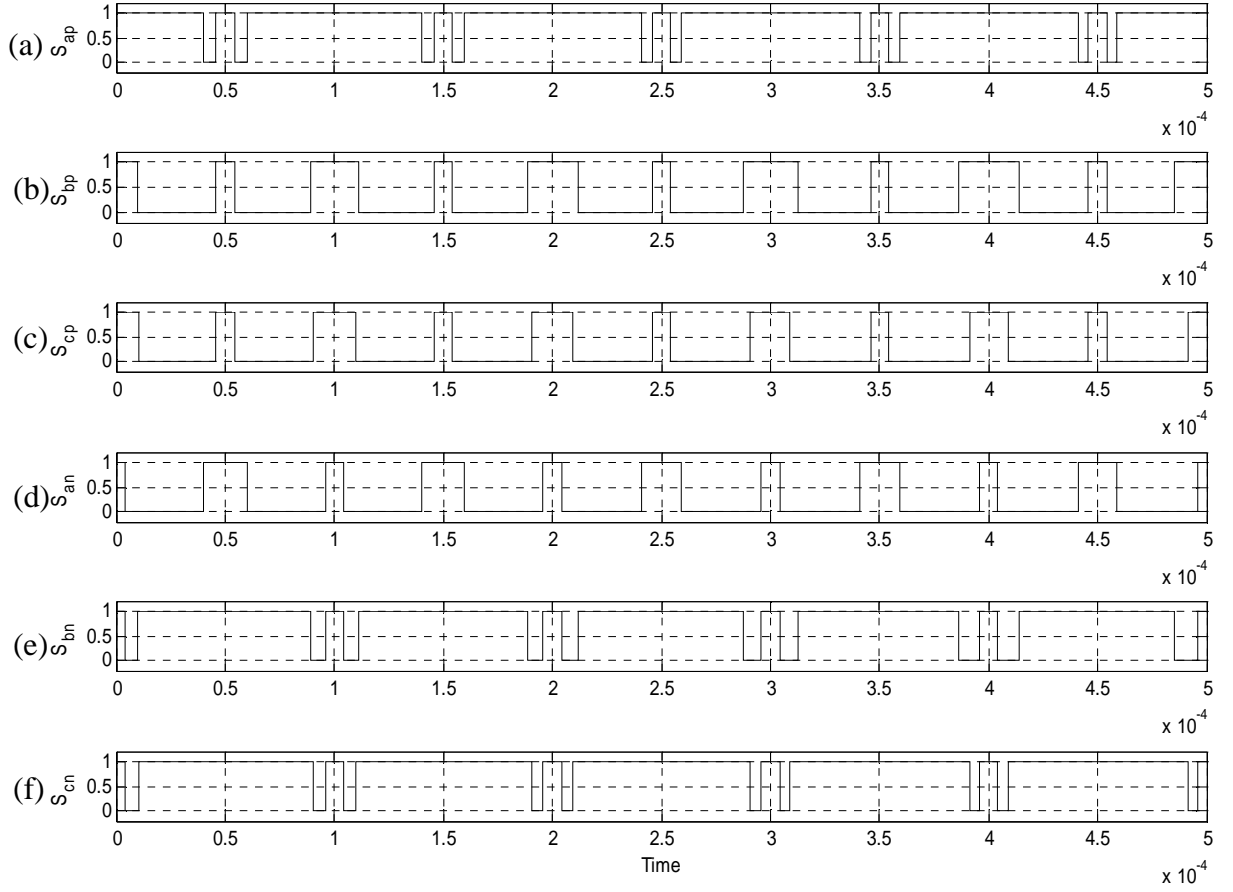
Figure 7.6: Switching function for the individual devices (a) phase 'a' – top device, (b) phase 'b' – top device, (c) phase 'c' – top device, (d) phase 'a' – bottom device, (e) phase 'b' – bottom device, (f) phase 'c' – bottom device

171

7.5 Unity Power Factor Operation

The sum of the active state, shoot-through state, and null state switching functions are equal to unity. The expression is as shown in (7.70).

Since the shoot-through state can be represented as d, the sum of the active state and the null state is given as

$$S_A + S_C = 1 - d \tag{7.83}$$

where

d is the average of D_o

The generalized average model equations in the qd reference frame are given as shown in (7.84)-(7.94) when the expression in (7.83) is substituted.

$$V_{qs} = r_s I_{qs} + L_s p I_{qs} + L_s \omega_e I_{ds} + \frac{V_{dd} M_{qs}}{2} \tag{7.84}$$

$$V_{ds} = r_s I_{ds} + L_s p I_{ds} - L_s \omega_e I_{qs} + \frac{V_{dd} M_{ds}}{2} \tag{7.85}$$

$$L_1 p I_1 = V_{dd} - r_1 I_1 - V_{c2} \tag{7.86}$$

$$L_2 p I_2 = V_{dd} - r_2 I_2 - V_{c1} \tag{7.87}$$

$$C_1 p V_{c1} = I_2 - I_L \tag{7.88}$$

$$C_2 p V_{c2} = I_1 - I_L \tag{7.89}$$

$$C_o p V_o = (1-d)(I_1 + I_2) - \frac{3}{2}(M_{qs} I_{qs} + M_{ds} I_{ds}) - \frac{V_o}{R_o} \tag{7.90}$$

$$I_L = (1-d)(I_1 + I_2) - \frac{3}{2}(M_{qs} I_{qs} + M_{ds} I_{ds}) \tag{7.91}$$

$$V_{dd} = (1 - d)(V_{c1} + V_{c2} - V_o)$$ (7.92)

$$I_n = \frac{3}{2}(M_{qs}I_{qs} + M_{ds}I_{ds}) + d(I_1 + I_2)$$ (7.93)

$$I_o = \frac{V_o}{R_o}$$ (7.94)

The steady state analysis of the Z-Source Rectifier is performed when the derivative terms of the synchronous reference frame qd model equations are made zero.

To obtain unity power factor, the input reactive power has to be equal to zero. The equation for the reactive power is

$$Q = \frac{3}{2}(V_{ds}I_{qs} - V_{qs}I_{ds}) = 0$$ (7.95)

Now, $V_{qs} = V_m \cos(\theta_{eo} - \theta_o)$ (7.96)

$$V_{ds} = -V_m \sin(\theta_{eo} - \theta_o)$$ (7.97)

Where θ_{eo} - initial angle of the supply voltage

θ_o - initial angle of the reference frame

The initial angle of the reference frame is forced to be equal to the initial angle of the supply voltage

$$\Rightarrow \theta_{eo} = \theta_o$$ (7.98)

This results in the qd input voltages to be

$$V_{qs} = V_m$$ (7.99)

$$V_{ds} = 0$$ (7.100)

When $Q = 0$ and when $V_{ds} = 0$, it automatically implies that

$$I_{ds} = 0$$ (7.101)

7.6 Conclusion

In this chapter, the Z-Source Rectifier's operating modes were explained in detail. It was seen that there were only three operating states in this case because the switch connecting the Z-source network and the load was kept open during the shoot-through state. That switch could have been open during the null state also but it was avoided in order to make sure that the load was not left open. The averaging technique was illustrated in detail to obtain the generalized model equations. The simplified dynamic model equations were derived in the qd synchronous reference frame. The conditions for unity power factor were derived and laid out.

CHAPTER 8

ANALYSIS OF Z-SOURCE RECTIFIERS

8.1 Introduction

The Z-Source rectifier can accurately produce the correct volt-sec average at its output along with simultaneously achieving inductive voltage boosting through careful control. These performances are obtained at no increase of the number of semiconductor devices and commutations. Minimal passive elements are utilized in this case. The characteristics of the model of the Z-source rectifier has to be studied in order to verify the theory stated.

The steady state analysis is performed while the objective is to achieve unity power factor. The model equations are combined using the averaging technique and harmonic balance technique is used to derive the steady state equations. The results of the steady state analysis are utilized in the dynamic analysis to study the transients of the system. Eventually the steady state and simulation results verify the proposed theories. The small signal analysis is performed to study the stability of the system.

8.2 Harmonic Balance Technique

The equations for the steady state analysis as well as the equation for the ripple current and voltage in the Z-network can be determined using the harmonic balance technique. Harmonic balance technique for a linear system states that, for a given system, for example the output will have the same form as the input. That is, both sides of an equation will be of the same order.

The qd synchronous dynamic equations of the Z-source rectifier are as shown in equations (7.71)-(7.82). With the assumption that the Z–source network is symmetrical, such that the currents through the two inductors and the voltages across the capacitors are equal, the state equations can be re-written as shown in (8.1) and (8.2). The shoot-through duty ratio D_o is averaged to become d.

$$LpI = 2(1-d)(V_{sc} - V_o) - r_{12}I - V_{sc}$$ (8.1)

$$CpV_{sc} = I(-1+2d) + 3(M_{qs}I_{qs} + M_{ds}I_{ds})$$ (8.2)

$$C_o pV_o = (1-d)I - \frac{3}{2}(M_{qs}I_{qs} + M_{ds}I_{ds}) - \frac{V_o}{R_o}$$ (8.3)

where

$$I = I_1 + I_2$$

$$V_{sc} = V_{c1} + V_{c2}$$

The Fast Fourier Transformation (FFT) was performed on the variables and they can be expressed as shown in (8.4)-(8.12)

$$I_{qs} = \text{Re}(I_{qso} + I_{qs1}e^{j\theta_e})$$ (8.4)

$$I_{ds} = \text{Re}\left(I_{dso} + I_{ds1}e^{j\theta_e}\right) \tag{8.5}$$

$$V_{dd} = \text{Re}\left(V_{ddo} + V_{dd1}e^{j\theta_e}\right) \tag{8.6}$$

$$I = \text{Re}\left(I_o + I_1 e^{j\theta_e} + I_5 e^{j5\theta_e} + I_6 e^{j6\theta_e}\right) \tag{8.7}$$

$$d = \text{Re}\left(d_o + d_6 e^{j6\theta_e}\right) \tag{8.8}$$

$$M_{qs} = \text{Re}\left(M_{qso} + M_{qs6}e^{j6\theta_e}\right) \tag{8.9}$$

$$M_{ds} = \text{Re}\left(M_{dso} + M_{ds6}e^{j6\theta_e}\right) \tag{8.10}$$

$$V_{sc} = \text{Re}\left(V_{sco} + V_{sc1}e^{j\theta_e}\right) \tag{8.11}$$

$$V_o = \text{Re}\left(V_{oo} + V_{o1}e^{j\theta_e}\right) \tag{8.12}$$

The equations (8.4)-(8.12) are substituted in the average dynamic equations to obtain (8.13)-(8.17)

$$V_{qs} = r_s \,\text{Re}\left(I_{qso} + I_{qs1}e^{j\theta_e}\right) + L_s p\,\text{Re}\left(I_{qso} + I_{qs1}e^{j\theta_e}\right) + L_s \omega_e\,\text{Re}\left(I_{dso} + I_{ds1}e^{j\theta_e}\right)$$

$$+ \frac{1}{2}\text{Re}\left(V_{ddo} + V_{dd1}e^{j\theta_e}\right)\text{Re}\left(M_{qso} + M_{qs6}e^{j6\theta_e}\right) \tag{8.13}$$

$$V_{ds} = r_s \,\text{Re}\left(I_{dso} + I_{ds1}e^{j\theta_e}\right) + L_s p\,\text{Re}\left(I_{dso} + I_{ds1}e^{j\theta_e}\right) + L_s \omega_e\,\text{Re}\left(I_{qso} + I_{qs1}e^{j\theta_e}\right)$$

$$+ \frac{1}{2}\text{Re}\left(V_{ddo} + V_{dd1}e^{j\theta_e}\right)\text{Re}\left(M_{dso} + M_{ds6}e^{j6\theta_e}\right) \tag{8.14}$$

$$Lp\,\text{Re}\left(I_o + I_1 e^{j\theta_e} + I_5 e^{j5\theta_e} + I_6 e^{j6\theta_e}\right) = 2\left(1 - \text{Re}\left(d_o + d_6 e^{j6\theta_e}\right)\right)\left(\begin{array}{c}\text{Re}\left(V_{sco} + V_{sc1}e^{j\theta_e}\right)\\ -\,\text{Re}\left(V_{oo} + V_{o1}e^{j\theta_e}\right)\end{array}\right)$$

$$-\, r_{12}\,\text{Re}\left(I_o + I_1 e^{j\theta_e} + I_5 e^{j5\theta_e} + I_6 e^{j6\theta_e}\right) - \text{Re}\left(V_{sco} + V_{sc1}e^{j\theta_e}\right) \tag{8.15}$$

$$Cp\,\text{Re}\left(V_{sco} + V_{sc1}e^{j\theta_e}\right) = \text{Re}\left(I_o + I_1 e^{j\theta_e} + I_5 e^{j5\theta_e} + I_6 e^{j6\theta_e}\right)\left(-1 + 2\,\text{Re}\left(d_o + d_6 e^{j6\theta_e}\right)\right)$$
$$+ 3\left(\text{Re}\left(M_{qso} + M_{qs6}e^{j6\theta_e}\right)\text{Re}\left(I_{qso} + I_{qs1}e^{j\theta_e}\right) + \text{Re}\left(M_{dso} + M_{ds6}e^{j6\theta_e}\right)\text{Re}\left(I_{dso} + I_{ds1}e^{j\theta_e}\right)\right)$$

$$\tag{8.16}$$

$$C_o p \operatorname{Re}\left(V_{oo} + V_{o1}e^{j6\theta_e}\right) = \left(1 - \operatorname{Re}\left(d_o + d_6 e^{j6\theta_e}\right)\right)\operatorname{Re}\left(I_o + I_1 e^{j\theta_e} + I_5 e^{j5\theta_e} + I_6 e^{j6\theta_e}\right)$$

$$- \frac{3}{2}\left(\operatorname{Re}\left(M_{qso} + M_{qs6}e^{j6\theta_e}\right)\operatorname{Re}\left(I_{qso} + I_{qs1}e^{j\theta_e}\right) + \operatorname{Re}\left(M_{dso} + M_{ds6}e^{j6\theta_e}\right)\operatorname{Re}\left(I_{dso} + I_{ds1}e^{j\theta_e}\right)\right)$$

$$- \frac{1}{R_o}\operatorname{Re}\left(V_{oo} + V_{o1}e^{j\theta_e}\right) \tag{8.17}$$

The identity given in (8.18) is used to solve the equations (8.13)-(8.17) to obtain (8.19)-(8.23).

$$\operatorname{Re}(A)\operatorname{Re}(B) = \frac{\operatorname{Re}(AB)}{2} + \frac{\operatorname{Re}(AB^*)}{2} \tag{8.18}$$

$$V_{qs} = r_s I_{qso} + L_s p I_{qso} + L_s \omega_e I_{dso} + \frac{V_{ddo}M_{qso}}{2} + r_s \operatorname{Re} I_{qs1}e^{j\theta_e} + L_s \operatorname{Re} p I_{qs1}e^{j\theta_e}$$

$$+ jL_s\omega_e \operatorname{Re} I_{qs1}e^{j\theta_e} + L_s\omega_e \operatorname{Re} I_{ds1}e^{j\theta_e} + \frac{\operatorname{Re}}{2}\left(V_{dd1}M_{qso}e^{j\theta_e}\right) + \operatorname{Re} V_{ddo}M_{qs6}e^{j6\theta_e}$$

$$+ \frac{\operatorname{Re}}{2}\left(V_{dd1}M_{qs6}e^{j7\theta_e}\right) + \frac{\operatorname{Re}}{2}\left(V_{dd1}M_{qs6}e^{-j5\theta_e}\right) \tag{8.19}$$

$$V_{ds} = r_s I_{dso} + L_s p I_{dso} - L_s \omega_e I_{qso} + \frac{V_{ddo}M_{dso}}{2} + r_s \operatorname{Re} I_{ds1}e^{j\theta_e} + L_s \operatorname{Re} p I_{ds1}e^{j\theta_e}$$

$$+ jL_s\omega_e \operatorname{Re} I_{ds1}e^{j\theta_e} - L_s\omega_e \operatorname{Re} I_{qs1}e^{j\theta_e} + \frac{\operatorname{Re}}{2}\left(V_{dd1}M_{dso}e^{j\theta_e}\right) + \operatorname{Re} V_{ddo}M_{ds6}e^{j6\theta_e}$$

$$+ \frac{\operatorname{Re}}{2}\left(V_{dd1}M_{ds6}e^{j7\theta_e}\right) + \frac{\operatorname{Re}}{2}\left(V_{dd1}M_{ds6}e^{-j5\theta_e}\right) \tag{8.20}$$

$$Lp \operatorname{Re}\left(I_o + I_1 e^{j\theta_e} + I_5 e^{j5\theta_e} + I_6 e^{j6\theta_e}\right) = 2\left(\begin{array}{l} \operatorname{Re}\left(V_{sco} - V_{oo} + \left(V_{sc1} - V_{o1}\right)e^{j\theta_e}\right) \\ - \frac{\operatorname{Re}}{2}\left(\begin{array}{l} 2d_o V_{sco} + \left(2d_o V_{sc1} - d_o V_{o1}\right)e^{j\theta_e} - 2d_o V_{oo} \\ + \left(2d_6 V_{sco} - 2d_6 V_{oo}\right)e^{j6\theta_e} + \left(d_6 V_{sc1} - d_6 V_{o1}\right)e^{j7\theta_e} \\ + \left(d_6 V_{sc1} - d_6 V_{o1}\right)e^{j5\theta_e} \end{array}\right) \end{array}\right)$$

$$+ r_{12} \operatorname{Re}\left(I_o + I_1 e^{j\theta_e} + I_5 e^{j5\theta_e} + I_6 e^{j6\theta_e}\right) - \operatorname{Re}\left(V_{sco} - V_{sc1}e^{j\theta_e}\right) \tag{8.21}$$

$$C\,\mathrm{Re}\!\left(pV_{sco} + pV_{sc1}e^{j\theta_e} + j\omega_e V_{sc1}e^{j\theta_e}\right) = -\mathrm{Re}\!\left(I_o + I_1 e^{j\theta_e} + I_5 e^{j5\theta_e} + I_6 e^{j6\theta_e}\right)$$

$$+\,\mathrm{Re}\!\begin{pmatrix} 2I_o d_o + I_6 d_6 + \left(2I_o d_6 + 2I_6 d_o\right)e^{j6\theta_e} + 2I_1 d_o e^{j\theta_e} + I_1 d_6 e^{j7\theta_e} + 2I_5 d_o e^{j5\theta_e} \\ +\, I_5 d_6 e^{j11\theta_e} + I_6 d_6 e^{j12\theta_e} + I_1 d_6 e^{-j5\theta_e} + I_5 d_6 e^{-j\theta_e} \end{pmatrix}$$

$$+\,\frac{3\,\mathrm{Re}}{2}\!\begin{pmatrix} 2M_{qso}I_{qso} + 2M_{qso}I_{qs1}e^{j\theta_e} + 2M_{qs6}I_{qso}e^{j6\theta_e} + M_{qs6}I_{qs1}e^{j7\theta_e} + M_{qs6}I_{qs1}e^{j5\theta_e} \\ +\, 2M_{dso}I_{dso} + 2M_{dso}I_{ds1}e^{j\theta_e} + 2M_{ds6}I_{dso}e^{j6\theta_e} + M_{ds6}I_{ds1}e^{j7\theta_e} + M_{ds6}I_{ds1}e^{j5\theta_e} \end{pmatrix}$$

$$(8.22)$$

$$C_o\,\mathrm{Re}\!\left(pV_{oo} + pV_{o1}e^{j\theta_e} + j\omega_e V_{o1}e^{j\theta_e}\right) = \mathrm{Re}\!\left(I_o + I_1 e^{j\theta_e} + I_5 e^{j5\theta_e} + I_6 e^{j6\theta_e}\right)$$

$$-\,\frac{\mathrm{Re}}{2}\!\begin{pmatrix} 2d_o I_o + d_6 I_6 + \left(2d_o I_o + d_6 I_5\right)e^{j\theta_e} + \left(2d_o I_5 + d_6 I_1\right)e^{j5\theta_e} \\ +\, \left(2d_o I_6 + d_6 I_o\right)e^{j6\theta_e} + d_6 I_1 e^{j7\theta_e} + d_6 I_5 e^{j11\theta_e} + d_6 I_6 e^{j12\theta_e} \end{pmatrix}$$

$$-\,\frac{3\,\mathrm{Re}}{4}\!\begin{pmatrix} 2M_{qso}I_{qso} + 2M_{qso}I_{qs1}e^{j\theta_e} + 2M_{qs6}I_{qs6}e^{j6\theta_e} + M_{qs6}I_{qs1}e^{j7\theta_e} \\ +\, M_{qs6}I_{qs1}e^{j5\theta_e} + 2M_{dso}I_{dso} + 2M_{dso}I_{ds1}e^{j\theta_e} + 2M_{ds6}I_{ds6}e^{j6\theta_e} \\ +\, M_{ds6}I_{ds1}e^{j7\theta_e} + M_{ds6}I_{ds1}e^{j5\theta_e} \end{pmatrix}$$

$$-\,\frac{\mathrm{Re}}{R_o}\!\left(V_{oo} + V_{o1}e^{j\theta_e}\right) \qquad (8.23)$$

By separating the average terms from the above equations, the average equations can be obtained as shown in (8.24)-(8.28)

$$V_{qs} = r_s I_{qso} + L_s pI_{qso} + L_s \omega_e I_{dso} + \frac{V_{ddo}M_{qso}}{2} \qquad (8.24)$$

$$V_{ds} = r_s I_{dso} + L_s pI_{dso} - L_s \omega_e I_{qso} + \frac{V_{ddo}M_{dso}}{2} \qquad (8.25)$$

$$LpI_o = 2\!\left(\left(1 - d_o\right)\left(V_{sco} - V_{oo}\right)\right) - r_{12}I_o - V_{sco} \qquad (8.26)$$

$$CpV_{sco} = I_o\!\left(-1 + 2d_o\right) + I_6 d_6 + 3\!\left(M_{qso}I_{qso} + M_{dso}I_{dso}\right) \qquad (8.27)$$

$$C_o pV_{oo} = I_o\!\left(1 - d_o\right) + \frac{d_6 I_6}{2} - \frac{3}{2}\!\left(M_{qso}I_{qso} + M_{dso}I_{dso}\right) - \frac{V_{oo}}{R_o} \qquad (8.28)$$

8.3 Steady State Analysis of ZSR

The steady state analysis is performed when all the derivative terms of the dynamic equations are zero.

8.3.1 Steady State Analysis Derivation

By substituting (7.100) and (7.101) in (7.84) and (7.85), the q-axis input voltage and current can be obtained as shown in (8.29) and (8.30).

$$V_{qs} = r_s I_{qs} + \frac{M_{qs} V_{dd}}{2} \qquad (8.29)$$

$$I_{qs} = \frac{M_{qs} V_{dd}}{2\omega_e L_s} \qquad (8.30)$$

From (7.88) and (7.89), it is known that the Z-network inductor currents are equal to the output of the Z-network.

$$I_1 = I_2 = I_L \qquad (8.31)$$

From (7.86) and (7.87), the following expressions are obtained

$$V_{c1} = V_{dd} - r_2 I_2 \qquad (8.32)$$

$$V_{c2} = V_{dd} - r_1 I_1 \qquad (8.33)$$

Also from (7.90),

$$I_L = \frac{V_o}{R_o} \qquad (8.34)$$

By substituting (8.30) and (8.31) in (7.91), the dc output current of the Z-network is given as shown in (8.35)

$$I_L = \frac{3M_{qs}M_{ds}V_{dd}}{4\omega_e L_s \left(1 - 2D_o\right)} \tag{8.35}$$

Substituting (8.35) in (8.34),

$$\frac{3M_{qs}M_{ds}V_{dd}}{4\omega_e L_s \left(1 - 2D_o\right)} = \frac{V_o}{R_o} \tag{8.36}$$

By substituting (8.32) and (8.33) in (7.92), the output voltage of the rectifier can be expressed as shown in (8.37)

$$V_o = -rI_L + V_{dd}\left(\frac{1 - 2D_o}{1 - D_o}\right) \tag{8.37}$$

where $r_1 + r_2 = r$

Substituting (8.37) in (8.36)

$$\frac{3M_{qs}M_{ds}V_{dd}}{4\omega_e L_s \left(1 - 2D_o\right)} = \frac{-rI_L}{R_o} + \frac{V_{dd}}{R_o}\left(\frac{1 - 2D_o}{1 - D_o}\right) \tag{8.38}$$

Eliminating I_L from the above expression, the product of the q-axis and d-axis modulation signals is given as shown in (8.39)

$$M_{qs}M_{ds} = \frac{4\omega_e L_s \left(1 - 2D_o\right)^2}{3\left(r - R_o\right)\left(1 - D_o\right)} \tag{8.39}$$

The product of the q-axis and d-axis modulation signals is a constant for a given value of shoot-through duty ratio as seen in (8.39). Hence is it defined as Y.

$$Y = \frac{4\omega_e L_s \left(1 - 2D_o\right)^2}{3\left(r - R_o\right)\left(1 - D_o\right)}$$

Now, $M_{ds} = \dfrac{Y}{M_{qs}}$ (8.40)

Also the modulation index M is defined as $M^2 = M_{qs}^2 + M_{ds}^2$ (8.41)

Hence by substituting (8.40) in (8.41), the q-axis modulation signal can be solved for.

$$M_{qs}^4 - M^2 M_{qs}^2 + Y^2 = 0$$

The other steady state parameters of the system can be solved for using the above equations. By substituting (7.77) in (7.76), the q-axis input voltage can be obtained as

$$V_{qs} = \dfrac{2\omega_e L_s V_{qs} M_{qs}}{r_s Y + \omega_e L_s M_{qs}}$$ (8.42)

Hence the other parameters are obtained as follows

$$V_{dd} = \dfrac{2\omega_e L_s V_{qs}}{r_s M_{ds} + \omega_e L_s M_{qs}}$$ (8.43)

$$I_L = \dfrac{3M_{qs} I_{qs}}{2(1 - 2D_o)} = I_1 = I_2$$ (8.44)

$$V_o = I_L R_o$$ (8.45)

$$V_c = V_{dd} - rI_L$$ (8.46)

$$I_n = \dfrac{3}{2}\left(M_{qs} I_{qs}\right) + 2D_o I_L$$ (8.47)

$$I_o = I_L$$ (8.48)

8.3.2 Steady State Results

The steady state results shown are obtained by using the parameters shown in Table 8.1. To illustrate the relationship between the q-axis and d-axis modulation signals, four different values of modulation index, m = 0.6, 0.7, 0.8, 0.9 has been used. It is seen from Figure 8.1 - Figure 8.4 that for a reasonable output, the values of the q-axis modulation signal is large compared to that of the q-axis modulation signal while the shoot-through duty ratio D_o is varied from its minimum to its maximum. All the other parameters are plotted for four different values of the modulation index, namely m = 0.6, 0.7, 0.8, and 0.9.

Table 8.1: Parameters used in the steady state analysis and their values

Parameter	Value
V_{qs}	180 V
r_s	0.5 Ω
L_s	2 mH
f	60 Hz
R	50 Ω
r	0.24 Ω
L	3.615 mH
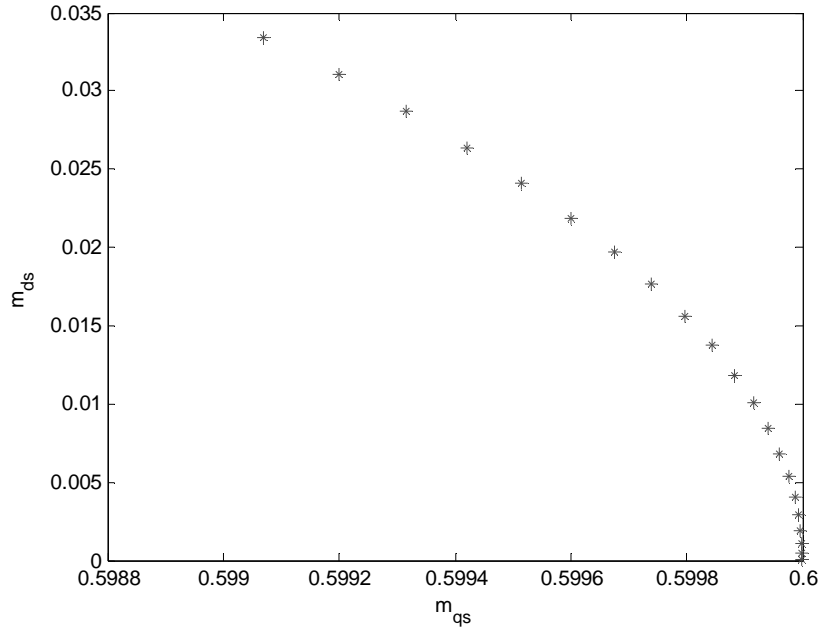
Figure 8.1: Relationship between M_{qs} and M_{ds} for m = 0.6 for varying D_o
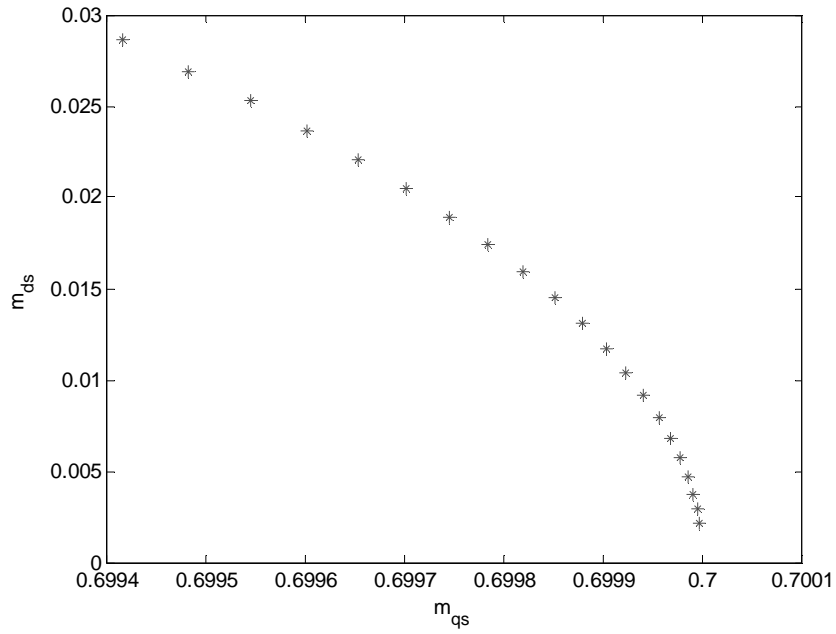
Figure 8.2: Relationship between M_{qs} and M_{ds} for m = 0.7 for varying D_o
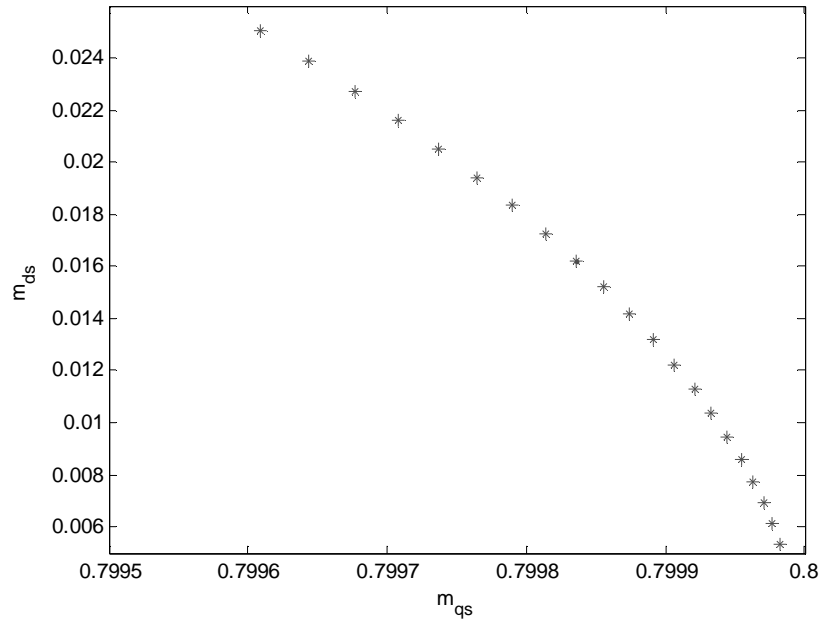
Figure 8.3: Relationship between M_{qs} and M_{ds} for m = 0.8 for varying D_o
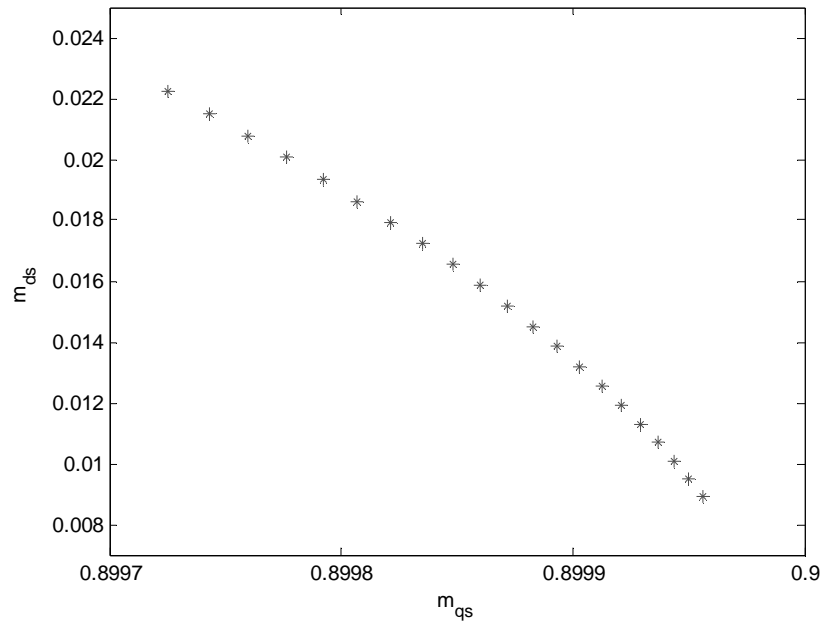
Figure 8.4: Relationship between M_{qs} and M_{ds} for m = 0.9 for varying D_o

Figure 8.5 shows the input supply power P_{in} for the four different values of the modulation index. Figure 8.6 shows the input current to the Z-source network I_n which is also the output dc current of the rectifier. Figure 8.7 illustrates the input power factor for the Z-source rectifier. It is seen that the input power factor is always one for all the operating conditions. Figure 8.8 shows the output load power P_o. The load used here is a resistive load. Hence the relationship between the power and voltage is given as $P_o = V_o I_o$. Figure 8.9 shows the Z-source network capacitor voltages. V_{c1}, V_{c2}. It is seen that for lower values of the modulation index, the capacitor voltages are higher. Figure 8.10 explains the behavior of the inductor currents in the Z-source network I_1, I_2. A similar trend compared to that of the capacitor voltages is seen in this case also where as the modulation index increases, the inductor current decreases. Figure 8.11 shows the q-axis input current I_{qs}. Figure 8.12 shows the plots of the dc current coming out of the Z-source network I_L. Figure 8.13 illustrates the behavior of the load voltage V_o. Figure 8.14 shows the behavior of the dc input voltage to the Z-source network V_{dd}.
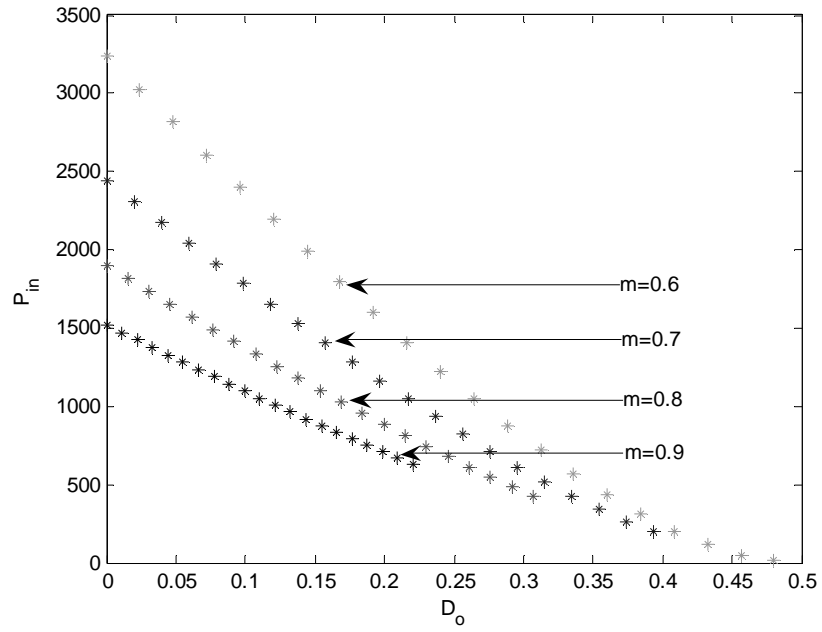
Figure 8.5: Input power, P_{in} for various values of m while varying D_o at 50 Ω load
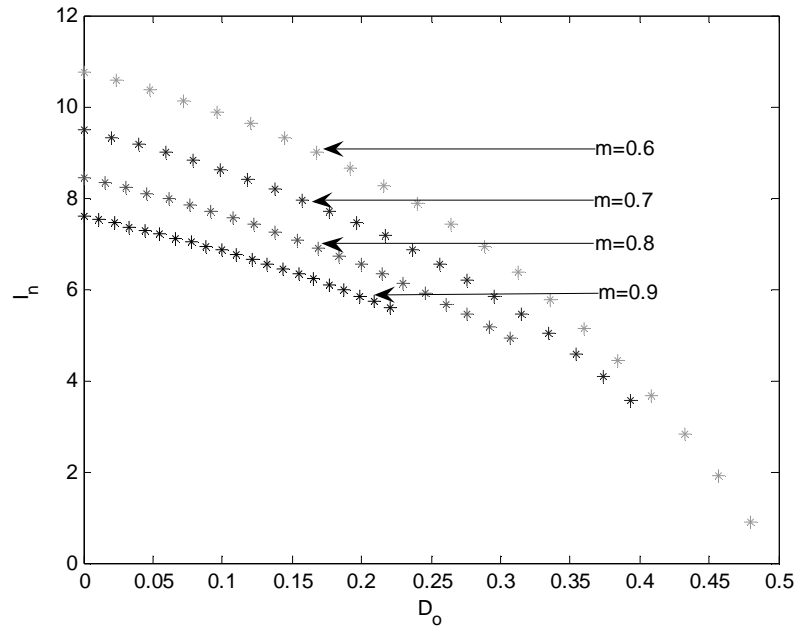
resistance

Figure 8.6: Input current to the Z-network, I_n for various values of m while varying D_o

at 50 Ω load resistance
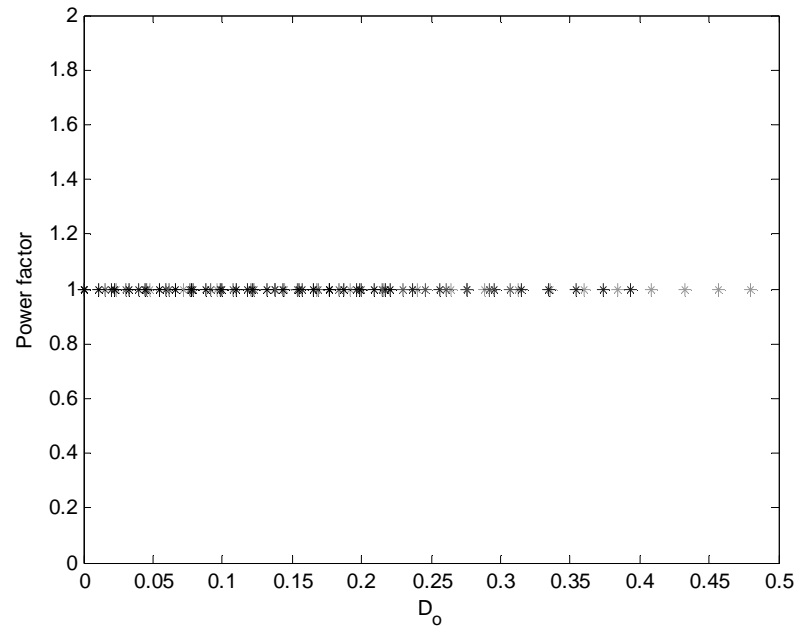
Figure 8.7: Input power factor for various values of m while varying D_o at 50 Ω load
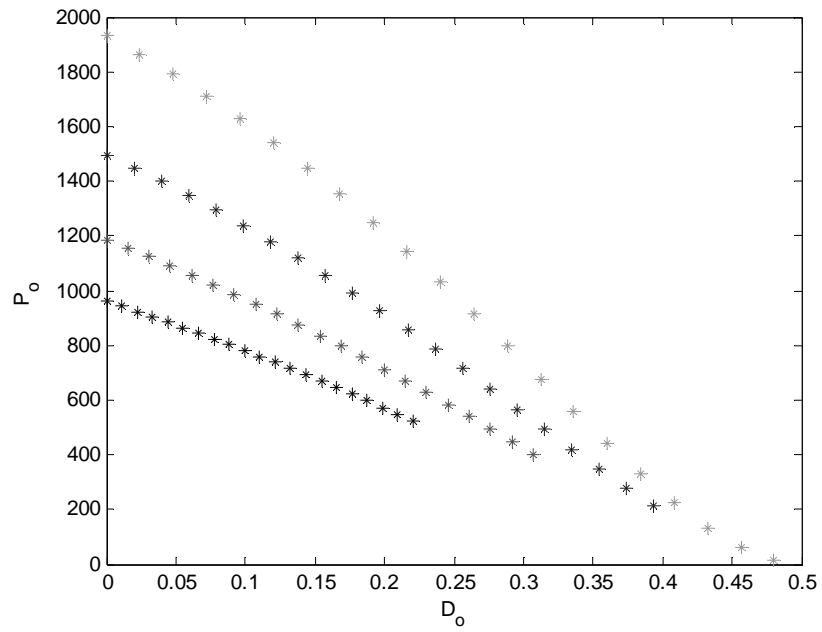
resistance

Figure 8.8: Output load power, P_o for various values of m while varying D_o at 50 Ω
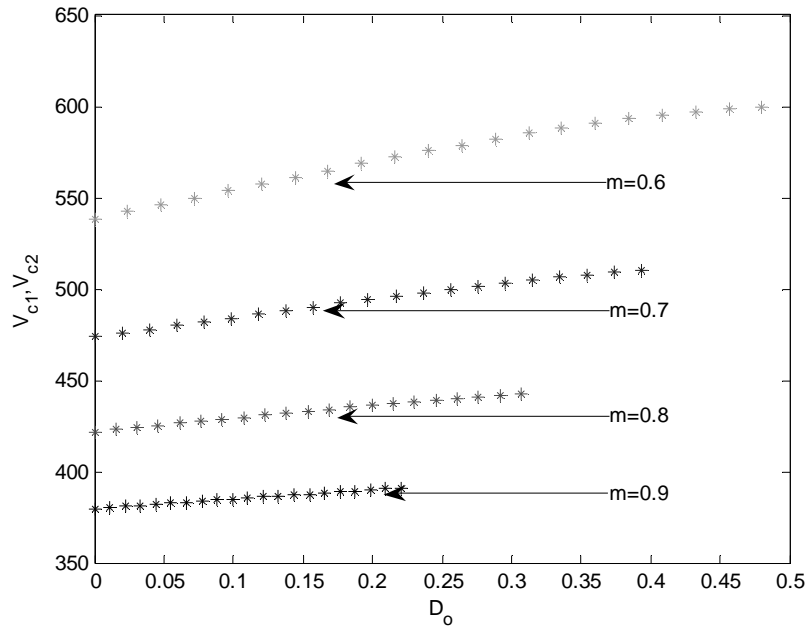
load resistance

Figure 8.9: Capacitor voltages V_{c1}, V_{c2} of the Z-network for various values of m while

varying D_o at 50 Ω load resistance
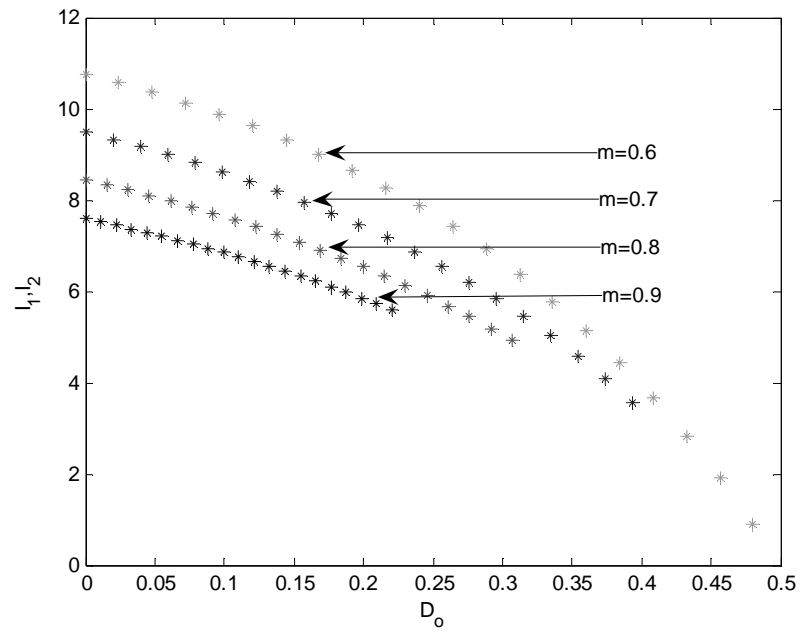
Figure 8.10: Inductor currents I_1, I_2 of the Z-network for various values of m while

varying D_o at 50 Ω load resistance

189
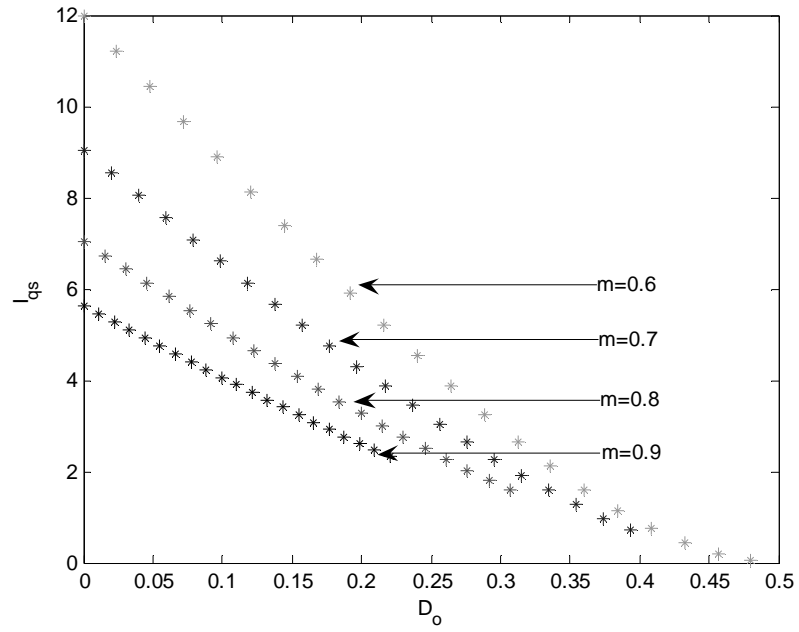
Figure 8.11: Input q-axis current I_{qs} for various values of m while varying D_o at 50 Ω
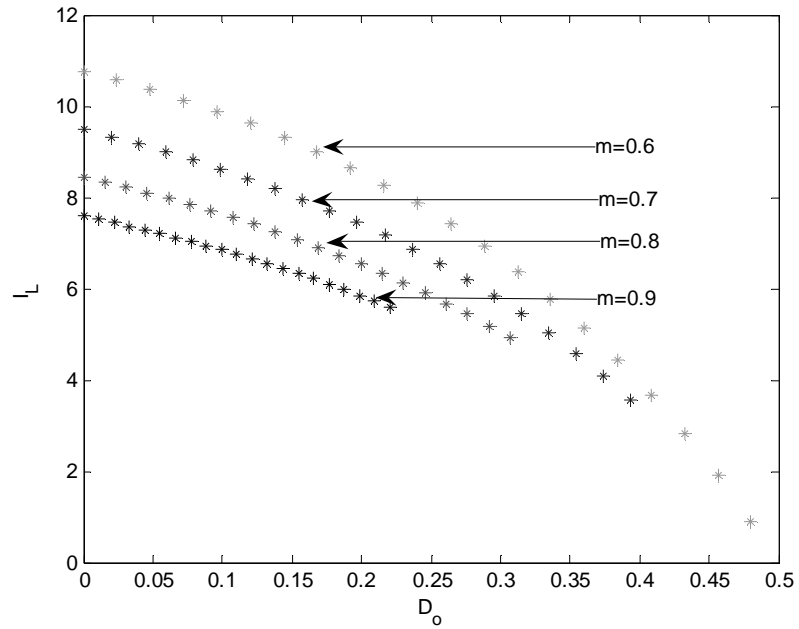
load resistance

Figure 8.12: Output current of the Z-network, I_L for various values of m while varying

D_o at 50 Ω load resistance
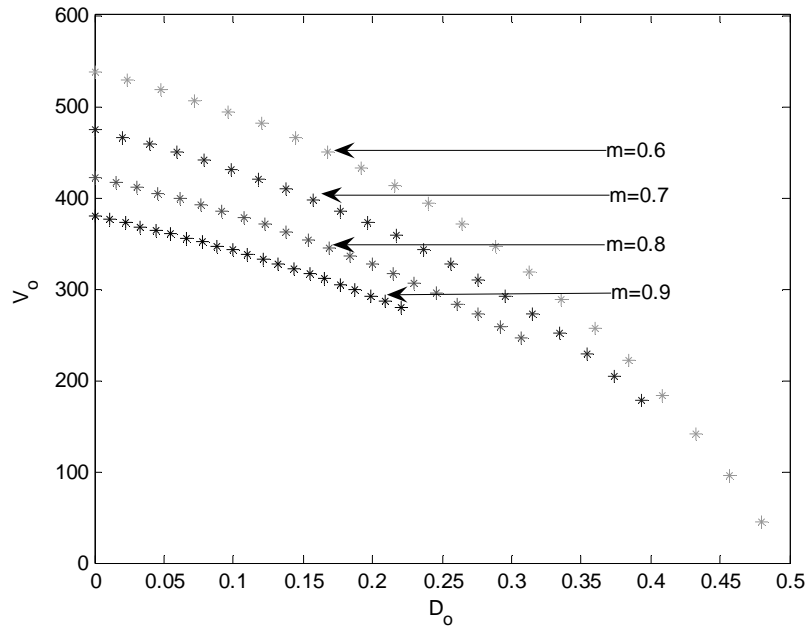
Figure 8.13: Output load voltage, V_o for various values of m while varying D_o at 50 Ω
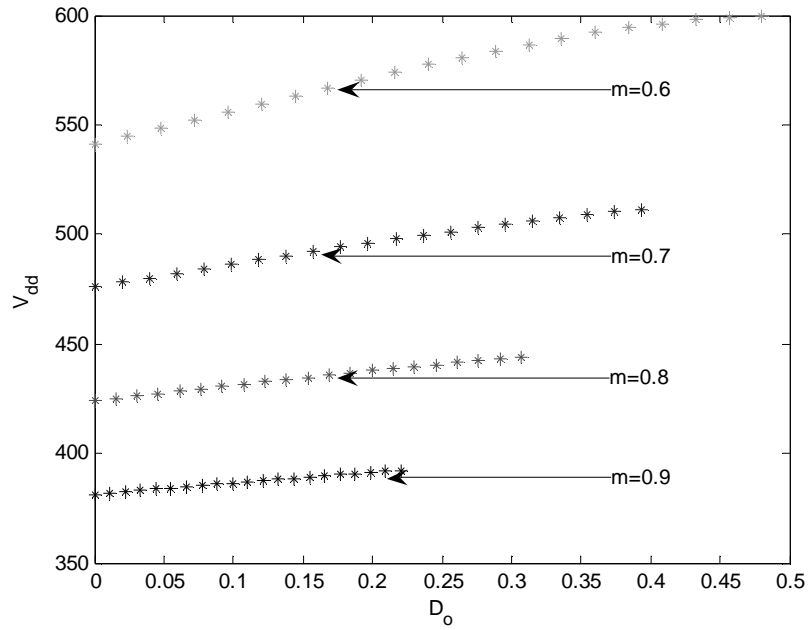
load resistance

Figure 8.14: Output dc voltage, V_{dd} of the Z-network for various values of m while

varying D_o at 50 Ω load resistance

8.4 Simplified Model Equations

The simplified model equations of the Z-source network in the qd synchronous reference frame can be written as

$$V_{qs} = r_s I_{qs} + L_s p I_{qs} + L_s \omega_e I_{ds} + \frac{(1 - D_o)(V_{c1} + V_{c2} - V_o)M_{qs}}{2} \tag{8.49}$$

$$V_{ds} = r_s I_{ds} + L_s p I_{ds} - L_s \omega_e I_{qs} + \frac{(1 - D_o)(V_{c1} + V_{c2} - V_o)M_{ds}}{2} \tag{8.50}$$

$$L_1 p I_1 = (1 - D_o)(V_{c1} + V_{c2} - V_o) - r_1 I_1 - V_{c2} \tag{8.51}$$

$$L_2 p I_2 = (1 - D_o)(V_{c1} + V_{c2} - V_o) - r_2 I_2 - V_{c1} \tag{8.52}$$

$$C_1 p V_{c1} = I_2 - (1 - D_o)(I_1 + I_2) + \frac{3}{2}(M_{qs} I_{qs} + M_{ds} I_{ds}) \tag{8.53}$$

$$C_2 p V_{c2} = I_1 - (1 - D_o)(I_1 + I_2) + \frac{3}{2}(M_{qs} I_{qs} + M_{ds} I_{ds}) \tag{8.54}$$

$$C_o p V_o = (1 - D_o)(I_1 + I_2) - \frac{3}{2}(M_{qs} I_{qs} + M_{ds} I_{ds}) - \frac{V_o}{R_o} \tag{8.55}$$

$$I_L = (1 - D_o)(I_1 + I_2) - \frac{3}{2}(M_{qs} I_{qs} + M_{ds} I_{ds}) \tag{8.56}$$

$$V_{dd} = (1 - D_o)(V_{c1} + V_{c2} - V_o) \tag{8.57}$$

$$I_n = \frac{3}{2}(M_{qs} I_{qs} + M_{ds} I_{ds}) + D_o(I_1 + I_2) \tag{8.58}$$

$$I_o = \frac{V_o}{R_o} \tag{8.59}$$

$$\text{where} \quad S_A + S_C = 1 - D_o \tag{8.60}$$

$$\text{since} \quad S_A + S_B + S_C = 1$$

Equations (8.49)-(8.60) are used for the simulation of the Z-source rectifier. The results for the system when a resistive load of 50 Ω and a shoot-through duty ratio of 0.15 are used are as illustrated in Section 8.3.2. The system simulation is performed under unity power factor operation. Here, the results of the q-axis and d-axis modulation signals are obtained from the steady state results and are used in the simulation.

8.4.1 Simulation Results

The simulation of the system model is performed in MATLAB/SIMULINK and the results are as shown below. Figure 8.15 shows the three-phase input currents I_{as}, I_{bs}, I_{cs}. Figure 8.16 illustrates the concept of unity power factor. Here the input phase voltage and the input phase current is shown on the same plot. It is seen that the zeroes of both the curves are the same. Hence unity power factor is achieved through the proposed method. Figure 8.17 shows the load output voltage of the Z-source rectifier when a resistive load of 50 Ω is used. Figure 8.18 shows the behavior of the input dc voltage to the Z-source network. Figure 8.19 shows the load dc current for the resistive load. Figure 8.20 shows the input dc current to the Z-source network which is also the output current of the rectifier.
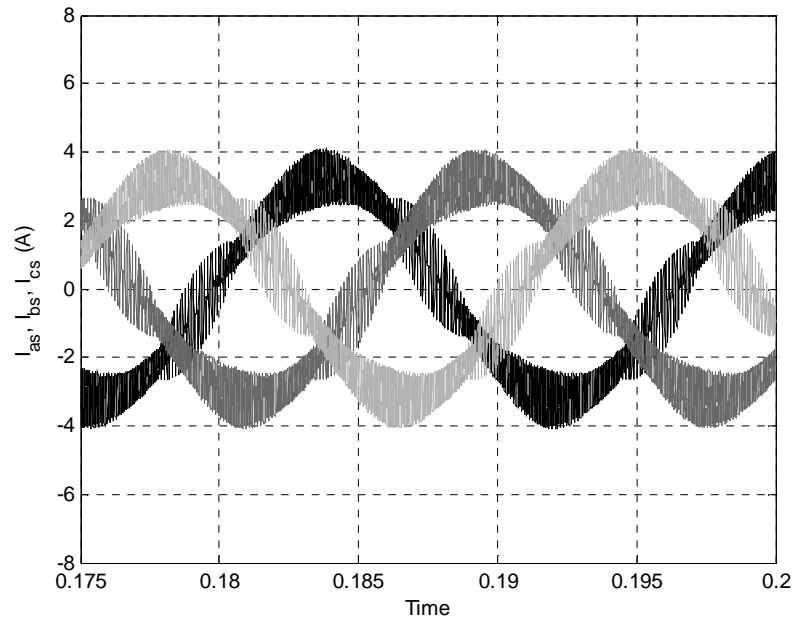
Figure 8.15: Three phase input currents I_{as}, I_{bs}, I_{cs}
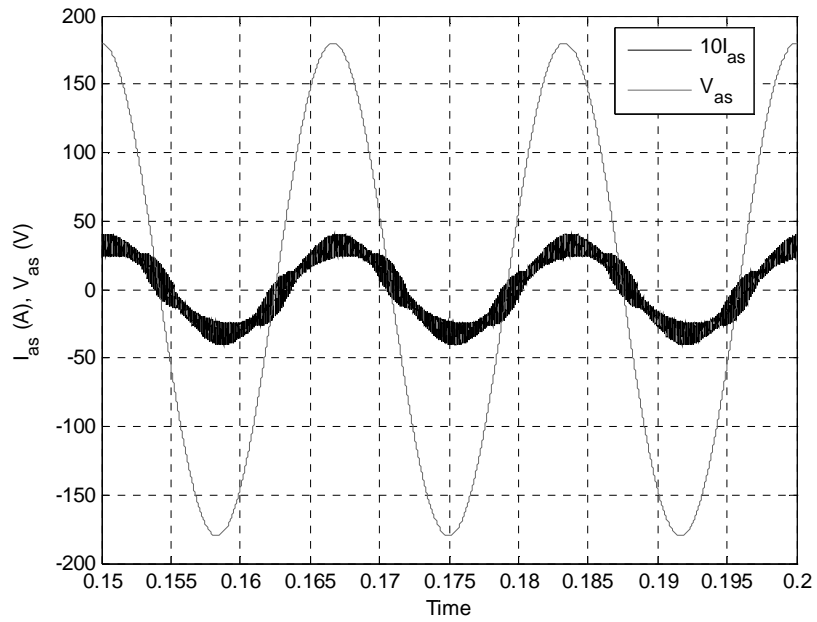
Figure 8.16: Superimposition of input phase voltage V_{as} and ten times the input phase

current I_{as} to show unity power factor
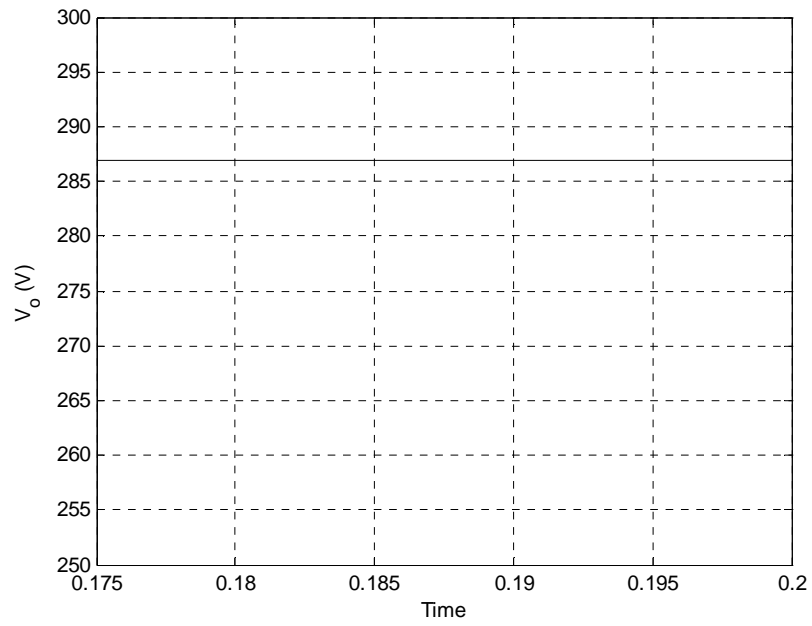
Figure 8.17: Load output voltage V_o of the Z-Source Rectifier
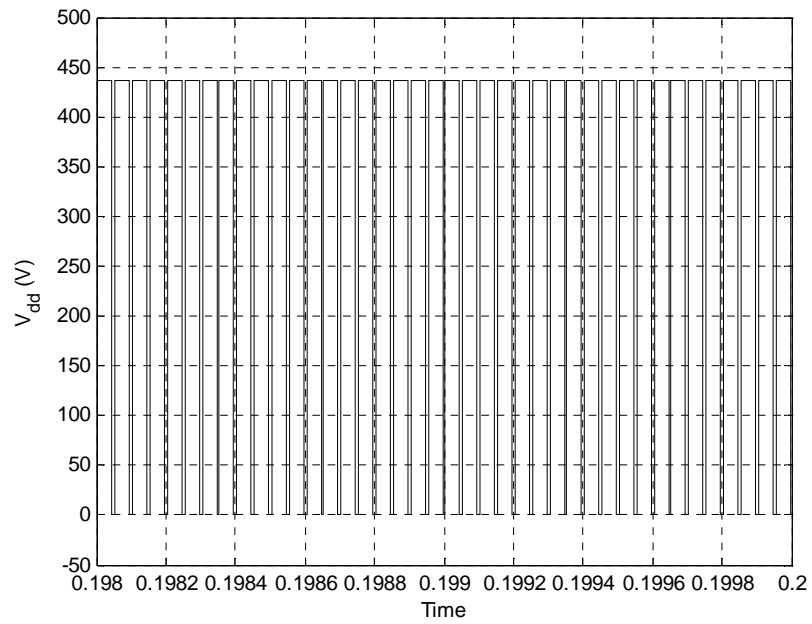
Figure 8.18: Input voltage to the Z-source network V_{dd}
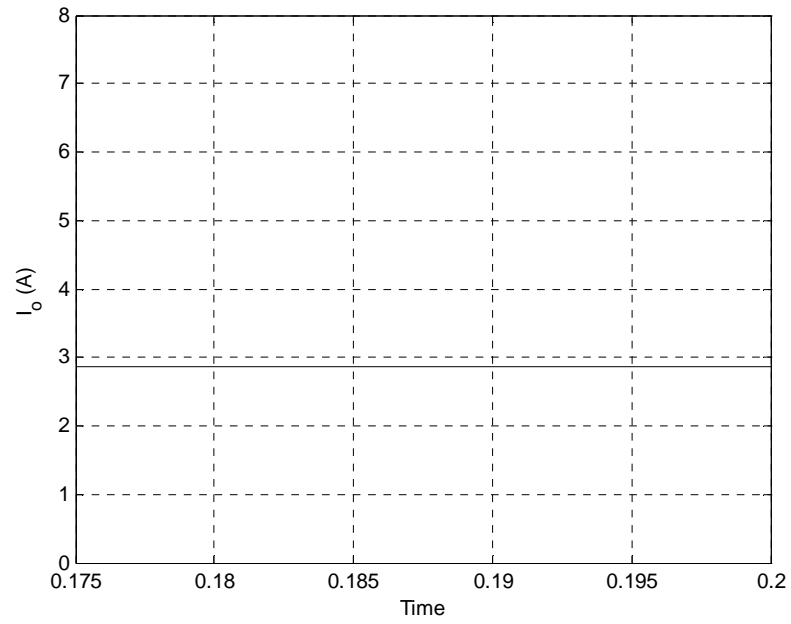
Figure 8.19: Load current for a resistive load I_o
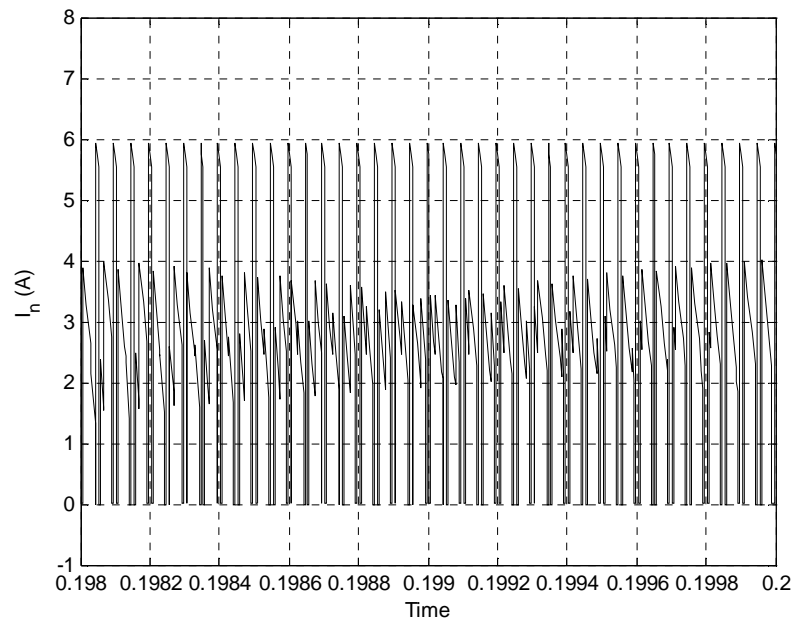
Figure 8.20: Input dc current to the Z-source network I_n

8.5 Small Signal Analysis

The small signal analysis is performed by state space averaging which is performed as follows.

8.5.1 Derivation of Characteristic Matrix

The characteristic matrix is represented as A and it is used to study the stability of the system.

Let the state equations be of the form

$$\dot{x} = f(x, u)$$

where

x = state variable

u = input variable

A small change is introduced in all the state variables and they are simplified in order to get the expression as shown below.

$$\Delta \dot{x}(s) = A\Delta x(s) + B\Delta u(s) + D\Delta e(s) \tag{8.61}$$

where x - equilibrium (dc) state vector

e - equilibrium (dc) control vector

u - equilibrium (dc) input vector

A, B, D - co-efficient matrices

The assumptions used in this section are

$$\delta = 1 - D_o \tag{8.62}$$

$$C_1 = C_2 = C$$

$$r_1 = r_2 = r_{12}$$

$$L_1 = L_2 = L$$

$$I_1 + I_2 = I$$

$$V_{c1} + V_{c2} = V_{sc}$$

The state equations are given from (8.49)-(8.59) as

$$pI_{qs} = \frac{1}{L_s}\left(V_{qs} - r_s I_{qs} - L_s \omega_e I_{ds} - \frac{(1 - D_o)(V_{c1} + V_{c2} - V_o)M_{qs}}{2}\right) \tag{8.63}$$

$$pI_{ds} = \frac{1}{L_s}\left(V_{ds} - r_s I_{ds} + L_s \omega_e I_{qs} - \frac{(1 - D_o)(V_{c1} + V_{c2} - V_o)M_{ds}}{2}\right) \tag{8.64}$$

$$pI_1 = \frac{1}{L_1}\left((1 - D_o)(V_{c1} + V_{c2} - V_o) - r_1 I_1 - V_{c2}\right) \tag{8.65}$$

$$pI_2 = \frac{1}{L_2}\left((1 - D_o)(V_{c1} + V_{c2} - V_o) - r_2 I_2 - V_{c1}\right) \tag{8.66}$$

$$pV_{c1} = \frac{1}{C_1}\left(I_2 - (1 - D_o)(I_1 + I_2) + \frac{3}{2}\left(M_{qs} I_{qs} + M_{ds} I_{ds}\right)\right) \tag{8.67}$$

$$pV_{c2} = \frac{1}{C_2}\left(I_1 - (1 - D_o)(I_1 + I_2) + \frac{3}{2}\left(M_{qs} I_{qs} + M_{ds} I_{ds}\right)\right) \tag{8.68}$$

$$pV_o = \frac{1}{C_o}\left((1 - D_o)(I_1 + I_2) - \frac{3}{2}\left(M_{qs} I_{qs} + M_{ds} I_{ds}\right) - \frac{V_o}{R_o}\right) \tag{8.69}$$

By using the assumptions mentioned in the above state equations

$$pI_{qs} = \frac{1}{L_s}\left(V_{qs} - r_s I_{qs} - L_s \omega_e I_{ds} - \delta \frac{(V_{sc} - V_o)M_{qs}}{2} \right) \tag{8.70}$$

$$pI_{ds} = \frac{1}{L_s}\left(V_{ds} - r_s I_{ds} + L_s \omega_e I_{qs} - \delta \frac{(V_{sc} - V_o)M_{ds}}{2} \right) \tag{8.71}$$

$$pI_1 = \frac{1}{L_1}\left(\delta(V_{sc} - V_o) - r_1 I_1 - V_{c2} \right) \tag{8.72}$$

$$pI_2 = \frac{1}{L_2}\left(\delta(V_{sc} - V_o) - r_2 I_2 - V_{c1} \right) \tag{8.73}$$

$$pV_{c1} = \frac{1}{C_1}\left(I_2 - \delta I + \frac{3}{2}\left(M_{qs} I_{qs} + M_{ds} I_{ds} \right) \right) \tag{8.74}$$

$$pV_{c2} = \frac{1}{C_2}\left(I_1 - \delta I + \frac{3}{2}\left(M_{qs} I_{qs} + M_{ds} I_{ds} \right) \right) \tag{8.75}$$

$$pV_o = \frac{1}{C_o}\left(\delta I - \frac{3}{2}\left(M_{qs} I_{qs} + M_{ds} I_{ds} \right) - \frac{V_o}{R_o} \right) \tag{8.76}$$

Adding (8.72) and (8.73)

$$p(I_1 + I_2) = pI$$

$$pI = \frac{1}{L}\left(2(V_{sc} - V_o)\delta - r_{12} I - V_{sc} \right) \tag{8.78}$$

Adding (8.74) and (8.75),

$$p(V_{c1} + V_{c2}) = pV_{sc}$$

$$pV_{sc} = \frac{1}{C}\left((1 - 2\delta)I + 3\left(M_{qs} I_{qs} + M_{ds} I_{ds} \right) \right) \tag{8.79}$$

By perturbing the above equations using the following expressions to bring in a very small change, (8.80)-(8.84) is obtained.

$$V_o = V_{oo} + \Delta V_o$$

$$V_{sc} = V_{sco} + \Delta V_{sc}$$

$$I = I_o + \Delta I$$

$$I_{qs} = I_{qso} + \Delta I_{qs}$$

$$I_{ds} = I_{dso} + \Delta I_{ds}$$

$$V_{qs} = V_{qso} + \Delta V_{qs}$$

$$V_{ds} = V_{dso} + \Delta V_{ds}$$

$$M_{qs} = M_{qso} + \Delta M_{qs}$$

$$M_{ds} = M_{dso} + \Delta M_{ds}$$

$$\delta = \delta_o + \Delta \delta$$

By substituting the above equations in the state equation and ignoring the dc terms as well as the second order terms gives the following set of equations

$$p\Delta I_{qs} = \frac{1}{L_s} \left(\begin{array}{l} \Delta V_{qs} - r_s \Delta I_{qs} - \omega_e L_s \Delta I_{ds} - \frac{1}{2}(\delta_o V_{sco} - \delta_o V_{oo})\Delta M_{qs} - \frac{1}{2}\delta_o M_{qso}\Delta V_{sc} \\ + \frac{1}{2}\delta_o M_{qso}\Delta V_o - \frac{1}{2}(V_{sco} M_{qso} - V_{oo} M_{qso})\Delta \delta \end{array} \right)$$

(8.80)

$$p\Delta I_{ds} = \frac{1}{L_s} \left(\begin{array}{l} \Delta V_{ds} - r_s \Delta I_{ds} + \omega_e L_s \Delta I_{qs} - \frac{1}{2}(\delta_o V_{sco} - \delta_o V_{oo})\Delta M_{ds} - \frac{1}{2}\delta_o M_{dso}\Delta V_{sc} \\ + \frac{1}{2}\delta_o M_{dso}\Delta V_o - \frac{1}{2}(V_{sco} M_{dso} - V_{oo} M_{dso})\Delta \delta \end{array} \right)$$

(8.81)

$$p\Delta I = \frac{1}{L}(-r_{12}\Delta I + (2\delta_o - 1)\Delta V_{sc} - 2\delta_o \Delta V_o + 2(V_{sco} - V_{oo})\Delta \delta)$$
(8.82)

$$p\Delta V_{sc} = \frac{1}{C}\left((1 - 2\delta_o)\Delta I - 2I_o\Delta\delta + 3\left(M_{qso}\Delta I_{qs} + M_{dso}\Delta I_{ds} + I_{qso}\Delta M_{qs} + I_{dso}\Delta M_{ds}\right)\right)$$

(8.83)

$$p\Delta V_o = \frac{1}{C_o}\left(\delta_o\Delta I + I_o\Delta\delta - \frac{3}{2}\left(M_{qso}\Delta I_{qs} + M_{dso}\Delta I_{ds} + I_{qso}\Delta M_{qs} + I_{dso}\Delta M_{ds}\right) - \frac{\Delta V_o}{R_o}\right)$$

(8.84)

Equations (8.80)-(8.84) can be written in the form of a matrix. The simplified

matrix equation of the Z-source rectifier model is as shown in the next page.

$$
\begin{bmatrix} p\Delta I_{qs} \\ p\Delta I_{ds} \\ p\Delta I \\ p\Delta V_{sc} \\ p\Delta V_o \end{bmatrix} = \begin{bmatrix} -\dfrac{r_s}{L_s} & -\omega_e & 0 & -\dfrac{\delta_o M_{qso}}{2L_s} & \dfrac{\delta_o M_{qso}}{2L_s} \\[3mm] \omega_e & -\dfrac{r_s}{L_s} & 0 & -\dfrac{\delta_o M_{dso}}{2L_s} & \dfrac{\delta_o M_{dso}}{2L_s} \\[3mm] 0 & 0 & -\dfrac{r_{12}}{L} & \dfrac{(2\delta_o-1)}{L} & -\dfrac{2\delta_o}{L} \\[3mm] \dfrac{3M_{qso}}{C} & \dfrac{3M_{dso}}{C} & \dfrac{(1-2\delta_o)}{C} & 0 & 0 \\[3mm] -\dfrac{3M_{qso}}{C_o} & -\dfrac{3M_{dso}}{C_o} & \dfrac{\delta_o}{C_o} & 0 & -\dfrac{1}{R_o C_o} \end{bmatrix} \begin{bmatrix} \Delta I_{qs} \\ \Delta I_{ds} \\ \Delta I \\ \Delta V_{sc} \\ \Delta V_o \end{bmatrix}
$$

$$
+ \begin{bmatrix} -\dfrac{1}{2L_s}(\delta_o V_{sco}-\delta_o V_{oo}) & 0 & -\dfrac{1}{2L_s}(V_{sco}M_{qso}-V_{oo}M_{qso}) \\[3mm] 0 & -\dfrac{1}{2L_s}(\delta_o V_{sco}-\delta_o V_{oo}) & -\dfrac{1}{2L_s}(V_{sco}M_{dso}-V_{oo}M_{dso}) \\[3mm] 0 & 0 & \dfrac{2(V_{sco}-V_{oo})}{L} \\[3mm] \dfrac{3I_{qso}}{C} & \dfrac{3I_{dso}}{C} & -\dfrac{2I_o}{C} \\[3mm] -\dfrac{3I_{qso}}{2C_o} & -\dfrac{3I_{dso}}{2C_o} & \dfrac{I_o}{C_o} \end{bmatrix} \begin{bmatrix} \Delta M_{qs} \\ \Delta M_{ds} \\ \Delta \delta \end{bmatrix} + \begin{bmatrix} \dfrac{1}{L_s} & 0 \\[3mm] 0 & \dfrac{1}{L_s} \\[3mm] 0 & 0 \\[3mm] 0 & 0 \\[3mm] 0 & 0 \end{bmatrix} \begin{bmatrix} \Delta V_{qs} \\ \Delta V_{ds} \end{bmatrix} \qquad (8.85)
$$

Here the A matrix is known as the characteristic matrix. The characteristics and the eigen values of the system model can be obtained from this matrix. In the system described, the characteristic matrix is given as

$$A = \begin{bmatrix} -\dfrac{r_s}{L_s} & -\omega_e & 0 & -\dfrac{\delta_o M_{qso}}{2L_s} & \dfrac{\delta_o M_{qso}}{2L_s} \\[2mm] \omega_e & -\dfrac{r_s}{L_s} & 0 & -\dfrac{\delta_o M_{dso}}{2L_s} & \dfrac{\delta_o M_{dso}}{2L_s} \\[2mm] 0 & 0 & -\dfrac{r_{12}}{L} & \dfrac{(2\delta_o-1)}{L} & -\dfrac{2\delta_o}{L} \\[2mm] \dfrac{3M_{qso}}{C} & \dfrac{3M_{dso}}{C} & \dfrac{(1-2\delta_o)}{C} & 0 & 0 \\[2mm] -\dfrac{3M_{qso}}{C_o} & -\dfrac{3M_{dso}}{C_o} & \dfrac{\delta_o}{C_o} & 0 & -\dfrac{1}{R_o C_o} \end{bmatrix} \qquad (8.86)$$

$$B = \begin{bmatrix} -\dfrac{1}{2L_s}(\delta_o V_{sco} - \delta_o V_{oo}) & 0 & -\dfrac{1}{2L_s}(V_{sco} M_{qso} - V_{oo} M_{qso}) \\[2mm] 0 & -\dfrac{1}{2L_s}(\delta_o V_{sco} - \delta_o V_{oo}) & -\dfrac{1}{2L_s}(V_{sco} M_{dso} - V_{oo} M_{dso}) \\[2mm] 0 & 0 & \dfrac{2(V_{sco} - V_{oo})}{L} \\[2mm] \dfrac{3I_{qso}}{C} & \dfrac{3I_{dso}}{C} & -\dfrac{2I_o}{C} \\[2mm] -\dfrac{3I_{qso}}{2C_o} & -\dfrac{3I_{dso}}{2C_o} & \dfrac{I_o}{C_o} \end{bmatrix}$$

$$(8.87)$$

$$C = \begin{bmatrix} \dfrac{1}{L_s} & 0 \\[2mm] 0 & \dfrac{1}{L_s} \\[2mm] 0 & 0 \\[2mm] 0 & 0 \\[2mm] 0 & 0 \end{bmatrix} \qquad (8.88)$$

8.5.2 Stability Analysis

The state equations are represented in the form of a matrix equation after the small signal analysis has been performed as shown in (8.85). The characteristic matrix is used to study the stability analysis of the Z-source rectifier. The characteristic matrix is shown in (8.86) and is utilized to determine the eigen values of the system. The real part of the eigen values are plotted against the imaginary values of the eigen values for each of the state variables as one of the control parameters are varied. In this case, the shoot-through duty ratio is varied from 0 to 0.2. The real part of all the eigen values of all the state parameters should be less than zero in order for the system to be stable. Figure 8.21 shows the plot of the eigen values of the Z-source rectifier for varying shoot-through duty ratio.
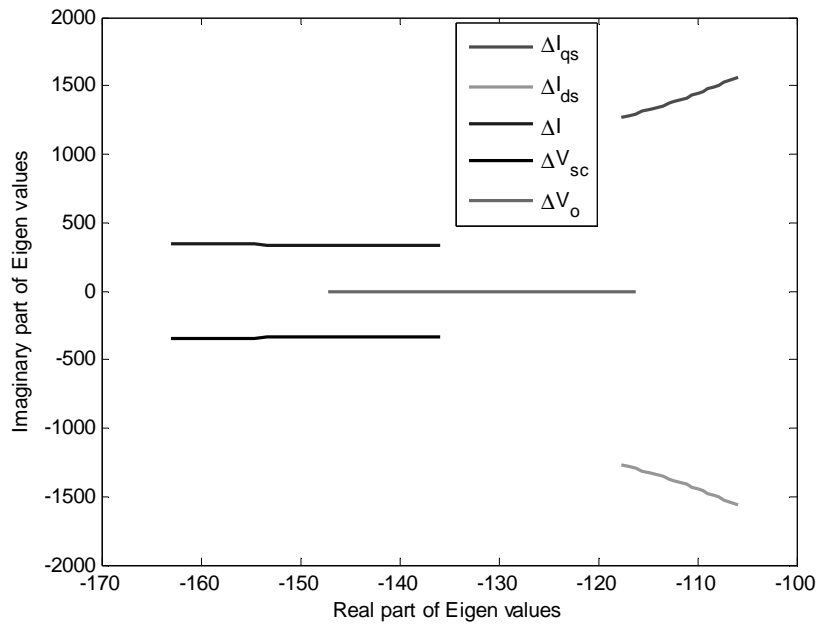
Figure 8.21: Eigen values of the state variables of the Z-source rectifier

It is seen that the real part of the eigen values of the state parameters are negative in this case. Hence for the given operating conditions, it can be concluded that the Z-source rectifier is stable.

8.6 Conclusion

The steady state results under the condition of unity input power factor was shown for a resistive load. The system parameters were plotted for various values of modulation index while varying shoot-through duty ratio D_o from zero to its corresponding maximum. It was noticed that as the shoot-through duty ratio, D_o increased, the ripple in the circuit increased. The simulation results showed the system's behavior under transient conditions as well as loaded operating conditions. The small signal analysis was performed and the characteristic matrix was obtained in order to perform the stability analysis of the system. The eigen values were obtained and plotted to show that the system was stable.

CHAPTER 9

DESIGN OF CONTROLLER FOR Z-SOURCE RECTIFIER

9.1 Introduction

This chapter explores the control scheme for the Z-source Rectifier using a feedback linearized method with decoupling. Here the strategy is to obtain linear approximation of the relationship between input and output control variables with each output-input pair decoupled from each other

Converters designed using reduced active semiconductor devices can be of interest to the industry because of their lower cost and enhanced reliability linked to their less complex gating and control circuitries. Despite their simplicity, most of the reduced component count inverters reported to date can only either perform voltage-buck or boost operation with buck-boost operation usually attained by adding additional actively controlled dc-dc converters. Although effective, the adding of dc-dc converters introduces additional active switches, which somehow dilute advantages associated with a reduced component count topology. There are three control variables in the case of the Z-source rectifier. Hence three variables can be controlled. It is advantageous to control the variables of the system using the given control variables itself. This further reduces the size and the component count of the system model.

9.2 Input-Output Linearization

The control scheme for the dc voltage is set forth with the help of the input-output linearization technique which enables the linearization and decoupling of the model equations in the synchronous reference frame. It can be observed from the system model equations that the Z-source rectifier is a non-linear model where the parameters are coupled with each other. Therefore, is it obvious that it is not easy to design the controller and study the behavior of the outputs by using the input signals. This problem can be overcome if a direct and simple relationship between system inputs and outputs can be found.

Input-output linearization and decoupling technique algebraically approximate a nonlinear system dynamics into that of a linear system and decouple the coupled terms. The simplest form of feedback linearization in order to obtain the closed-loop dynamics in linear form is to cancel the nonlinearities in a nonlinear system so that the. The input-output linearization method of controlling a system is one of the methods for nonlinear control design. The fundamental idea is to transform a nonlinear system into a fully or partly linear system. After that is done, any of the traditional linear control techniques can be applied for the design of the controller. The input-output linearization method with decoupling is used to remove the non-linearity and coupled terms which permits the classic linear system control methodology to be used to determine the parameters of the controllers. This method is possible since the input-output linearization and decoupling strategy ensure the linear relationship between the input control variables and the output controlled variables with each output-input pair decoupled from each other.

9.3 Control of the Z-Source Rectifier

The scheme of using a cascaded controller is divided into two sections: the derivation of the algorithm of the system and derivation of the controllers.

9.3.1 Algorithm of the Cascaded Control Scheme

The Z-Source rectifier controller equations are derived and are illustrated as follows.

The following are the assumptions made for easier understanding

$$\delta = 1 - D_o \tag{9.1}$$

$$I = I_1 + I_2 \tag{9.2}$$

$$V_{cc} = V_{c1} + V_{c2} - V_o \tag{9.3}$$

$$V_{sc} = V_{c1} + V_{c2} \tag{9.4}$$

$$\hat{r}_{12} = \hat{r}_1 = \hat{r}_2 \tag{9.5}$$

$$\hat{L} = \hat{L}_1 = \hat{L}_2 \tag{9.6}$$

$$\hat{C} = \hat{C}_1 = \hat{C}_2 \tag{9.7}$$

If the parameters are assumed to be measured values, then they become

$$r_s = \hat{r}_s$$

$$L_s = \hat{L}_s$$

$$r_{12} = \hat{r}_{12}$$

$$L = \hat{L}$$

$$C = \hat{C}$$

$$C_o = \hat{C}_o$$

$$R_o = \hat{R}_o$$

The state equations are given in Chapter 7 in (7.58)-(7.64). By using the assumptions (9.1)-(9.7), the following expressions are obtained.

$$V_{qs} = r_s I_{qs} + L_s p I_{qs} + L_s \omega_e I_{ds} + \frac{V_{dd} M_{qs}}{2} \tag{9.8}$$

$$V_{ds} = r_s I_{ds} + L_s p I_{ds} - L_s \omega_e I_{qs} + \frac{V_{dd} M_{ds}}{2} \tag{9.9}$$

$$Lp(I_1 + I_2) = LpI = 2\delta V_{cc} - r_{12} I_1 - r_{12} I_2 - V_{c1} - V_{c2}$$

$$LpI = 2\delta V_{cc} - r_{12} I - V_{sc} \tag{9.10}$$

$$Cp(V_{c1} + V_{c2}) = I_1 + I_2 - 2\delta(I_1 + I_2) + 3(M_{qs} I_{qs} + M_{ds} I_{ds})$$

$$CpV_{sc} = I - 2\delta I + 3(M_{qs} I_{qs} + M_{ds} I_{ds})$$

$$CpV_{sc} = (1 - 2\delta)I + 3(M_{qs} I_{qs} + M_{ds} I_{ds}) \tag{9.11}$$

$$CpV_o = \delta I - \frac{3}{2}(M_{qs} I_{qs} + M_{ds} I_{ds}) - \frac{V_o}{R_o} \tag{9.12}$$

The seven state equations are simplified to five state equations in (9.8)-(9.12). The like terms are combined in order to eliminate the coupling in the equations and the controllers are defined for each state equation and is given in (9.13)-(9.17).

Hence, by using the measured values, the state equations can be represented as the following.

$$\hat{r}_s I_{qs} + \hat{L}_s \, pI_{qs} = V_{qs} - \hat{L}_s \, \omega_e I_{ds} - \frac{\delta V_{cc} M_{qs}}{2} = \sigma_{qs} \tag{9.13}$$

$$\hat{r}_s I_{ds} + \hat{L}_s \, pI_{ds} = V_{ds} + \hat{L}_s \, \omega_e I_{qs} - \frac{\delta V_{cc} M_{ds}}{2} = \sigma_{ds} \tag{9.14}$$

$$\hat{L} \, pI + \hat{r}_{12} I = 2\delta V_{cc} - V_{sc} = \sigma_I \tag{9.15}$$

$$\hat{C} \, pV_{sc} = (1 - 2\delta)I + 3\left(M_{qs} I_{qs} + M_{ds} I_{ds}\right) = \sigma_c \tag{9.16}$$

$$\hat{C}_o \, pV_o + \frac{V_o}{\hat{R}_o} = \delta I - \frac{3}{2}\left(M_{qs} I_{qs} + M_{ds} I_{ds}\right) = \sigma_o \tag{9.17}$$

The dc output load voltage V_o and the sum of the capacitor voltages V_c in the Z-network V_{sc} are controlled in this scheme. In addition to these a unity input power factor is also achieved which means that the d-axis input current is forced to be zero. The reference values of the output load voltage V_o and the sum of the capacitor voltages are specified by the user.

The PI controllers are defined as

$$\sigma_{qs} = k_q \left(I_{qs}^* - I_{qs}\right) \tag{9.18}$$

$$\sigma_{ds} = k_d \left(I_{ds}^* - I_{ds}\right) \tag{9.19}$$

$$\sigma_I = k_I \left(I^* - I\right) \tag{9.20}$$

$$\sigma_c = k_c \left(V_{sc}^* - V_{sc}\right) \tag{9.21}$$

$$\sigma_o = k_o \left(V_o^* - V_o\right) \tag{9.22}$$

Hence when the output load voltage and the sum of the capacitor voltages' reference values are known, the controllers σ_o and σ_c are known. Also, when unity input power factor is required, $I_{ds} = 0$. Equations (9.16) and (9.17) are solved assuming that the d-axis input current is zero for the reference value of the sum of the Z-network inductor currents.

$$I^* = \sigma_c + 2\sigma_o \tag{9.23}$$

When the reference value of the sum of the Z-network inductor currents is obtained, the controller σ_I is obtained from (9.20). When the inductor current controller is in action, the reference value of the shoot-through duty ratio is obtained from (9.15) when $V_{cc} = V_{sc} - V_o$ is assumed.

$$\delta^* = \frac{\sigma_I + V_{sc}}{2(V_{sc} - V_o)} \tag{9.24}$$

Therefore, the shoot-through duty ratio is obtained from (9.1) and (9.24). The q-axis input current reference value can be obtained from the (9.17) and is given by the expression (9.25)

$$I_{qs}^* = \frac{2(\delta(\sigma_c + 2\sigma_o) - \sigma_o)}{3M_{qs}} \tag{9.25}$$

Now that the reference values of the q-axis and d-axis input currents are known, the controllers σ_{qs} and σ_{ds} can be determined from (9.18) and (9.19). The derivation of the controller gains is given in the following section. The reference values of the q-axis and d-axis modulation signals can be obtained from (9.13) and (9.14) as

$$M_{qs} = \frac{2}{\delta V_{cc}}\left(V_{qs} - \hat{L}_s \omega_e I_{ds} - \sigma_{qs}\right) \tag{9.26}$$

$$M_{ds} = \frac{2}{\delta V_{cc}} \left(V_{ds} + \hat{L}_s \omega_e I_{qs} - \sigma_{ds} \right)$$ (9.27)

Now that δ^* is known, the value of σ can also be determined.

$$\delta^* = 1 - D_o^*$$

$$\Rightarrow \delta^* = 1 - \left((1-\sigma)\left(1 - \frac{\sqrt{3}m}{2}\right)\right)$$

$$= \frac{\sqrt{3}m}{2} + \sigma - \frac{\sqrt{3}\sigma m}{2}$$

Also, $\sigma = 1 - \dfrac{\left(1-\delta^*\right)}{\left(1 - \dfrac{\sqrt{3}m}{2}\right)}$ (9.28)

9.3.2 Derivation of the Controllers

The controllers are defined in Equations (9.18)-(9.22). The design of the controller parameters is a vital part of control system determination. There are different types of controller structures. Namely

- Proportional controller (P)

- Proportion-Integral controller (PI)

- Integration-Proportional controller (IP)

- Proportional- Integral-Derivative controller (PID)

- Proportion-Derivative controller (PD)

The stability constraint has to be considered for the design of the controller. The parameters design is brought about by the Butterworth method, in which the gain parameters are selected to locate the eigen-values of the transfer functions uniformly in the left half of the s-plane, on a circle of radius ω_o, with its center at the origin [B.8]. The second order Butterworth polynomial can be expressed as

$$p^2 + \sqrt{2}\omega_o p + \omega_o^2 \tag{9.29}$$

The pole placement method used in this design is called the Butterworth method. The dynamic response of the controller is determined by the value of ω_o. In a control system with multiple controllers, the values of ω_o for different controllers must be properly selected and designed. Generally, the inner loop controller should have a value of ω_o 10 times greater than that of the outer control loop. The poles are evenly distributed around the circle whose radius is ω_o. The diagram of pole placement for a second order system is shown in Figure 9.1.

Among the steps to design the controller firstly the transfer function of the controller is obtained, then the denominator of the transfer function is compared with the Butterworth polynomial which is given in (9.29). When the value of ω_o is specified, the controller parameters are obtained since the Butterworth polynomial is expressed only in term of ω_o.

The design methodology of the Butterworth method requires that none of the terms in the denominator are zero. This leads to a limitation for the controller determination. The absence of any term in (9.29) leads to the conclusion that ω_o has to be zero, which yields unreasonable controller parameters.
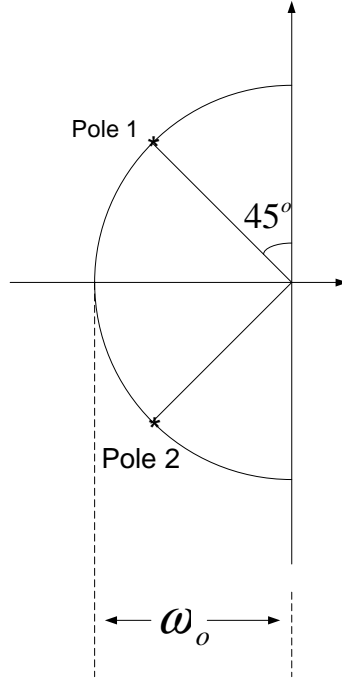
Figure 9.1: Diagram of pole placement using Butterworth method

On the other hand, zero value for ω_o means that the poles of the controllers overlap the original point, which makes the system unstable for practical purposes. The zeros of the transfer functions also greatly influence the system performance. When any zero of a transfer function of a system has positive real part (the system is non-minimum phase), the closed-loop performance is compromised as the right half-plane zero induces additional phase shift of -180. The determination of controller parameters should ensure the minimum phase system requirement [T.6].

The transfer functions of the controller parameters are obtained as follows

From (9.16), the controller is also defined as

$$\hat{C}\, pV_{sc} = \sigma_c \qquad\qquad (9.30)$$

By equating (9.21) and (9.30), we get

$$\hat{C}\, pV_{sc} = k_c \left(V_{sc}^* - V_{sc} \right)$$

214

where

$$k_c = k_{pc} + \frac{k_{ic}}{p}$$ is defined as the PI capacitor voltage controller gain

The transfer function of the sum of the capacitor voltages is obtained as

$$\frac{V_{sc}}{V_{sc}^*} = \frac{pk_{pc} + k_{ic}}{p^2 C + pk_{pc} + k_{ic}} \tag{9.31}$$

By comparing the denominator of the transfer function which is known as the characteristic equation with the Butterworth's second order polynomial, the controller gains can be obtained as

$$k_{pc} = \sqrt{2}\omega_o C \tag{9.32}$$

$$k_{ic} = \omega_o^2 C \tag{9.33}$$

Similarly the output voltage controller gain constant can be determined

From (9.17), the controller is also defined as

$$\hat{C}_o \, pV_o + \frac{V_o}{\hat{R}_o} = \sigma_o \tag{9.34}$$

By equating (9.22) and (9.34), we get

$$\hat{C}_o \, pV_o + \frac{V_o}{\hat{R}_o} = k_o \left(V_o^* - V_o \right)$$

where

$$k_o = k_{po} + \frac{k_{io}}{p}$$ is defined as the PI output voltage controller gain

The transfer function of the output load voltages is obtained as

$$\frac{V_o}{V_o^*} = \frac{pk_{po} + k_{io}}{p^2 + p\left(\dfrac{1}{R_o C_o} + \dfrac{k_{po}}{C_o}\right) + \dfrac{k_{io}}{C_o}}$$ (9.35)

By comparing the denominator of the transfer function which is known as the characteristic equation with the Butterworth's second order polynomial, the controller gains can be obtained as

$$k_{po} = \sqrt{2}\omega_o C_o - \frac{1}{R_o}$$ (9.36)

$$k_{io} = \omega_o^2 C_o$$ (9.37)

From (9.14), the controller is also defined as

$$\hat{r}_s I_{ds} + \hat{L}_s \, pI_{ds} = \sigma_{ds}$$ (9.38)

By equating (9.19) and (9.38), we get

$$\hat{r}_s I_{ds} + \hat{L}_s \, pI_{ds} = k_d \left(I_{ds}^* - I_{ds}\right)$$

where

$$k_d = k_{pd} + \frac{k_{id}}{p}$$ is defined as the PI d-axis input current controller gain

The transfer function of the output load voltages is obtained as

$$\frac{I_{ds}}{I_{ds}^*} = \frac{pk_{pd} + k_{id}}{p^2 + p\left(\dfrac{r_s}{L_s} + \dfrac{k_{pd}}{L_s}\right) + \dfrac{k_{id}}{L_s}}$$ (9.39)

By comparing the denominator of the transfer function which is known as the characteristic equation with the Butterworth's second order polynomial, the controller gains can be obtained as

$$k_{pd} = \sqrt{2}\omega_o L_s - r_s \tag{9.40}$$

$$k_{id} = \omega_o^2 L_s \tag{9.41}$$

From (9.15), the controller is also defined as

$$\hat{L}\, pI + \hat{r}_{12}\, I = \sigma_I \tag{9.42}$$

By equating (9.20) and (9.42), we get

$$\hat{L}\, pI + \hat{r}_{12}\, I = k_I \left(I^* - I\right)$$

where

$$k_I = k_{pI} + \frac{k_{iI}}{p} \quad \text{is defined as the PI sum of the Z-network inductor currents}$$

controller gain

The transfer function of the output load voltages is obtained as

$$\frac{I}{I^*} = \frac{p k_{pI} + k_{iI}}{p^2 + p\left(\dfrac{r_{12}}{L} + \dfrac{k_{pI}}{L}\right) + \dfrac{k_{iI}}{L}} \tag{9.43}$$

By comparing the denominator of the transfer function which is known as the characteristic equation with the Butterworth's second order polynomial, the controller gains can be obtained as

$$k_{pI} = \sqrt{2}\omega_o L - r_{12} \tag{9.44}$$

$$k_{id} = \omega_o^2 L \tag{9.45}$$

From (9.13), the controller is also defined as

$$\hat{r}_s I_{qs} + \hat{L}_s \, pI_{qs} = \sigma_{qs} \tag{9.46}$$

By equating (9.18) and (9.46), we get

$$\hat{r}_s I_{qs} + \hat{L}_s \, pI_{qs} = k_q \left(I_{qs}^* - I_{qs} \right)$$

where

$$k_q = k_{pq} + \frac{k_{iq}}{p} \text{ is defined as the PI q-axis input current controller gain}$$

The transfer function of the output load voltages is obtained as

$$\frac{I_{qs}}{I_{qs}^*} = \frac{pk_{pd} + k_{id}}{p^2 + p\left(\dfrac{r_s}{L_s} + \dfrac{k_{pq}}{L_s} \right) + \dfrac{k_{iq}}{L_s}} \tag{9.47}$$

By comparing the denominator of the transfer function which is known as the characteristic equation with the Butterworth's second order polynomial, the controller gains can be obtained as

$$k_{pq} = \sqrt{2}\omega_o L_s - r_s \tag{9.48}$$

$$k_{iq} = \omega_o^2 L_s \tag{9.49}$$

When the system is put together, the block diagram of the controller system is formed. It is shown in Figure 9.2.

Figure 9.2: Block Diagram of the Z-source rectifier control scheme

9.3.3 Relationship Between Load Voltage and Capacitor Voltage
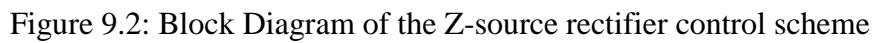
The output load voltage can be written in terms of the capacitor voltage and the expression is derived as follows.

From (6.65), the input dc voltage to the Z-network is given as

$$V_{dd} = (1 - D_o)(V_{c1} + V_{c2} - V_o)$$

The same equation is re-arranged to obtain the load voltage equation

$$V_o = V_{c1} + V_{c2} - \frac{V_{dd}}{1 - D_o}$$

$$= 2V_c - \frac{V_{dd}}{1 - D_o} \tag{9.29}$$

Also, $V_{dd} = V_c + r_{12}I_L$ $\tag{9.30}$

By substituting (9.30) in (9.29), we get

$$V_o = 2V_c - \frac{V_c + r_{12}I_L}{1 - D_o}$$

$$= \frac{(1 - D_o)2V_c - V_c + r_{12}I_L}{1 - D_o} \tag{9.31}$$

Re-arranging the above equation leads to

$$V_c = \frac{(1 - D_o)V_o - r_{12}I_L}{1 - 2D_o} \tag{9.32}$$

If the resistance is negligible, then the ratio between the load voltage and the capacitor voltage is given as

$$\frac{V_o}{V_c} = \frac{1 - 2D_o}{1 - D_o} \tag{9.33}$$

To get an idea of the relationship between the load voltage and the capacitor voltage, (9.33) is useful. It is considered while calculating the reference values of the load voltage and the sum of the capacitor voltages.

9.3.4 Z-Source Rectifier Controller Results

The controller system for the Z-source rectifier was tested using MATLAB/SIMULINK software. The controller is introduced at 0.06 seconds of the simulation. The three parameters for control in this case are the output DC voltage, the

sum of the Z-network capacitor voltages and obtaining the unity input power factor. The

reference output voltage V_o^* is 250 V and the reference sum of the capacitor voltages V_{sc}^*

is 500 V. The input three-phase voltage is 180 V peak. Figure 9.3 shows the reference

output voltage as well as the controlled output voltage when the controller is introduced

in the simulation at 0.06 seconds. Figure 9.4 shows the reference sum of the Z-network

capacitor voltages and the controlled sum of the Z-network capacitor voltages. Figure 9.5

shows the input phase 'a' voltage and ten times the input phase 'a' current. They are in

phase with each other and hence it shows that unity input power factor has been achieved.
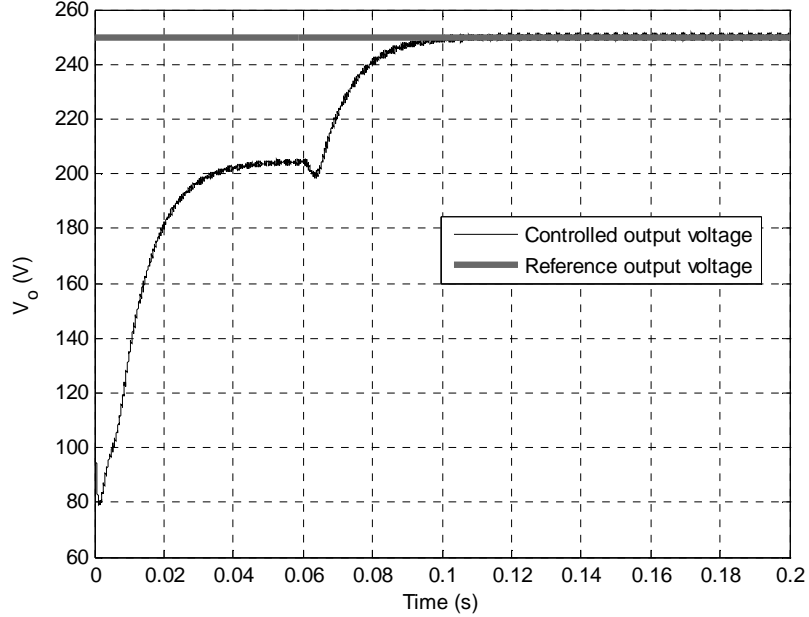
Figure 9.3: Controlled output voltage
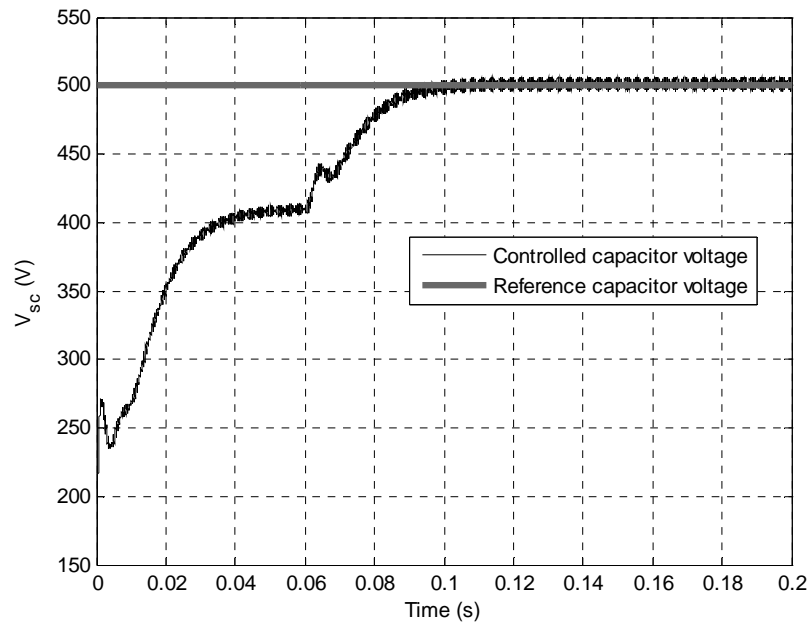
Figure 9.4: Controlled sum of the capacitor voltages
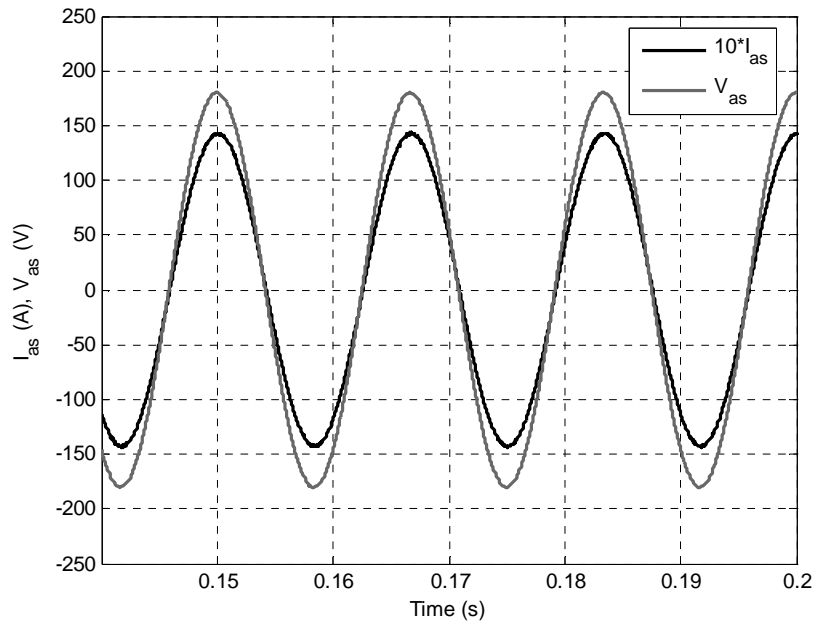
Figure 9.5: Controlled input current is in phase with the input voltage proving unity

power factor

9.4 Conclusion

This chapter dealt with the control schemes of the Z-source rectifier. The cascaded control scheme was demonstrated in the case of the Z-source rectifier. The proposed block diagram of the controller controlling the output DC voltage, the Z-network capacitor voltages and the unity input power factor was shown. It was validated with simulation results performed in MATLAB/SIMULINK. Hence it was shown that the cascaded control scheme proposed for the Z-source rectifier can be implemented practically.

CHAPTER 10

DESIGN OF CONTROLLER FOR INDUCTION MOTOR DRIVEN BY A Z-SOURCE INVERTER

10.1 Introduction

Induction motors have been widely used in the industrial drive system as a means of converting electric power to mechanical power. With the development of the vector control technology, the induction machine drive systems offer high performance as well as independent control on torque and flux linkages. Furthermore, it is possible to drive the induction machines above their rated speed through flux weakening, which also finds a lot of industrial applications. The major applications include pumps, fans, electric vehicles, machine tools, robotics, and many kinds of electric propulsions. The vector control is referred for controlling both amplitude and phase of the AC excitation. And the vector control of voltages and currents results in the control of spatial orientation of the electromagnetic fields in the machine, which leads to the field orientation. It is usually desired to have the 90° orientation between the MMF due to the armature current and the field.

10.2 Vector Control of Induction Machine

There are different types of control schemes available for the induction motor drives. Namely

- scalar control

- direct torque control

- adaptive control

- vector or field-oriented control.

In this section, the vector control is discussed. In the case of induction machines, the rotor flux oriented control is usually employed in the case of induction machines, although it is possible to implement stator flux oriented and also magnetizing flux oriented control. The stator and rotor flux linkages of the induction machine are necessary to implement the vector control method. Then again, there are different methods to obtain the flux linkages. The field oriented induction machine drive systems are classified into two categories

- direct field-oriented system with flux sensors

- indirect field-oriented system.

The vector control of voltages and currents result in the control of spatial orientation of the electromagnetic fields in the machine, which leads to the field orientation. As the name suggests, it controls both amplitude and phase of the AC excitation.

10.2.1 Derivation of Indirect Vector Control of Induction Machine

In the indirect vector control of induction machine, the Z-source inverter has to drive the machine so that the slip frequency can be changing according to the particular requirement. Assuming the rotor speed is measured, the slip frequency is derived from the rotor voltage equations. The rotor voltage equations in the synchronous reference frame are

$$0 = r_r' I_{qr}' + p\lambda_{qr}' + (\omega_e - \omega_r)\lambda_{dr}' \qquad (10.1)$$

$$0 = r_r' I_{dr}' + p\lambda_{dr}' - (\omega_e - \omega_r)\lambda_{qr}' \qquad (10.2)$$

where

The slip frequency is given by the difference between the supply speed and the rotor speed.

$$\Rightarrow \omega_s = \omega_e - \omega_r \qquad (10.3)$$

The q-axis and d-axis rotor flux linkages are defined as

$$\lambda_{qr}' = L_r' I_{qr}' + L_m I_{qs} \qquad (10.4)$$

$$\lambda_{dr}' = L_r' I_{dr}' + L_m I_{ds} \qquad (10.5)$$

In the rotor flux control,

$$\lambda_{qr}' = 0 \qquad (10.6)$$

By substituting (10.6) in (10.1)-(10.2) and (10.4) yields

$$0 = r_r' I_{qr}' + (\omega_e - \omega_r)\lambda_{dr}' \qquad (10.7)$$

$$0 = r_r' I_{dr}' + p\lambda_{dr}' \qquad (10.8)$$

$$0 = L_r^{'} I_{qr}^{'} + L_m I_{qs}$$ (10.9)

From (10.9) and (10.5), the q-axis and d-axis input currents to the induction machine are obtained as

$$I_{qr}^{'} = \frac{-L_m I_{qs}}{L_r^{'}}$$ (10.10)

$$I_{dr}^{'} = \frac{\lambda_{dr}^{'} - L_m I_{ds}}{L_r^{'}}$$ (10.11)

By substituting (10.10) and (10.11) in (10.7) and (10.8), we get the slip frequency and the derivative of the d-axis rotor flux linkage

$$\omega_s = \omega_e - \omega_r = \frac{r_r^{'} L_m I_{qs}}{L_r^{'} \lambda_{dr}^{'}}$$ (10.12)

$$p\lambda_{dr}^{'} = -r_r^{'} \left(\frac{\lambda_{dr}^{'} - L_m I_{ds}}{L_r^{'}} \right)$$ (10.13)

The stator flux is eliminated by the following procedure. It is assumed that

$$L_\sigma = L_s - \frac{L_m^2}{L_r^{'}}$$ (10.14)

$$r = r_s + \frac{r_r^{'} L_m^2}{L_r^{'2}}$$ (10.15)

The voltage equations of the induction machine can be rewritten as

$$V_{qs} = r I_{qs} + L_\sigma p I_{qs} + \omega_e L_\sigma I_{ds} - \frac{r_r^{'} L_m}{L_r^{'2}} \lambda_{qr}^{'} + \frac{\omega_r L_m}{L_r^{'}} \lambda_{dr}^{'}$$ (10.16)

$$V_{ds} = r I_{ds} + L_\sigma p I_{ds} - \omega_e L_\sigma I_{qs} - \frac{r_r^{'} L_m}{L_r^{'2}} \lambda_{dr}^{'} - \frac{\omega_r L_m}{L_r^{'}} \lambda_{qr}^{'}$$ (10.17)

$$0 = \frac{r_r^{'}}{L_r^{'}} \lambda_{qr}^{'} + p\lambda_{qr}^{'} - \frac{r_r^{'} L_m}{L_r^{'}} I_{qs} + (\omega_e - \omega_r)\lambda_{dr}^{'}$$ (10.18)

$$0 = \frac{r_r^{'}}{L_r^{'}} \lambda_{dr}^{'} + p\lambda_{dr}^{'} - \frac{r_r^{'} L_m}{L_r^{'}} I_{ds} - (\omega_e - \omega_r)\lambda_{qr}^{'}$$ (10.19)

$$T_e = \frac{3PL_m}{4L_r^{'}} \left(I_{qs} \lambda_{dr}^{'} - I_{ds} \lambda_{qr}^{'} \right)$$ (10.20)

By using (10.6), Equations (10.16)-(10.20) yield

$$rI_{qs} + L_\sigma pI_{qs} = V_{qs} - \omega_e L_\sigma I_{ds} - \frac{\omega_r L_m}{L_r^{'}} \lambda_{dr}^{'}$$ (10.21)

$$rI_{ds} + L_\sigma pI_{ds} = V_{ds} + \omega_e L_\sigma I_{qs} + \frac{r_r^{'} L_m}{L_r^{'2}} \lambda_{dr}^{'}$$ (10.22)

$$\frac{r_r^{'}}{L_r^{'}} \lambda_{dr}^{'} + p\lambda_{dr}^{'} = \frac{r_r^{'} L_m}{L_r^{'}} I_{ds}$$ (10.23)

$$T_e = \frac{3PL_m}{4L_r^{'}} \left(I_{qs} \lambda_{dr}^{'} \right)$$

$$= K_e \left(I_{qs} \lambda_{dr}^{'} \right)$$ (10.24)

where $K_e = \frac{3PL_m}{4L_r^{'}}$

The rotor speed equation is given as

$$p\omega_r = \frac{P}{2J} \left(K_e I_{qs} \lambda_{dr}^{'} - T_L \right)$$ (10.25)

The control scheme is derived from the above equations.

$$\sigma_{qs} = rI_{qs} + L_\sigma pI_{qs} = k_{qs} \left(I_{qs}^{*} - I_{qs} \right)$$ (10.26)

$$\sigma_{ds} = rI_{ds} + L_\sigma pI_{ds} = k_{ds} \left(I_{ds}^{*} - I_{ds} \right)$$ (10.27)

Now, the reference q-axis and d-axis currents are defined as

$$I_{ds}^{*} = k_{dr} \left(\lambda_{dr}^{'*} - \lambda_{dr}^{'} \right)$$ (10.28)

$$I_{qs}^* = k_\omega \left(\omega_r^* - \omega_r \right) \qquad (10.29)$$

k_{qs}, k_{ds}, k_{dr} and k_ω can be any type of controller.

The desired q-axis and d-axis stator voltages are calculated based on the input-output linearization technique which is given by

$$V_{qs}^* = \sigma_{qs} + \omega_e L_\sigma I_{ds} + \frac{\omega_r L_m}{L_r'} \lambda_{dr}' \qquad (10.30)$$

$$V_{ds}^* = \sigma_{ds} - \omega_e L_\sigma I_{qs} - \frac{r_r' L_m}{L_r'^2} \lambda_{dr}' \qquad (10.31)$$

When the reference q-axis and d-axis stator voltages are known, the Z-source inverter equations can be brought in

$$V_{qs}^* = \left(\sqrt{M_{qs}^2 + M_{ds}^2} + D_o \right)\left(V_{sc}^* - V_{dd}^* \right)\frac{M_{qs}}{2} \qquad (10.32)$$

$$V_{ds}^* = \left(\sqrt{M_{qs}^2 + M_{ds}^2} + D_o \right)\left(V_{sc}^* - V_{dd}^* \right)\frac{M_{ds}}{2} \qquad (10.33)$$

The desired sum of the capacitor voltage is specified and hence σ_c is known since it is defined as

$$\sigma_c = k_c \left(V_{sc}^* - V_{sc} \right) \qquad (10.34)$$

This yields the reference Z-network inductor currents to be

$$I^* = \sigma_c + 2I_L \qquad (10.35)$$

Hence the controller σ_I is determined through the expression

$$\sigma_I = k_I \left(I^* - I \right) \qquad (10.36)$$

Therefore the reference dc voltage supplied to the Z-network circuit is given by the expression

$$V_{dd}^* = \frac{1}{2}\left(\sigma_I - V_{sc}\right) \tag{10.37}$$

When V_{dd}^* is known, the shoot-through duty ratio of the Z-source inverter is obtained from the expression (10.38)

$$D_o = \frac{2}{V_{sc}^* - rI^*}\left(V_{dd}^* - V_{dc} - \frac{V_{sc}^*}{2} - \frac{rI^*}{2}\right) \tag{10.38}$$

By substituting (10.38) in (10.32) and (10.33), the desired stator voltages can be obtained as

$$V_{qs}^* = \left(\sqrt{M_{qs}^2 + M_{ds}^2} + \left(\frac{2}{V_{sc}^* - rI^*}\left(V_{dd}^* - V_{dc} - \frac{V_{sc}^*}{2} - \frac{rI^*}{2}\right)\right)\right)\left(V_{sc}^* - V_{dd}^*\right)\frac{M_{qs}}{2} \tag{10.39}$$

$$V_{ds}^* = \left(\sqrt{M_{qs}^2 + M_{ds}^2} + \left(\frac{2}{V_{sc}^* - rI^*}\left(V_{dd}^* - V_{dc} - \frac{V_{sc}^*}{2} - \frac{rI^*}{2}\right)\right)\right)\left(V_{sc}^* - V_{dd}^*\right)\frac{M_{ds}}{2} \tag{10.40}$$

Hence the three control parameters are obtained and the block diagram of the control scheme is as shown in Figure 10.1.
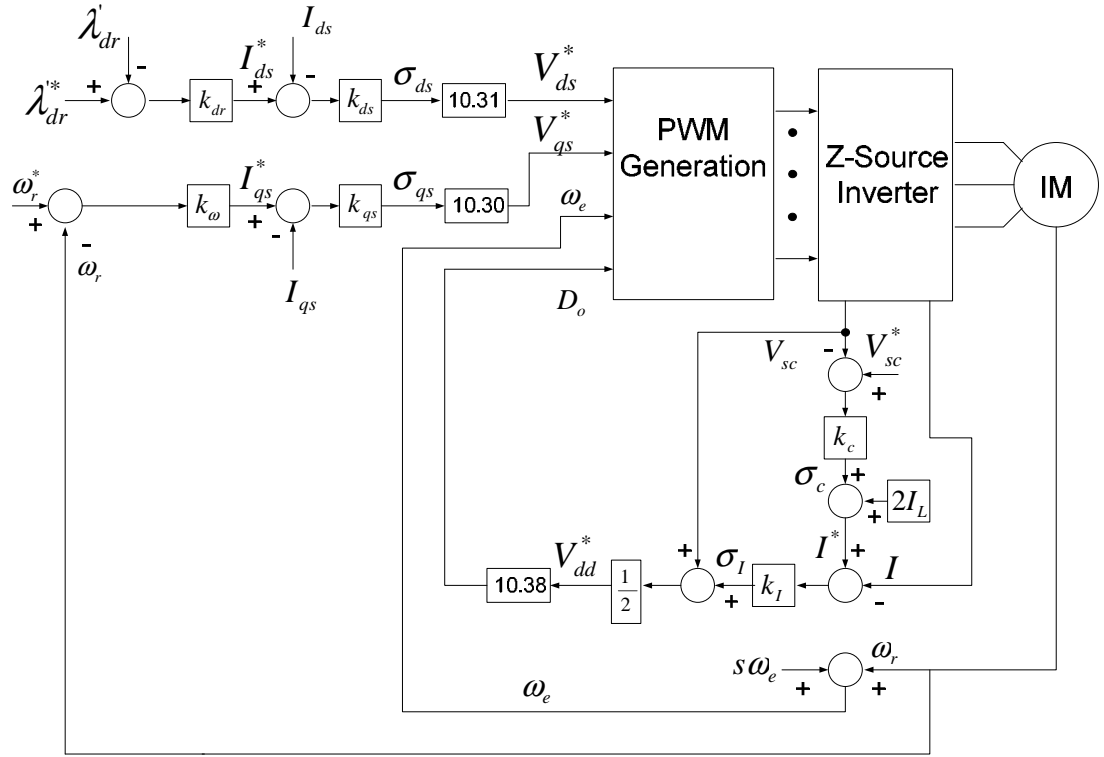
Figure 10.1: Proposed indirect vector control scheme for the induction machine fed by

the Z-Source Inverter

10.3 Conclusion

This chapter dealt with the control schemes of the induction motor fed by the Z-source inverter. The indirect vector control scheme was proposed for the induction motor. The block diagram of the control scheme was shown.

CHAPTER 11

HARDWARE IMPLEMENTATION

11.1 Introduction

This section of the chapter presents the design details of the three-phase Z-Source converters. In the laboratory a three-phase Z-Source Inverter is being built. The primary purpose of the prototype is to verify the analytical and control algorithms that are developed in this thesis. The prototype built is flexible and robust enough to conduct the experiments. The prototype can be used both as an inverter and also as the rectifier. There are several steps involved in implementing the hardware.

- Inverter design.

- DSP coding using the code composer studio.

- Designing the logic circuit to inject the shoot-through pulses.

- Designing the inductors used in the Z-network.

The implementation has been carried out on a three phase, 1 hp, 60 Hz induction machine, using the TMS320LF2407A floating point DSP with 40 MHz cycle frequency. This chapter also explains how the simple gates are used to implement the logic circuit developed in order to bring in the shoot-through pulses. This chapter also gives a description of the types of switches and diodes used in constructing the converter.

11.2 Inverter Design

This section deals with requirements of the inverter and the IGBT used in this case. In the case of the Z-source Inverter, a diode is used which connects the dc power supply to the Z-network. The type of diode used and the rating of the same is also mentioned.

11.2.1 Inverter Specifications

The requirements of the inverter are given as follows

- Voltage rating of 200 V dc input

- Current rating of 10 A

- Switching frequency of less than 50 KHz. In this case, 10 KHz switching frequency is used

- All the devices used in the construction of the inverter are isolated and have separate gate driving circuits

The assumptions in the design of the inverter are that for this case, a separate short circuit protection is not necessary since the Z-network acts as a protection circuit automatically. The control signals for this inverter are through an external source like DSP or micro-controller. Power devices and clamping diode selection are among the important selection criterions. The other important tasks in the implementation of the

inverter are building the power circuit, building driving circuit board, and to build the power supplies for the driver circuits.

11.2.2 IGBT Selection

The IGBT required for this operation requires the following specifications

- Low conduction and switching losses

- Low stray inductance design

- High operating frequencies of 50 KHz

- Low EMI

- High voltage applications of greater than 800 V

- High output power of greater than 5 kW

The IGBT used in this case which meets the specifications is the "Half-Bridge" IGBT MTP – 50MT060WH. It is a product of IRF rectifier and the schematic of the same is shown in Figure 11.1.

(a)   (b)
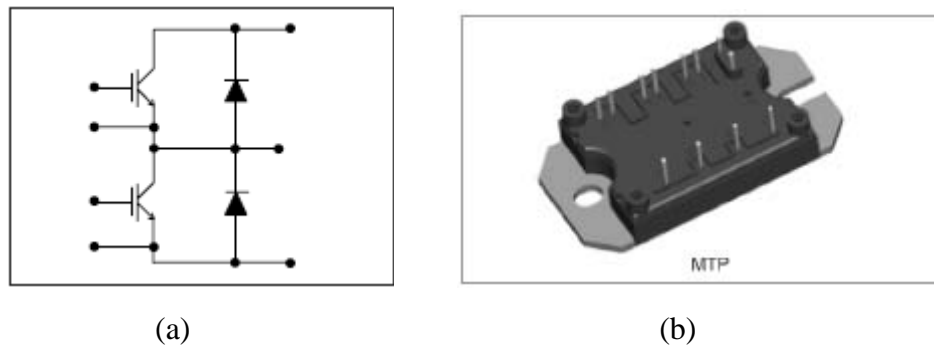
Figure 11.1: (a) Schematic of IGBT module, (b) Warp speed IGBT – 50MT060WH

11.2.3 Diode Specifications

The diode used in the circuit is mainly used for clamping the dc bus voltage. The specifications required in this case are as follow

- Wide current range of maximum of at least 50 A

- Short reverse recovery time

- Good surge capabilities

- Low stored charge

The power diode used in this case is the IRF product - IRD3913R fast recovery diode. The case style and dimensions are as shown in Figure 11.2.
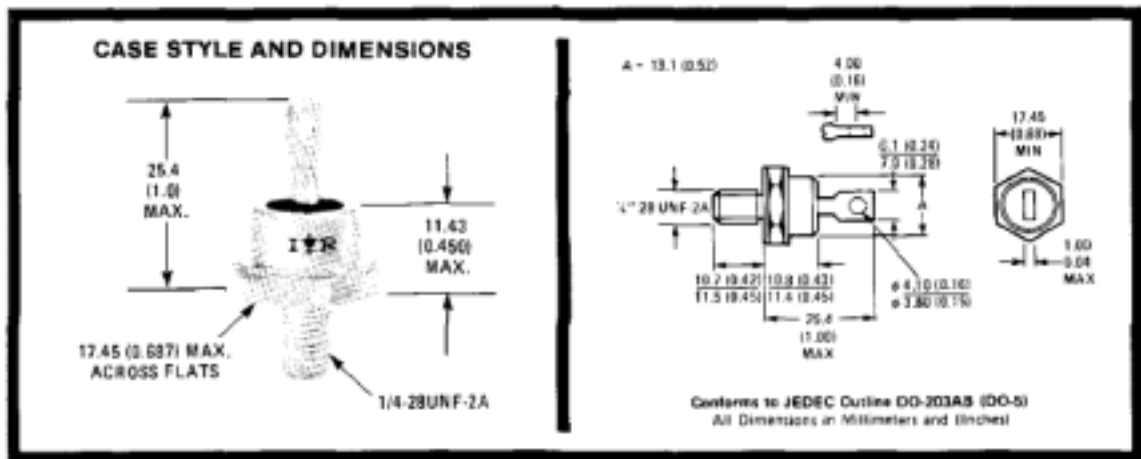
Figure 11.2: Case style and dimensions of the power diode-IRD3913R

11.3 Design of IGBT Gate Drive Circuit

The IGBT gate drive circuit involves using different components. The basic layout of the schematic of the gate drive circuit is discussed in this section. Among the different components, the power supply used is one of the important topics. The multiple output power supply is discussed too in this section.

11.3.1 Gate Drive

The threshold gate voltage of the IGBT is around 4 V, but to ensure switching ON and OFF of the devices at higher frequencies, the gate voltage range is between +12 V and –12 V. A DSP1 Series dual output is designed to convert a nominal 5 V input into two isolated output voltages. The dual semi-regulated output voltages are designed to allow analog circuits and three terminal regulators to operate within their most efficient input voltage range. The DSP1 Series block diagram is shown in Figure 11.3.

A positive three terminal voltage regulator is used as a part of the gate drive circuit. It can deliver an output current up to 1.5 A. The internal current-limiting and thermal-shutdown features of this regulator essentially make them immune to overload. It is very high power-dissipation capability along with internal short-circuit current limiting properties. The schematic of the positive-voltage regulator is shown in Figure 11.4. The schematic of the gate drive circuit is shown in Figure 11.6.
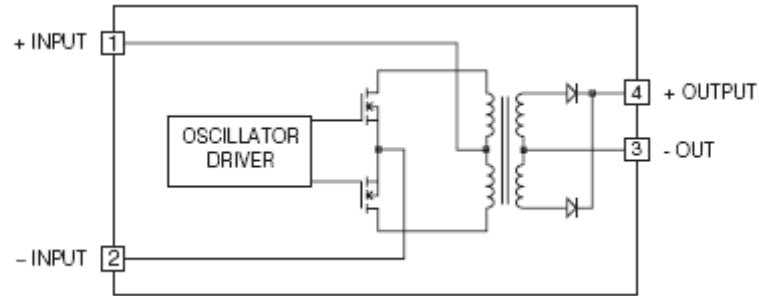
Figure 11.3: DSP1 Series – Dual output block diagram

The hybrid IC driver for the IGBT – EXB841 is a product of Fuji Electric. It has a wide range of operating conditions. It has a built-in photo coupler for high isolation voltage of 2500 V Ac for one minute and also a built-in over current protection circuit. It can be operated with a single supply. The functional block diagram of the IGBT-Driving hybrid IC is shown in Figure 11.5.
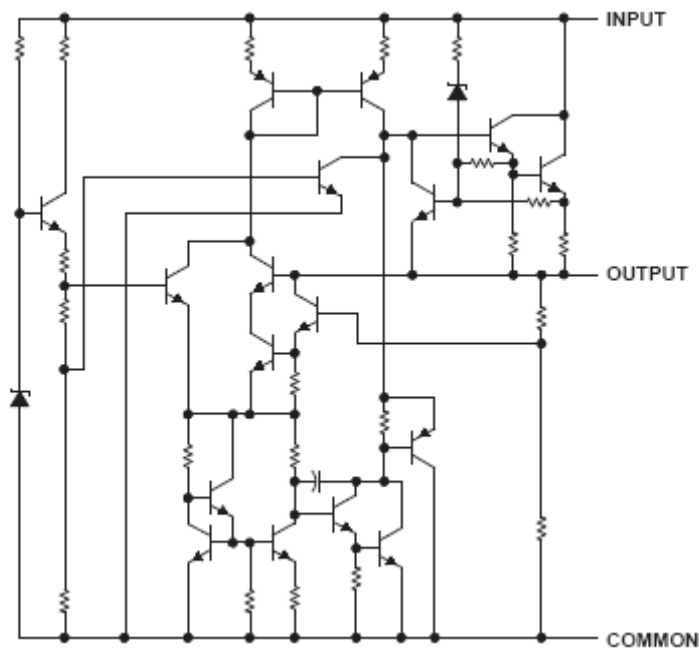
Figure 11.4: Schematic of the three terminal positive voltage regulator
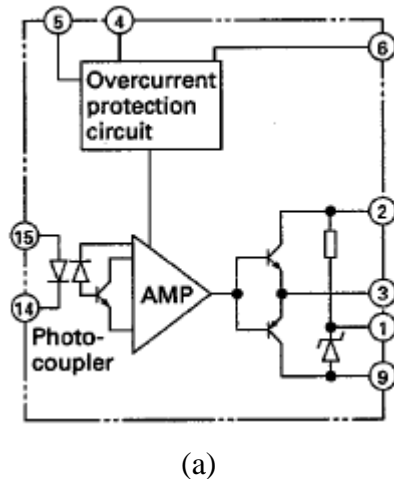
Pin number	Description
①	Connected to smoothing capacitor for reverse bias power supply
②	Power supply (+20 V)
③	Drive output
④	For connecting an external capacitor to protect against malfunction of the overcurrent protection circuit. (The capacitor is not needed in most cases.)
⑤	Overcurrent detection output
⑥	Collector voltage monitoring
⑦ ⑧	Not connected
⑨	Power supply (0 V)
⑩ ⑪	Not connected
⑭	Drive signal input (–)
⑮	Drive signal input (+)

(a)   (b)

Figure 11.5: IGBT-Driving hybrid IC (a) Functional block diagram, (b) Notations used in the block diagram.

11.3.2 Power Supply

In implementing the inverter, the power supplies have to isolate from each other, i.e., having separate grounds. By having separate isolated power supplies for the gate drives, any dv/dt coupled noise generated by the power device switching stays within the gate power supply circuits. Also since there is problem of shorting of shorting between the devices, the driver boards connected to the power switches have to be supplied with isolated power supplies to avoid the shoot through current to pass through the devices.

Figure 11.6: Schematic of the gate drive circuit

The voltage sensors and current sensors are also supplied with different power supplies.

The power supply with multiple outputs is as shown in Figure 11.7.

Figure 11.7: Multiple output power supply of the gate drive circuit

11.4 Design of External Logic Gate Circuit

An external logic circuit is introduced in this case to inject the shoot-through pulses. Basically, the shoot-through pulses are added to the conventional PWM pulses. The shoot-through pulses are generated separately in the DSP and it is brought out to the logic circuit. Similarly, the PWM pulses are also generated separately in the DSP and brought to the external logic circuit. A simple logic circuit is designed with the usage of OR gates (LM7432) to add the shoot-through pulses and the conventional PWM pulses. An important point to be considered in this juncture is that the ground of all the ports used in the DSP has to be grounded along with the ground of the logic circuit. The schematic of the external logic circuit is illustrated in Figure 11.8.
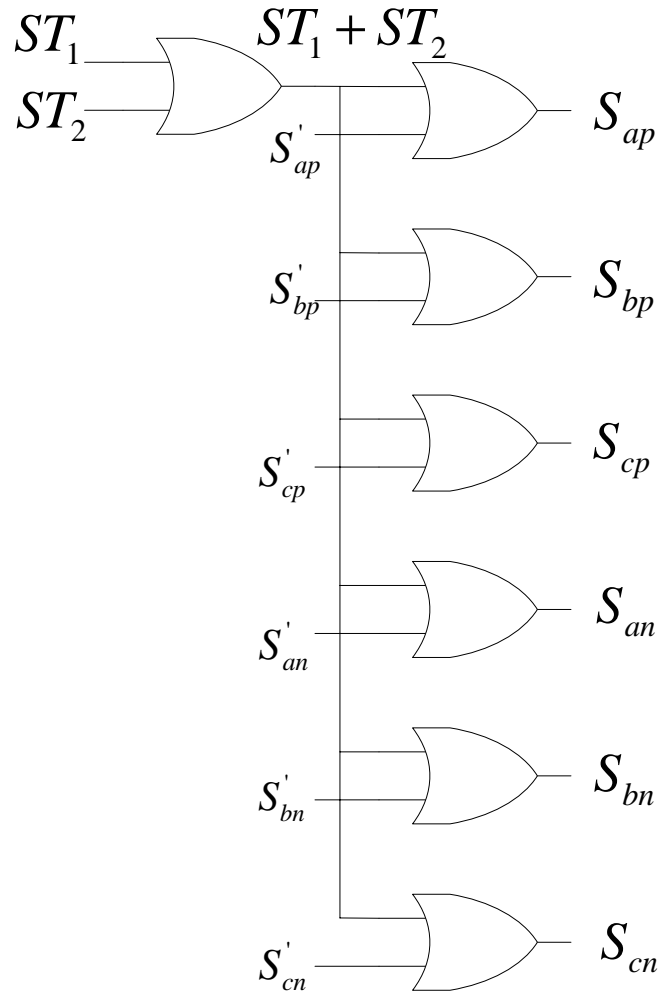
Figure 11.8: Logic circuit to combine the shoot-through pulses along with the

conventional PWM pulses.

In this case, ST_1 and ST_2 are the two individual shoot-through pulses generated in the DSP. They are initially summed together and this sum is added with the other conventional PWM signals in order to get the signal S_{ij} which is supplied to the gate drive.

where i - a, b, c

j - p, n

11.5 Z-network Inductor Design

The inductors used in the Z-network are very sensitive. Both the inductors have to be identical. Hand wound inductors are not very accurate. They are noisy even at very low supply voltages. It has been decided to use manufactured reactors or chokes for this purpose.

In a Z-source rectifier, the current through the capacitor in one switching cycle =0 [I.6].

$$D_o\left(-I_1\right)+\left(1-D_o\right)I_c = 0$$

$$I_c = \frac{D_o I_1}{1-D_o}$$

The load Current, $I_o = I_c + I_1$

$$= I_1 + \frac{D_o I_1}{1-D_o}$$

$$= I_1\left(1+\frac{D_o}{1-D_o}\right)$$

$$= I_1\left(\frac{1}{1-D_o}\right)$$

$$I_n = I_1 - I_c$$

$$= I_1\left(1-\frac{D_o}{1-D_o}\right)$$

$$= I_1\left(\frac{1-2D_o}{1-D_o}\right)$$

Since it is of lossless nature, the input power = output power

$$V_{dd} I_n = V_o I_o$$

$$V_o = \frac{V_{dd} I_n}{I_o}$$

$$= V_{dd}(1 - 2D_o)$$

$$\Delta I_1 = I_{1\max} - I_{1\min}$$

$$= \frac{V_L}{L}(1 - D_o)T$$

During the shoot-through state, $V_L = V_c = \dfrac{1 - D_o}{1 - 2D_o} V_o$

During the non-shoot-through state, $V_L = \dfrac{D_o}{1 - 2D_o} V_o$

So, $\Delta I_1 = \dfrac{D_o(1 - D_o)TV_o}{L(1 - 2D_o)}$

In the continuous conduction mode,

$$I_o - \frac{D_o(1 - D_o)TV_o}{2L(1 - 2D_o)} > 0$$

$$I_o > \frac{D_o(1 - D_o)TV_o}{2L(1 - 2D_o)}$$

$$L > \frac{D_o(1 - D_o)TV_o}{2I_o(1 - 2D_o)}$$

Also, $\Delta I_1 = \dfrac{I_{1\max}}{2}$

$$\frac{D_o(1 - D_o)TV_o}{L(1 - 2D_o)} \geq \frac{I_o}{2} + \frac{D_o(1 - D_o)TV_o}{4L(1 - 2D_o)}$$

$$\frac{D_o(1 - D_o)TV_o}{(1 - 2D_o)}\left(\frac{1}{L} - \frac{1}{4L}\right) \geq \frac{I_o}{2}$$

$$L \leq \frac{3D_o(1-D_o)TV_o}{2(1-2D_o)I_o}$$

Hence limits of the value of the inductor is given as,

$$\frac{D_o(1-D_o)TV_o}{2I_o(1-2D_o)} < L \leq \frac{3D_o(1-D_o)TV_o}{2(1-2D_o)I_o} \qquad (11.1)$$

Using the above equation and for D_o =0.15 and a reasonable value of output voltage and the required current (~10 A), the limits of the inductor values are shown in Figure 11.9.
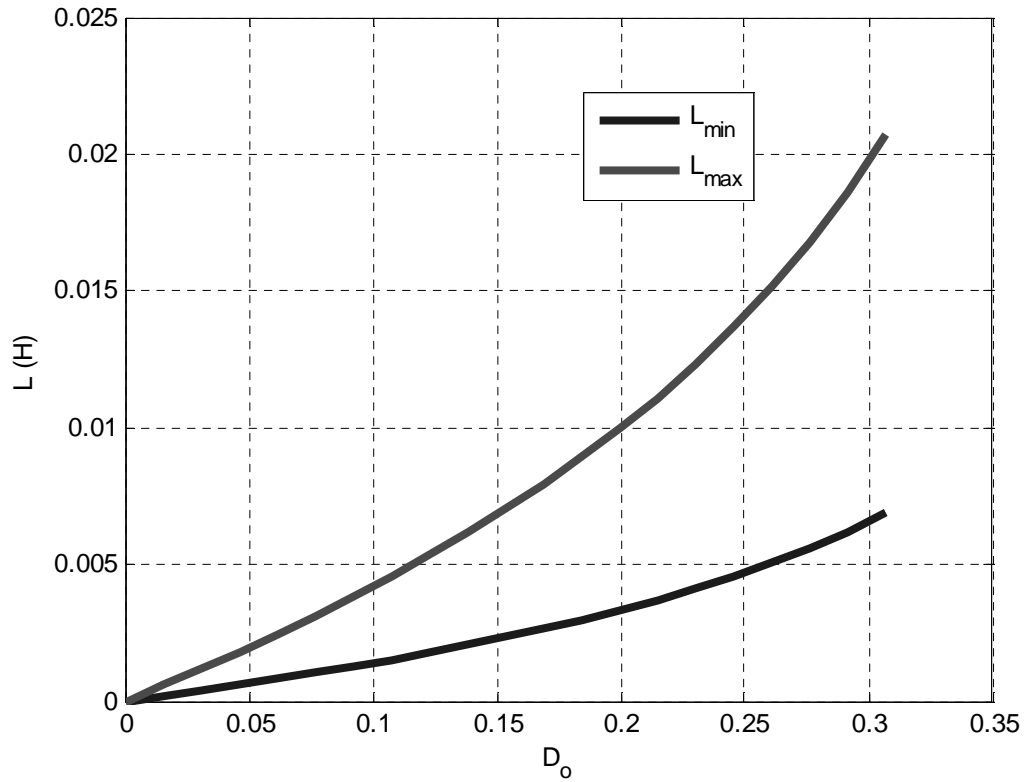
Figure 11.9: Limits of the inductor used in the Z-network

A nominal value of inductor which has been picked for the experiment is 10 mH. A product of Stancor is used with the specifications of 12.5 A dc current and 0.11 Ω dc resistance. It is noted that the dc resistance should be minimum in order to make sure that the current still exits in the circuit.

11.6 PWM Generation

TMS320LF2407 DSP is being used in the laboratory to obtain the gating signals.To obtain pulse width modulated waveforms, a triangular carrier at the switching frequency needs to be generated. The cosine and sine routine programs of the DSP generate the modulation signals and the zero sequence voltage expression is added to obtain the discontinuous modulation signals. In the DSP, the carrier-based implementation, there is no actual triangle that is being compared with the modulation signals to generate the gating signals. In each modulation cycle (triggered by the PWMSYNC interrupt service routine) the DSP must compute the new on-time value to write to the six duty cycle registers of the PWM generation unit. These on times are loaded into the compare registers of the DSP and when the timer reaches the loaded value in the compare register, a pulse of + 12 V is given out. Hence the carrier-based scheme can be implemented using the above method.

11.7 Conclusion

This chapter dealt with the design and implementation of the experimental setup of the Z-source converter. The inverter design along with the type of IGBT and type of power diode used in this particular case has been discussed. The IGBT gate drive circuit is discussed in detail. A simple logic circuit consisting of OR gates has been designed for introducing the shoot-through pulses. Stancor manufactured inductors are used in the Z-network in order to obtain a clean and smooth waveform. The dc resistance of the inductor chosen is very small. The generation of the PWM signal in the DSP is explained in detail.

CHAPTER 12

CONCLUSION AND FUTURE WORK

12.1 Introduction

A summary of the major contributions of this work is presented in the following sections. The significance of these contributions towards the advancement of understanding the topologies of a Z-source converter is included in this chapter. The previous work done in this area has been detailed in Chapter 2 to establish some background on the work carried out in this thesis. Towards the end, future investigations on alternate topologies, modulation strategies, and control schemes that can be carried out are discussed.

12.2 Conclusions

A chapter wise conclusion is presented in this chapter. Chapter one gives the detailed description of the introduction of the thesis and the work performed in each chapter. Chapter two gives a detailed illustration of the previous work done in the same field. The previous work on conventional converters, namely, voltage source inverters, boost rectifiers, boost-buck ac-dc converters, and buck-boost ac-dc converters have been

studied. In addendum, the work done on the Z-source inverters and Z-source rectifiers have been studied. The modulation schemes, analysis methods, characteristics and control scheme for the both the types of Z-source converters has been reviewed in the past

Chapter three gives a description of the performances of continuous and discontinuous PWM strategies, their limitations, and advantages. It was studied in different conventional power converters (a) Three Phase VSI, (b) Three Phase Boost Rectifier. The simulation of both the conventional converters was performed such that the difference between the same and the Z-source converter can be shown.

Chapter four studies the PWM modulation scheme utilized in the Z-Source Converters. The PWM modulation techniques are presented including both carrier-based PWM and space vector PWM. The equivalence is set up between these two methods for the normal operation. The space vector diagram is drawn using the generalized transformation and then used to synthesize the reference voltages. The calculation of zero sequence voltage expressions is done by choosing the appropriate active and null states and then these expressions are generalized and added to the reference voltage to generate the modulation signals. The switching signals are generated using carrier-based PWM through the comparison between these modulation signals and the high frequency carrier signals. This method is easy to implement compared with the direct space vector approach and can be used for any system. The same scheme is adopted for the Z-source converter also and corresponding results are presented. The modulation principles are carefully formulated in order to achieve minimum number of device commutations in each cycle of operation.

Chapters five and six model the Z-source inverter feeding an impedance load and an induction machine respectively. The Z-source inverter is analyzed in all its six operating modes and a detailed dc and ac analysis to study its transient and steady state behavior is laid out in detail. For dc analysis, the small-signal analysis method is used with an intention of developing a comprehensive guide on Z-source impedance modeling. It is also carefully analyzed to ensure that the current ripple and the voltage stress is minimized. When the above factors are considered, the size of the system reduces to a great extent. Dynamic analysis of the Z-source inverter is also performed. The simulations are performed using MATLAB/SIMULINK. The induction machine used in this case is a 3 phase, 1 hp, 60 Hz squirrel cage induction machine. The system is studied in the transient state as well as when it reaches steady state. The induction machine is loaded and its effects are shown in the results. The results prove that by controlling the shoot-though duty ratio, the load voltage can either be boosted or bucked.

The section following the Z-source Inverters involves the description of the Z-source Rectifier which is provided in chapters seven and eight. The Z-source rectifier can buck and boost the input voltage by using the extra shoot-through state. Actually, the three-phase rectifier without the Z-network connecting it to the load is the conventional boost rectifier. In order to buck the voltage, the shoot-through state is introduced. It prevents the usage of a dc-dc converter. It provides a low-cost, reliable, and highly efficient single-stage structure for buck-boost power conversion. Similar to that of the Z-source inverter, the Z-source rectifier is analyzed in all its operating modes and the steady state and transient analysis is performed. A simple resistive load is used in this analysis. The small signal analysis is performed in order to study the stability criterion of the of the

249

system model. In the case of the rectifier, the operating condition which is achieved is unity power factor. This effect is studied in both the cases of dynamic analysis and steady state analysis.

A PI controller is designed to develop the cascaded controller of the Z-source rectifier in chapter nine. This is designed while is system is studied in the synchronous reference frame. The Z-source rectifier basically has three control variables. Namely – q-axis and d-axis modulation signals, M_{qs}, M_{ds} and the shoot through duty ratio, D_o. Hence the system can be controller for three parameters which is the output dc voltage, the capacitor voltage and the unity power factor. The control is implemented and the simulation results are provided.

The later section involves the development of the vector control scheme of the Induction machine which is fed by the Z-source inverter. This constitutes chapter ten. This adjustable speed drive is studied and a cascaded PI controller is proposed and designed.

Chapter eleven provides the hardware description used in the practical experiment. The design of the inverter, base drives, external logic circuit, and the design of the Z-network inductor is presented in detail.

To conclude the continuous and discontinuous PWM strategies have been developed and laid out in an analytical way in this thesis. The Z-source converter employs a unique impedance network (or circuit) to couple the converter main circuit to the power source, thus providing unique features that cannot be observed in the traditional voltage-source and current-source converters where a capacitor and inductor are used, respectively. The Z-source converter overcomes the conceptual and theoretical

barriers and limitations of the traditional voltage-source converter and current-source converter and provides a novel power conversion concept which can be utilized in a wide field of applications. The Z-source converter can boost–buck voltage, minimize component count, increase efficiency, and reduce cost.

12.3 Future Work

The scope for future work is highlighted in this section. The suggestions made are discussed with respect to the work done in this thesis.

Due to laboratory limitations, the ratings used in this study as well as the experiments is not that which can be used for high rated machines. The design developed can be used in order to make it compatible for other machines.

Photovoltaic systems and fuel cells can be used instead of the dc supply being used in this thesis.

The system can be extended to multi-phase/multi-leg converters and the effect of the Z-source network can be studied in detail.

Mutually coupled inductors can be used instead of the two individual inductors used in the Z-network and the effects of this can be studied and compared to that of the conventional Z-source converters.

In this thesis, only unity power factor is aimed at and achieved. In the future, other power factors can be aimed at achieving.

Other methods of designing the controller can be followed to determine other control schemes. Say for example, instead of a PI controller, a PID controller can be

designed and the output can be studied. In this study, the Butterworth's polynomial method is used to study the system. In the future, other analytical tools like the Chebyshev polynomial can also be used in order to compare the different tools which can be used and the better method can be concluded.

REFERENCES

Conventional Converters

[C.1]   Ahmet M. hava, Russel J. Kerkman, Thomas A. Lipo, "Simple Analytical and Graphical Methods for Carrier-Based PWM-VSI Drives," *IEEE Transactions on Power Electronics*, Vol. 14, No. 1, pp. 49-61, January 1999.

[C.2]   Olorunfemi Ojo, "The Generalized Discontinuous PWM Scheme for Three-Phase Voltage Source Inverters," *IEEE Transactions on Industrial Electronic*, Vol. 51, No. 6, pp. 1280-1289, December 2004

[C.3]   Ahmet M. hava, Russel J. Kerkman, Thomas A. Lipo, "A High Performance Generalized Discontinuous PWM Algorithm," *IEEE Transactions on Industry Applications*, Vol. 34, No. 5, pp. 1059-1071, September/October 1998.

[C.4]   Keliang Zhou, Danwei Wang, "Relationship between Space-Vector Modulation and Three Phase Carrier-Based PWM:A Comprehensive Analysis," *IEEE Transactions on Industrial Electronics,* Vol. 49, No. 1, pp. 186-196, February 2002.

[C.5]   Yongsug Suh, Valentin Tijeras, Thomas A. Lipo, "A Control Method in dq Synchronous Frame for PWM Boost Rectifier under Generalized Unbalanced Operating Conditions," *IEEE 33rd Annual Power Electronics Specialists Conference*, Vol. 3, pp. 1425-1430, June 2002.

[C.6]   Po-Wa Lee, Yim-Shu Lee, David K. W. Cheng, Xiu-Cheng Liu, "Steady-State Analysis of an Interleaved Boost Converter with Coupled Inductors," *IEEE Transactions on Industrial Electronics*, Vol. 47, No. 4, pp. 787-795, August 2000.

[C.7]   Z. Ye, D. Boroyevich, J. Choi and F. C. Lee, "Control of Circulating Current in Two Parallel Three-Phase Boost Rectifiers," *IEEE Transactions on Power Electronics,* vol. 17, no. 5, pp. 609–615, September. 2002.

[C.8]   Ching-Tsai Pan, Jenn-Jong Shieh, "A Family of Closed-Form Duty Cycle Control Laws for Three-Phase Boost AC/DC Converter," *IEEE Transactions on Industrial Electronic*, Vol. 45, No. 4, pp. 530-543, August 1998.

[C.9]   Ching-Tsai Pan, Jenn-Jong Shieh, "A Single-Stage Three-Phase Boost-Buck AC/DC Converter based on Generalized Zero-Space Vectors," *IEEE Transactions on Power Electronics*, Vol. 14, No. 5, pp. 949-958, September 1999.

[C.10] Ching-Tsai Pan, Jenn-Jong Shieh, "New Space-Vector Control Strategies for Three-Phase Step-Up/Down AC/DC Converter," *IEEE Transactions on Industrial Electronics*, Vol. 47, No. 1, pp. 25-35, February 2000.

[C.11] Michael T. Madigan, Robert W. Erickson, Esam Hamid Ismail, "Integrated High-Quality Rectifier-Regulators," *IEEE Transactions on Industrial Electronics*, Vol. 46, No. 4, pp. 749-758, August 1999.

[C.12] D. S. L. Simonetti, J. Sebastian, and J. Uceda, "The Discontinuous Conduction mode sepic and cuk Power Factor Pre-regulators: Analysis and Design," *IEEE Transactions on Industrial Electronics,* Vol. 44, pp. 630–637, October. 1997.

[C.13] J. C. Salmon, "Techniques for minimizing the input current distortion of current-controlled single-phase boost rectifiers," *IEEE Transactions on Power Electronics*, Vol. 8, No. 4, pp. 509-520, October 1993.

[C.14] C. T. Pan, J. J. Shieh, "A single-stages three-phase boost-buck AC/DC converter based on generalized zero-space vedtors," *IEEE Transactions on Power Electronics*, Vol. 14, No. 5, pp. 949-958, 1999.

[C.15] J. J. Sheih, "SEPIC derived three-phase switching mode rectifier with sinusoidal input current," *IEE Proceedings Part B – Electrical Power Applications*, Vol. 147, No. 4, pp. 286-294, 2000.

[C.16] R. Itoh, K. Ishizaka, "Three-phase flyback ac-dc converter with sinusoidal supply currents," *IEE Proceedings Part B - Electrical Power Applications*, Vol. 138, No. 3, pp. 143- 151, 1991.

[C.17] C. T. Pan, T. C. Chen, "Step-up/down three-phase ac to dc converter with sinusoidal input current and unity power factor," *IEE Proceedings Part B – Electrical Power Applications*, Vol. 141, No. 2, pp. 77-84, 1994.

[C.18] V. F. Pires, J. F. Silva, "A new single stage three-phase step-up/down rectifier with low effects on the mains," *IEEE Conference Proceedings of IAS 2000*, pp. 2389-2396, 2000.

Z-Source Inverters

[I.1] Fang Zheng Peng, "Z-Source Inverter," *IEEE Transactions on Industry Applications*, Vol. 39, No. 2, pp. 504-510, March/April 2003

[I.2] Fang Xheng Peng, Xiaoming Yuan, Xupeng Fang, Zhaoming Qian, "Z-Source Inverter for Adjustable Speed Drives," *IEEE Power Electronics Letters*, Vol. 1, No. 2, pp. 33-35, June 2003.

[I.3]   Xinping Ding, Zhaoming Qian, Shuitao Yang, Bin Cui, Fang Zheng Peng, "A PID Control Strategy for DC-link Boost Voltage in Z-Source Inverter," *22nd Annual IEEE Applied Power Electronics Conference and Exposition*, pp. 1145-1148, February 2007.

[I.4]   Xinping Ding, Zhaoming Qian, Shuitao Yang, Bin Cui, Fang Zheng Peng, "A Direct Peak DC-link Boost Voltage Control Strategy in Z-Source Inverter," *22nd Annual IEEE Applied Power Electronics Conference and Exposition*, pp. 648-653, February 2007.

[I.5]   Xinping Ding, Zhaoming Qian, Shuitao Yang, Bin Cui, Fang Zheng Peng, "A High Performance Z-Source Inverter Operating with Small Inductor at Wide-Range Load," *22nd Annual IEEE Applied Power Electronics Conference and Exposition*, pp. 615-620, February 2007.

[I.6]   Tran-Quang Vinh, Tae-Won Chun, Jung-Ryol Ahn, Hong-Hee Lee, "Algorithms for Controlling both the DC Boost and AC Output Voltage of the Z-Source Inverter," *32nd Annual Conference of IEEE Indusrial Electronics Society,* pp. 970-974, November 2005.

[I.7]   P. C. Loh, D. M. Vilathgamuwa, C. J. Gajanayake, Y. R. Lim, C. W. Teo, "Transient Modeling and Anlaysis of Pulse-Width modulated Z-source Inverter," *IEEE Transactions on Power Electronics*, Vol. 22, No. 2, pp. 498-507, March 2007.

[I.8]   P. C. Loh, F. Blaabjerg, S. Y. Feng, K. N. Soon, "Pulse-Width Modulated Z-Source Neutral-Point Clamped Inverter," *21st Annual IEEE Applied Power Electronics Conference and Exposition,* pp. 431-437, March 2006.

[I.9]   Jingbo Liu, Jiangang Hu, Longya Xu, "A modified Space vector PWM for Z-source Inverter – Modeling and Design," *Proceedings of the 8th International Conference on Electrical Machines and Systems*, Vol. 2, pp. 1242-1247, September 2005.

[I.10] Fang Zheng Peng, Miaosen Shen, Zhaoming Qian, "Maximum Boost Control of the Z-Source Inverter," *IEEE Transactions on Power Electronics*, Vol. 20, No. 4, pp. 833-838, July 2005.

[I.11] Miaosen Shen, Jin Wang, Alan Joseph, Fang Zheng Peng, Leon M. Tolbert, Donald J. Adams, "Constant Boost Control of the Z-source Inverter to Minimize Current Ripple and Voltage Stress," *IEEE Transactions on Industry Applications*, Vol. 42, No. 3, pp. 770-778, May/June 2006.

[I.12] Yi Huang, Miaosen Shen, Fang Zheng Peng, Jin Wang, "Z-Source Inverter for Residential Photovoltaic Systems," *IEEE Transactions on Power Electronics*, Vol. 21, No. 6, pp. 1776-1782, November 2006.

[I.13]   Poh Chiang Loh, D. Mahinda Vilathgamuwa, Yue Sen Lai, Geok Tin Chua, Yunwei Li, " Pulse-Width Modulation of Z-Source Inverters," *IEEE Transactions on Power Electronics*, Vol. 20, No. 6, pp. 1346-1335, November 2005.

[I.14]   F. Gao, P. C. Loh, D. M. Vilathgamuwa, F. Blaabjerg, "Performance Analysis of Random Pulse-Width Modulated Z-Source Inverter with Reduced Common Mode Switching," *37th IEEE Power Electronics Specialists Conference*, pp. 1536-1542, June 2006.

[I.15]   D. M. Vilathgamuwa, C. J. Gajanayake, P. C. Loh, Y. W. Li, "Voltage Sag Compensation with Z-Source Inverter Based Dynamic Voltage Restorer," *41st IAS Annual Meeting, Conference Record of IEEE Industry Applications Conference*, Vol. 5, pp. 2242-2248, October 2006.

[I.16]   Miaosen Shen, Fang Zheng Peng, "Control of the Z-Source Inverter for Fuel Cell-Battery Hybrid vehicles to Eliminate Undesirable Operation Modes," *41st IAS Annual Meeting, Conference Record of IEEE Industry Applications Conference*, Vol. 4, pp. 1667-1673, October 2006.

[I.17]   Keping You, M. F. Rahman, "Constructing a Novel Power Converter by Matrix Converter Theory and Z-Source Inverter Concepts for ISA 42 V PwerNet System," *41st IAS Annual Meeting, Conference Record of IEEE Industry Applications Conference*, Vol. 4, pp. 2101-2108, October 2006.

[I.18]   Keping You, M. F. Rahman, "Analytical Comparison of Conduction and Switching Losses of a Novel Matrix-Z-Source Converter and a Conventional VSI Converter for Automotive ISA 42 V System," *37th IEEE Power Electronics Specialists Conference*, pp. 146-152, June 2006.

[I.19]   P.C. Loh, F. Blaabjerg, C. P. Wong, "Comparative Evaluation of Pulse-Width Modulation Strategies for Z-Source Neutral-Point-Clamped Inverter," *37th IEEE Power Electronics Specialists Conference*, pp. 1316-1322, June 2006.

[I.20]   C. J. Gajanayake, D. M. Vilathgamuwa, P. C. Loh, "Modeling and Design of Multi-loop Closed Loop Controller for Z-Source Inverter for Distributed Generation," *37th IEEE Power Electronics Specialists Conference*, pp. 1353-1359, June 2006.

[I.21]   F. Gao, P. C. Loh, D. M. Vilathgamuwa, F. Blaabjerg, "Performance Evaluation of Three-Level Z-Source Inverters Under Semiconductor Failure Conditions," *22nd IEEE Applied Power Electronics Conference*, pp. 626 – 632, February 2007.

[I.22]   Tae-Won Chun, Quang-Vinh Tran, Jung-Ryol Ahn, Jih-Sheng Lai, "AC Output Voltage Control with Minimization of Voltage Stress Devices in the Z-Source Inverter Using Modified SVPWM," *37th IEEE Power Electronics Specialists Conference*, pp. 3030-3034, June 2006

[I.23] F. Gao, P. C. Loh, F. Blaabjerg, D. M. Vilathgamuwa, "Dual Z-Source Inverter with Three-Level Reduced Common Mode Switching," *41st IAS Annual Meeting, Conference Record of IEEE Industry Applications Conference*, Vol. 4, pp. 619-626, October 2006.

[I.24] Babak Farhangi, Shahrokh Farhangi, "Comparison of Z-Source and Boost-Buck Inverter as a Single Phase Transformer-less Photovoltaic Grid-connected Power Conditioner," *37th IEEE Power Electronics Specialists Conference*, pp. 74-79, June 2006.

[I.25] Jin-Woo Jung, Ali Keyhani, "Control of a Fuel Cell Based Z-Source Converter," *IEEE Transactionson Energy Conversion*, Vol. 22, No. 2, pp. 467-476, June 2007.

[I.26] Fang Zheng Peng, Alan Joseph, Jin Wang, Miaosen Shen, Lihua Chen, Zhiguo Pan, Eduardo Ortiz-Rivera, Yi Huang, "Z-Source Inverter for Motor Drives," *IEEE Transactions on Power Electronics*, Vol. 20, No. 4, pp. 857-863, July 2005.

[I.27] Miaosen Shen, Alan Joseph, Jin Wang, Fang Z. Peng, Donald J. Adams, "Comparison of Traditional Inverters and Z-Source Inverter for Fuel Cell Vehicles," *IEEE Transactions on Power Electronics*, Vol. 22, No. 4, pp. 1453-1463, July 2007.

[I.28] F. Gao, P. C. Loh, F. Blaabjerg, R. Teodorescu, "Modulation Schemes of Multi-phase Three-level Z-Source Inverters," *38th IEEE Power Electronics Specialists Conference*, pp. 1905-1911, June 2007.

[I.29] Miaosen Shen, Qingsong Tang, Fang Z. Peng, "Modeling and Controller Design of the Z-Source Inverter with Inductive Load," *38th IEEE Power Electronics Specialists Conference*, pp. 1804-1809, June 2007.

Z-Source Rectifiers

[R.1] Xinping Ding, Zhaoming Qian, Yeyuan Xie, Fang Zheng Peng, "A Novel ZVS Z-Source Rectifier," *21st Annual IEEE Applied Power Electronics Conference and Exposition*, pp. 951-955, March 2006.

[R.2] Yeyuan Xie, Zhaoming Qian, Xinping Ding, Fang Zheng Peng, "A Novel Buck-Boost Z-Source Rectifier," *37th IEEE Power Electronics Specialists Conference*, pp. 1225-1229, June 2006.

[R.3] Xinping Ding, Zhaoming Qian, Yeyuan Xie, Fang Zheng Peng, "Transient Modeling and Control of the Novel ZVS Z-Source Rectifier," *37th IEEE Power Electronics Specialists Conference*, pp. 898-902, June 2006.

[R.4]   Jun Kikuchi, Thomas A. Lipo, "Three-Phase PWM Boost-Buck Rectifiers with Power-Regenerating Capability," *IEEE Transactions on Industry Applications*, Vol. 38, No. 5, pp. 1361-1369, September/October 2002.

[R.5]   Poh Chiang Loh, Feng Gao, Pee-Chin Tan, Frede Blaabjerg, "Three-level AC-DC-AC Z-Source Converter Using Reduced Passive Component Count," *38th IEEE Power Electronics Specialists Conference*, pp. 2691-2697, June 2007.

Books

[B.1]   Philip T. Krein, *Elements of Power Electronics*, Oxford University Press, 1998.

[B.2]   Robert W. Erickson, Dragan Maksimovic, *Fundamentals of Power Electronics*, Springer Science+Business Media, Inc., 2001.

[B.3]   Colonel Wm. T. McLyman, *Transformer and Inductor Design Handbook*, Marcel Dekker, Inc., 1978.

[B.4]   Jean-Jacques E. Slotine, Weiping Li, *Applied Nonlinear Control*, Prentice Hall, Englewood Cliffs, New Jersey, 1991.

[B.5]   Muhammad H. Rashid, *Power Electronics-Circuits, Devices and Applications*, Second Edition, Prentice Hall, 2001.

[B.6]   D. Grahame Holmes, Thomas A. Lipo, *Pulse Width Modulation for Power Converters*, IEEE Press, John Wiley & Sons, Inc., 2003.

[B.7]   Peter Wood, *Switching Power Converters*, Robert E. Krieger Publishing Company, Florida, 1981.

[B.8]   B.Friedland, *Control System Design, An Introduction to State-Space Methods*, McGraw-Hill Inc., New York, 1986.

Thesis

[T.1]   Glenn Sugita, "**Analysis of Three-Phase Pulse Width Modulation AC-to-DC Buck Converter Under Modulation Magnitude and Phase Control**," M.S. Thesis, Tennessee Technological University, Cookeville, TN, 1994.

[T.2]   Jingbo Liu, "**Modeling, Analysis and Design of Integrated Starter Generator System Based on Field Oriented Controlled Induction Machines**," Ph.D. dissertation, Ohio State University, OH, 2005.

[T.3]   Kent Daniel Holland, "**Z-Source Inverter Control for Traction Drive of Fuel Cell-Battery Hybrid Vehicles**," M.S. thesis, Michigan State University, MI, 2005.

[T.4]   Jun Kikuchi, "**Analysis and Control of Three-Phase AC-DC PWM Boost-Buck and Buck-Boost Bidirectional Power Converters**," Ph.D. dissertation, University of Wisconsin-Madison, WI, 2002.

[T.5]   Jin Woo Jung, "**Modeling and Control of Fuel Cell Based Distributed Generation Systems**," Ph.D. dissertation, Ohio State University, OH, 2005.

[T.6]   Zhiqiau Wu, "**An Investigation Of Dual Stator Winding Induction Machines**," Ph.D. dissertation, Tennessee Technological University, TN, December 2006.

[T.7]   Gan Dong, "**Sensorless and Efficiency Optimized Induction Machine Control with Associated Converter PWM Modulation Schemes,**" Ph.D. dissertation, Tennessee Technological University, TN, December 2005

VITA

Gayathri Murthi was born in Chennai, India, on November 4, 1983. She finished her Bachelor of Engineering degree program in Electrical and Electronics Engineering in May 2005 in Anna University, Chennai, India. She joined Tennessee Technological University in August 2005 and is currently a Master of Science graduate student in Electrical Engineering. Her research area and interest includes Power Electronics, Control Systems, and Drives.